Source, transport, and fate of particulate organic carbon in the largest Chinese rivers

Yutian Ke

université PARIS-SACLAY

Source, transport, and fate of particulate organic carbon in the largest Chinese rivers

Origine et devenir du carbone organique particulaire transporté par les plus grands fleuves de Chine

Thèse de doctorat de l'université Paris-Saclay

École doctorale n° 579, Sciences mécaniques et énergétiques, matériaux et géosciences (SMEMAG)
Spécialité de doctorat : Terre solide : géodynamique des enveloppes supérieures, paléobiosphère
Unité de recherche : Université Paris-Saclay, CNRS, GEOPS, 91405, Orsay, France
Graduate School : Géosciences, climat, environnement et planètes
Référent : Faculté des sciences d'Orsay

Thèse présentée et soutenue à Paris-Saclay, le 15 décembre 2021, par

Yutian KE

Composition du Jury

Christian FRANCE-LANORD DR CNRS, CRPG	Président
Isabelle BASILE-DOELSCH DR INRAE, Aix-Marseille Université, CEREGE	Rapporteure & Examinatrice
Robert HILTON Professeur, University of Oxford, Department of Earth Sciences	Rapporteur & Examinateur
Jiubin CHEN Professeur, Tianjin University, ISESS	Examinateur
Laure GANDOIS CR CNRS, Laboratoire Ecologie Fonctionnelle et Environnement	Examinatrice
Christophe RABOUILLE DR CEA, LSCE	Examinateur

Direction de la thèse

Cécile QUANTIN Professeure, Université Paris-Saclay, GEOPS	Directrice de thèse
Damien CALMELS MCF, Université Paris-Saclay, GEOPS	Co-encadrant de thèse

Thèse de doctorat

NNT : 2021UPASJ021

Abstract

Continental erosion and riverine transport of particulate organic carbon (POC) to the Ocean play a central role in the global carbon cycle. Rivers provide key and integrated information on the origin, mobilization processes and metabolism of POC transiting from terrestrial to marine reservoirs. Once in the marine environment, POC may eventually have antagonist feedbacks on the long-term CO_2 content of the atmosphere, depending on its origin (biospheric vs petrogenic) and its fate (burial vs mineralization). Large rivers in China are of crucial importance in our understanding of POC delivery at both regional and global scales, as they encompass a large spectrum of climatic and geomorphic conditions, drain various lithologies, and are subject to varied but increasing anthropogenic pressure.

This thesis focuses on three parts: 1) the sources and transport mechanisms of POC in one of the most turbid large rivers, the Huanghe; 2) the impact of dam-building on POC export in the Changjiang, a large catchment that experiences massive anthropogenic perturbation with > 50,000 dams; 3) the development of a global database that gathers 3,300 data on riverine POC along with co-localized data of its possible geoenvironmental controls. To fulfill the goals of this thesis, multiple sampling expeditions were carried out on the largest rivers in China to collect monthly time series of suspended particulate matter (SPM) at the channel surface and multiple vertical depth profiles of SPM along channel transects. Fluvial sediment was analyzed for particle size and major elements as well as for POC content and dual carbon isotopes (^{13}C and ^{14}C). Coupling POC content with particle size (or aluminum to silicon ratios) and ADCP acquisitions allows accessing the loading and transport mode of POC as well as an accurate estimate of instantaneous POC fluxes.

The Huanghe, which has experienced a 90% decrease in sediment load since the 1950s, carries relatively ^{14}C-depleted POC ($\Delta^{14}C$: −453‰ to −331‰) although POC mainly originates from the biospheric pool (67%-79%). This is explained by enhanced physical erosion of unconsolidated loess-paleosol sequences in the Chinese Loess Plateau region. Gully erosion would mobilize aged (and even dead) carbon from deep horizons that can still be considered as biospheric carbon in the long-term carbon cycle. In addition, POC heterogeneities at the scale of a river cross-section suggest that bank erosion and bedload resuspension are operational processes.

In the Changjiang River system, long-term fluxes of erosion and POC export have been greatly impacted by human activities, especially since the operation of dams. A substantial amount of POC is not anymore transferred to the ocean but end-up buried in reservoirs upstream of dams. Nowadays, there would be 4 times more POC retained in reservoirs along the Changjiang than the amount of POC exported to the ocean at the mouth. For the first time, the impact of cascade mega reservoirs (CMRs) in the lower Jinshajiang (upper reaches of the Changjiang) on fluvial POC transfer is quantitatively evaluated. Distinct POC signature and loading are observed before and after CMRs operation, which prevented POC coming from the Qinghai-Tibet Plateau from traveling downstream and favored rapid and efficient burial of this OC on the continent rather than in the ocean.

Finally, a global database archiving 3,300 published and unpublished elemental and isotopic data on worldwide riverine POC: MOdern River archivEs of Particulate Organic Carbon (MOREPOC) has been built. It records the fluvial memory of SPM collected at 229 main channels and tributaries in 118 river systems. MOREPOC is then used to investigate the global pattern of POC loading and the possible environmental factors (*i.e.*, geomorphology, climate, and tectonics) that can control the radiocarbon signatures of POC in global rivers.

Résumé

Les processus d'érosion et de transport de carbone organique particulaire (POC) des continents vers l'océan jouent un rôle central dans le cycle du carbone. Les rivières fournissent des informations clés et intégrées sur l'origine, les processus de mobilisation et le métabolisme du carbone organique transitant des réservoirs terrestres aux réservoirs marins. Cet apport de POC à l'océan peut avoir des impacts variés sur la teneur en CO_2 de l'atmosphère à long terme, suivant son origine (biosphérique vs pétrogénique) et son devenir (enfouissement vs minéralisation). Il est donc crucial d'améliorer notre compréhension des processus de mobilisation et de transport de POC dans les fleuves et d'en identifier les sources, notamment face aux perturbations anthropiques actuelles. En ce sens, les grands fleuves chinois sont des terrains d'études privilégiés car ils sont caractérisés par une diversité de conditions climatiques et géomorphologiques, drainent des lithologies variées et sont soumis à une pression anthropique variable mais croissante.

Cette thèse se décompose en trois parties : 1) quantifier les sources et mécanismes de transport du POC dans un grand fleuve ayant l'une des charges sédimentaires les plus importantes au monde, le Huanghe ; 2) quantifier l'impact des barrages sur l'export de POC dans le Changjiang, un fleuve soumis à une pression anthropique massive (> 50,000 barrages) ; 3) développer une base de données mondiale qui rassemble 3,300 données de POC ainsi que des données de ses éventuels contrôles géo-environnementaux. Pour atteindre ces objectifs, des campagnes de prélèvements ont été menées sur les plus grands fleuves de Chine. Il a ainsi été possible d'exploiter des séries temporelles mensuelles de matière en suspension (SPM) prélevée en surface ainsi que de multiples échantillons de SPM prélevés suivant des profils verticaux distribués le long de transects de rivière. La distribution en taille des grains et la composition chimique de ces SPM ont été analysés au même titre que la teneur en carbone organique et ses compositions isotopiques en $d^{13}C$ et C^{14}.

Le fleuve Huanghe, qui a connu une diminution d'environ 90 % de sa charge sédimentaire depuis 1950, transporte du POC relativement appauvri en C^{14} ($\Delta^{14}C$: −453‰ à −331‰) et cela, bien que la majorité de ce POC provienne de sources biosphériques (67% - 79%). L'érosion physique intense des séquences de loess-paléosols dans le bassin expliquerait cette mobilisation de carbone relativement ancien

(et même “mort” pour partie) provenant d'horizons profonds. De plus, l’hétérogénéité verticale et latérale de la composition élémentaire et isotopique du POC à l'échelle d'un transect de rivière montrent que l'érosion des berges et la remise en suspension du sable de fond sont des processus actifs.

Dans le bassin du fleuve Changjiang, les flux d'érosion à long terme et l'exportation de POC ont été fortement impactés par les activités humaines, notamment par la mise en place de barrages. A l’heure actuelle, il y aurait 4 fois plus de POC retenus à l’arrière des barrages du Changjiang que la quantité de POC exportée à l'embouchure. Le développement des méga-réservoirs en cascade (CMR) dans le Jinshajiang (cours supérieur du Changjiang) a bloqué le transfert jusqu’à l’océan du POC provenant du plateau du Qinghai-Tibet et a favorisé un enfouissement rapide et efficace de ce carbone organique sur le continent plutôt que dans l'océan.

Enfin, une base de données mondiale archivant 3,300 données élémentaires et isotopiques de POC dans le monde : Modern River Archives of Particulate Organic Carbon (MOREPOC), a été construite. Elle enregistre la mémoire fluviale des SPM collectés dans 229 rivières de 118 systèmes fluviaux. MOREPOC est construite pour étudier de manière globale les facteurs environnementaux majeurs pouvant contrôler l’export de POC et sa signature isotopique.

Acknowledgments

Vouloir, c'est pouvoir.

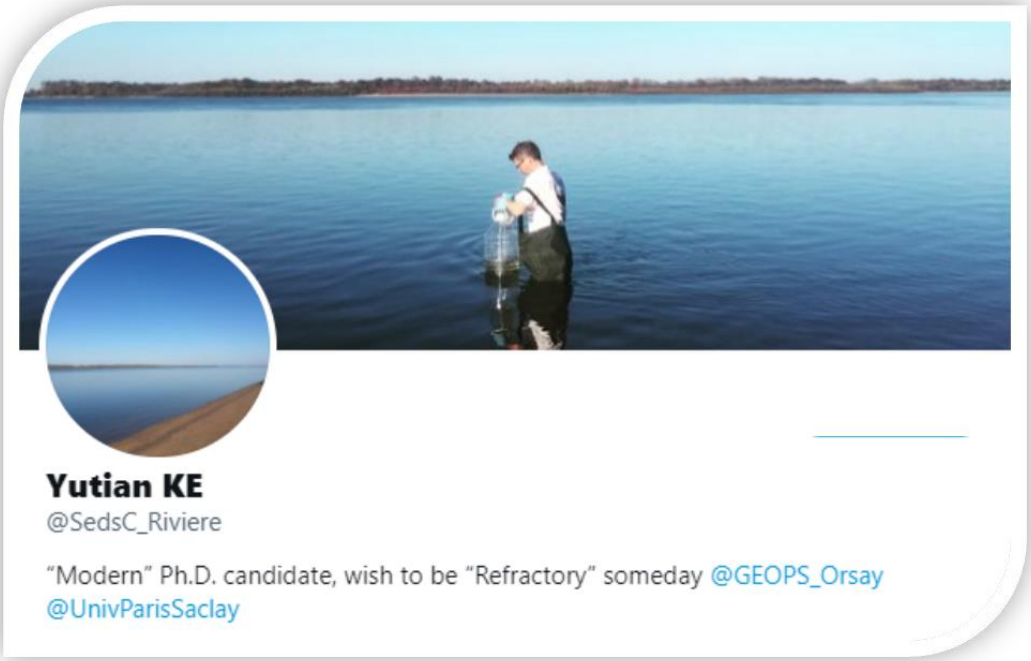

When I finished writing this thesis, I can't help myself looking back to the past four years, a truly wonderful journey, many people are involved in this adventure. Some people always ask why I decided to jump into another "river" of science instead of sticking into the old one, now the answers are hidden in the following words. In my life philosophy, I do believe the decision that you can truly embrace is usually a good one.

To begin with, I would like to give my sincere thanks to my master advisor, Prof. Shouyun LIANG at Lanzhou University, who was constantly giving strength and trust in raising my scientific motivation for geoscience research. Therefore, I was offered a lot of opportunities in participating in different scientific projects (concerning the failure mechanism of loess landslides, spatial prediction of landslide susceptibility, and conglomerate landform evolution, etc.), field expeditions, and conferences. I am truly grateful for his support and guidance.

À Paris, J'ai commencé ma vie romantique de doctorat, c'est dommage que je n'ai pas amélioré mon français. Je suis resté dans ma zone de confort en parlant anglaise. Il faut blâmer mes directeurs de thèse (Damien Calmels et Cécile Quantin) car ils parlent très bien anglaise. Here, I appreciate the China Scholarship Council for funding my study under the ANR project "SEDIMAN" in Paris.

Damien is both a mentor and a friend to me. I am a rookie in the field of river geochemistry. It was a really hard start when I was trying to figure out what I should learn and what I should do. Nonetheless, so many unexpected experimental problems occurred. Thanks to Damien, his talents, patience, trust, and enthusiasm helped me get through the clouds. I learned a lot from him in science, experiments, and fields with specific details, most importantly, the way of flexible and critical thinking. Dans la vie, he is really humorous and optimistic, we had a lot of fun. I have received countless help from Damien,

thank you for being an incredible advisor and an incredible listener. Cécile is so nice and wise that impressed me a lot. I felt overwhelmed when she invited me for a Christmas after my arrival. She helped me solve many administrative problems and always tried her best to seek possible solutions to my experimental problems. I have a nice Ph.D. life largely because of the joint effort of Damien and Cécile.

I sincerely thank the help provided by my dear colleagues, without whom this thesis won't be possible to come real. First of all, I thank Xavier Quidelleur, Thi Kim Ngan Ho, and Raboux Georgette for their kind help in handling administrative procedures of registration and thesis for the doctoral school. Then, I also want to thank Christophe Colin for joining my first-year committee. Here comes my solid supporters, I have endless appreciations, Marc Massault, the man who calls me "Arsène Lupin" because I "stole" a lot of materials and skills from him for elemental and isotopic carbon analysis. Aurelie Noret, the "Wonderwoman" assisted me to measure the organic carbon content and stable carbon isotopic composition using IRMS-EA. François Thil, a true master on MICADAS at LSCE, generously guided me to manipulate MICADAS for ^{14}C analysis, which is an essential component of this thesis. Jean-Pascal Dumoulin, taught me to master the quartz tube sealing technique, which is really helpful to reduce atmospheric CO_2 contamination. Agrinier Pierre, helped me to analyze the stable carbon isotope of carbon and oxygen of riverine inorganic particulate carbon at IPGP. Pierre Barré, provided me place and equipment to conduct particle size analysis on sediment samples. Nadine Tissenerat, Christophe Rabouille and Christine Hatté are thanked for those wonderful talks and technical sharings at LSCE.

I would like to give my sincere thanks to Julien Bouchez, who has been actively participating in my research, I benefited a lot from his insightful ideas and comments. Besides, Julien helped me to access different experiment resources to boost my study. Benjamin Chetelat, Jérôme Gaillardet, and Jiubin Chen are thanked for providing constructive scientific inputs and SPM samples. During the field, Damien, Julien, Hongming, Antoine, Benjamin, Shengliu, Yilong, Jianfeng, Yulong helped to collect sediment samples and to conduct the pretreatment procedure. Jiubin Chen and Jérôme Gaillardet are thanked for their valuable suggestions, discussions, and supports of my research.

This thesis is coming to a final stage, I appreciate that Robert Hilton and Isabelle Basile-Doelsch for agreeing to review my thesis in the midst of pressing affairs. I had a wonderful chat with Bob at IPGP, your work on mountain-building-related organic carbon cycles is so juicy that boost my addiction to this field. Then, I want to give my sincere thanks to Christian France-Lanord, Christophe Rabouille, Jiubin CHEN, and Laure Gandois for agreeing to be a member of the jury.

I am glad I have met so many great souls here in Paris at GEOPS, Claire Ansart, Claire Froger, Heller Beatrix, Brandon Margaux, Alexis Derycke, etc. These amazing people helped me to adapt to la vie en France, we had nice moments drinking, eating, chatting. Besides, Alexis, I will never forget chartreuse. The 3rd floor is a center of good people, Gaël Monvoisin, thanks for being my great neighbor, and for all the chatting and talented musical suggestions. Emmanuel Leger, thanks for being willing to listen to me, all your encouragement and care matter to me.

With my whole heart, I would like to thank my Chinese friends in Paris, Wei XIE, Rongxing LI, Xinquan ZHOU, Jaozhi YE, Xu ZHANG, Jing KONG, Xu

CHEN, Yanli XIANG, Xia GAO, Yue TONG, Xi CHEN, etc. It is lucky to know you guys in a foreign country, thanks for the precious time spent together to get over sorrows and to enjoy happiness.

I have endless thanks for my family back in China, especially for my parents Hong KE (柯红) and Xiaomei TANG (汤小梅), providing me love, support, and encouragement throughout. It has been eleven years since I entered the college, and also the eleven years that I have been far away and giving you very few accompany. The pandemic kept us from coming back for two years, it has always been a hard time for you to wait for your son to come back home. I would also like to thank my grandma, with who I spent my entire childhood, her kindness and love give me the strength to carry on, I wish I would have more time with you but it will never be fulfilled, I will be missing you forever.

Finally, and with my whole heart, I send my essential thanks to Liping ZHU (朱丽萍), I think I hit the jackpot by choosing you to be my wife, for glowing me when I was in the dark, for completing me by being who you are, for dancing in my every heartbeat. The beautiful views in the world shall be the happy melody in our life with each other till the end. Grow old along with me, the best is yet to be.

Merci beaucoup, tout le monde!

25/09/2021

Lille

Yutian

柯雨田

Contents

General Introduction

Since the Earth has entered the Anthropocene, in which human activities act as a geological force comparable to tectonics and climate, terrestrial and aquatic environments have experienced drastic and unprecedently fast disruption to their functioning (Zalasiewicz et al., 2015). Fluvial sediments, which integrate erosion, weathering, and anthropogenic processes at the scale of the river catchment, provide essential information to unravel key earth surface processes and behind drivers.

In the delivery trajectory of sediments from source to sink in the Earth's sedimentary cycle, rivers are the main conveyor of terrestrial materials in the form of suspended particulate matter (SPM) and dissolved load from inland regions to continental margins (Blair and Aller, 2012; Leithold et al., 2016). Along with SPM, terrestrial organic carbon is transported as particulate organic carbon (POC) from continents to their final burial site in ocean sediments and represents a main component of the global carbon cycle (Ittekkot, 1988; Meybeck, 1993; Galy et al., 2007; 2008a; 2015; Blair and Aller, 2012). Globally, rivers transport a total POC flux of 125-335 megatonnes of carbon per year (MtC/yr), consisting of 110-230 MtC/yr derived from the terrestrial biosphere (OC_{bio}) and 20-100 MtC/yr as rock-derived (petrogenic) organic carbon (OC_{petro}) (Galy et al., 2015; Ludwig et al., 1996). Oxidation and/or sequestration of these two organic carbon pools lead to different net effects on the atmospheric CO_2 content over geological and shorter time scales. On geological timescales (> 100,000 years), the balance between sequestration of POC_{bio} and oxidation of POC_{petro} governs the net lithosphere-atmosphere CO_2 exchange of the global organic carbon cycle (Berner, 1982; Galy et al., 2008a; Galy and Eglinton, 2011). Before entering estuaries, riverine POC including different fractional contributions goes through processes such as mineralization, aggregation, disaggregation, and sedimentation, determining its role, behavior, and fate in the aquatic ecosystem (Blair and Aller, 2012). However, these processes and the behind governing mechanisms are mostly qualitatively interpreted, quantitative information is still highly needed.

This thesis is supported (field campaigns and analytical costs) by the France-China corporated ANR (Agence nationale de la recherche) project ' Les SEDIments des grands fleuves chinois, Messagers des processus géologiques et chANgements environnementaux – SEDIMAN' (ANR-15-CE01-0012), aiming to determine the controls on the chemical and physical alteration of POC during the fluvial transfer in large rivers. A major concern is to decipher and quantify provenances of POC (POC_{bio} vs POC_{petro}). On this basis, the transport mode involving physical and chemical alteration is interpreted in detail. The mechanism governing this alteration is thus further investigated, aside from natural controls (*i.e.,* climate, geomorphology, and tectonics), anthropogenic perturbations and regulations are emphasized. Altogether, this thesis aims at better constraining the role of large rivers under coupled multi-environmental processes in the global carbon cycle.

Accordingly, the elemental and isotopic compositions of the biologically important carbon element were determined to probe the sources of POC spanning the entire fluvial transport routine in the largest Chinese rivers, with a special focus on the Huanghe (Yellow River) and on the Changjiang (Yangtze River). These rivers drain very contrasted basins in terms of geomorphology, lithology, climatic conditions, and anthropogenic pressure. The major environmental drivers (natural vs anthropogenic) regulating riverine POC metabolism, quality, and fluxes are assessed, especially the impact of anthropogenic perturbations (*e.g.,* dam-building). To achieve the research purposes, three main questions will be answered: 1) what are the dominant sources of POC in river sediments? 2) what are the main processes regulating the behavior of riverine POC? Particularly, how do hydrodynamic sorting processes impact the transport mode of POC in large Chinese rivers? 3) how and to what extent do anthropogenic activities impact the delivery of POC from the terrestrial source to the oceanic sink?

Following the detailed overview of riverine POC in **Chapter 1**, **Chapter 2** gives a detailed description of the tectonic, lithologic, geomorphic, climatic, hydrologic, and anthropogenic background of the largest Chinese rivers, with a special focus on Huanghe and Changjiang. **Chapter 2** also provides detailed information on the sampling strategy and the collected sediment samples. Analytical technics are then

detailed as well as the method used to model and estimate the transect-integrated elemental and isotopic distribution and fluxes.

Chapter 3 presents a study based on SPM samples collected over a whole channel cross-section in the Huanghe (Yellow River). This chapter presents two main emphases: 1) how riverine POC responds to the enhanced physical erosion to deeper soil horizon of loess-paleosol sequences in the Chinese Loess Plateau, 2) the determination of the transport mode of POC in this turbulent river system.

Chapter 4 carries out systematic research on the impact of dam-building on POC alteration in the source-to-sink trajectory of the Changjiang river sediments. To the first order, it provides a pristine investigation on the components and fluxes of POC in Jinshajiang, a large mountainous river of the upper Changjiang in the tectonic active region. Subsequently, an assessment was carried on the composition of riverine POC in the Changjiang River Basin after the "blocking" by newly build mega cascade reservoirs in lower Jinshajiang. Lastly, this chapter seeks to constrain the means and the scale dam-building enhances POC burial in the large fluvial system and its role in the carbon cycle over different timescales.

Chapter 5 presents an extensive compilation of POC data from global rivers, namely *Modern River Archives of Particulate Organic Carbon (MOREPOC) version 1.0*, recording the fluvial memory of SPM. Besides, with a further discussion on the climatic, geomorphic, and tectonic controls on the POC radiocarbon around the globe.

Chapter 6 summarizes the findings of this thesis and puts forward a new look into the terrestrial organic carbon and some related earth surface processes that possibly have significance for the global carbon cycle on Earth.

Synthèse en français

Depuis que la Terre est entrée dans l'Anthropocène, où les activités humaines agissent comme une force géologique comparable à la tectonique et au climat, le fonctionnement des environnements terrestres et aquatiques a connu des perturbations majeures et d'une rapidité sans précédent (Zalasiewicz et al., 2015). Les sédiments fluviaux, qui intègrent l'érosion, l'altération et les processus anthropiques à l'échelle du bassin versant, fournissent des informations essentielles pour comprendre les processus clés agissant à la surface terrestre ainsi que leur moteur.

Dans le processus de transfert de sédiments des zones source aux zones de dépôt, i.e., dans le cycle sédimentaire terrestre, les rivières jouent un rôle essentiel transportant du matériel continental sous forme de particules en suspension (SPM) et de charge dissoute des terres émergées aux marges continentales (Blair et Aller, 2012 ; Leithold et al., 2016). Associé à la charge particulaire (SPM, pour suspended particulate matter), le carbone organique terrestre est transporté sous forme de carbone organique particulaire (POC) des continents vers leur site d'enfouissement final dans les sédiments océaniques, et représente une composante principale du cycle global du carbone (Ittekkot, 1988 ; Meybeck, 1993 ; Galy et al., 2007 ; 2008a ; 2015 ; Blair et Aller, 2012). Ces informations sont présentées dans la figure 1. À l'échelle mondiale, les cours d'eau transportent un flux de POC compris entre 125 et 335 mégatonnes de carbone par an (MtC/an), dont 110 à 230 MtC/an provenant de la biosphère terrestre (OC_{bio}) et 20 à 100 MtC/an provenant de l'érosion de roches sédimentaires (OC_{petro}) (Galy et al., 2015 ; Ludwig et al., 1996). Des effets antagonistes sur la teneur en CO_2 de l'atmosphère sont attendus sur des échelles de temps géologiques et plus courtes selon le devenir de ces deux sources de carbone organique, i.e., oxydation ou séquestration. Sur des échelles de temps géologiques (> 100 000 ans), l'équilibre entre la séquestration de POC_{bio} et l'oxydation de POC_{petro} régit le sens du transfert net de CO_2 entre la lithosphère et l'atmosphère pour le cycle global du carbone organique (Berner, 1982 ; Galy et al., 2008a ; Galy et Eglinton, 2011). Avant d'arriver à l'estuaire, le POC transporté par les fleuves peut être affecté par un ensemble de processus tels que la minéralisation,

l'agrégation, la désagrégation et la sédimentation, qui vont déterminer son rôle, son comportement et son devenir dans l'écosystème aquatique (Blair et Aller, 2012). Cependant, ces processus et les mécanismes qui les régissent sont pour la plupart interprétés de manière qualitative, des informations quantitatives sont encore grandement nécessaires.

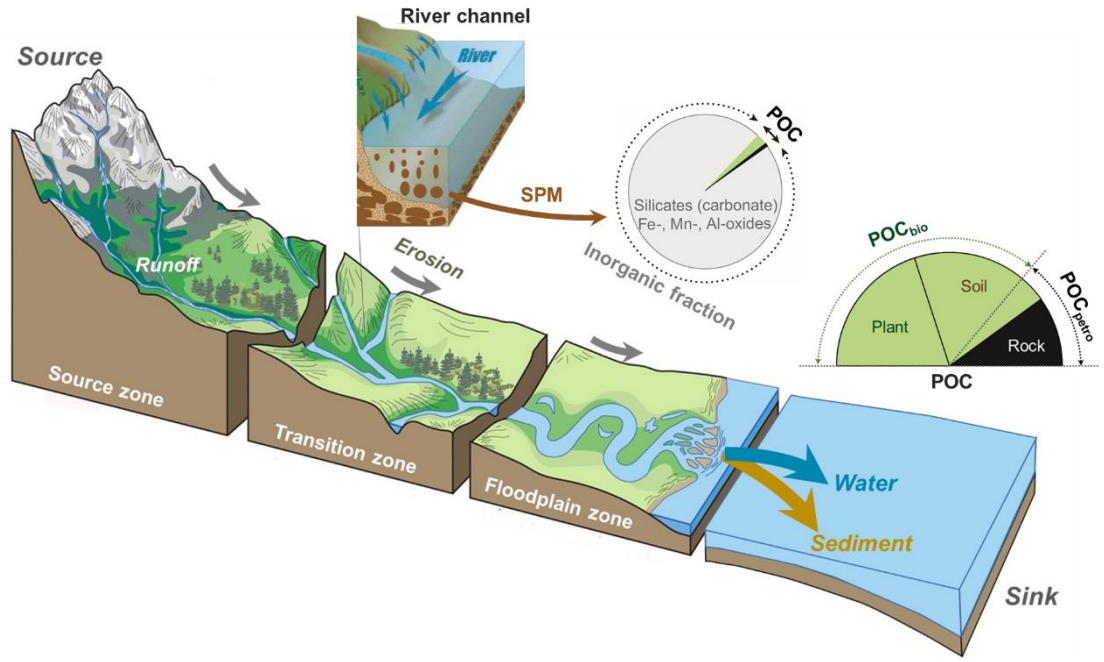

Figure 1 Le processus de la source au puits des matériaux terrestres par le transport fluvial. La figure est modifiée de Gaillardet et al., 2018, OZCAR et une figure créée par Trista L. Thornberry-Ehrlich (Colorado State University).

Ce travail de thèse ' Origine et devenir du carbone organique particulaire transporté par les plus grands fleuves de Chine ' intervient dans le cadre d'un projet ANR PRCI (Agence nationale de la recherche) France-Chine ' Les SEDIments des grands fleuves chinois, Messagers des processus géologiques et chANgements environnementaux - SEDIMAN' (ANR-15-CE01-0012), et vise à déterminer les contrôles de l'altération chimique et physique du POC pendant son transfert dans les grands fleuves. Un des enjeux majeurs est de déchiffrer et de quantifier les provenances des POC (POC $_{bio}$vs POC $_{petro}$). Sur cette base, le mode de transport impliquant une altération physique et chimique est interprété en détail. Outre les contrôles naturels (i.e., le climat, la géomorphologie et la tectonique), le rôle des perturbations anthropiques est étudié comme un mécanisme clé impactant le transport et le devenir du POC. Dans l'ensemble, cette thèse vise à mieux contraindre le rôle des multiples processus environnementaux

couplés (naturels et/ou anthropiques) sur le cycle global du carbone, par le prisme des grandes fleuves.

Dans cette optique, les compositions élémentaires et isotopiques du carbone organique particulaire ont été déterminées pour d'une part, en identifier ses origines et d'autre part, contraindre les mécanismes l'ayant affecté qualitativement et quantitativement au cours de son transport dans les fleuves. Les fleuves chinois Changjiang (fleuve Yangtze) et Huanghe (fleuve Jaune) ont été spécifiquement étudiés car ils drainent des bassins très contrastés en termes de géomorphologie, lithologie, conditions climatiques et pression anthropique (figure 1). Les principaux facteurs environnementaux (naturels ou anthropiques) qui régulent le métabolisme, la qualité et les flux de POC fluviaux sont évalués, en particulier l'impact des perturbations anthropiques, comme la construction de barrages. Pour répondre à ces questions fondamentales, nous répondrons à **trois questions principales :**

1) Quelles sont les sources dominantes de POC dans les sédiments fluviaux ?
2) Quels sont les principaux processus (notamment le tri hydrodynamique) régulant le mode de transport du POC dans les rivières chinoises ?
3) Comment et dans quelle mesure les activités anthropiques ont-elles un impact sur le transport et le devenir du POC des zones sources (surfaces continentales) au puits océanique ?

Après une présentation détaillée, dans le Chapitre 1, de nos connaissances actuelles sur l'origine et le devenir du carbone organique particulaire transporté par les grands fleuves et de son rôle dans le cycle du carbone global, le **chapitre 2** donne une description détaillée du contexte tectonique, lithologique, géomorphologique, climatique, hydrologique et anthropique des plus grands fleuves chinois, avec un accent particulier sur le Huanghe et le Changjiang. Le **chapitre 2** fournit également des informations détaillées sur la stratégie d'échantillonnage et les échantillons de sédiments collectés. Les techniques d'analyse sont ensuite détaillées ainsi que la méthode utilisée pour modéliser et estimer la distribution et les flux élémentaires et isotopiques intégrés dans les transects.

Le **chapitre 3** présente une étude basée sur des échantillons de SPM collectés sur

une section transversale complète du Huanghe (fleuve Jaune). Ce chapitre met l'accent sur deux points principaux : 1) la manière dont le POC fluvial répond à l'érosion physique accrue des horizons profonds des séquences de loess-paléosol du plateau de lœss chinois, 2) la détermination du mode de transport du POC dans ce système fluvial qui est l'un des plus turbides au monde.

Le **chapitre 4** s'attache à comprendre l'impact de la construction d'une succession de barrages le long du fleuve Changjiang sur l'altération et le devenir du POC lors de son transport. En premier lieu, ce chapitre fournit une étude détaillée et inédite des compositions et flux de POC dans le Jinshajiang, un grand fleuve montagneux drainant la région tectoniquement active du haut Changjiang. Par la suite, nous avons estimé l'impact du "blocage" de POC par les méga-réservoirs en cascade nouvellement construits dans le bas Jinshajiang sur la composition du POC fluvial dans le bassin du fleuve Changjiang.. Enfin, ce chapitre discute des nouvelles voies de séquestrations du carbone organique des fleuves mais aussi des échelles de temps sur lesquelles ces processus impactent le cycle global et régional du carbone.

Le **chapitre 5** présente une compilation exhaustive des données de POC des rivières mondiales, à savoir *Modern River Archives of Particulate Organic Carbon (MOREPOC) version 1.0*, enregistrant la mémoire élémentaire et isotopique des particules en suspension transportées par les fleuves. MOREPOC archivant 3,300 données élémentaires et isotopiques de POC dans le monde. Elle enregistre la mémoire fluviale des SPM collectés dans 229 rivières de 118 systèmes fluviaux. MOREPOC est construite pour étudier de manière globale les facteurs environnementaux majeurs pouvant contrôler l'export de POC et sa signature isotopique. Par ailleurs, nous discutons de façon approfondie les contrôles climatiques, géomorphologiques et tectoniques sur le composition isotopique (stable et radioactif) du POC à l'échelle mondiale.

Le **chapitre 6** résume les résultats de cette thèse et propose des perspectives d'étude du carbone organique et de certains processus connexes opérant à la surface de la Terre qui ont potentiellement une importance pour notre compréhension du cycle global du carbone sur Terre.

Chapter 1

State of the Art

1. The Earth's long-term carbon cycle

The long-term carbon cycle on Earth operates over millions of years and involves the exchange of carbon between deep and surface reservoirs, namely the mantle, the crust, the ocean, the atmosphere, and the biosphere (Berner, 1994, 1999, 2003; Berner and Berner, 2012). Surface reservoirs together have a carbon mass of over 78×10^9 MtC, and the vast majority is essentially found in rock reservoirs in the form of either inorganic carbon (mass: 65.3×10^9 MtC) or organic carbon (12.5×10^9 MtC) with a storage ratio of approximately 5:1 (Figure 1) (Li, 2000; Holland, 1978; Petsch, 2014). The pre-industrial atmosphere comprises 590×10^3 MtC (Sundquist, 1993), while the biosphere has an organic carbon mass of over $2{,}300 \times 10^3$ MtC (Sundquist, 1993; Tarnocai et al., 2009). The atmosphere is a relatively small carbon reservoir compared to the biosphere (including soils and plants) and ocean (mass: $39{,}000 \times 10^3$ MtC, Sundquist, 1993), much smaller when compared to the lithosphere. Therefore, even a very small fraction of carbon released from the lithosphere would drive large variations in atmospheric CO_2 content. Multiple Earth surface processes together influence the atmospheric CO_2 dynamics over geologic timescales (>100,000 years), these carbon exchange processes can be separated into two primary cycles based on the dominant cycling and reacting material. One is dominated by the oxidation, erosion, and sedimentation of organic carbon (organic carbon cycle), and the other is centered on the chemical weathering of rocks and carbonate deposition that control inorganic carbon exchange fluxes (inorganic carbon cycle). Both sub-cycles constitute geologic reactions and transfers, exerting sources or sinks relatively to the atmospheric CO_2.

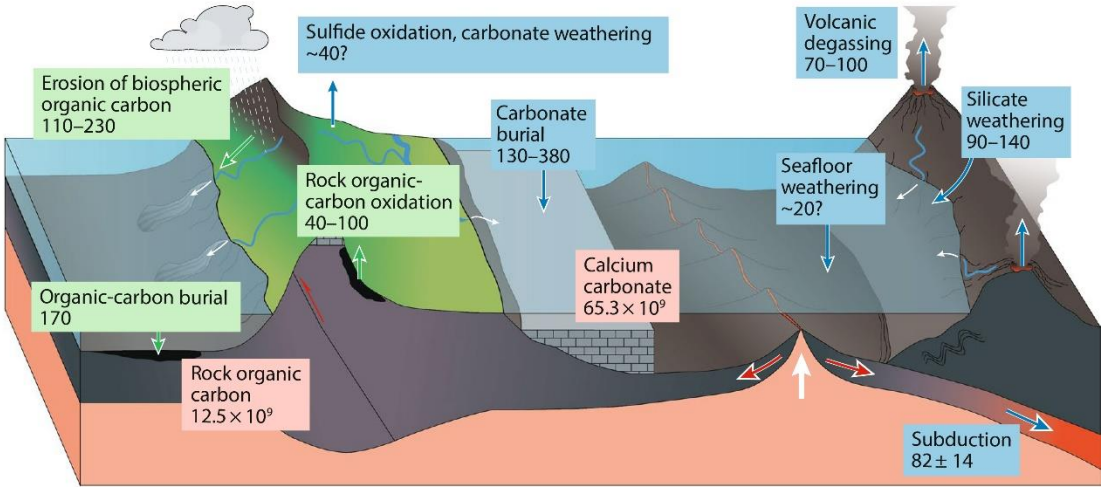

Fig.1 The geological carbon cycle and carbon transfer between the atmosphere and the lithosphere (rocks). The red labels are the storage of organic carbon and calcium carbonate in the Earth's crust. The blue labels are the traditional view of major processes in the long-term carbon cycle concerning mainly inorganic carbon; the green labels represent organic carbon transfers in the long-term carbon cycle supported by recent advances. Numbers are provided in megatonnes of carbon per year (MtC/yr) for carbon fluxes and MtC for carbon stocks. Figure from Hilton and West (2020).

1.1 The inorganic carbon cycle

Volcanism (Kerrick et al., 1995; Robock, 2000), metamorphic outgassing (Kerrick et al., 1998; Becker et al., 2008; Evans et al., 2008), subduction of sedimentary and oceanic crust (Plank and Manning, 2019), and rock weathering followed by carbonate deposition (Walker et al., 1981) are well recognized as the geologic processes regulating the inorganic carbon cycle at geologic timescales. It is estimated that volcanism emits CO_2 to the atmosphere at a rate of 70-100 MtC/yr (Plank and Manning, 2019; Kerrick et al., 1995; Robock, 2000). Subduction brings the same magnitude of carbon (ca. 82 MtC/yr) into the deeper crust, the quantity of metamorphic outgassing is poorly constrained but possibly has a similar magnitude (Becker et al., 2008; Hilton and West, 2020). Rock weathering mainly refers to silicate weathering because carbonate weathering overall has no net effect on the long-term regulation of atmospheric CO_2 (Berner and Berner, 2012). Silicate minerals, as well as carbonate minerals, break down during the reaction with carbonic acid (H_2CO_3) produced by the dissolution of atmospheric/soil CO_2 in surface waters (Reaction 1). As a result, rivers deliver cations and bicarbonate ions (HCO_3^-) produced by continental weathering (*e.g.*,

Meybeck, 1987; Gaillardet et al., 1999) into the oceans where carbonate precipitation happens (Reaction 2).

$$2CO_2 + H_2O + CaSiO_3 \rightarrow Ca^{2+} \text{ the } + 2HCO_3^- + SiO_2 \quad (1)$$

$$Ca^{2+} + 2HCO_3^- \rightarrow CaCO_3 + CO_2 + H_2O \quad (2)$$

Carbonate precipitation leads to long-term sequestration of atmospheric CO_2 but also to a returning flux of CO_2 back to the atmosphere. While carbonate weathering followed by carbonate precipitation in the ocean eventually returns an equal amount of CO_2 than the one consumed on land (*i.e.*, no net effect), silicate weathering only returns half of the consumed CO_2 on land, therefore representing a net sink. Silicate weathering as a long-term CO_2 sink is a key process that extensively occurs on Earth as proved by the widespread presence of carbonate rocks at the Earth's surface (Ébelmen, 1845; Urey, 1952; Holland et al., 1986; Berner, 2012). This process is estimated to consume up to 140 MtC/yr on land, which eventually results in a long-term atmospheric CO_2 drawdown of 70 MtC/yr (Gaillardet et al., 1999). A recent report suggests that silicate weathering fluxes would be overestimated by 12 to 28% by excluding the non-silicate origin from the dissolved load (Tipper et al., 2021). Recently, an important process, namely sulfide oxidation, has been demonstrated to act as a long-term carbon source to the atmosphere when coupled with carbonate weathering (Calmels et al., 2007; Torres et al., 2014), which is estimated to release ca. 40 MtC/yr from the lithosphere to the atmosphere (Hilton and West, 2020).

1.2 The organic carbon cycle

The organic carbon cycle comprises processes concerning the burial and oxidation of different components of terrestrial organic carbon. The atmospheric CO_2 is fixed by the biomass (C_3 and C_4 plants) via photosynthesis (Reaction 3, CH_2O represents organic carbon in biomass) and returns to the atmosphere through respiration (Reaction 4).

$$CO_2 + H_2O \xrightarrow{\text{photosynthesis}} CH_2O + O_2 \quad (3)$$

$$CH_2O + O_2 \xrightarrow{\text{respiration}} CO_2 + H_2O \quad (4)$$

As referred to in the **General Introduction** of the thesis, OC_{bio} and OC_{petro} are the two major constituents of terrestrial organic carbon in a global carbon cycle perspective (Galy et al., 2007; Galy et al., 2015; Leithold et al., 2006). Oxidative degradation of OC_{bio} produces CO_2 back to the atmosphere over the present to millennial timescales

depending on the residence time of OC_{bio}, only representing a short-term atmospheric CO_2 source that does not enter the geologic carbon cycle (Galy and Eglinton, 2011). However, the recently-photosynthesized organic carbon (OC_{bio}) that survives from mineralization along the pathway from source to sink is eventually buried in ocean sediments and transformed into a solid-phase, macromolecular organic matter termed kerogen through diagenesis and catagenesis, representing a long-term atmospheric CO_2 sink (Berner, 1982; Galy et al., 2007). Globally, rivers deliver approximately 200 MtC/yr in the form of POC to the ocean, the majority is OC_{bio}, representing ~80% of the annual POC flux (Galy et al., 2015; Ludwig et al., 1996). Even though the riverine OC_{bio} flux only represents less than 0.2% of the global net primary production, the quantity that can be eventually buried and preserved in the oceanic sediments is of the same magnitude as the net flux of CO_2 consumed by silicate weathering. This process continuously removes terrestrial OC_{bio} that has fixed atmospheric CO_2 and avoids respiration processes. In Bengal fan, the net burial of OC during Himalayan sediment deposition is estimated to be 2–3 times the amount of CO_2 consumed by chemical weathering of silicate in the Himalayas (France-Lanord and Derry, 1997). Globally, 55%–80% of the exported terrestrial POC is remineralized along the continental margins (Burdige, 2005; 2007). Applying the global mean remineralization rate of an equivalent 70% for OC_{bio}, then the estimated burial of terrestrial OC_{bio} is up to ca. 70 MtC/yr. The burial of terrestrial and marine POC is estimated to be ca. 170 MtC/yr due to the high remineralization rate (Hedge and Keil, 1995; Smith et al., 2015). In this total burial flux, OC_{petro} represents a significant fraction as well. However, the burial of OC_{petro} only corresponds to a spatial redistribution (from land to ocean) of OC already present in rocks and has thus no net impact on the carbon cycle. In contrast, if OC_{petro} is oxidized along its fluvial (*e.g.*, floodplains) and marine pathway or directly in rocks at the continental surface (*e.g.*, in shales), it could act as positive feedback to the atmospheric CO_2 over geologic timescales (Petsch, 2014; Derry, 2014; Hilton et al., 2014; Soulet et al., 2018, 2021; Horan et al., 2019; Bouchez et al., 2010; Hemingway et al., 2019). This CO_2 source flux is estimated at 40-100 MtC/yr (Petsch, 2014). The balance between the weathering of OC_{petro} and the burial of OC_{bio} within ocean sediments partly modulates atmospheric CO_2 and O_2 over geologic timescales (Galy et al., 2007).

Overall, different geologic processes yield CO_2 fluxes with nearly similar

magnitude, and it is reported that river catchment could be either a net source or a net sink of atmospheric CO_2 over geological timescales. Thus it is highly needed to accurately calculate the corresponding fluxes to understand what role the fluvial system plays in the geologic carbon cycle. In this thesis, one of the focuses is on the fluxes of riverine POC and its compositional fractions in the largest rivers in China.

1.3 Net rock-atmosphere CO_2 exchange of fluvial systems

For the large river systems in the world, the Mackenzie River Basin is the only one for which the net rock-atmosphere CO_2 exchanges have been determined, including organic and inorganic carbon components (Horan et al., 2019). It reveals that the Mackenzie river basin acts as an overall carbon sink of atmospheric CO_2 over geologic timescales (Horan et al., 2019), although some sub-catchments such as the Arctic Red and Peel rivers are net sources of CO_2 mainly because of high rates of sulfide oxidation (Calmels et al., 2007; Horan et al., 2019). Regarding the organic carbon cycle at the catchment scale, small mountainous rivers in the western Southern Alps of New Zealand show either CO_2 emissions by oxidation of OC_{petro} greatly exceeding sequestrated CO_2 through OC_{bio} burial (*e.g.*, Waiho and Haast) or OC_{bio} burial larger than OC_{petro} oxidation (*e.g.*, Hokitika and Whataroa) (Horan et al., 2017; Hilton and West, 2020). It is therefore fundamental to understand the controls and quantify rock-atmosphere CO_2 exchanges processes to evaluate the overall net carbon balance in a river basin. Calculations for the net balance of carbon cycles are as follows (Horan et al., 2019):

The net balance of the organic carbon cycle: $J_{OC} = J_{OCpetro\text{-}ox} - J_{OCbio\text{-}burial}$

The net balance of the inorganic carbon cycle: $J_{IC} = J_{Carb\text{-}sulf} - J_{Silicate}$

The net balance of the overall Earth's carbon cycle: $J_{net} = J_{OC} + J_{IC}$

where the balance between CO_2 emissions from OC_{petro} oxidation ($J_{OCpetro\text{-}ox}$) and CO_2 sequestration by OC_{bio} burial ($J_{OCbio\text{-}burial}$) determines whether the organic carbon cycle at the catchment scale is a net atmospheric CO_2 source or sink at geologic time scale, and the balance between CO_2 emission from sulfide oxidation coupled to carbonate weathering ($J_{Carb\text{-}sulf}$) and CO_2 sequestration by silicate weathering ($J_{Silicate}$) corresponds to the net exchange flux of inorganic carbon between rocks and the atmosphere. The total net rock-atmosphere carbon flux (J_{net}) can be calculated by summing the net balances of organic (J_{OC}) and inorganic (J_{IC}) carbon cycles. A negative value will represent a net atmospheric CO_2 sink while a positive value will mean that the river

basin acts as a net source of CO_2 to the atmosphere (Horan et al., 2019; Hilton and West, 2020). In this thesis, fluxes of riverine POC and its source fractions (biospheric [POC_{bio}] vs. petrogenic [POC_{petro}]) in the largest Chinese rivers are calculated to better constrain the impact of anthropogenic activities on the geologic carbon cycle, especially on the natural and long-term fluxes of POC.

2. Riverine particulate organic carbon delivery in large river systems

Global rivers deliver about 19×10^3 Mt/yr of terrestrial solid material to the coastal ocean, which corresponds to an average global sediment yield of 190 t/km^2/yr for exorheic continental areas (Figure 2, Milliman and Farnsworth, 2011). Those riverine sediments carry ca. 200 Mt/yr of POC (Galy et al., 2015; Ludwig et al., 1996). Riverine POC originates from numerous terrestrial OC sources having a wide range of signatures, ages, and reactivities, undergoing multiple remobilizations and alteration processes at almost all temporal and spatial scales (Hedge and Keil, 1995; Blair and Aller, 2012; Leithold et al., 2016). Rivers in Southern Asia and Oceania contribute over 65% of the global sediment input to the ocean. The four largest rivers in China (*i.e.*, Changjiang, Huanghe, Heilongjiang, and Zhujiang) account for 43% of the total sediment delivery by Chinese rivers that is ca. 2,240 Mt/yr (Figure 2B) (Milliman and Farnsworth, 2011). POC components (POC_{bio} and POC_{petro}) and yields in global fluvial systems are greatly influenced by physical erosion (Galy et al., 2015; Hilton, 2017), which is itself mostly controlled by tectonic and climatic forcing (Whittaker et al., 2010; Coulthard and Wiel, 2013). Intense physical erosion promotes high POC yields and eventually more efficient sequestration of both POC_{bio} and POC_{petro} in sedimentary basins in response to higher sedimentation rates (Hilton and West, 2020). Large Chinese rivers span a large variety of climatic, tectonic, topographic, and lithologic contexts from steep mountainous areas in the upper source regions to vastly distributed plains in the lower reaches. All put together, the large Chinese river basins offer contrasted settings that may help to understand the controls on POC export and represent massive sediment suppliers to the ocean suggesting that they could play a significant role in the global carbon cycle.

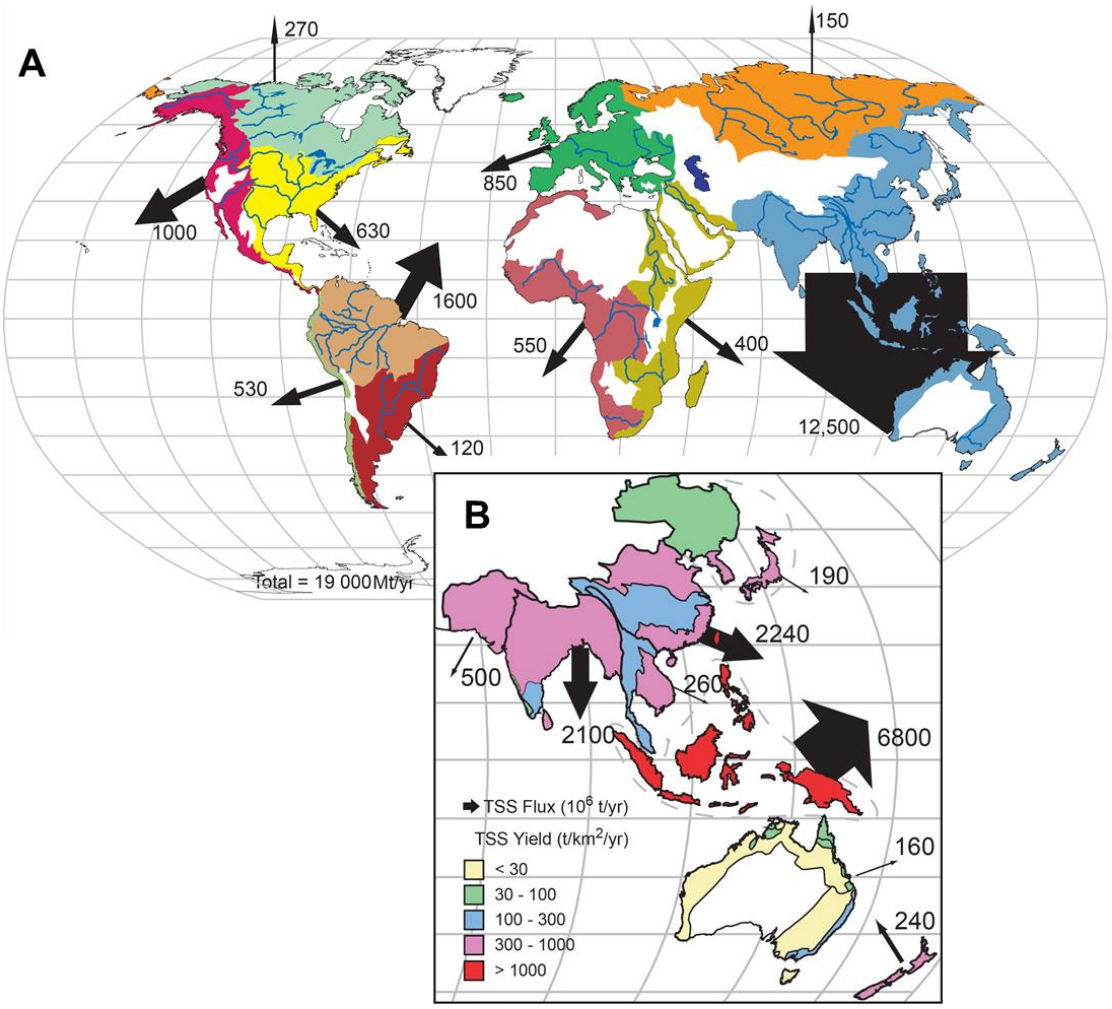

Fig. 2 Fluvial sediment load to the coastal ocean. A) Annual global fluvial sediment load; B) annual regional fluvial sediment load and yield from Austral-Asian rivers. Global rivers export sediment in a flux of 19,000 Mt/yr to the coastal ocean, the largest rivers in China (e.g., Changjiang, Huanghe, Zhujiang) contribute a substantial fraction to the global export budget. Figure modified from Milliman and Farnsworth, (2011).

2.1 POC Provenances

The balance between oxidation of OC_{petro} (kerogen) derived from uplifted and weathered sedimentary rocks and burial of OC_{bio} in the ocean governs the organic part of the global carbon cycle at geological timescale, regulating CO_2 and O_2 inventories in the atmosphere as well as climate (Berner, 1982; Galy et al., 2008a; Galy and Eglinton, 2011). However, the biospheric and petrogenic fractions of OC from different sources have varying reactivity. Carbon atoms are usually of high-bond strength in OC_{petro}, leading to its intrinsic recalcitrant nature (it already survives a sedimentary cycle), while the low-energy bonded OC_{bio} is comparatively more labile. OC_{petro} is thus

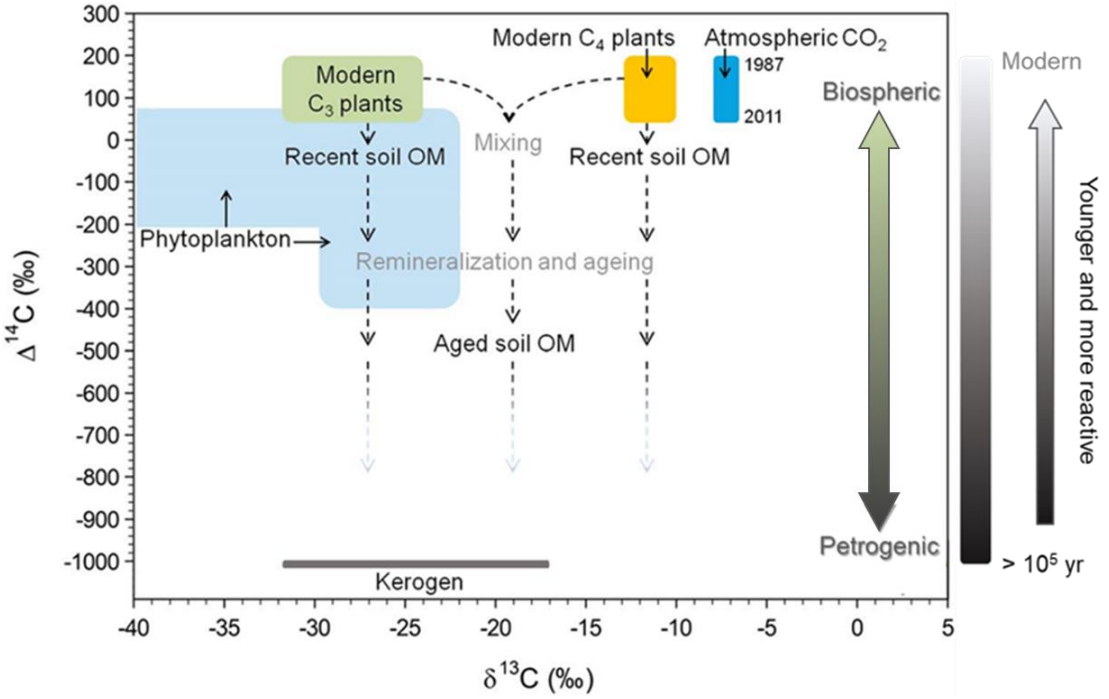

Fig. 3 Major sources of fluvial POC using a mixing space of dual carbon isotopes ($\delta^{13}C$ and $\Delta^{14}C$). Different color bars represent different organic carbon pools, the two-way arrow indicates that POC with high $\Delta^{14}C$ values tends to be preferentially biospheric sourced and POC with low $\Delta^{14}C$ values tends to be preferentially petrogenic sourced. The black-to-grey spectrum indicates the intrinsic reactivity of organic carbon. Figure modified from Marwick et al. (2015) and Leithold et al. (2016).

more resistant to remineralization preventing it from reentry into the active carbon cycle (Figure 3) (Hedge and Keil., 1995; Mayorga et al., 2005; Leithold et al., 2016; Hemingway et al., 2019). In the biospheric OC pool, modern to aged OC_{bio} that reside in continental environments also has variable intrinsic reactivity as reflected by its thermal stability (Rosenheim and Galy, 2012; Hemingway et al., 2019). It is widely observed that POC fractions coming from mountainous upstream regions would be partially replaced by downstream terrestrial OC contributions (Mayorga et al., 2005; Blair and Aller, 2012). Understanding the dynamics of riverine POC along the fluvial system provides information on which POC enters the marine burial environment. As shown in Figure 3, OC_{bio} generally includes two OC components: the primary production of modern C_3 and C_4 plants; recent to aged soil OC (mainly a mixture of C_3 and C_4 plants that undergoes aging and mineralization in soils) (Blair et al., 2010). In addition, aquatic autochthonous phytoplankton could contribute to riverine POC but,

apparently to a minor extent (Cole et al., 2007; Marwick et al., 2015). Overall, the organic components of fluvial SPM can have widely contrasted molecular, isotopic, and elemental compositions (*e.g.*, Freymond et al., 2018; Yu et al., 2019). Regarding the substantial amount of riverine POC that is delivered to the coastal ocean, it is essential to unravel the various POC fractions to better constrain how solid organic carbon dynamics at catchment scale may impact regional and global biogeochemical cycles at different timescales.

Two naturally occurring stable isotopes of carbon, ^{12}C (98.89% of the total mass) and ^{13}C (1.11% of the total mass), are unevenly distributed among the different carbon pools on Earth because various physical, chemical, and biological processes generate isotope partitioning, namely isotopic fractionation. The isotopic composition ($\delta^{13}C$) of atmospheric CO_2 is around −8 to −6.5‰ (Figure 3), whereas that of plant and algal tissues is depleted in ^{13}C (relative to atmospheric CO_2), owing to the preferential uptake of ^{12}C during photosynthesis. The globally dominant C_3 pathway results in biomass $\delta^{13}C$ values ranging from −32‰ to −24‰, while the C_4 pathway results in biomass having $\delta^{13}C$ signature (in ‰) ranging from −13‰ to −10‰ (Cerling et al., 1997). Soil OC (SOC) is composed of a mixture of OC from C_3 and C_4 pathway biomass that undergoes mineralization and aging. As confirmed by molecular analysis, the various biospheric fractions that contribute to fluvial POC_{bio} have ages spanning from modern to multi-millennia (Galy and Eglinton, 2011), which is largely dependent on the residence time of OC in soils within the catchment (Eglinton et al., 2021). Actual kerogen has been fixed by photosynthetic organisms in the geologic past (typically multi-million years ago), and then buried in sediments on land or in the ocean, and eventually lithified along with mineral grains in sedimentary rocks. Thus, $\delta^{13}C$ signatures of kerogen range from −32‰ to −17‰ which could overlap with ^{13}C signals of soil OC (Whiticar, 1996). The above information highlights the difficulty in differentiating varying OC sources based on ^{13}C only. As long as the POC_{bio} pool has an age <50,000 years, the radiocarbon composition of POC provides unique information on age, residence time, and fractional contribution of POC pools as well as on potential recycling in the different carbon reservoirs (atmosphere, lithosphere, and biosphere). Radiocarbon atoms are produced when protons knocked loose by cosmic ray impacts encounter the nuclei of atmospheric nitrogen atoms, the content of atmospheric radiocarbon significantly increased during the early bomb period from the

mid-1950s to the late 1960s due to nuclear tests (Hua et al., 2013). Thus, OC of modern biomass is enriched in ^{14}C ($\Delta^{14}C$ in ‰, which can be expressed as fraction modern, F_m) and kerogen is devoid of ^{14}C ($\Delta^{14}C$=−1000‰ and F_m=0). Recycled kerogen is termed ^{14}C-dead (see detail in Chapter 2). OC that resides in soils has an intermediate ^{14}C composition. Aged POC_{bio} signatures could be compromised by bomb ^{14}C contribution, which needs special attention in provenance interpretation (Hemingway et al., 2017). Scholars also have adopted ^{14}C analysis on specific size fractions and particle separates (Mayorga et al., 2005; Bouchez et al., 2014); compound-specific radiocarbon measurements of terrestrial biomarkers such as fatty acids and lignin phenols (Galy and Eglinton, 2011; Freymond et al., 2018); ramped pyrolysis thermal-stability dependent ^{14}C measurement (Rosenheim and Galy, 2012; Hemingway et al., 2018; 2019). There are widely adopted methods to estimate the contributions of different sources to the riverine POC based on isotopic analysis on bulk OC. Assuming that POC_{petro} is radiocarbon-dead and average POC_{bio} is still radiocarbon-active, a binary mixing model (see detail in Chapter 4) between POC content and modern OC content (Fm times POC content) can be built based on linear regression to quantitatively estimate the fractional contents of POC_{petro} and POC_{bio}, and the average F_m of POC_{bio} (Galy et al., 2008a; 2015). The use of isotopic mass balance can also be a good approach to decipher more OC provenances by assigning each end-member appropriate dual carbon isotope values (see detail in Chapters 3 and 4). This method needs to constrain the average isotopic values of each end-member, which could be problematic, especially at the scale of large river systems. This approach can yield relatively large uncertainties if we lack representative data. Consequently, careful identification of the end-members is needed and a posteriori validation of the calculated results is recommended.

Anthropogenic activities have been impacting river systems for centuries, and so natural routing of terrestrial OC mobilization and natural in-channel POC transfer. Human interference could affect the relative abundance of source fractions in fluvial POC through enhancing or prohibiting specific OC fractions into the fluvial system: 1) land-use change would alter OC sources and fluxes mobilized into fluvial systems; 2) anthropogenic engineering constructions, such as dam-building would interrupt the transfer downstream of some SPM and POC fraction and favor the production of autochthonous OC; 3) human-induced climate warming, would help the release of aged soil OC in permafrost regions and potentially favor the oxidation of OC. Land-use

change induced by *e.g.*, increased agriculture, deforestation, and mining influence OC formation in its original residing environment and enhanced physical erosion within the catchment (Moore et al., 2013). The latter may facilitate the erosion of deeper soil horizons with more degraded and aged OC_{bio} or of fragmented clastic rocks resulting in inputs of ^{14}C-dead OC_{petro} (Wilmshurst et al., 2008). On the contrary, afforestation, as well as artificial levees and bank stabilization will weaken the link between terrestrial OC pool and aquatic environment, thus reducing the quantity of terrestrial OC entering river channels as observed in the Mississippi (Shen et al., 2021; Meade and Moody, 2010). Anthropogenic engineering constructions have been seriously influencing the natural OC exchange between terrestrial and aquatic environments and in-channel transport (Maavara et al., 2017, Shen et al., 2021). Dam-building, on the one hand, can enhance the input of terrestrial materials by inducing mass wasting events such as landslides – *e.g.*, the Three Gorges Dam in Changjiang River Basin has induced many landslides (Li et al., 2013) – and, on the other hand, creates large low-velocity areas which favor the sedimentation of coarse SPM fractions and the production of autochthonous organic matter. The latter input in reservoirs has almost doubled from 1970 to 2000 globally due to the increased catchment area upstream of dams (Cole et al., 2007; Marwick et al., 2015; Maavara et al., 2017). Bank stabilization in the lower Mississippi has led to the drastic reduction of river-floodplain sediment exchange by ca. 90%, modulating the riverine POC composition by effectively decreasing its OC component loss and enhancing the delivery of younger POC to marine sediments (Shen et al., 2021). Since the Second Industrial Revolution, accelerated and intensified emissions of greenhouse gases led to global warming, permafrost regions are sensitive to temperature change, resulting in the release of aged soil OC into rivers such as in Circum-Arctic large rivers (Vonk et al., 2013; Wild et al., 2019). This mechanism could be at play in the source regions of the Changjiang and Huanghe as well as in the Heilongjiang basin that includes vast permafrost-dominated areas. The Anthropocene has experienced so many environmental changes, sometimes antagonist in terms of POC sources and transport, that further research is highly needed, especially in large Chinese river systems.

2.2 Transport behavior of fluvial POC

Understanding the fluvial transport mode of detrital sediments and their controls advances the diagnosis of riverine organic and inorganic chemical compositions and

fluxes. It is therefore crucial to address the role of continental erosion in the global carbon cycle (Galy et al., 2008b; Bouchez et al., 2011a, b; Hilton and West, 2020). Transport behavior of fluvial POC (*i.e.*, composition, metabolism, and fluxes) is expected to vary from one river system to another depending on geoenvironmental, climatic, and anthropogenic conditions. In addition, the transport behavior of POC can change along the river channel in response to heterogeneous river dynamics in the different sub-catchments of a river basin. Globally, POC shows a general depleting trend of both content and radiocarbon activity with increasing turbidity (suspended sediment load), indicating a dilution by OC-poor materials of older ages from deeper soil horizons and/or source rocks (Ludwig et al., 1996; Marwick et al., 2015; Leithold et al., 2016). Wet, steep, short mountainous rivers at active continental margins present a transport mode of high sediment load and low POC abundancy, *e.g.*, rivers in Taiwan and New Zealand (Blair et al., 2010; Hilton, 2017), while in low-gradient long rivers, the transport mode is reverse in terms of sediment load and POC content, *e.g.*, Pan-Arctic large rivers (Lena, Yenisey, and Ob', etc.) and African rivers (Congo, Zambezi, and Tana, etc.) (Vonk et al., 2013; Marwick et al., 2015).

Three major properties of SPM load exert controls on POC loading of fluvial delivery: 1) the specific area of mineral particles (Mayer, 1994; Hedge and Keil, 1995; Blair and Aller, 2012); 2) the particle size (Galy et al., 2008b; Bouchez et al., 2014; Yu et al., 2019); 3) the mineralogy (Ransom et al., 1998; Hemingway et al., 2019). Even though earlier studies proposed that the specific surface area exerts a dominant control over the POC loading (Hedge and Keil, 1995; Hedge, 1997; Mayer, 1994), Galy et al. (2008b) made a debate and concluded that hydrodynamic-induced sorting processes determine sediment properties in the fluvial transport, exerting a primary control on POC loading in the Ganges-Brahmaputra river system for instance. The mineralogical, chemical and isotopic compositions of sediments are particle-size dependent, and the hydrodynamic sorting would redistribute particles of different sizes within the water column (Galy et al., 2008b; Garzanti et al., 2011; Bouchez et al., 2011a). This idea is later examined by some recent studies in some global significant large river systems, such as the Amazon (Bouchez et al., 2011a; 2014) and the Mackenzie (Hilton et al., 2015). To understand the particle size effect of sediments on POC loading, the Al/Si ratio is widely accepted as an efficient proxy to infer particle sizes (Galy et al., 2008b; Bouchez et al., 2011a; 2014). The slope of the Al/Si ratio versus the POC content of

sediments can be used to constrain the POC loading at a given location (See the global compilation in Chapter 5). The mineralogy and particle size of sediments are generally not totally independent of each other, coarse particles tend to be quartz-rich (low Al/Si ratios) and fine particles tend to be clay-rich (high Al/Si ratios) (Galy et al., 2008b). POC contents are usually positively correlated with proportions of fine-grained fractions (Keil et al., 1997; Galy et al., 2008b; Martin et al., 2013), indicating POC is either abundant in fine particles due to the low density coupled with hydrodynamics or there is an association with minerals through aggregation or encapsulation. In addition, organo-mineral aggregates are preferentially formed from clays, suggesting the larger abundance of POC in fine fractions of fluvial sediments (Galy et al., 2008b; Bouchez et al., 2014; Hilton et al., 2015). The manually separated size fractions of sediments allow some scholars to access the impact of particle size on POC loading in the Yellow River, the results are consistent with the mechanism afore-described (Yu et al., 2019; Ge et al., 2020). Although the community agrees on the sorting effect in the river channel, whether the mechanism behind sorting determines the sediment characteristics and controls POC loading needs to be further explored.

Hydrodynamic segregation processes will be investigated in detail in this thesis. In general, coarse-grained sediments that are enriched in quartz are preferentially delivered to the river bottom due to high density, while fine-grained sediments, relatively clay-rich, are usually transported near the surface. In this way, SPM concentration usually shows an increasing trend with depth. It is widely observed that POC contents and radiocarbon activities in SPM generally show depleting trends with water depth in large river systems (Galy et al., 2007; 2015; Bouchez et al., 2014; Hilton et al., 2015). The heterogeneity (both vertically and laterally in a cross-section) of SPM concentration and the associated POC nature must be taken into account when calculating corresponding fluxes and overall POC compositions. The sorting effect is generally very pronounced with vertical depth profiles, especially in low-gradient systems or during low-discharge events (Blair and Aller, 2012). This also suggests differences in sediment transport behaviors between upper mountainous regions and downstream plain areas which are driven by contrasted geomorphic, climatic, and tectonic conditions. However, some studies on large river systems report relatively weak vertical sorting effect, such as for the Danube that shows a relative homogeneity for SPM concentration and POC characteristics (elemental and isotopic compositions

of bulk and molecular POC) with depth (Freymond et al., 2018) or for the Amazon at Madeira that exhibits invariant POC contents and stable carbon isotope ^{13}C compositions with depth (Bouchez et al., 2014). Systematic vertical sampling is thus highly necessary to access SPM and POC heterogeneities in large rivers as each river system will have its transport behavior.

Lateral heterogeneity of POC transport needs to be considered aside from the vertical heterogeneity. Significant physical and chemical heterogeneity of SPM and POC have been observed laterally in river cross-sections, such as in the Amazon at Obidos (Bouchez et al., 2014), in the Salween at Hpa-An, and in the Irrawaddy at Pyay (Baronas et al., 2020). This phenomenon might be owing to the complex hydrodynamic and sediment carrying capacity in the channel (Bouchez et al., 2014) but still lacks clear explanations. Erosion to river flanks could instantaneously contribute external materials to near-bank transport thus affecting the lateral variability (See detail in Chapter 3). However, this lateral pattern can be very weak and is also reported in some cases (Bouchez et al., 2014; Freymond et al., 2014; Baronas et al., 2020). Despite extensive literature focusing on the composition of riverine POC in the largest Chinese rivers, studies mostly rely on SPM and POC collected at the surface or middle depth of channels (*e.g.*, Bianchi et al., 2007; Bouillon et al., 2012; Ellis et al., 2012; Ge et al., 2020), assuming homogeneous distribution in the water column both vertically and laterally. These studies failed to access the full range of particle size and POC components in rivers, resulting in less representative estimates of fluxes and POC sources. If POC transport follows the regular pattern of a preferential high abundance of POC in SPM delivered at channel-surface, the overall bulk POC load could be overestimated in most cases, so does the flux of POC_{bio}. Analyzing the transport behavior of sediments in both vertical and lateral directions is tedious but remains one of the most efficient ways to explore and explicit the mechanism behind POC transport mode.

Furthermore, large Chinese rivers are experiencing varied (and increasing) human pressure, meaning that the natural transport of SPM has been greatly perturbated with a dramatic decrease in total suspended load exported after the dam-building (Milliman and Farnsworth, 2011). Taking dam-building as an example, substantial sediments are retained upstream of dams owing to the slowing-down water velocity and the anthropogenic blocking-up of SPM to rivers, resulting in a diluted selective transport

of sediments downstream which alters riverine POC load. The scale and the way that the sediment transport in these large rivers responds to the anthropogenic perturbation is a key problem that needs to be investigated.

2.3 Fate of riverine POC

Understanding the fate of riverine POC in the ocean is fundamental to quantifying its role in the Earth's geologic carbon cycle (Berner, 1982). Key net effects of riverine POC_{bio} burial and POC_{petro} oxidation within both the terrestrial source and marine sink regions to atmospheric CO_2 are reviewed in Section 1.2.2. As shown in Figure 4, whether the riverine POC could be efficiently preserved depends on its intrinsic recalcitrance (*e.g.*, molecular compounds and mineral matrix) and the series of supply-reaction transport mechanisms (Blair and Aller, 2012). Broadly speaking, the preservation rate of terrestrial POC is systematically contrasted between drainage basins delivering SPM at passive- and active- continental margins. The former typically deliver POC dominated by biospheric fractions derived from modern biomass and aged soil to the continental boundaries, while the latter is generally characteristic of most small mountainous rivers (SMRs) exporting higher petrogenic fraction in fluvial POC (Blair and Aller, 2012; Blair et al., 2003; Hilton et al., 2011; Galy et al., 2015). SMRs in active mountain belts usually have high physical erosion rates. In this context, steep terrains and short pathways lead to fast sediment transfer into the ocean and, the high sediment accumulation rate and limited oxygen exposure together favor the efficient burial of terrestrial POC (Blair and Aller, 2012; Burdige, 2005). Concerning large river systems, most of them deliver POC that is eventually buried with a low preservation efficiency (20%-30%) due to the prolonged exposure time to oxygen in refluxing deltaic fluidized muds, such as the Amazon, Mississippi, Changjiang, Zhujiang (Aller and Blair, 2006; Blair and Aller, 2012; Hou et al., 2020). However, some large river systems at passive margins can have very high terrestrial POC preservation of 70%-100%, because of fast burial at high sediment accumulation rates (Galy et al., 2007; Hou et al., 2020). On average, it is estimated that ~70% of terrestrial POC are lost in the marine "incinerator" before its sequestration in sediments, the "survived" fraction in sediments is mainly preserved through selectivity and protection (Burdige, 2005; Hedge and Keil, 1995; Mayer et al., 1994). Some OC fractions become strongly bound to minerals during aging in the terrestrial environment, in turn, mineral interaction promotes OC preservation (Hemingway et al., 2019). For example, 13%-30% of the

OC in marine sediments is directly bound to reactive iron phases (Hedges and Keil, 1995; Lalonde et al., 2012), and the secondary clay mineral smectite favors OC sequestration (Kennedy et al., 2011; Blattmann et al., 2019). Large river systems are usually extended from mountainous/upland source regions to the subsequent lowlands until final transfer to oceans. Even though mountainous regions might only cover a small proportion of the whole river basin, it could contribute a dominant fraction of the total sediment load of the entire fluvial system, associated with a substantial amount of POC (Milliman and Farnsworth, 2011; Hilton, 2017). Dam-building in mountainous regions could function as a temporal "active margin", its POC preservation could be way higher than if SPM were exported to the passive margin in a free-flow condition. Human-induced regulation on transfer and burial of riverine POC is a globally significant mechanism and its role in the carbon cycle over different timescales requires careful consideration.

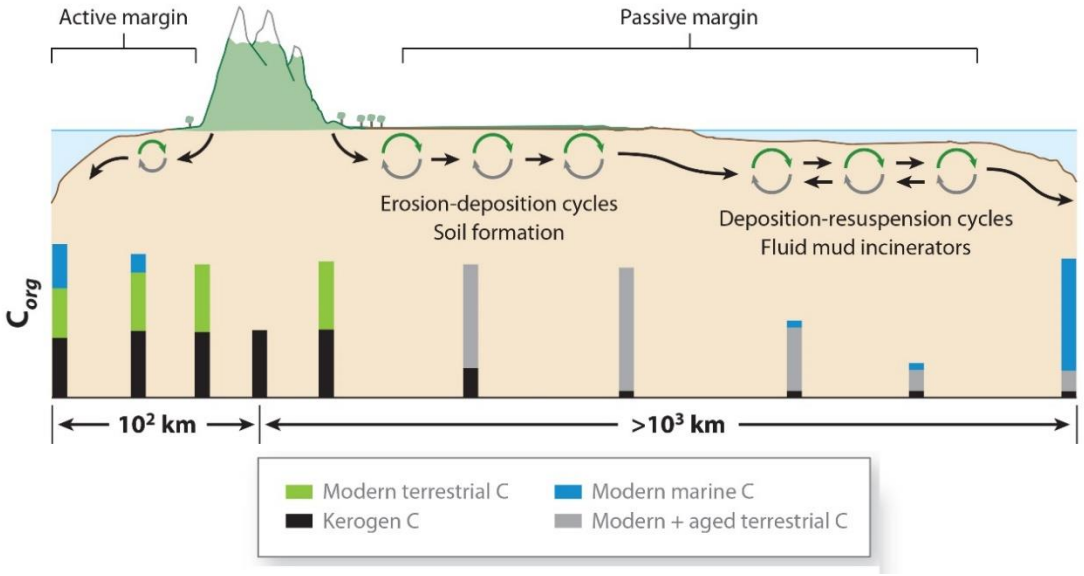

Fig. 4 The serial transport-reaction systems of fluvial particulate organic carbon in the contrasting active- and passive- margin. Figure modified from Blair and Aller (2012).

Dam-building results in pronounced retainment of sediments in reservoirs instead of entering the estuary, companies a sound decrease of POC load (Battin et al., 2009; Milliman and Farnsworth, 2011; Maavara et al., 2017). Although this human perturbation surely leads to a drastic decrease in POC export and preservation at continental margins, it does not mean that fewer riverine POC is involved in the global

carbon cycle. In fact, significant amounts of POC could be even more efficiently buried in artificial reservoirs (Mendonça et al., 2012, 2017; Dean and Gorham, 1998; Tranvik et al., 2009). It is estimated that reservoirs had replaced oceans as being the site of the largest burial rate of terrestrial riverine POC (Dean and Gorham, 1998; Maavara et al., 2017). It remains debated whether reservoirs are a net carbon source or sink, many studies demonstrate a negligible amount of carbon emissions compared to POC sink, thus supporting the idea that reservoirs could be an efficient sink of atmospheric CO_2 (Dean et al., 1998; Tranvik et al., 2009; Knoll et al., 2013; Mendonça et al., 2012, 2017). It can be summarized that three major processes related to dam-building could enhance the carbon sink of river basins:

- 1) the increased sedimentation rate in artificial reservoirs compared to that in oceans largely reduces the oxygen exposure time of POC, providing a favorable burial environment for the efficient burial of POC (Blair and Aller, 2012; Galy et al., 2007; Mendonça et al., 2012);
- 2) the intensified erosion of river banks and reduced sediment deposition (Yang et al., 2005) potentially add external terrestrial POC_{bio} into the fluvial system and to burial sites;
- 3) with the shorter pathway of POC from source to sink due to "blocking" by reservoirs, substantial POC could escape from metabolism and oxidation compared to the longer transport-deposition pathway (Bouchez et al., 2010; Galy et al., 2008a).

All processes are interfering with the natural alteration and decomposition of riverine POC, continuously impacting the global carbon cycle at least on the lifespan of reservoirs. The overall timescales of human perturbation on the global carbon cycle remain to be further constrained. The Changjiang River Basin, a highly regulated system over the last five decades (approximately 50,000 dams are in operation), is a suitable large fluvial system for accessing the alteration to the fate of riverine POC due to dam-building (Chapter 4).

Reference

Aller, R. C., and Blair, N. E. (2006). Carbon remineralization in the Amazon–Guianas tropical mobile mudbelt: A sedimentary incinerator. Continental Shelf Research, 26(17-18), 2241-2259.

Aufdenkampe, A. K., Mayorga, E., Raymond, P. A., Melack, J. M., Doney, S. C., Alin, S. R., ... and Yoo, K. (2011). Riverine coupling of biogeochemical cycles between land, oceans, and atmosphere. Frontiers in Ecology and the Environment, 9(1), 53-60.

Becker, J. A., Bickle, M. J., Galy, A., and Holland, T. J. (2008). Himalayan metamorphic CO_2 fluxes: Quantitative constraints from hydrothermal springs. Earth and Planetary Science Letters, 265(3-4), 616-629.

Berner, R. A. (1982). Burial of organic carbon and pyrite sulfur in the modern ocean: its geochemical and environmental significance. American Journal of Science, 282.

Berner, R. A. (1994). GEOCARB II: A revised model of atmospheric CO_2 over phanerozoic time. American Journal of Science;(United States), 294(1).

Berner, R. A. (1999). Atmospheric oxygen over Phanerozoic time. Proceedings of the National Academy of Sciences, 96(20), 10955-10957.

Berner, R. A. (2003). The long-term carbon cycle, fossil fuels and atmospheric composition. Nature, 426(6964), 323-326.

Berner, E. K., and Berner, R. A. (2012). Global environment: water, air, and geochemical cycles. Princeton University Press.

Blair, N. E., and Aller, R. C. (2012). The fate of terrestrial organic carbon in the marine environment. Annual Review of Marine Science, 4, 401-423.

Blair, N. E., Leithold, E. L., Brackley, H., Trustrum, N., Page, M., and Childress, L. (2010). Terrestrial sources and export of particulate organic carbon in the Waipaoa sedimentary system: Problems, progress and processes. Marine Geology, 270(1-4), 108-118.

Blattmann, T. M., Liu, Z., Zhang, Y., Zhao, Y., Haghipour, N., Montluçon, D. B., ... and Eglinton, T. I. (2019). Mineralogical control on the fate of continentally derived organic matter in the ocean. Science, 366(6466), 742-745.

Bianchi, T. S., Wysocki, L. A., Stewart, M., Filley, T. R., and McKee, B. A. (2007). Temporal variability in terrestrially-derived sources of particulate organic carbon in the lower Mississippi River and its upper tributaries. Geochimica et Cosmochimica

Acta, 71(18), 4425-4437.

Bouillon, S., Yambélé, A., Spencer, R. G. M., Gillikin, D. P., Hernes, P. J., Six, J., ... and Borges, A. V. (2012). Organic matter sources, fluxes and greenhouse gas exchange in the Oubangui River (Congo River basin). Biogeosciences, 9(6), 2045-2062.

Bouchez, J., Beyssac, O., Galy, V., Gaillardet, J., France-Lanord, C., Maurice, L., and Moreira-Turcq, P. (2010). Oxidation of petrogenic organic carbon in the Amazon floodplain as a source of atmospheric CO_2. Geology, 38(3), 255-258.

Bouchez, J., Gaillardet, J., France-Lanord, C., Maurice, L., and Dutra-Maia, P. (2011a). Grain size control of river suspended sediment geochemistry: Clues from Amazon River depth profiles. Geochemistry, Geophysics, Geosystems, 12(3).

Bouchez, J., Galy, V., Hilton, R. G., Gaillardet, J., Moreira-Turcq, P., Pérez, M. A., ... and Maurice, L. (2014). Source, transport and fluxes of Amazon River particulate organic carbon: Insights from river sediment depth-profiles. Geochimica et Cosmochimica Acta, 133, 280-298.

Bouchez, J., Lupker, M., Gaillardet, J., France-Lanord, C., and Maurice, L. (2011b). How important is it to integrate riverine suspended sediment chemical composition with depth? Clues from Amazon River depth-profiles. Geochimica et Cosmochimica Acta, 75(22), 6955-6970.

Burdige, D. J. (2005). Burial of terrestrial organic matter in marine sediments: A re-assessment. Global Biogeochemical Cycles, 19(4).

Burdige, D. J. (2007). Preservation of organic matter in marine sediments: controls, mechanisms, and an imbalance in sediment organic carbon budgets?. Chemical Reviews, 107(2), 467-485.

Calmels, D., Gaillardet, J., Brenot, A., and France-Lanord, C. (2007). Sustained sulfide oxidation by physical erosion processes in the Mackenzie River basin: Climatic perspectives. Geology, 35(11), 1003-1006.

Cerling, T. E., Harris, J. M., MacFadden, B. J., Leakey, M. G., Quade, J., Eisenmann, V., and Ehleringer, J. R. (1997). Global vegetation change through the Miocene/Pliocene boundary. Nature, 389(6647), 153-158.

Cole, J. J., Prairie, Y. T., Caraco, N. F., McDowell, W. H., Tranvik, L. J., Striegl, R. G., ... and Melack, J. (2007). Plumbing the global carbon cycle: integrating inland waters into the terrestrial carbon budget. Ecosystems, 10(1), 172-185.

Coulthard, T. J., and Van de Wiel, M. J. (2013). Climate, tectonics or morphology: what

signals can we see in drainage basin sediment yields?. Earth Surface Dynamics, 1(1), 13-27.

Dean, W. E., and Gorham, E. (1998). Magnitude and significance of carbon burial in lakes, reservoirs, and peatlands. Geology, 26(6), 535-538.

Derry, L. A. (2014). Organic Carbon Cycling and the Lithosphere. In Reference Module in Earth Systems and Environmental Sciences Treatise on Geochemistry (Second Edition) (Vol. 12, pp. 239–249).

Ebelmen, J. J. (1845). Sur les produits de la décomposition des espèces minérales de la famille des silicates. In Annales des Mines (Vol. 7, No. 3, p. 66).

Ellis, E. E., Keil, R. G., Ingalls, A. E., Richey, J. E., and Alin, S. R. (2012). Seasonal variability in the sources of particulate organic matter of the Mekong River as discerned by elemental and lignin analyses. Journal of Geophysical Research: Biogeosciences, 117(G1).

Evans, M. J., Derry, L. A., and France-Lanord, C. (2008). Degassing of metamorphic carbon dioxide from the Nepal Himalaya. Geochemistry, Geophysics, Geosystems, 9(4).

France-Lanord, C., and Derry, L. A. (1997). Organic carbon burial forcing of the carbon cycle from Himalayan erosion. Nature, 390(6655), 65-67.

Freymond, C. V., Lupker, M., Peterse, F., Haghipour, N., Wacker, L., Filip, F., ... and Eglinton, T. I. (2018). Constraining instantaneous fluxes and integrated compositions of fluvially discharged organic matter. Geochemistry, Geophysics, Geosystems, 19(8), 2453-2462.

Gaillardet, J., Dupré, B., Louvat, P., and Allegre, C. J. (1999). Global silicate weathering and CO_2 consumption rates deduced from the chemistry of large rivers. Chemical Geology, 159(1-4), 3-30.

Galy, V., and Eglinton, T. (2011). Protracted storage of biospheric carbon in the Ganges–Brahmaputra basin. Nature Geoscience, 4(12), 843-847.

Galy, V., Beyssac, O., France-Lanord, C., and Eglinton, T. (2008a). Recycling of graphite during Himalayan erosion: A geological stabilization of carbon in the crust. Science, 322(5903), 943-945.

Galy, V., France-Lanord, C., and Lartiges, B. (2008b). Loading and fate of particulate organic carbon from the Himalaya to the Ganga–Brahmaputra delta. Geochimica et Cosmochimica Acta, 72(7), 1767-1787.

Galy, V., France-Lanord, C., Beyssac, O., Faure, P., Kudrass, H., and Palhol, F. (2007).

Efficient organic carbon burial in the Bengal fan sustained by the Himalayan erosional system. Nature, 450(7168), 407-410.

Galy, V., Peucker-Ehrenbrink, B., and Eglinton, T. (2015). Global carbon export from the terrestrial biosphere controlled by erosion. Nature, 521(7551), 204-207.

Garzanti, E., Andó, S., France-Lanord, C., Censi, P., Vignola, P., Galy, V., and Lupker, M. (2011). Mineralogical and chemical variability of fluvial sediments 2. Suspended-load silt (Ganga–Brahmaputra, Bangladesh). Earth and Planetary Science Letters, 302(1-2), 107-120.

Ge, T., Xue, Y., Jiang, X., Zou, L., and Wang, X. (2020). Sources and radiocarbon ages of organic carbon in different grain size fractions of Yellow River-transported particles and coastal sediments. Chemical Geology, 534, 119452.

Hedges, J. I., and Keil, R. G. (1995). Sedimentary organic matter preservation: an assessment and speculative synthesis. Marine Chemistry, 49(2-3), 81-115.

Hedges, J. I., and Keil, R. G. (1995). Sedimentary organic matter preservation: an assessment and speculative synthesis. Marine Chemistry, 49(2-3), 81-115.

Hemingway, J. D., Hilton, R. G., Hovius, N., Eglinton, T. I., Haghipour, N., Wacker, L., ... and Galy, V. V. (2018). Microbial oxidation of lithospheric organic carbon in rapidly eroding tropical mountain soils. Science, 360(6385), 209-212.

Hemingway, J. D., Rothman, D. H., Grant, K. E., Rosengard, S. Z., Eglinton, T. I., Derry, L. A., and Galy, V. V. (2019). Mineral protection regulates long-term global preservation of natural organic carbon. Nature, 570(7760), 228-231.

Hemingway, J. D., Schefuß, E., Spencer, R. G., Dinga, B. J., Eglinton, T. I., McIntyre, C., and Galy, V. V. (2017). Hydrologic controls on seasonal and inter-annual variability of Congo River particulate organic matter source and reservoir age. Chemical Geology, 466, 454-465.

Hilton, R. G. (2017). Climate regulates the erosional carbon export from the terrestrial biosphere. Geomorphology, 277, 118-132.

Hilton, R. G., and West, A. J. (2020). Mountains, erosion and the carbon cycle. Nature Reviews Earth and Environment, 1(6), 284-299.

Hilton, R. G., Gaillardet, J., Calmels, D., and Birck, J. L. (2014). Geological respiration of a mountain belt revealed by the trace element rhenium. Earth and Planetary Science Letters, 403, 27-36.

Hilton, R. G., Galy, A., Hovius, N., Chen, M. C., Horng, M. J., and Chen, H. (2008). Tropical-cyclone-driven erosion of the terrestrial biosphere from mountains. Nature

Geoscience, 1(11), 759-762.

Hilton, R. G., Galy, A., Hovius, N., Horng, M. J., and Chen, H. (2011). Efficient transport of fossil organic carbon to the ocean by steep mountain rivers: An orogenic carbon sequestration mechanism. Geology, 39(1), 71-74.

Hilton, R. G., Galy, V., Gaillardet, J., Dellinger, M., Bryant, C., O'Regan, M., ... and Calmels, D. (2015). Erosion of organic carbon in the Arctic as a geological carbon dioxide sink. Nature, 524(7563), 84-87.

Holland, H. D. (1978). The chemistry of the atmosphere and oceans. New York: Wiley.

Horan, K., Hilton, R. G., Dellinger, M., Tipper, E., Galy, V., Calmels, D., ... and Burton, K. W. (2019). Carbon dioxide emissions by rock organic carbon oxidation and the net geochemical carbon budget of the Mackenzie River Basin. American Journal of Science, 319(6), 473-499.

Horan, K., Hilton, R. G., Selby, D., Ottley, C. J., Gröcke, D. R., Hicks, M., and Burton, K. W. (2017). Mountain glaciation drives rapid oxidation of rock-bound organic carbon. Science Advances, 3(10), e1701107.

Hou, P., Yu, M., Zhao, M., Montluçon, D. B., Su, C., and Eglinton, T. I. (2020). Terrestrial biomolecular burial efficiencies on continental margins. Journal of Geophysical Research: Biogeosciences, 125(8), e2019JG005520.

Keil, R. G., and Mayer, L. M. (2014). Mineral Matrices and Organic Matter. In Reference Module in Earth Systems and Environmental Sciences Treatise on Geochemistry (Second Edition) (Vol. 12, pp. 337–359).

Kennedy, M. J., and Wagner, T. (2011). Clay mineral continental amplifier for marine carbon sequestration in a greenhouse ocean. Proceedings of the National Academy of Sciences, 108(24), 9776-9781.

Kerrick, D. M., and Caldeira, K. (1998). Metamorphic CO_2 degassing from orogenic belts. Chemical Geology, 145(3-4), 213-232.

Kerrick, D. M., McKibben, M. A., Seward, T. M., and Caldeira, K. (1995). Convective hydrothermal C02 emission from high heat flow regions. Chemical Geology, 121(1-4), 285-293.

Knoll, L. B., Vanni, M. J., Renwick, W. H., Dittman, E. K., and Gephart, J. A. (2013). Temperate reservoirs are large carbon sinks and small CO_2 sources: Results from high-resolution carbon budgets. Global Biogeochemical Cycles, 27(1), 52-64.

Krissansen-Totton, J., Buick, R., and Catling, D. C. (2015). A statistical analysis of the carbon isotope record from the Archean to Phanerozoic and implications for the rise

of oxygen. American Journal of Science, 315(4), 275-316.

Lalonde, K., Mucci, A., Ouellet, A., and Gélinas, Y. (2012). Preservation of organic matter in sediments promoted by iron. Nature, 483(7388), 198-200.

Li, K., Zhu, C., Wu, L., and Huang, L. (2013). Problems caused by the Three Gorges Dam construction in the Yangtze River basin: a review. Environmental Reviews, 21(3), 127-135.

Li, Y. H. (2000). A compendium of geochemistry: from solar nebula to the human brain. Princeton University Press.

Maavara, T., Lauerwald, R., Regnier, P., and Van Cappellen, P. (2017). Global perturbation of organic carbon cycling by river damming. Nature communications, 8(1), 1-10.

Maavara, T., Lauerwald, R., Regnier, P., and Van Cappellen, P. (2017). Global perturbation of organic carbon cycling by river damming. Nature communications, 8(1), 1-10.

Martin, E. E., Ingalls, A. E., Richey, J. E., Keil, R. G., Santos, G. M., Truxal, L. T., ... and Druffel, E. R. (2013). Age of riverine carbon suggests rapid export of terrestrial primary production in tropics. Geophysical Research Letters, 40(21), 5687-5691.

Marwick, T. R., Tamooh, F., Teodoru, C. R., Borges, A. V., Darchambeau, F., and Bouillon, S. (2015). The age of river-transported carbon: A global perspective. Global Biogeochemical Cycles, 29(2), 122-137.

Mayer, L. M. (1994). Surface area control of organic carbon accumulation in continental shelf sediments. Geochimica et Cosmochimica Acta, 58(4), 1271-1284.

Meade, R. H., and Moody, J. A. (2010). Causes for the decline of suspended-sediment discharge in the Mississippi River system, 1940-2007. Hydrological Processes: An International Journal, 24(1), 35-49.

Mendonca, R., Kosten, S., Sobek, S., Barros, N., Cole, J. J., Tranvik, L., and Roland, F. (2012). Hydroelectric carbon sequestration. Nature Geoscience, 5(12), 838-840.

Mendonça, R., Müller, R. A., Clow, D., Verpoorter, C., Raymond, P., Tranvik, L. J., and Sobek, S. (2017). Organic carbon burial in global lakes and reservoirs. Nature communications, 8(1), 1-7.

Meybeck, M. (1993). Riverine transport of atmospheric carbon: sources, global typology and budget. Water, Air, and Soil Pollution, 70(1), 443-463.

Milliman, J. D., and Farnsworth, K. L. (2011). River Discharge to the Coastal Ocean: A Global Synthesis.

Moore, S., Evans, C. D., Page, S. E., Garnett, M. H., Jones, T. G., Freeman, C., ... and Gauci, V. (2013). Deep instability of deforested tropical peatlands revealed by fluvial organic carbon fluxes. Nature, 493(7434), 660-663.

Petsch, S. T. (2014). Weathering of Organic Carbon. In Reference Module in Earth Systems and Environmental Sciences Treatise on Geochemistry (Second Edition) (Vol. 12, pp. 217–238).

Petsch, S. T., Berner, R. A., and Eglinton, T. I. (2000). A field study of the chemical weathering of ancient sedimentary organic matter. Organic Geochemistry, 31(5), 475-487.

Plank, T., and Manning, C. E. (2019). Subducting carbon. Nature, 574(7778), 343-352.

Ransom, B., Kim, D., Kastner, M., and Wainwright, S. (1998). Organic matter preservation on continental slopes: importance of mineralogy and surface area. Geochimica et Cosmochimica Acta, 62(8), 1329-1345.

Robock, A. (2000). Volcanic eruptions and climate. Reviews of Geophysics, 38(2), 191–219.

Rosenheim, B. E., and Galy, V. (2012). Direct measurement of riverine particulate organic carbon age structure. Geophysical Research Letters, 39(19).

Shen, Z., Rosenheim, B. E., Törnqvist, T. E., and Lang, A. (2021). Engineered Continental-Scale Rivers Can Drive Changes in the Carbon Cycle. AGU Advances, 2(1), e2020AV000273.

Smith, R. W., Bianchi, T. S., Allison, M., Savage, C., and Galy, V. (2015). High rates of organic carbon burial in fjord sediments globally. Nature Geoscience, 8(6), 450-453.

Soulet, G., Hilton, R. G., Garnett, M. H., Dellinger, M., Croissant, T., Ogrič, M., and Klotz, S. (2018). In situ measurement of flux and isotopic composition of CO_2 released during oxidative weathering of sedimentary rocks. Biogeosciences, 15(13), 4087-4102.

Soulet, G., Hilton, R. G., Garnett, M. H., Roylands, T., Klotz, S., Croissant, T., ... and Le Bouteiller, C. (2021). Temperature control on CO_2 emissions from the weathering of sedimentary rocks. Nature Geoscience, 1-7.

Sundquist, E. T. and Ackerman, A. V. (2014). The geological history of the carbon cycle. In Reference Module in Earth Systems and Environmental Sciences Treatise on Geochemistry (Second Edition) (Vol. 12, pp. 239–249).

Sundquist, E. T. (1993). The global carbon dioxide budget. Science, 934-941.

Syvitski, J. P. M., Vörösmarty, C. J., Kettner, A. J., and Green, P. (2005). Impact of Humans on the Flux of Terrestrial Sediment to the Global Coastal Ocean. Science, 308(5720), 376–380.

Tarnocai, C., Canadell, J. G., Schuur, E. A., Kuhry, P., Mazhitova, G., and Zimov, S. (2009). Soil organic carbon pools in the northern circumpolar permafrost region. Global Biogeochemical Cycles, 23(2).

Torres, M. A., West, A. J., and Li, G. (2014). Sulphide oxidation and carbonate dissolution as a source of CO_2 over geological timescales. Nature, 507(7492), 346-349.

Urey, H. C. (1952). The planets: their origin and development. Mrs. Hepsa Ely Silliman Memorial Lectures.

Walker, J. C., Hays, P. B., and Kasting, J. F. (1981). A negative feedback mechanism for the long-term stabilization of Earth's surface temperature. Journal of Geophysical Research: Oceans, 86(C10), 9776-9782.

West, A. J., Galy, A., and Bickle, M. (2005). Tectonic and climatic controls on silicate weathering. Earth and Planetary Science Letters, 235(1-2), 211-228.

Whiticar, M. J. (1996). Stable isotope geochemistry of coals, humic kerogens and related natural gases. International Journal of Coal Geology, 32(1-4), 191-215.

Whittaker, A. C., Attal, M., and Allen, P. A. (2010). Characterising the origin, nature and fate of sediment exported from catchments perturbed by active tectonics. Basin Research, 22(6), 809-828.

Wild, B., Andersson, A., Bröder, L., Vonk, J., Hugelius, G., McClelland, J. W., ... and Gustafsson, Ö. (2019). Rivers across the Siberian Arctic unearth the patterns of carbon release from thawing permafrost. Proceedings of the National Academy of Sciences, 116(21), 10280-10285.

Wilmshurst, J. M., Anderson, A. J., Higham, T. F., and Worthy, T. H. (2008). Dating the late prehistoric dispersal of Polynesians to New Zealand using the commensal Pacific rat. Proceedings of the National Academy of Sciences, 105(22), 7676-7680.

Yang, S. L., Zhang, J., Zhu, J., Smith, J. P., Dai, S. B., Gao, A., and Li, P. (2005). Impact of dams on Yangtze River sediment supply to the sea and delta intertidal wetland response. Journal of Geophysical Research: Earth Surface, 110(F3).

Yu, M., Eglinton, T. I., Haghipour, N., Montluçon, D. B., Wacker, L., Wang, Z., and Zhao, M. (2019). Molecular isotopic insights into hydrodynamic controls on fluvial suspended particulate organic matter transport. Geochimica et Cosmochimica Acta,

262, 78-91.

Zalasiewicz, J., Waters, C. N., Williams, M., Barnosky, A. D., Cearreta, A., Crutzen, P., ... and Oreskes, N. (2015). When did the Anthropocene begin? A mid-twentieth century boundary level is stratigraphically optimal. Quaternary International, 383, 196-203.

Chapter 2

Materials and Analytical Methods

This chapter aims to provide a general framework for analyzing the physico-chemical properties of collected sediment samples in the thesis. It starts by introducing the geo-environmental background of the four largest Chinese rivers, and follows with the sampling strategy and sample information, and then with a focus on the pretreatment techniques and analyzing procedures of geochemistry analysis, and finishing with special attention paid to the integrated transect elemental and isotopic flux calculation based on Rouse model by taking advantages of hydrodynamic sorting. Measurement of elemental and stable isotopic carbon and nitrogen composition is outlined, with emphasis on the radiocarbon composition analysis using *EchoMICADAS*.

1. Study area and sampling strategy

1.1 The four largest rivers in China

The four largest river systems in China, namely, Changjiang (CJ, Yangtze River), Huanghe (HH, Yellow River), Zhujiang (ZJ, Pearl River), and Heilongjiang (HLJ, Amur River), drain around the two-fifths continental area of China, spanning very contrasted geomorphology, lithology, climatic conditions, and anthropogenic pressure. The geographic location and basin limitation of each river is shown in Figure 1, below is the brief introduction (The Ministry of Water Resources of China, MWRC).

Changjiang is the longest river in Asia and the third-longest in the world. It flows 6,387 km eastward from Jari Hill in the Tanggula Mountain (Qinghai-Tibet Plateau) to the East China Sea, draining an area of 180×10^4 km^2. Its upper reaches range from the source to the Yichang city. The section between Yushu and Yibin city is also named the Jinshajiang River (JSJ), with a length of around 3,481 km draining an area of 50.2×10^4 km^2. The largest tributary of JSJ is the Yalong River (YR). The middle reaches lie within Yichang and Hukou city running 950 km long, and the section after Hukou till the river mouth is the lower reaches, the length is around 850 km.

Huanghe is the second-longest river in China with a length of 5,464 km draining an area of 75.19×10^4 km^2. It starts at the northern Bayan Har Mountains (Qinghai-

Tibet Plateau) and flows into the Bohai Sea. Its upper reaches span from the source (an elevation of 4,500 m) to Toudaoguai (TDG, an elevation of 1,000 m) in variable gradient with a length of 3,472 km, the middle reaches ends at Huayuankou (HYK, an elevation of 110 m) in relatively continuous gradient with a length of 1,206 km and the lower reaches flow eastwards across the fluvial plain over a length of 786 km, these three sections control 53.8%, 43.3% and 2.9% of the whole river basin (Wang et al., 2007).

Zhujiang is the second largest river in China in terms of water discharge, whilst the third-largest river with respect to the flowing length. It originates from the Maxiong Mountain in Yunnan Province and exports to the South China Sea. Its length is 2320 km and the drainage basin is 41.52×10^4 km^2. ZJ River is an expansive river network consisting of Xijiang (West River, 2075 km), Beijiang (North River, 573 km), and Dongjiang (East River, 562 km), among which Xijiang is the main stem representing around 64% annual discharge of ZJ, covering an area of 35×10^4 km^2.

Heilongjiang is the tenth longest river in the world with a length of 4,444 km flowing into the Sea of Okhotsk, covering a drainage basin of 185.6×10^4 km^2. It is shared by China, Russia, and Mongolia. HLJ along with its main tributary, the Ussuri River, are the national boundaries between China and Russia. The section of HLJ before Heihe is the upper reaches, then the middle reaches extend to Fuyuan, while the section after is the lower reaches that is totally in Russia. Its largest tributary in China, the Songhuajiang River (SHJ), has a length of 1927 km and drains 55.72×10^4 km^2 basin area, taking over most of the Northeast China Plain. SHJ has two sources, the north source is the Nenjiang River (NJ, 1,370 km) originated from the Greater Khingan Range, and the south source is the Di'er Songhuajiang (DSHJ, 795 km) originated from the Changbai Mountain.

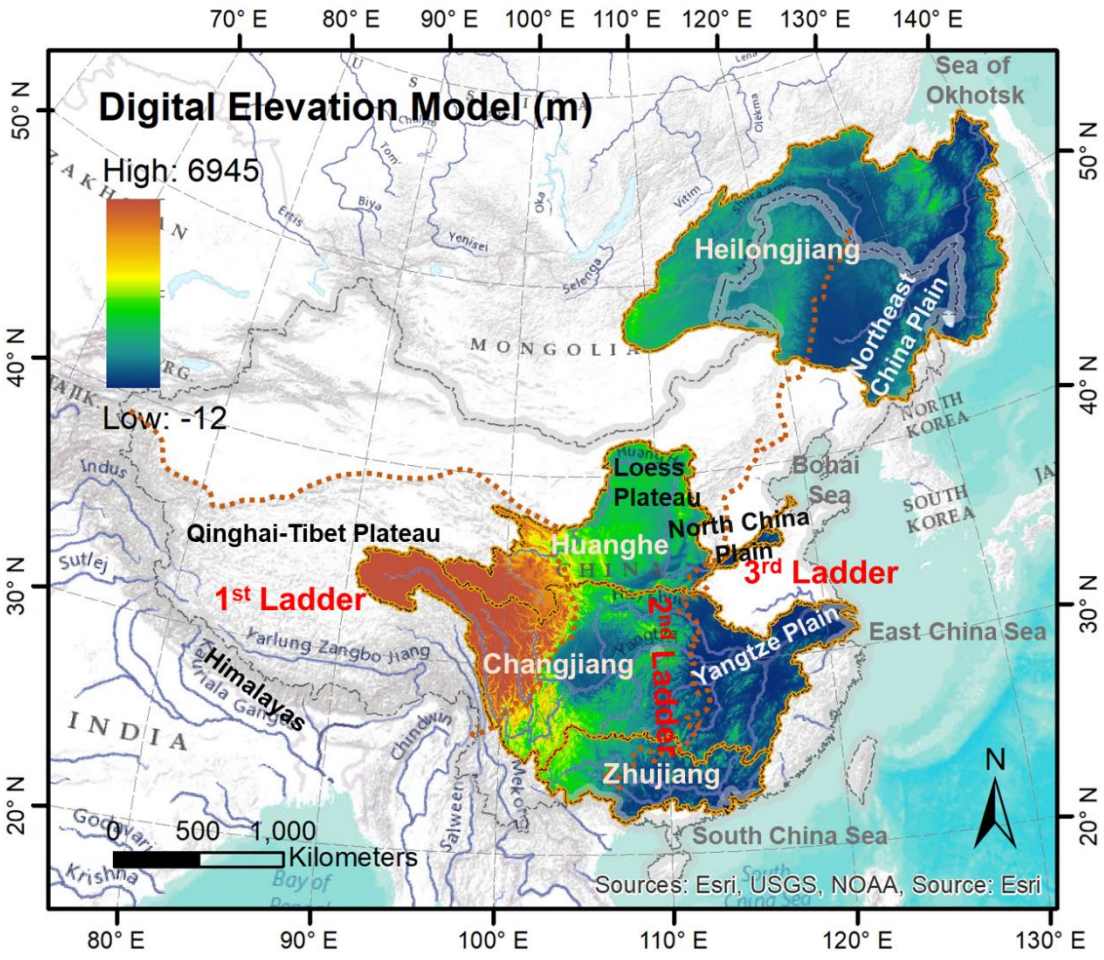

Fig. 1 Digital Elevation Model (DEM) of the four largest rivers in China (DEM is using Shuttle Radar Topography Mission [SRTM] 1 Arc-Second Global data). From south to north in geography, the four rivers are Zhujiang, Changjiang, Huanghe, and Heilongjiang, respectively (Hereinafter). The basin boundaries are limited by orange outlines. The brown dot lines represent the limitations of the three steps of China's terrain. The grey outline represents the boundary of China, hereinafter.

1.1.1 Hydrological condition under Anthropogenic pressure

Global rivers are getting more and more regulated owing to intensified human interference. While drainage land-use changes dramatically especially deforestation, farming, mining, and modern construction, accelerating the erosion rate and runoff in the watershed; dam construction effectively regulates the natural river transportation process by storing and trapping water and sediments resulting in a significant decrease of sediment flux (Milliman and Farnsworth, 2011; Syvitski et al., 2005; Syvitski and Kettner, 2011; Kondolf et al., 2014).

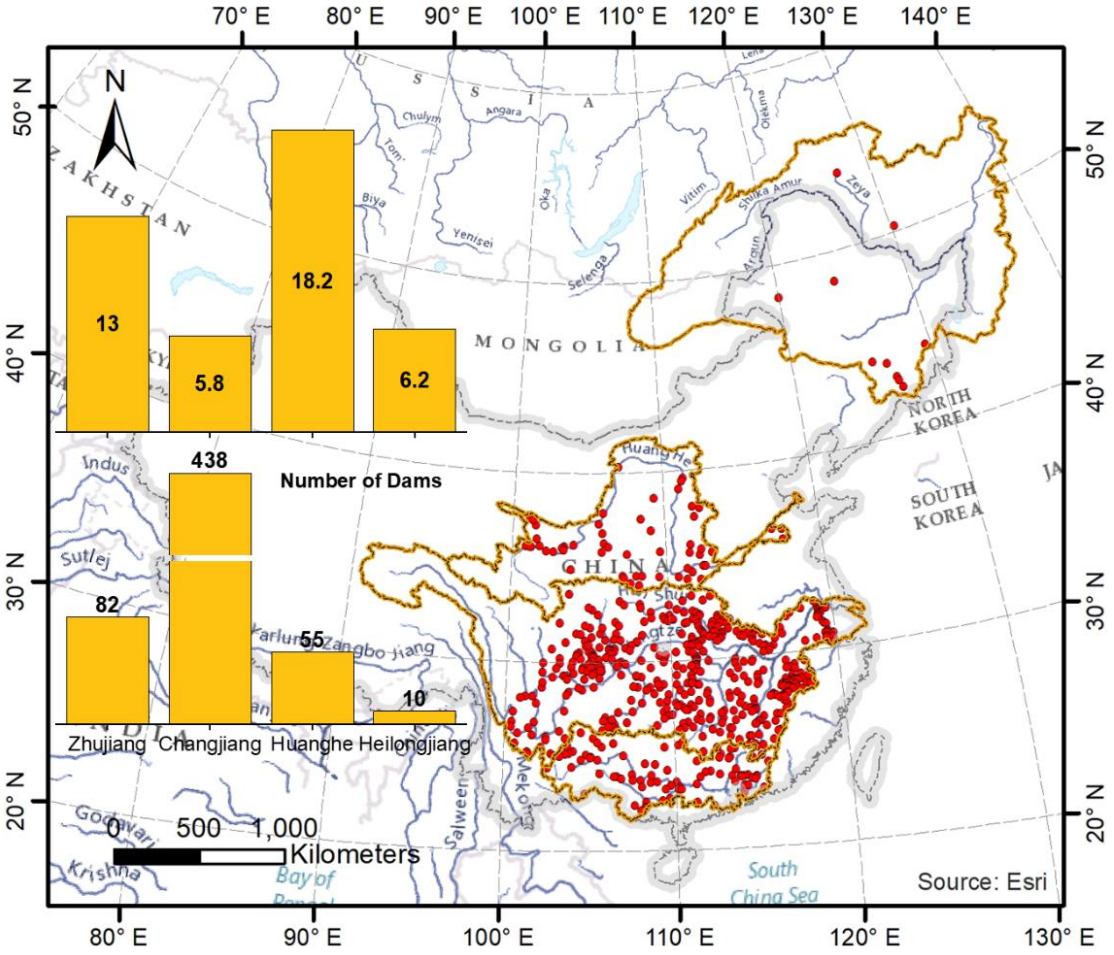

Fig. 2 Dams distributed in the four largest rivers in China (Dam number and capacity are extracted from the GRanD v1.3 database by Lehner et al., 2011). The column plot above shows the ratio of the dam capacity to river volume (river volume is extracted from the HydroSHEDS and WaterGAP v2.2 database by Lehner and Grill, 2013).

The Global Reservoir and Dam Database (GRanD v1.3, Lehner and Grill, 2013) com 7,320 dams greater than 15 m in height or with a reservoir of more than 0.1 km^3. In the absence of counting other smaller dams, there are 82 (reservoir capacity 93.85 × 10^9 m^3, hereinafter), 438 (277.41 × 10^9 m^3), 55 (72.11 × 10^9 m^3), and 10 (114.88 × 10^9 m^3) dams in the ZJ, CJ, HH, and HLJ drainage basin until 2016, respectively (Figure 2). The cumulative reservoir capacity in China increased 15 times from 42.33 × 10^9 m^3 in 1953 to 679.23 × 10^9 m^3 in 2016 (Figure 3). In this circumstance, reservoir capacity exceeds the river volume to a great extent (Figure 2), using the ratio of the former to the latter, HH reaches the maximum by 18.2 and followed by ZJ (13.0), HLJ (6.2), and CJ (5.8).

Under efficient regulation of dams, the four case rivers underwent a decrease of water discharge and sediment flux in the last few decades to varying degrees (annual mean value from 1953 to 2017, data were retrieved from MWRC, Figure 3). HLJ is reported to have an average water discharge of 10,929 m^3/s which equals 344.66×10^9 m^3/yr with the sediment flux of 52×10^9 kg/yr (Tachibana et al., 2008; Milliman and Farnsworth, 2011). There are two discharge peaks within one annual cycle which normally occurs in June and September. As there is no access to the long-term hydrological data of the HLJ River, data of the SHJ River was used instead. The mean annual water discharge is 284.32×10^9 m^3/yr, 889.65×10^9 m^3/yr, 28.38×10^9 m^3/yr, and 62.84×10^9 m^3/yr for ZJ, CJ, HH, and SHJ, respectively, carrying a mean annual sediment flux of 65.49×10^9 kg/yr, 358.98×10^9 kg/yr, 646.58×10^9 kg/yr, and 12.24×10^9 kg/yr, correspondingly. Comparing hydrological data of the first recorded decade (1953-1962) with the latest decade (2008-2017), ZJ and CJ showed a relatively constant water discharge, while HH and SHJ decreased 63.2% and 33.3%, respectively. Concerning the sediment flux, HH had a dramatic decrease of 92.7%, follfollowed by CJ (72.7%), ZJ (64.5%), and SHJ (24.6%), and this trend is likely to continue in the future (Milliman and Farnsworth, 2011). In the 1950s, HH is the most turbid river system on the earth, delivering approximately 16 times more sediments than that of ZJ. However, sediment flux decreased two magnitudes since 2014, and is 10.6×10^9 kg in 2016 and is 7.7×10^9 kg in 2017, which are even far less than that of ZJ. The sharp dropping of riverine sediments suggests the total amount of particulate organic carbon that could be finally delivered into the ocean faced a significant reduction as well, thus impacting the global carbon cycle as less and less biospheric organic carbon will be buried, meanwhile, more and more organic carbon will be kept in the terrestrial river fluvial system.

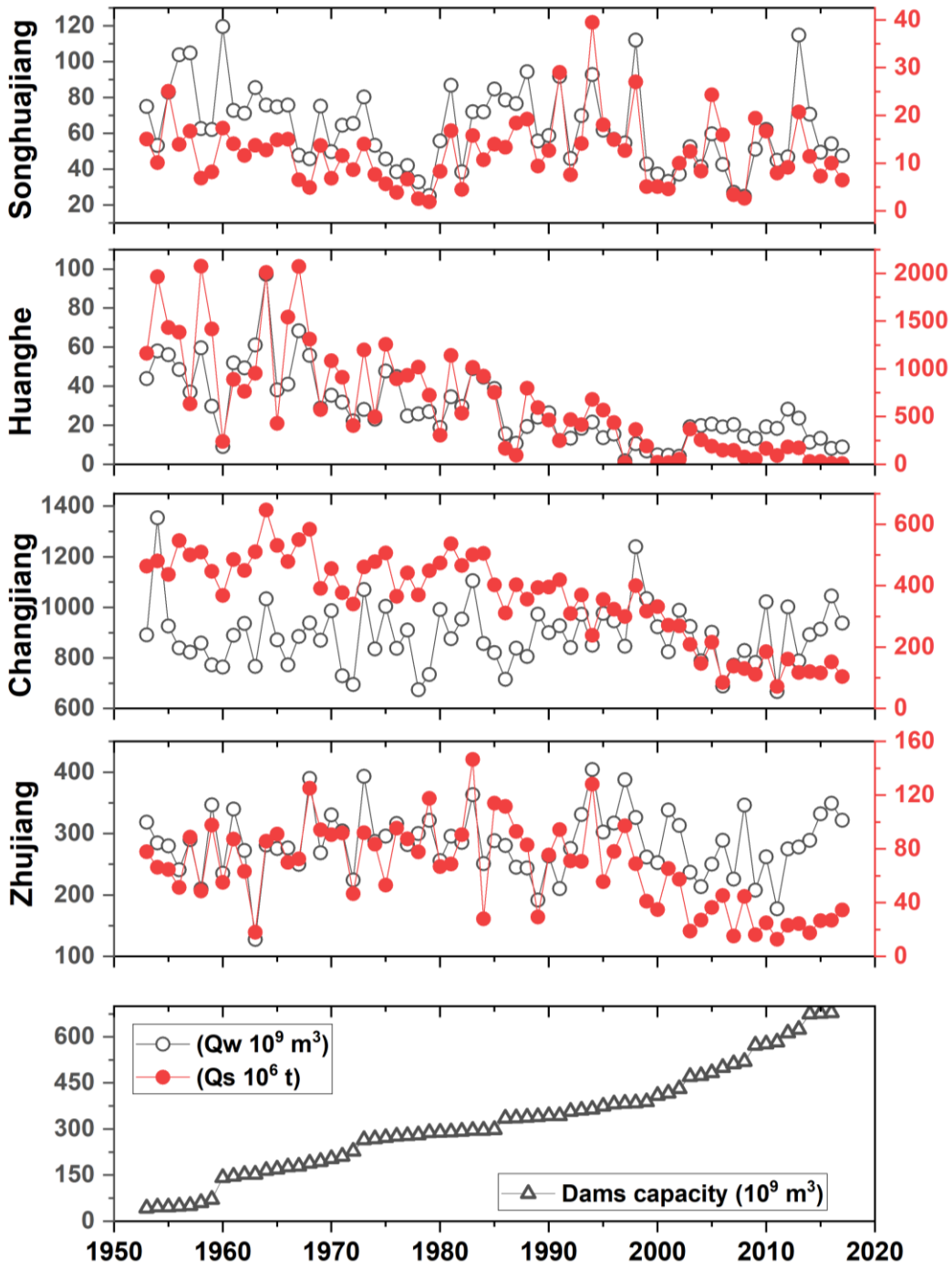

Fig. 3 Annual water discharge (Qw) and sediment flux (Qs) of the four largest rivers in China from 1953 to 2017 (in-situ historic monitoring data is from MWRC), with reservoir capacity in China from 1953 to 2016 (World reservoir capacity was from GRanD V1.3 database, Lehner et al., 2011). In absence of accessing historic Qw and Qs data from the Heilongjiang River, its main tributary in China, the Songhuajiang River was used instead.

1.1.2 Climatic condition: precipitation and temperature

The four large river basins exhibit distinct climatic features in precipitation and air temperature. In general, mean annual precipitation (MAP) decreases northeastwards, and mean annual temperature (MAT) decreases northwards in China. As shown in Figure 4 and Figure 5, the MAP of each drainage basin decreases following the order of ZJ (1,482 mm), CJ (1,037 mm), HLJ (525 mm), and HH (456 mm). MAT of each drainage basin decreases northwards in the order of ZJ (18.74 ℃), CJ (11.22 ℃), HH (6.01 ℃), and HLJ (-1.02 ℃).

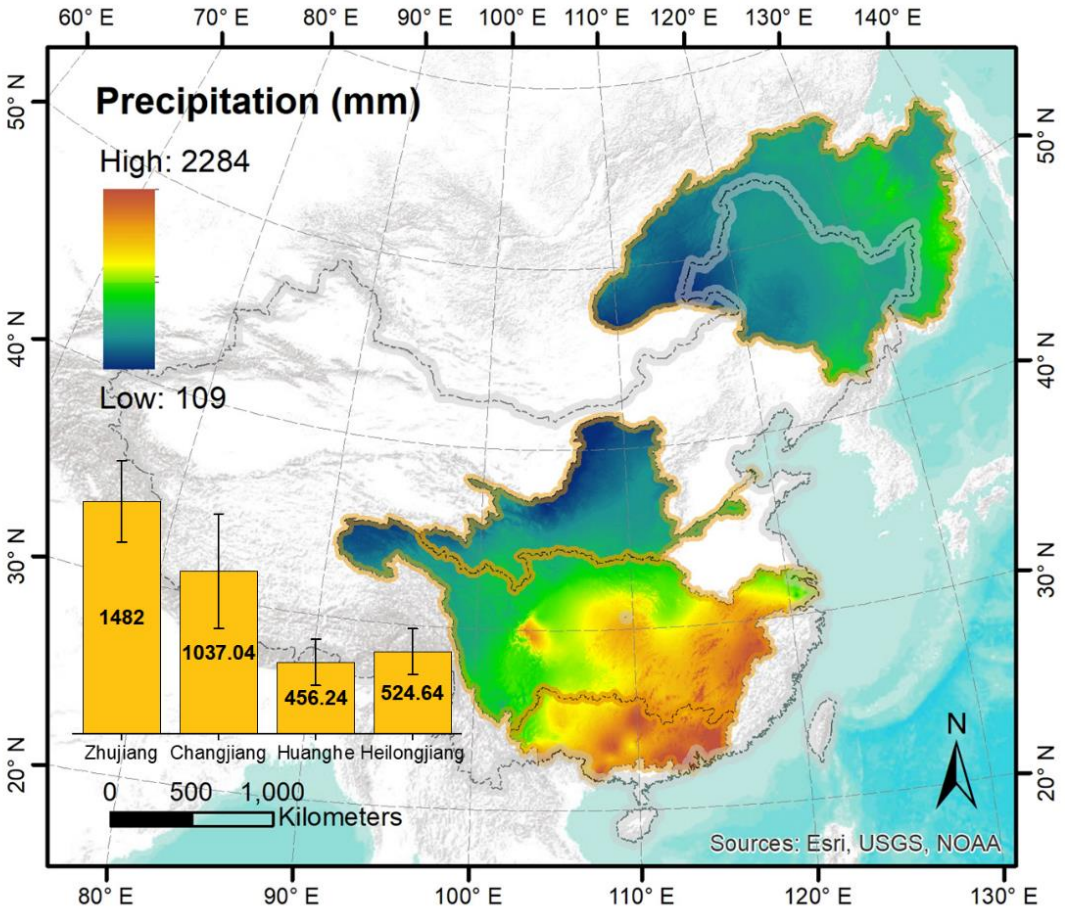

Fig. 4 Mean annual precipitation of the four largest rivers in China (MAP is extracted from the WorldClim 2 database by Fick and Hijmans, 2017).

The Zhujiang drainage basin is strongly affected by East Asian and South Asian monsoons, with 80% of annual precipitation occurring in the wet season from April to October, and 60% from June to September. Vegetation types of the drainage basin are evergreen monsoon rainforests, broad-leaf forests, and grassland, some forests have

been transformed into grasslands and farmlands due to the strong regulation of anthropogenic activities (Liu et al., 2017).

The Changjiang drainage basin is strongly affected by the humid sub-tropical Asian monsoon climate. Generally, the upper basin is subject to the Indian Summer Monsoon, while the mid-lower basin is dominated by the East Asian Summer Monsoon. At present, more than 70% of annual water discharge occurs from May to October, and mostly reaches the highest in July. The MAP is around 1,037 mm for the entire river basin; however, it varies a lot spatially showing an eastward decreasing trend of from over 2,000 mm/yr in eastern Yangtze Plain to less than 400 mm/yr in the western Qinghai-Tibet Plateau.

The Huanghe drainage basin spans the entire arid and semi-arid region of northern China in the upper and middle reaches as well as humid regions in the lower reaches, with MAP (from 1950 to 2000) of 368 mm, 530 mm, and 670 mm, respectively (Wang et al., 2007). Under the control of the East Asian summer and winter monsoon circulations, the vegetation is dominated by shrubs and grasses of both C3 and C4 plants (Liu and Ding, 1998; Liu et al., 2005). The rainy season (June to September) contributes 85% of the annual precipitation, resulting in the highest water discharge and sediment load (Wang et al., 2007). On the Loess Plateau, modern vegetation in the south-eastern region is dominated by C_3 trees and C_4 grasses, with MAT and MAP decreasing northwestwards, the proportion of C_3 trees and C_4 grasses decreasing.

The Heilongjiang drainage basin is strongly influenced by the seasonally alternating Asian monsoon. The strong Asian summer monsoon associated with anomalous cyclonic circulation over Eurasia strengthens the summer flux convergence at an interannual time scale, resulting in an anomalously large discharge in autumn (Tachibana et al., 2008). The strong Asian winter monsoon wind with a dry air mass, associated with the anomalously strong Siberian high and Aleutian low, activates evaporation, resulting in anomalously large flux divergence in autumn through winter and anomalously small discharge in spring (Tachibana et al., 2008). The rainy season (July to September) contributes nearly 80% of the annual precipitation. Taiga forest regions dominate the vegetation coverage in HLJ.

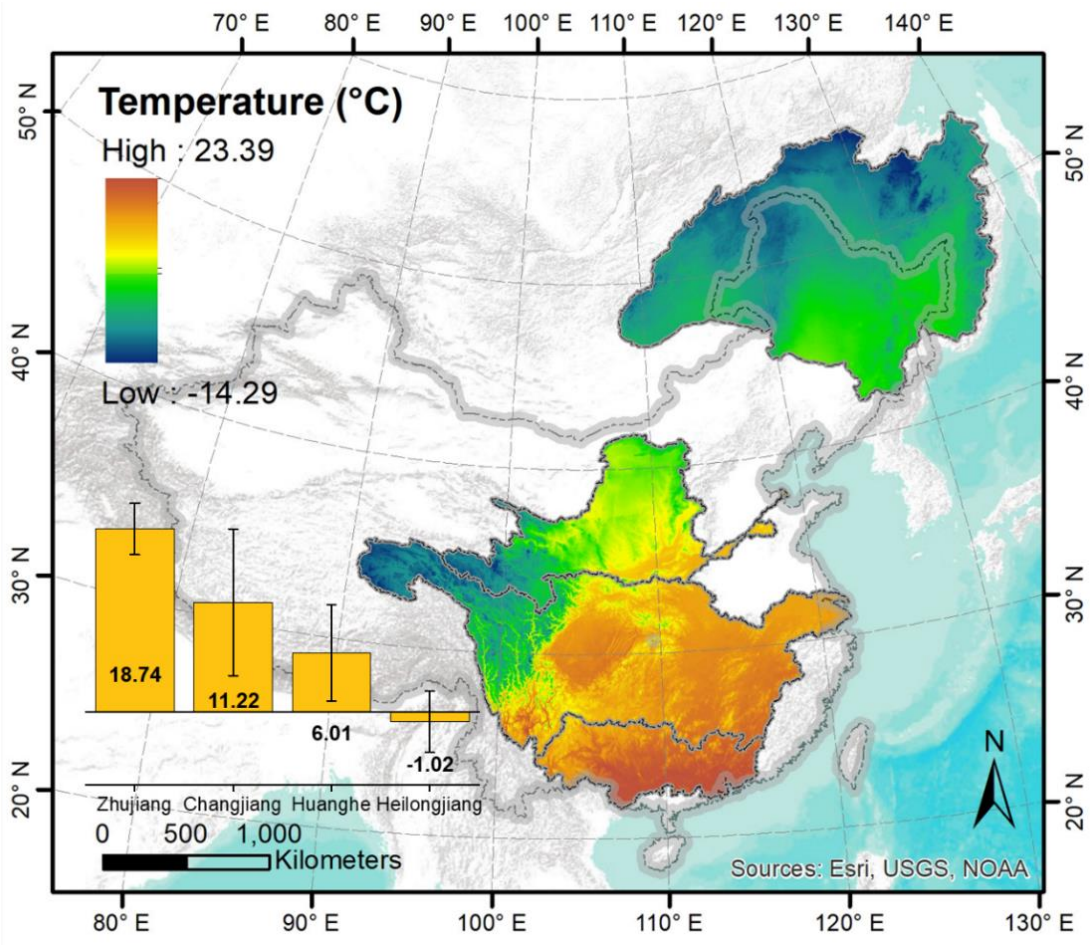

Fig. 5 Mean annual temperature of the four largest rivers in China (MAT is extracted from the WorldClim 2 database by Fick and Hijmans, 2017).

1.1.3 Geomorphic features

China's terrain can be generally characterized by three steps, including the 1st ladder with an elevation over 4,000 m at the Qinghai-Tibet Plateau, the 2nd ladder with elevation in a range from 1,000 to 2,000 m involving the Loess Plateau, the Inner Mongolia Plateau, and the Yungui Plateau, etc., and the 3rd ladder with elevation less than 500 m above sea level consisting of plains and hills. CJ and HH span three ladders while ZJ and HLJ only cross the 2nd and 3rd ladders (Figure 6).

The ZJ drainage basin is covered by 94.5% hill and mountainous regions, with the elevation decreasing southeastwards, and the rest 5.5% are the dispersedly distributed small plains. For CJ, its upper reaches are characterized by high relief and steep slopes incising deeply through high mountainous regions with a sharp decrease of elevation. Then with the joining of Minjiang, Tuojiang, and Jialingjiang rivers that are flowing

through the high-mountainous areas of steep terrains resulting in strong hydrodynamic and incision. The upper reaches are where the tectonic and fault activity is very active, inducing frequent earthquakes that trigger landslides and rockfalls to provide materials to riverine sediments (Jin et al., 2016). River water enters the hill and plain regions in the middle and lower reaches, where there are extensive floodplains and two big lakes, namely, the Dongting Lake and the Poyang Lake. As for HH, it starts at northeastern Qinghai-Tibet Plateau, then goes through the Loess Plateau, finally passes the North China Plain. The Loess Plateau serves as the long-term major net supplier to HH (Stevens et al., 2013). The erodible deposited loess-paleosols (formed spanning from modern to 2.58 Myr), accumulating a thickness from a few meters to more than 500 meters with an average of 100 m, and the underlying Cretaceous sedimentary rocks are continuously incised by the mainstem and tributaries, together contributing more than 90% materials to the riverine sediments (Shi and Shao, 2000; Wang and Fu et al., 2016). Even though HLJ is of low relief and gentle slopes, mountain ranges, ridges, foothills, and plateaus cover two-thirds of the region. Three wide and parallel bands of mountain ranges cross the drainage basin in a nearly north-south direction. The Great Hinggan Range spans the upper reaches, the small Hinggan and Bureya Ranges cross the center and the Sikhotw-Alin Range in the lower reaches. Plains are also extensive, mainly at lower HLJ and confluence of HLJ with SHJ and Ussuri. The SHJ drainage basin is mostly covered by the Northeast China Plain.

Loss of terrestrial materials presents very contrasted intensity among the four large river basins. According to the summarization by the Food and Agriculture Organization of the United Nations (FAO, 2016), the HLJ drainage basin has a sediment yield of 28 t/km^2/yr, while HH has a sediment yield of 1,400 t/km^2/yr (Figure 6A). Without considering sediments trapped, deposited, or redirected in the river system, the physical erosion rate is calculated by dividing the mean annual sediment flux by the total drainage basin. From 1953 to 1962, the physical erosion rate (sediment yield) of the four large river basins span three orders of magnitude, with the most intensive erosion (1591.9 t/km^2/yr) happening in HH, and followed by CJ (260.4 t/km^2/yr), ZJ (168.8 t/km^2/yr), and SHJ (24.9 t/km^2/yr). However, in the present (from 2008 to 2017), there is a rapid decrease in the other three large river basins except in SHJ (Figure 6B).

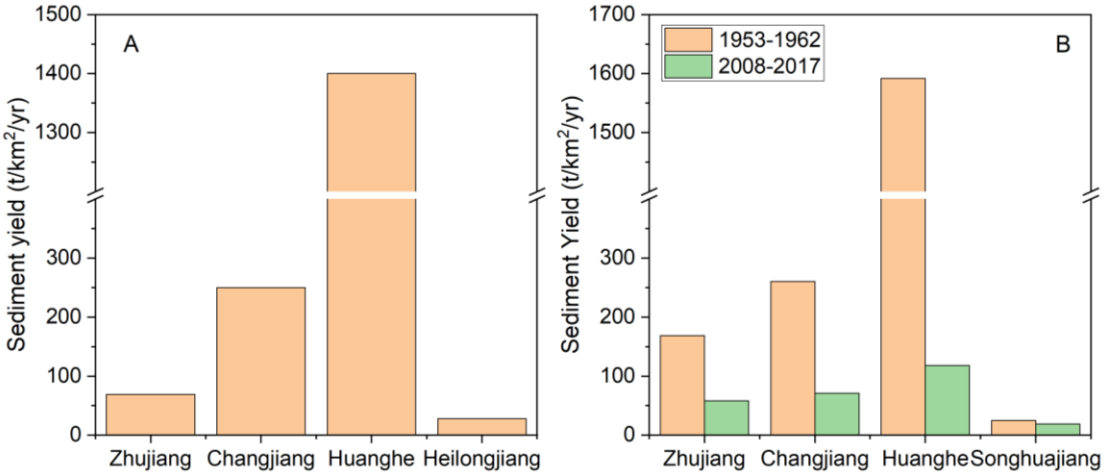

Fig. 6 Sediment yield of the four largest rivers in China. A, data is from FAO (2016); B, data is from MWRC, yellow columns represent the mean sediment yield from 1953 to 1962, and green columns are the mean sediment yield from 2008 to 2017.

1.1.4 Lithological Formation and Tectonic Settings

A general overview of the lithological formation of the four large rivers is shown in Figure 7, and the summarization of the proportion of each lithology is presented in Table. 1 in detail. Four large river drainage basin spans a vast area that exhibits complicated heterogeneous lithology characteristics.

The ZJ drainage basin is dominated by carbonate sedimentary rocks, covering around 35.8% of the entire basin, with great abundance in the upper and middle reaches of the Xijiang River. Siliciclastic sedimentary rocks are also widely distributed in the upper reaches and the Dongjiang drainage basin, while unconsolidated sediments such as Quaternary fluvial sediments are abundant in the fluvial plains of the middle and lower reaches, where is also abundant with igneous rock outcrops. The CJ drainage basin is characterized by various tectonic settings, from ongoing uplift Longmenshan in the upper reaches to the stable Yangtze Craton in the middle and lower reaches. The drainage basin is dominated by sedimentary rocks, covering around 72% of the total area, the lithologies are characterized by silicates, carbonates, and alluvial deposits from Precambrian to Quaternary in age. Metamorphic and plutonic rocks are sporadically distributed. In general, over 80% of the rock outcrops are sedimentary rocks in the upper reaches. In the JSJ drainage basin, siliciclastic sedimentary rocks are widely distributed (covering proportion is approximately 46.6%), while the carbonate sedimentary rocks (13.9%) are mainly distributed in the source regions and southern

parts, while in the mid-lower reaches such as at Datong, the fluvial unconsolidated sediments cover 41.7% of the watershed. The HH drainage basin is in the North China craton and bounded by several mountain belts, 46% of the watershed is covered by sedimentary rock outcrops (consist of the dominated siliciclastic and the minor carbonate), and 45% by unconsolidated sediments (mainly Quaternary loess deposits) as well as the remaining diverse lithological units including metamorphic, plutonic and volcanic rocks formed from Archean to Tertiary. The HHJ drainage basin is mainly covered by plutonic (24.5%), unconsolidated sediments (24.5%), and siliciclastic sedimentary rocks (16.6%). The unconsolidated Quaternary alluvial deposits cover 35.4% of the SHJ drainage basin.

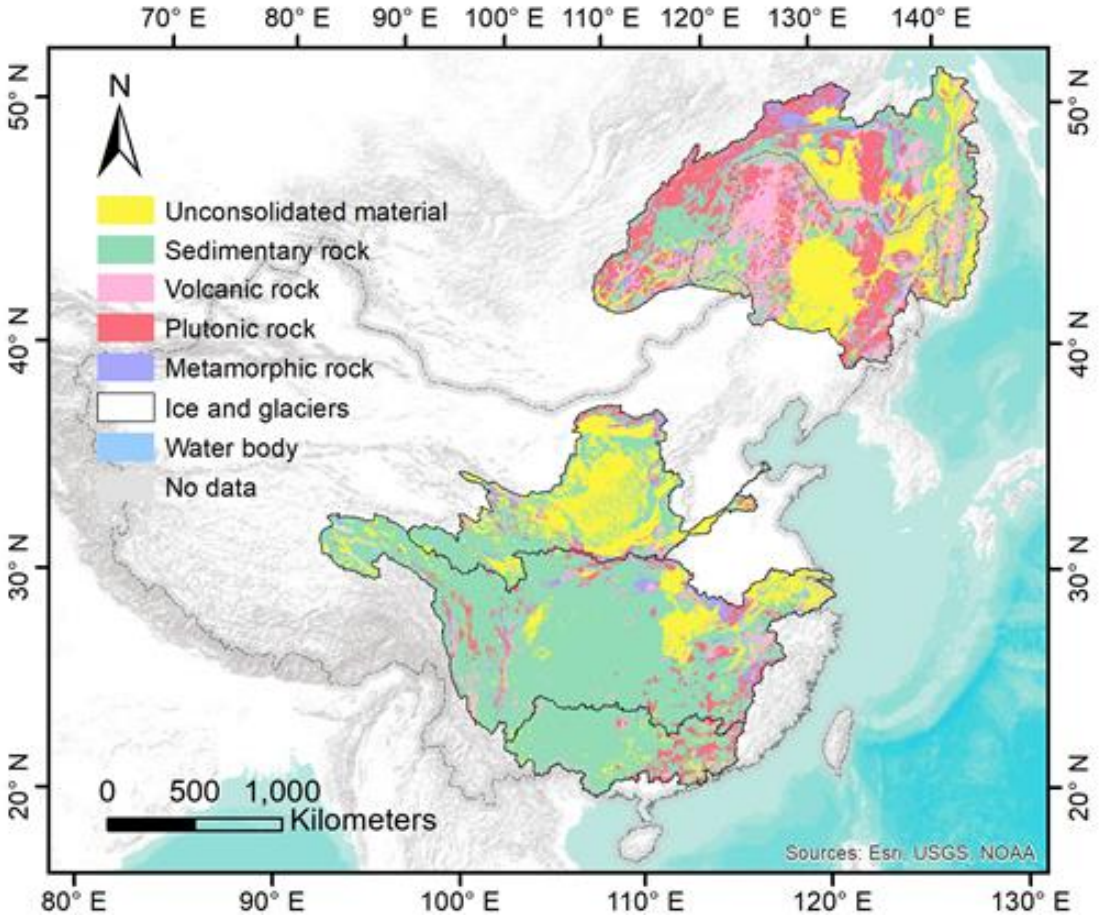

Fig. 7 Lithological map of the four largest rivers in China (data are from the GLiM v1.1 database by Hartmann and Mossdorf, 2012).

Table 1 Lithological proportions in the four largest rivers in China, the geometric calculation was performed in ArcGIS 10.3 environment based on Global Lithological Map provided by Hartmann and Mossdorf (2012).

Lithology/Proportion %	Zhujiang	Changjiang	Huanghe	Heilongjiang
Unconsolidated Sediments (SU)	4.85	11.90	44.68	24.49
Sedimentary rock	78.04	71.94	45.85	26.35
Volcanic Rocks	2.05	2.00	1.89	13.57
Plutonic Rocks	13.95	9.43	4.14	28.78
Metamorphic rock	0.76	3.09	2.90	6.33
Ice and Glaciers		0.08	0.02	
Waterbody	0.33	1.15	0.34	0.08
No data		0.41	0.19	0.41

1.1.5 Soil Organic Carbon Variation

Soils are thought to regulate overall terrestrial ecosystem carbon storage due to their large organic carbon stocks and potential to stabilize carbon on a range of timescales (Carvalhais et al., 2014; Bloom et al., 2016). The capacity of rivers to mobilize and transport particulate organic carbon is controlled by the physical erosion rate (Galy et al., 2015). Soils are easily eroded and mobilized to the rivers, serving as the main net supplier of riverine SPMs delivered into the sea. Thus, it is very important to look into the soil organic carbon storage of the four case large drainage basins (Figure 8).

Among the four large rivers, the HLJ drainage basin is the most organic carbon enriched in soils (depth within 30 cm), which is the most abundant in the northern basin that is influenced by the Siberian permafrost, and the most depleted in the basin center and boundary regions of the SHJ drainage basin. The mean soil organic carbon storage is 78.21 ± 86.78 Mg/ha in HLJ, and is equivalent between CJ (47.15 ± 43.04 Mg/ha) and ZJ (47.95 ± 41.73 Mg/ha), is the least in HH (38.91 ± 25.48 Mg/ha). HH has the largest soil organic carbon storage in the upper reaches that are on the Qinghai-Tibet Plateau, and the smallest in the area covered by eolian loess deposits. The northern part of the CJ drainage basin that is near the Loess Plateau is also depleted in organic carbon, while in the rest of that are mainly covered by mountainous and plain regions, organic carbon is relatively more enriched. The ZJ has the most depleted organic carbon in the southern parts where the urbanization is the most developed, showing contrasted storage properties between the south and north flanks of the main channel. However, the soil organic carbon storage data extracted in this section might not be able to provide very precise information to reflect the real situation in the drainage basin, because the

simulation and calculation are also limited by the number of soil depth profiles.

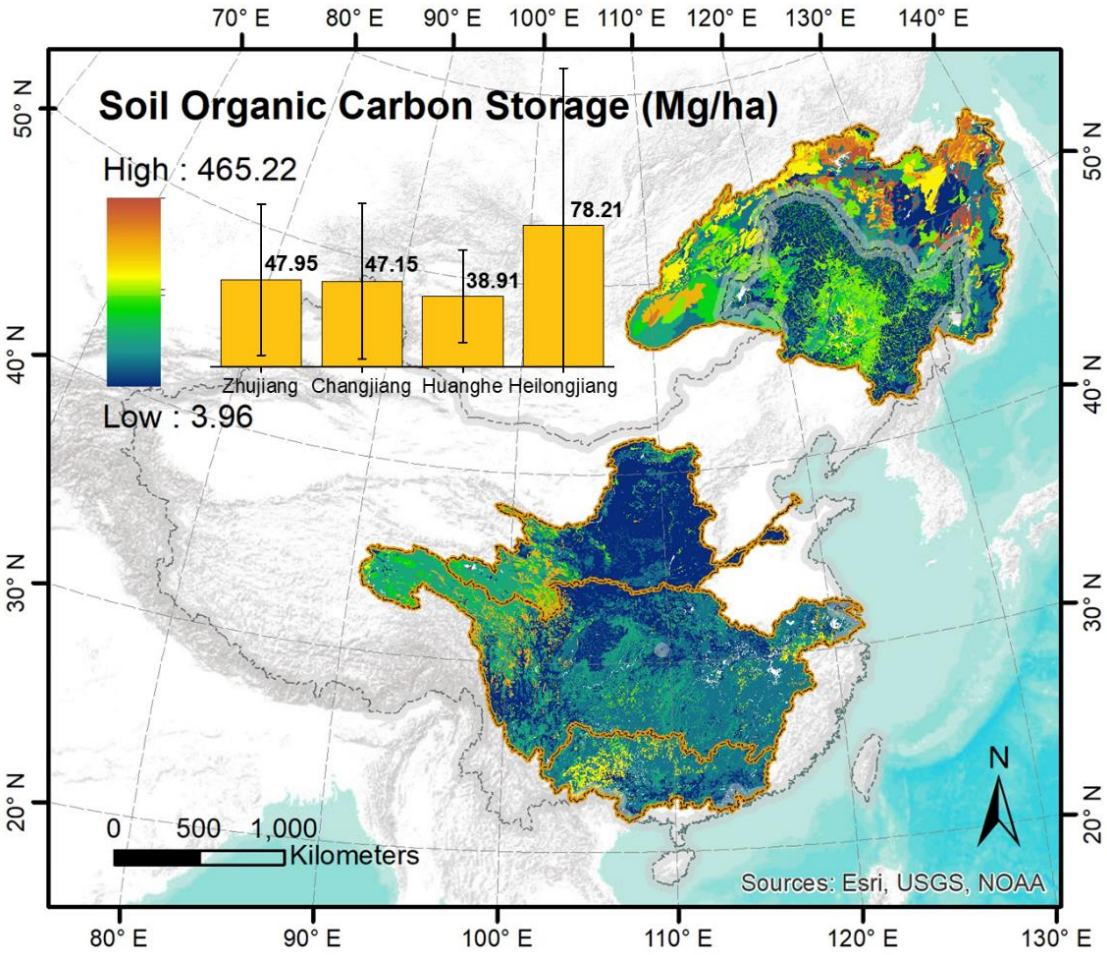

Fig. 8 Soil organic carbon storage (within top 30 cm soil depth) of the four largest rivers in China (Data is extracted from Global Soil Organic Carbon Estimates raster layer in a resolution of 30 arc seconds constructed by Hiederer and Köchy, 2011).

1.2 Sediment sampling strategy

During sediment sampling from 2015 to 2018 in the four largest rivers in China (Figure 9), we collected suspended sediments using three different ways, transect multiple depth-profile sampling, individual depth-profile sampling, and channel surface (depth in 0.5 m) sampling (Figure 9). At the same time, bank and bed sediments were collected. Some sampling sites are absent of bed sediment samples due to the unavailability of sediment grabber. The full sampling information is shown as follows with details in Section 3:

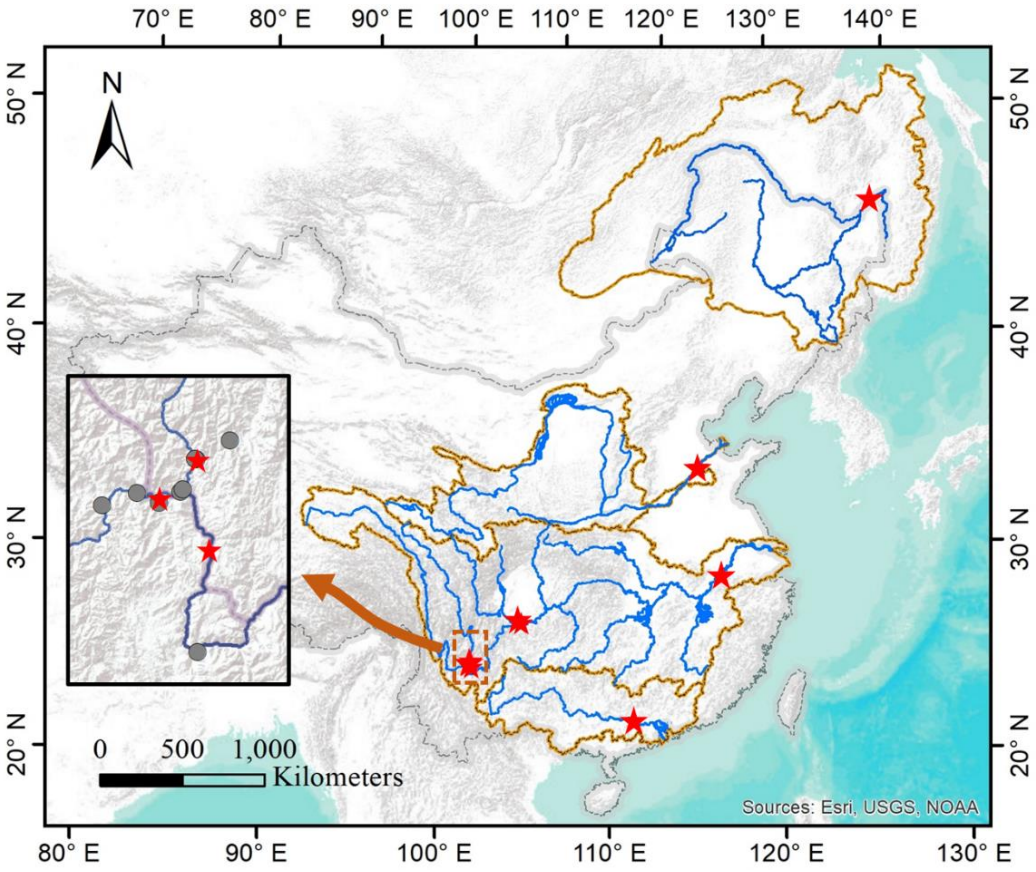

Fig. 9 Sampling scheme of sediment collection in the four largest rivers in China. Areas marked by dark yellow represent the catchment coverage of Zhujiang, Changjiang, Huanghe, and Heilongjiang from south to north, respectively. The blue lines are the river networks in China. The red stars show where the depth profiles were sampled, and the grey dots are the locations for sampling at the channel surface, time-series sampling at the surface was carried out at where the depth profiles were sampled, which is Xitan of Zhujiang, Yibin of Changjiang, and Fuyuan of Heilongjiang.

Changjiang (Yangtze River): Surface samples were collected upstream of CJ, which is the Jinshajiang River and its tributaries. 3 transect depth-profile samplings were performed at Panzhihua [3, 4] in September 2017 (JSJ), at Nanxi [3, 3, 3] in August 2016 (middle stream of Changjiang), and at Datong [5, 6, 6] in August 2017 (lower stream of CJ, near river mouth). Meanwhile, Nanxi is where one-year monthly time-series surface SPMs were collected from August 2016 to July 2017. Another three depth profiles were collected in the Jinshajiang River before the confluence with the Yalong River and in the Anning River during two rain events in September 2017.

Huanghe (Yellow River): The transect depth-profile sampling was near Luokou

Gauging station at Jibei [3, 3, 2, 1, 1] in July 2016. Two monthly SPM samples were collected at the channel surface to retrieve very fine materials in May 2017 and June 2017 before flooding.

Zhujiang (Pearl River): One-year monthly time-series surface SPMs were collected at Makou (near the river mouth) from July 2015 to June 2016. The transect depth-profile sampling was carried in August 2016 at Shapu, a total of 18 SPM samples were collected in a matrix [3, 4, 5, 4, 2], showing samples collected from the left flank to the right flank in each depth profile following the flowing direction, hereinafter. Except for one sample site at Beijiang, the rest sediments were all collected at Xijiang.

Heilongjiang (Amur River): The sampling expeditions could only be performed in part of the HLJ that belongs to Chinese territory. The transect depth-profile was performed in July 2016 at Fuyuan [3, 4], and is located after the confluence with SHR; another two depth profiles were collected in the middle of the river in December 2016 and October 2018 at the same place, where one-year monthly time-series surface SPMs from July 2016 to July 2017 were collected. Surface SPMs before the confluence with SHR and tributaries (Hailaer River, Ussuri River, etc.) were sampled, with a special focus on SHR and its tributaries in October 2018, a depth profile was collected in SHR at Harbin in the middle.

In general, an Acoustic Doppler Current Profiler (ADCP) was employed before sampling to characterize river bathymetry and access the water velocity profiles. In this way, the depth information and instantaneous water discharge were obtained. According to the ADCP profile, the number of profiles and samples per profile was determined based on the river turbidity. For each river cross-section, either a multiple depth-profile sampling or a single depth-profile sampling was realized, depending on the spatial variability of the water velocity (Figure 10). The sampling device is equipped with a 10 L Van Dorn type stratified sampler mounted on an orientation plummet in the flow direction, and a 50kg fish lead to facilitate its immersion and resistance to the force of the water flow. The whole system is attached to a winch fixed on a boat. The sampler is opened and immersed at the depth of interest and is closed via a 'messenger' on the rope (Figure 11). Afterward, the sampler was retrieved back to the boat and the collected samples are transferred to 10 L pre-cleaned bottles. Before each sampling at the depth of interest and during the process of transfer, the sampler is cleaned and rinsed several times with a squeeze bottle filled with river water to ensure that all the particles

have been collected and to avoid possible cross-contamination. In some cases, due to the absence or malfunction of ADCP due to the high turbidity, water velocity was measured using a current meter attached to the sampling device (Figure 11). In general, to obtain enough SPM for all the analyses, from 30 to 40 L river water was collected for each sample, and then weighed before conducting filtration using a peristaltic pump using Millipore 0.22 μm cellulose acetate, 142 mm membrane within 24 hours after collection. In each sampling, pH value, dissolved oxygen (DO), electrical conductivity (EC), and temperature (T) for river water were measured simultaneously.

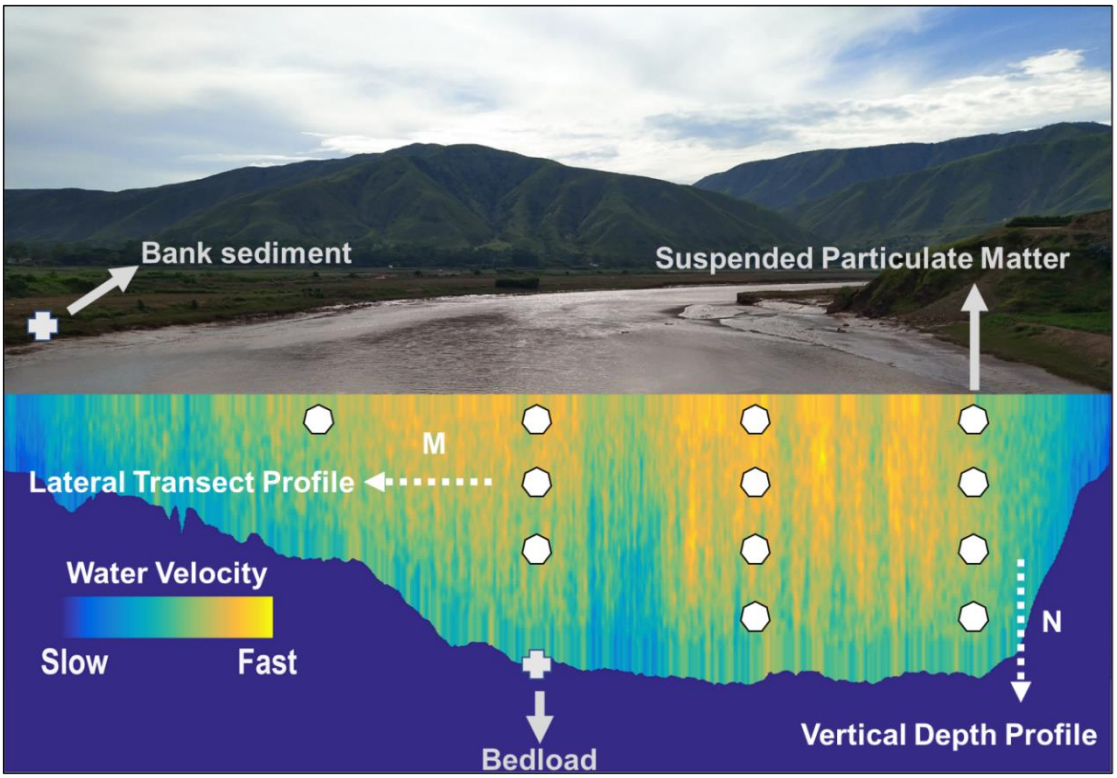

Fig. 10 Sketch of sediment sampling scheme, the river transect profile shows the water velocity distribution, N denotes sampling number in vertical depth profiles, and M denotes profile number in the lateral direction. In this regard, concerning suspended particulate matter (SPM) sampling, there are three ways, surface SPM sampling when both N and M equal to 1; single depth profile SPM sampling when N is larger than 3 and M equals to 1; multiple depth profile SPM sampling when N and M are not less than 2. Bedload (bed sediment) was collected using a sediment grabber, and bank sediment was collected at the river flank merged by shallow river water.

Concerning the storage and transfer of sediments, filter membranes with collected sediments were freeze-dried after being taken back from the field. Then the membranes

were moistened and washed by adding the corresponding filtered water, a nanoparticle brush was used to scrape and transfer the SPM into a 50 ml centrifuge tube. Afterward, another freeze-drying process was performed until completely dry. Each SPM sample was divided into two heterogeneous parts, one aliquot was used for the analysis of particle size distribution, and the remaining was crushed to 200 meshes in an agate mortar with a pestle for other elemental and isotopic geochemistry.

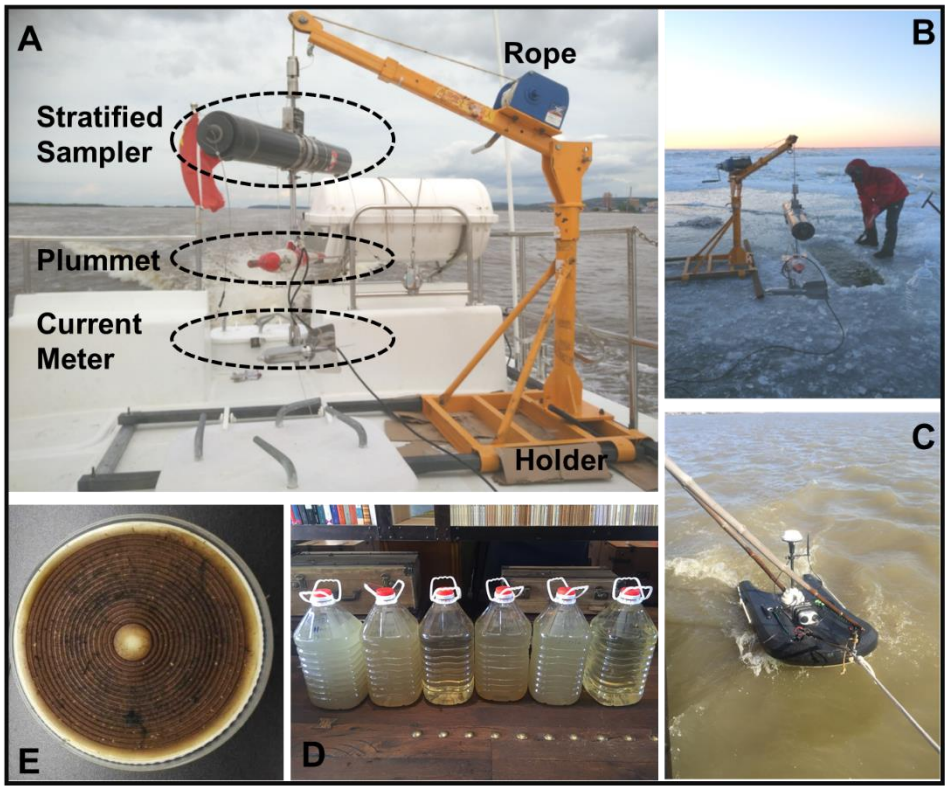

Fig. 11 River sediment sampling equipment. A, depth profile sampler install on a boat; B, winter (December 2016) sampling expedition in Heilongjiang River at Fuyuan, snow and ice samples were collected simultaneously; C, an ADCP survey on transect profile of the Songhua River at Jiamusi; D, some collected river water samples in October expedition in Songhuajiang and its tributaries; E, SPM stayed on a Teflon filtering membrane.

2. Elemental and isotopic chemistry

This section presents the sample pretreatment scheme prior to organic and inorganic composition analysis, and the detailed measurement procedures that were adopted to accurately acquire the carbon, nitrogen, and oxygen chemistry.

2.1 Organic carbon analysis

2.1.1 Removal of inorganic carbon (IC)

To remove the IC/carbonate composition from sediment, hydrochloric acid (HCl) was used based on two different techniques, vaporous acid fumigation, and liquid acid leaching. We performed the former technique to pretreat sediments collected in Zhujiang, Changjiang, and Huanghe River, and the latter one on sediments collected in Heilongjiang River. All sediment samples were mechanically ground and mixed into homogenized powder using an agate mortar with a pestle before acidification.

Vaporous acid fumigation. Ground homogenized samples were acidified with 12M HCl fumes in a closed Teflon tank under 60 °C for 48 hours to remove the carbonate fraction (Komada et al., 2008), and then were dried under a pumping vacuum line prior to analysis. Sediment samples were loaded either in silver (Ag) capsules for stable isotope analysis or in Pyrex mini tubes for radiocarbon analysis. Ag capsules were pre-combusted for 2.5 hours at 550 °C to remove any extraneous OC contamination (Welte et al., 2018), then the loaded capsules were held by a homemade 16-position Teflon plate. Pyrex mini tubes were rinsed with 0.1 M HCl solution, then were cleaned using pure ethanol and distilled water, subsequently, were put into a 500 °C furnace for over 12 hours. It is worthy to point out that silver capsules are very fragile after high-temperature combustion and concentrated HCl fumigation, therefore, we used another Tin capsule to package a fumigated silver capsule. Besides, there would be massive chlorides in carbonate-rich sediments after acid fumigation, especially the generation of calcium chloride, absorbing water from the atmosphere, and wetting the de-carbonated samples. In this case, we prefer to prepare the acid-processed samples within 24 hours before the analysis and store them using a microtiter at a dry and dust-free environment using an ADS (Air Dépoussiéré Stérile Laminaire) container.

Liquid acid leaching. To remove any existence of carbonate before OC analysis on samples collected from the Heilongjiang River, we adopted the acid leaching with the carbonate removal reaction carried out in a Tin capsule. We started by evaluating the relative compositions of inorganic carbon and organic carbon in the sediment based on $\delta^{13}C$ of the total carbon, considering it is a binary mixing of terrestrial OC and IC. We arbitrarily used -30‰ for $\delta^{13}C$ of terrestrial OC because C3 plants are dominant species in the Heilongjiang River basin; and we took 0‰, the average $\delta^{13}C$ value for sedimentary IC (Sharp, 2017), as the IC for endmember in our estimation. Afterward,

the highest possible content of IC was considered to acquire the corresponding volume of diluted 1M HCl solution to get rid of it. To make sure the decarbonization is sufficient and complete, another 4 times more equivalent 1M HCl solution was added into the Tn capsules in a microtiter. The leaching decarbonization process was performed at room temperature (25 °C) for at least 8 hours and the subsequent drying was conducted at 50 °C oven environment for more than 24 hours. The fragility of the Tin capsules was unavoidable, another Tin capsule would be used to package the processed one. Then the decarbonated samples were kept in a microtiter and stored in the ADS container. This treatment technique to sediment sample would allow us to keep all the OC without losing any fraction of labile organic compounds (private communication with Christine Hatte at LSCE).

2.1.2 Element and stable isotope analysis of carbon and nitrogen

The determination of CN and the stable isotopes were performed on an Organic Elemental Analyser (OEA, Thermo Scientific Flash 2000) coupled with Isotope Ratio Mass Spectrometry (IRMS, Thermo Scientific Delta V Advantage) under continuous flow mode at the Laboratoire Géosciences Paris Saclay (GEOPS), Orsay, France. The measured aliquots of each sample were weighed and encapsulated and placed inside the MAS 200R autosampler (a 32-position tray), and then dropped into a combustion/reduction quartz reactor kept at a temperature of 950 °C. The exact amount of oxygen required for an optimum sample is delivered into the combustion reactor at a precise time. The reaction of Oxygen with the Tin capsule at elevated temperature generates an exothermic reaction which raises the temperature to 1800 °C for a few seconds. At this high temperature, both organic and inorganic substances encapsulated by either Ag or Tin capsules are efficiently converted into elemental gases which, after further reduction, are separated in a chromatographic column and finally detected by a highly sensitive thermal conductivity detector (TCD), weight percentage of Carbon and Nitrogen are obtained. Afterward, elemental gases go through the continuous flow interface (CFI) and are finally detected by the IRMS to get the stable isotope ratios for Carbon and Nitrogen. stable isotope ratios of carbon and nitrogen are expressed as $\delta^{13}C$ and $\delta^{15}N$, respectively, which are defined as:

$$\delta^{13}\mathrm{C}\ (\text{in } ‰) = \left[\frac{(^{13}\mathrm{C}/^{12}\mathrm{C})_{sample}}{(^{13}\mathrm{C}/^{12}\mathrm{C})_{standard}} - 1\right] * 1000$$

and

$$\delta^{15}\mathrm{N}\ (\text{in}\ ‰) = \left[\frac{(^{13}\mathrm{N}/^{12}\mathrm{N})_{sample}}{(^{13}\mathrm{N}/^{12}\mathrm{N})_{standard}} - 1\right] * 1000$$

reported relative to the Pee Dee Belemnite (VPDB) and air (AIR) respectively (Coplen, 1995).

Subjected to the blank subtraction by linearity test, two international standards including USGS-40 and IAEA-600 as well as an internal standard (GG-IPG) were used to build linear regression equations to calibrate the elemental and isotopic values for both carbon and nitrogen (Table 2). In general, for each sample, we prepared two to three aliquots for both untreated and acidified sediment based on its mass size. Thus, we obtained the weight percentage of total carbon (TC %), particulate organic carbon (POC %), total nitrogen (TN %), and particulate organic nitrogen (PON %), meanwhile, we got the corresponding isotopic values. The estimated weight percentage of particulate inorganic carbon (PIC %) was acquired by subtracting POC from TC, however, this value will be slightly higher than the real PIC % of the sediments that were acidified using vaporous HCl fumigation because it incorporates the content of thermal labile OC.

Table 2 Overview of standards for POC elemental and stable isotope analysis

Name	C (%)	δ^{13}C (‰)	N (%)	δ^{15}N (‰)
USGS-40	40.816	-26.389	9.524	-4.52
IAEA-600	49.484	-27.771	28.866	1.00
GG-IPG	59.890	-23.220	7.880	10.02

2.2 Radiocarbon analysis

The compact AMS (accelerator mass spectrometer) systems equipped with hybrid ion sources (MICADAS, MIni CArbon DAting System) realized the measurement of small (less than 100 µg C) and ultra-small (less than 25 µg C) samples, which is allowed to perform ^{14}C analysis on samples containing less than 10 µg C (Wacker et al., 2010a, 2013). All ^{14}C analysis was performed on the *ECHo*MICADAS system either by a gas ion source (GIS) interface (GIS-AMS) or by the coupling of an elemental analyzer (EA) to the GIS (EA-GIS-AMS) at the Laboratoire des Sciences du Climat et de l'Environnement (LSCE), Gif Sur Yvette, France (Figure 13). Regarding GIS-AMS ^{14}C analysis, carbon in the gas phase (CO_2) is delivered in Pyrex mini ampoules and then released in an automated ampoule cracker to the individual syringe, while for EA-GIS-

AMS, samples in solid-phase were used, the decarbonated sediment samples were encapsulated using Tin capsules to ensure their complete delivery to an EA for combustion. Encapsulated samples are loaded into the oxidation oven of the EA with an autosampler. The EA directs the gases through a water trap containing Sicapent (Merck, Germany) and through a zeolite trap which is later heated up stepwise by the EA to release N_2, CO_2, and residual gases at different temperatures. The outlet of the EA is connected to the GIS interface. The flow is directed to a second zeolite trap (zeolite X13, Sigma-Aldrich, Germany) located at the GIS. Consecutively, the GIS trap is heated up to 450 °C, the CO_2 is delivered into a syringe of known volume, the carbon amount is measured manometrically (Ruff et al., 2010; Salazar et al., 2015). In the gas handling system, a mixture of helium (He) and sample CO_2 was introduced into the GIS by the stepping-motor-driven syringe presses, allowing measurements to be continuous and stable (Wacker et al., 2013; Ruff et al., 2010; Salazar et al., 2015). Data reduction was performed using Bats software (version 4.07, Wacker et al., 2010b). The first few scans were routinely discarded to account for possible surface contamination of the target due to its contact with ambient air. Measurement parameters such as ^{12}C current and ^{13}CH current were checked. Time and isobar corrections were made prior to validation.

To prepare gas samples for GIS-AMS analysis, we used around 200 μg C that was stored in individually sealed Pyrex mini ampoules closed by a handheld torched flame on a vacuum line. OC must be converted into gas phase CO_2 prior to storage in mini ampoules. Subjected to the carbonate removal process, all decarbonated sediments were transferred to the quartz tubes correspondingly. A suitable amount of CuO was added and then silver wools were placed into the tubes. These loaded quartz tubes were purged of the atmosphere on a vacuum line before being sealed using an oxy-methane neutral flame and placed in a furnace at 900 °C to combust for 24 hours. All quartz tubes and CuO had been torched at 550 °C for 24 hours before this procedure. Aside from the blank PhA and standard NIST OX II gas in helium provided to the syringe by directly connecting gas bottles to the GIS used to do normalization, correction for fractionation and background corrections, untreated international standards including IAEA-C5, IAEA-C7, IAEA-C8, and blank PhA were prepared in different sizes to produce from 10 μg C to the equivalent amount of carbon as from OC fractions of sediment samples (blanks and standards are summarized in Table 4). For the preparation of analysis using

EA-GIS-AMS, the only difference with that of the GIS-AMS is all decarbonated sediments, standards, and blanks were prepared in the solid phase and wrapped up by Tin capsules. The constant contamination is approximately 0.5 μg C for the GIS-AMS and 0.8 μg C for the EA-GIS-AMS. The detailed method on the subtraction of constant contamination can be seen in Salazar et al. 2015, there are mainly two parts of contamination, including carbon mostly from Tin capsules as well as the remaining gas/memory effect from the last measured sample.

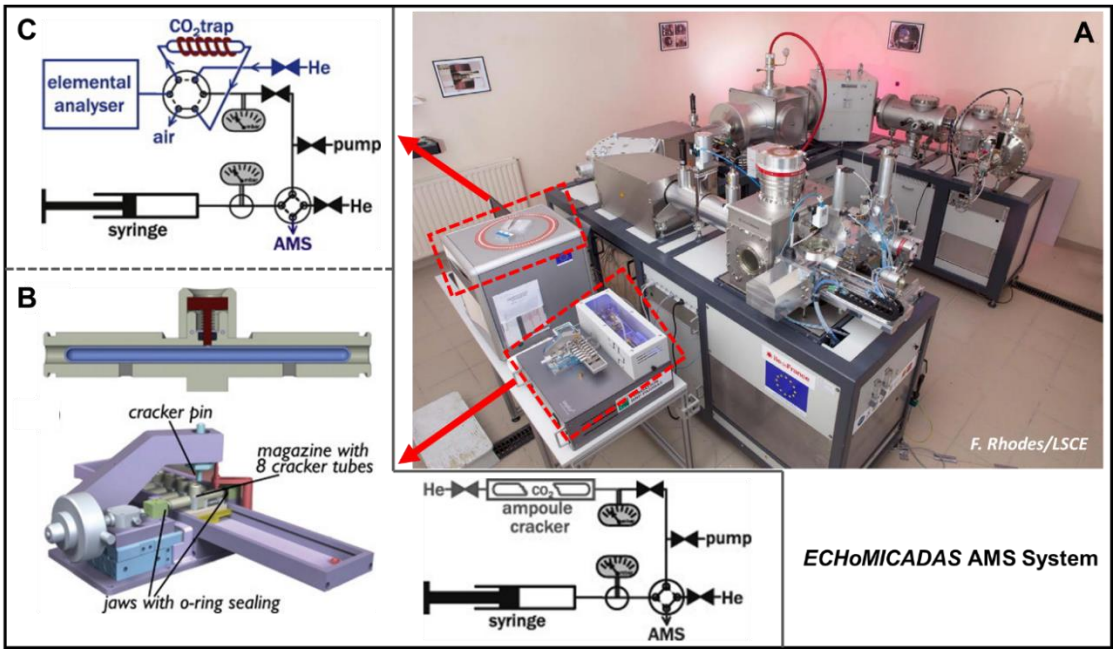

Figure 13 The ECHoMICADAS system at LSCE. A, an overview of the MICADAS system; B, the mini ampoule cracker and the GIS-AMS working procedure (Wacker et al., 2013); C, the EA-GIS-AMS working procedure (Wacker et al., 2013).

Fraction modern, $F^{14}C$ or F_m, is the deviation of a sample's ^{14}C atoms from that of the modern standard. $F^{14}C$ value is obtained and processed using Bats in the MICADAS AMS system through background corrections, blank subtraction, mass-fractionation correction, and standard normalization (Wacker et al., 2010b). The uncertainty is calculated by taking the ^{14}C counting statistic, the molecular correction, the variability of the blank contamination of the samples, and additional unassigned errors such as unstable measurement (Wacker et al., 2010b). Conventional Radiocarbon Ages (RCA) are quoted for standards as discussed by Stuiver and Polach (1977) using the Libby half-life of 5,568 years with the mean life of 8,033 for ^{14}C. RCA is expressed in units of years before present (BP), with year zero being 1950.

$$\mathrm{RCA} = -8{,}033 \ln (F^{14}\mathrm{C})$$

Δ^{14}C value, the relative difference between the absolute international standard (the base year 1950) and sample activity corrected for age and δ^{13}C (Stuiver and Polach, 1977), was reported as well. The calculation is defined as below.

$$\Delta^{14}\mathrm{C}\ (\text{in } ‰) = [F^{14}\mathrm{C} * exp\left(\frac{1950 - yr}{8267}\right) - 1] * 1000$$

Where *yr* is the collection year of the sample, 8267 is the true mean life of ^{14}C using the Cambridge half-life of 5,730 years.

Table 4 Overview of standards and blanks for radiocarbon analysis.

a. Standards from the International Atomic Energy Agency (IAEA);

Name	Material	Nature	Nominal value ($F^{14}C$)	Sample type
PhA	Phthalic acid	OC	0	Blank
NIST-OX II	Oxalic acid	OC	1.3407 ± 0.0005	Primary standard
IAEA-C5	Wood	OC	0.2305 ± 0.0002	Secondary standard[a]
IAEA-C7	Oxalic acid	OC	0.4953 ± 0.0012	Secondary standard[a]
IAEA-C8	Oxalic acid	OC	0.1503 ± 0.0007	Secondary standard[a]

2.3 Major and trace element composition analysis

The chemical composition was measured at the Centre de Recherches Pétrographiques et Géochimiques (CRPG), Vandoeuvre-lès-Nancy, France, using inductively coupled plasma optical emission spectrometry (ICP-OES) for major elements with typical uncertainties of 3% and inductively coupled plasma mass spectrometry (ICP-MS) for trace elements with typical uncertainties less than 10%.

2.4 Particle size analysis for sediments

All particle size analyses were performed on the Laser Diffraction Particle Size Analyzer (Beckman Coulter LS-12 320) at the École Normale Supérieure (ENS), Paris, France by measuring the pattern of light scattered by the particles in the sediment sample. The analyzer provides a dynamic range of 0.017 µm to 2000 µm based on PIDS (Polarization Intensity Differential Scattering) technology. Aliquots of untreated SPM were dispersed in deionized water, then ultrasonic pretreatment on the aliquot with an add-in of 0.5% sodium hexametaphosphate (SHMP) solution was used. Before

measuring the particle size distribution (PSD), the following procedures should be executed: 1) Rinse to avoid possible contamination, 2) De-bubble the suspending fluids to eliminate any air bubbles, 3) Measure and subtract the offset voltage from the scattering signal from the sample to accurately measure the light intensity, 4) Align the laser beam to the center of the detector array, 4) measure background to eliminate any interior particulate interference, 5) measure loading to add a suitable amount to get an acceptable signal-to-noise level in the detector channels with PIDS obscuration over 70% and diffraction obscuration over 8%. For each sediment sample, we made three sub-measurement and average particle size parameters (D90, D50 in μm, the portions of particles with diameters smaller and larger than this value are 90% and 50%, respectively), the uncertainty is better than 2%.

3. Flux calculation

Instantaneous depth-integrated fluxes of SPM and POC sources are calculated over the cross-section using a method developed by Lupker et al. (2011) and Bouchez et al. (2011a, b), this method is using the SPM concentration variation law in different size fractions along with the depth profiles based on the Rouse model (Rouse, 1950). In general. in the sampling expeditions, we used an acoustic Doppler current profiler (ADCP), a hydroacoustic current meter similar to a sonar, to measure water current velocities over a depth range using the Doppler effect of sound waves scattered back from particles within the water column at some depth-profile sampling sites. However, due to the malfunction or disability of applying an ADCP, we only used a current meter to measure the water velocity at different depths across a river transect. Based on the availability of ADCP velocities data, the integrated SPM and elemental and isotopic carbon fluxes across a river transect were calculated accordingly.

3.1 Modeling the distribution of water velocities in a river transect

In the absence of ADCP data, we used water velocity profiles measured with a current meter. After constructing a bathymetric profile of the river cross-section based on the depth profiles, the flow velocity distribution across the river transect was modeled by the so-called velocity-defect law (4) which assumes that the maximum flow velocity u_{max} takes place at the water surface is at $z=H$.

$$\frac{u_{max}-u}{u*} = -\frac{1}{\kappa} ln \frac{z}{H} \qquad (4)$$

where z is the height above the riverbed, H is the channel depth, u^* is the bottom shear velocity and κ is the von Karman's constant equal to 0.41.

Each velocity profile is fitted with the velocity-defect law and a pair of u_{max} and u^* values are estimated. Values of these two parameters are then linearly interpolated between profiles to model the water velocity distribution across the river section. For profiles where only one velocity data was measured, we assumed that the velocity was constant with depth.

To validate this method, we compared the water discharge measured at a gauging station or based on ADCP measurement with the value obtained by the integration over the river cross-section of the water velocity distribution measured by a current meter (Figure 14).

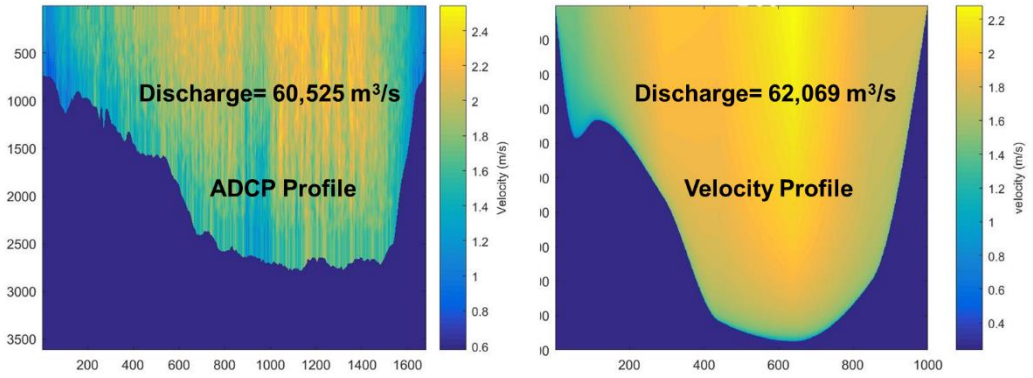

Figure 14 Velocity distributions based on ADCP data and modeled with the velocity-defect law across the Changjiang at Datong. The units of x and y axials represent the cell numbers, we adapted the x- and y- convert factor to calculate the real geometry (length and width of the channel) in the simulation, hereinafter.

We only have current velocity for the transect profile in Huanghe and Zhujiang, daily monitoring and average monthly water discharge were retrieved from the monitoring data of the adjacent gauge, which is Lijin in Huanghe and Gaoyao in Zhujiang, the data was provided by the Ministry of Water Resources of the People's Republic of China. The good agreement shows the accuracy of our method (Figure 15).

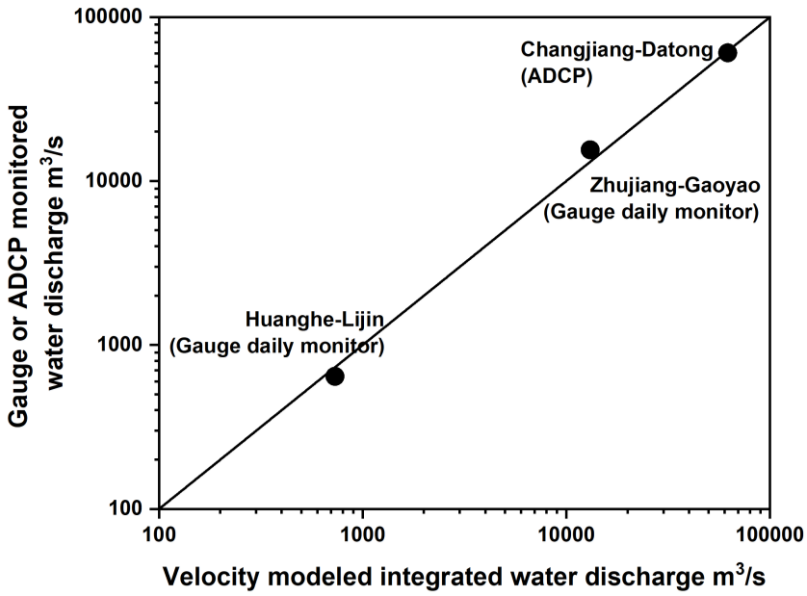

Fig. 15 Plot of velocity profile modeled integrated water discharge versus gauge monitored or ADCP simulated water discharge. The black line represents an ideal ratio of 1:1.

3.2 Modeling the distribution of the total SPM concentrations across a river transect and the concentration of SPM of different particle sizes

The distributions across a river transect of the total SPM concentrations as well as the concentrations of SPM of different grain sizes were modeled by the Rouse equation (5).

$$\frac{C(z)}{C(a)} = \left(\frac{H-z}{z} \times \frac{a}{H-a}\right)^{Z_R} \qquad (5)$$

where C is the total SPM concentration or the concentration of SPM of given grain size, z is the height above the river bed, a is a reference height above the river bed, here chosen equal to the height of the surface sampling point, H is the channel depth and Z_R is the Rouse number.

For each profile, the variations with a depth of the total SPM concentrations and the concentrations of SPM of different grain sizes are fitted with the Rouse equation to calculate a set of Rouse numbers for the total SPM concentrations and the different SPM grain sizes. Values of these parameters are then linearly interpolated between the profiles to model the distributions across the river transect of the total SPM concentrations and the concentrations of SPM of different grain sizes. Based on the distributions of the concentrations of SPM of different grain sizes, a mapping of the grain size distribution D90 across a river transect can be modeled (Figure 16).

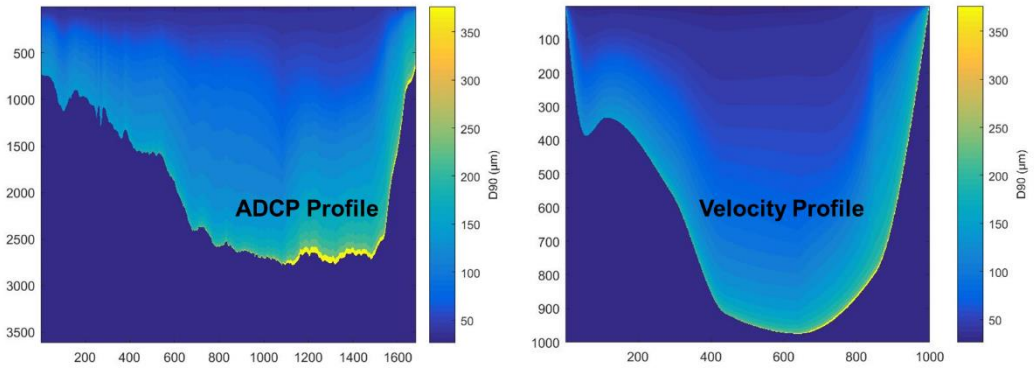

Fig:16 D90 distributions modeled with the Rouse equation based on the ADCP profile and for the velocity profiles across the Changjiang at Datong.

3.3 Calculation of integrated fluxes of element and isotopic composition

Distribution of the aluminum to silicon (Al/Si mass ratio) across a river transect can be then modeled, based on the relationship between D90 (or other grain size parameters such as D50) and the Al/Si ratio deduced from the profiles data (Figure 17). Al/Si ratio is proved to be a good proxy to indicate the particle size of riverine sediments, providing information about the sorting effect caused by river hydrodynamics, such as in Ganges-Brahmaputra, Amazon, and Mackenzie River, etc. (Galy et al., 2007; Bouchez et al., 2014; Hilton et al., 2015). Subsequently, based on the linear D90-Al/Si and then the linear TOC-Al/Si relationship using the integrated depth profiles, spatial TOC content distribution could be predicted in the cross-section. Finally, an instantaneous POC flux for the whole channel could be acquired with the aid of the afore-modeled water velocity, SPM concentration, and POC content. Like wisely, suing the correlations between Al/Si ratio and the elemental concentrations or isotopic compositions observed for the profiles data, integrated elemental fluxes or isotopic composition can be calculated.

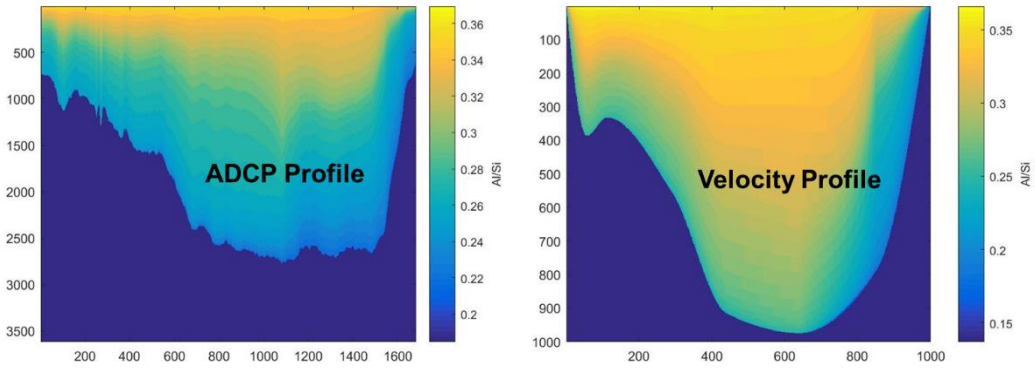

Fig.17 Al/Si ratio distribution based on the ADCP profile and the velocity profiles across the Changjiang at Datong.

Reference

Bloom, A. A., Exbrayat, J. F., Van Der Velde, I. R., Feng, L., and Williams, M. (2016). The decadal state of the terrestrial carbon cycle: Global retrievals of terrestrial carbon allocation, pools, and residence times. Proceedings of the National Academy of Sciences, 113(5), 1285-1290.

Bouchez, J., Gaillardet, J., France-Lanord, C., Maurice, L., and Dutra-Maia, P. (2011a). Grain size control of river suspended sediment geochemistry: Clues from Amazon River depth profiles. Geochemistry, Geophysics, Geosystems, 12(3).

Bouchez, J., Lupker, M., Gaillardet, J., France-Lanord, C., and Maurice, L. (2011b). How important is it to integrate riverine suspended sediment chemical composition with depth? Clues from Amazon River depth-profiles. Geochimica et Cosmochimica Acta, 75(22), 6955-6970.

Bouchez, J., Lupker, M., Gaillardet, J., France-Lanord, C., and Maurice, L. (2011b). How important is it to integrate riverine suspended sediment chemical composition with depth? Clues from Amazon River depth-profiles. Geochimica et Cosmochimica Acta, 75(22), 6955-6970.

Carvalhais, N., Forkel, M., Khomik, M., Bellarby, J., Jung, M., Migliavacca, M., ... and Reichstein, M. (2014). Global covariation of carbon turnover times with climate in terrestrial ecosystems. Nature, 514(7521), 213-217.

Coplen, T. B. (1995). Reporting of stable hydrogen, carbon, and oxygen isotopic abundances. Geothermics, 5(24), 707-712.

FAO. 2016. AQUASTAT, FAO's global water information system. Food and Agriculture Organization of the United Nations (FAO). Website accessed on [2020/12/12].

Fick, S. E., and Hijmans, R. J. (2017). WorldClim 2: new 1-km spatial resolution climate surfaces for global land areas. International Journal of Climatology, 37(12), 4302-4315.

Galy, V., France-Lanord, C., Beyssac, O., Faure, P., Kudrass, H., and Palhol, F. (2007). Efficient organic carbon burial in the Bengal fan sustained by the Himalayan erosional system. Nature, 450(7168), 407-410.

Galy, V., Peucker-Ehrenbrink, B., and Eglinton, T. (2015). Global carbon export from the terrestrial biosphere controlled by erosion. Nature, 521(7551), 204-207.

Hartmann, J., and Moosdorf, N. (2012). The new global lithological map database

GLiM: A representation of rock properties at the Earth surface. Geochemistry, Geophysics, Geosystems, 13(12).

Hiederer, R., and Köchy, M. (2011). Global soil organic carbon estimates and the harmonized world soil database. EUR, 79(25225), 10-2788.

Hilton, R. G., Galy, V., Gaillardet, J., Dellinger, M., Bryant, C., O'Regan, M., ... and Calmels, D. (2015). Erosion of organic carbon in the Arctic as a geological carbon dioxide sink. Nature, 524(7563), 84-87.

Jin, Z., West, A. J., Zhang, F., An, Z., Hilton, R. G., Yu, J., ... and Wang, X. (2016). Seismically enhanced solute fluxes in the Yangtze River headwaters following the AD 2008 Wenchuan earthquake. Geology, 44(1), 47-50.

Komada, T., Anderson, M. R., and Dorfmeier, C. L. (2008). Carbonate removal from coastal sediments for the determination of organic carbon and its isotopic signatures, $\delta^{13}C$ and $\Delta^{14}C$: comparison of fumigation and direct acidification by hydrochloric acid. Limnology and Oceanography: Methods, 6(6), 254-262.

Kondolf, G. M., Gao, Y., Annandale, G. W., Morris, G. L., Jiang, E., Zhang, J., ... and Yang, C. T. (2014). Sustainable sediment management in reservoirs and regulated rivers: Experiences from five continents. Earth's Future, 2(5), 256-280.

Lehner, B., and Grill, G. (2013). Global river hydrography and network routing: baseline data and new approaches to study the world's large river systems. Hydrological Processes, 27(15), 2171-2186.

Lehner, B., Liermann, C. R., Revenga, C., Vörösmarty, C., Fekete, B., Crouzet, P., ... and Wisser, D. (2011). High-resolution mapping of the world's reservoirs and dams for sustainable river-flow management. Frontiers in Ecology and the Environment, 9(9), 494-502.

Liu, Z., Zhao, M., Sun, H., Yang, R., Chen, B., Yang, M., ... and Zeng, H. (2017). “Old” carbon entering the South China Sea from the carbonate-rich Pearl River Basin: coupled action of carbonate weathering and aquatic photosynthesis. Applied Geochemistry, 78, 96-104.

Lupker, M., France-Lanord, C., Lavé, J., Bouchez, J., Galy, V., Métivier, F., ... and Mugnier, J. L. (2011). A Rouse-based method to integrate the chemical composition of river sediments: Application to the Ganga basin. Journal of Geophysical Research: Earth Surface, 116(F4).

Milliman, J. D., and Farnsworth, K. L. (2011). River discharge to the coastal ocean: a global synthesis. Cambridge University Press.

Rouse, H. (1950). Engineering hydraulics. In Hydraulics Conference 1949: Iowa Institute of Hydraulic Research); Hydraulics Conference (1949: University of Iowa). Wiley.

Ruff, M., Szidat, S., Gäggeler, H. W., Suter, M., Synal, H. A., and Wacker, L. (2010). Gaseous radiocarbon measurements of small samples. Nuclear Instruments and Methods in Physics Research Section B: Beam Interactions with Materials and Atoms, 268(7-8), 790-794.

Salazar, G., Zhang, Y. L., Agrios, K., and Szidat, S. (2015). Development of a method for fast and automatic radiocarbon measurement of aerosol samples by online coupling of an elemental analyzer with a MICADAS AMS. Nuclear Instruments and Methods in Physics Research Section B: Beam Interactions with Materials and Atoms, 361, 163-167.

Sharp, Z. (2017). Principles of stable isotope geochemistry.

Shi, H., and Shao, M. (2000). Soil and water loss from the Loess Plateau in China. Journal of Arid Environments, 45(1), 9-20.

Stevens, T., Carter, A., Watson, T. P., Vermeesch, P., Andò, S., Bird, A. F., ... and Sevastjanova, I. (2013). Genetic linkage between the Yellow River, the Mu Us desert and the Chinese loess plateau. Quaternary Science Reviews, 78, 355-368.

Stuiver, M., and Polach, H. A. (1977). Discussion reporting of ^{14}C data. Radiocarbon, 19(3), 355-363. Chemical Geology: Isotope Geoscience section, 86(2), 89-96.

Syvitski, J. P., and Kettner, A. (2011). Sediment flux and the Anthropocene. Philosophical Transactions of the Royal Society A: Mathematical, Physical and Engineering Sciences, 369(1938), 957-975.

Syvitski, J. P., Vörösmarty, C. J., Kettner, A. J., and Green, P. (2005). Impact of humans on the flux of terrestrial sediment to the global coastal ocean. Science, 308(5720), 376-380.

Tachibana, Y., Oshima, K., and Ogi, M. (2008). Seasonal and interannual variations of Amur River discharge and their relationships to large-scale atmospheric patterns and moisture fluxes. Journal of Geophysical Research: Atmospheres, 113(D16).

Wacker, L., Bonani, G., Friedrich, M., Hajdas, I., Kromer, B., Němec, M., ... and Vockenhuber, C. (2010a). MICADAS: routine and high-precision radiocarbon dating. Radiocarbon, 52(2), 252-262.

Wacker, L., Christl, M., and Synal, H. A. (2010b). Bats: a new tool for AMS data reduction. Nuclear Instruments and Methods in Physics Research Section B: Beam

Interactions with Materials and Atoms, 268(7-8), 976-979.

Wacker, L., Fahrni, S. M., Hajdas, I., Molnar, M., Synal, H. A., Szidat, S., and Zhang, Y. L. (2013). A versatile gas interface for routine radiocarbon analysis with a gas ion source. Nuclear Instruments and Methods in Physics Research Section B: Beam Interactions with Materials and Atoms, 294, 315-319.

Wang, H., Yang, Z., Saito, Y., Liu, J. P., Sun, X., and Wang, Y. (2007). Stepwise decreases of the Huanghe (Yellow River) sediment load (1950–2005): Impacts of climate change and human activities. Global and Planetary Change, 57(3-4), 331-354.

Wang, S., Fu, B., Piao, S., Lü, Y., Ciais, P., Feng, X., and Wang, Y. (2016). Reduced sediment transport in the Yellow River due to anthropogenic changes. Nature Geoscience, 9(1), 38-41.

Welte, C., Hendriks, L., Wacker, L., Haghipour, N., Eglinton, T. I., Günther, D., and Synal, H. A. (2018). Towards the limits: Analysis of microscale ^{14}C samples using EA-AMS. Nuclear Instruments and Methods in Physics Research Section B: Beam Interactions with Materials and Atoms, 437, 66-74.

Chapter 3

Transport of Particulate Organic Carbon in the Huanghe: Insights from Lateral and Vertical Heterogeneity in a River Cross-section

Yutian Ke[1], Damien Calmels[1], Julien Bouchez[2], Marc Massault[1], Benjamin Chetelat[3], Aurélie Noret[1], Hongming Cai[2], Jiubin Chen[3], Jérôme Gaillardet[2], Cécile Quantin[1]

[1] GEOPS, Université Paris-Saclay-CNRS, 91405 Orsay, France

[2] Université de Paris, Institut de Physique du Globe de Paris, CNRS, 75005 Paris, France

[3] School of Earth System Science, Institute of Surface-Earth System Science, Tianjin University, 300072 Tianjin, China

Abstract

The Huanghe (Yellow River), one of the largest turbid river systems in the world, has long been recognized as a major contributor of suspended particulate matter (SPM) to the ocean. However, over the last few decades, the SPM export flux of the Huanghe has decreased over 90% due to the high management, impacting the global export of particulate organic carbon (POC). To better constrain sources and modes of transport of POC beyond the previously investigated transportation of POC near the channel surface, SPM samples were for the first time collected over a whole channel cross-section in the lower Huanghe. Riverine SPM samples were analyzed for particle size and major element contents, as well as for POC content and dual carbon isotopes (^{13}C and ^{14}C). The results show clear vertical and lateral heterogeneity of SPM physical and chemical characteristics within the river cross-section, with for example finer SPM carrying more POC with higher ^{14}C activity near the surface and the right bank. Notably, we discuss how bank erosion in the alluvial plain is likely to generate lateral heterogeneity in POC composition. The Huanghe POC is millennial-aged (4,020 ± 500

radiocarbon years), dominated by organic carbon (OC) from the biosphere, while the lithospheric fraction reaches up to ca. 33%. The mobilization of aged and refractory OC from deeper soil horizons of the loess-paleosol sequence through erosion in the Chinese Loess Plateau is an important mechanism contributing to fluvial POC in the Huanghe drainage basin. The involvement of this OC fraction has significance for the regional and global carbon cycles, especially regarding its final fate in the estuary. Altogether, this study sheds light on the mechanism of fluvial transfer of POC and corresponding impacts on the carbon cycle in large river systems strongly perturbed by anthropogenic activities.

Keywords: Huanghe; particulate organic carbon; radiocarbon; bank erosion; depth profile sampling.

1. Introduction

Rivers are the main conveyor of rock and soil debris eroded from the continents to the ocean, where sediment deposition occurs, eventually leading to the formation of sedimentary rocks (Hay, 1998). Along with inorganic material, river sediments host particulate organic carbon (POC) derived mainly from three major sources: 1) recently photosynthesized OC of the biosphere, 2) aged and altered OC from soils, and 3) ancient OC contained in sedimentary rocks (Blair et al., 2010). Depending on its provenance and fate, POC transport may have opposite impacts on the carbon cycle and thus on the evolution of Earth's climate. For instance, the effective sedimentary burial of POC derived from the terrestrial biosphere (biospheric OC, OC_{bio}) will represent a net, long-term sink of atmospheric CO_2 (Galy et al., 2007, Bouchez et al., 2014; Hilton et al., 2015), while the oxidation of POC derived from continental rocks (petrogenic OC, OC_{petro}) will act as a net, long-term source of CO_2 to the atmosphere (Hilton et al., 2014). The erosion and burial of OC_{petro} escaping from oxidation will have no net effect on the long-term carbon cycle (Galy et al., 2008a; Bouchez et al., 2010; Hilton et al., 2011; Horan et al., 2019). In addition, upon oxidation, OC_{bio} transport might also result in CO_2 emission from river channels and recently-deposited sediments, in response to its intrinsically reactive nature (Mayorga et al., 2005; Galy and Eglinton, 2011; Blair and Aller, 2012).

Globally, rivers transport a total POC flux of *ca*. 200 Tg C/year, consisting of 157^{+74}_{-50} Tg C/year of OC_{bio} and 43^{+61}_{-25} Tg C/year of OC_{petro} (Galy et al., 2015; Ludwig

et al., 1996). Source-to-sink processes controlling the origin and fate of riverine POC are prominently river-specific, suggesting that the impact of POC on regional and global carbon cycles might significantly vary both spatially and temporally (Blair and Aller, 2012). It is thus crucial to understand the mechanisms behind riverine POC export by large rivers that integrate vast portions of the land surface, and quantify the potential sources of this large river POC.

The Huanghe (Yellow River) is a highly turbid river system that exports over 85% of its OC as particulate matter, with efficient deposition and preservation in the ocean (Cauwet and Mackenzie, 1993; Bianchi, 2011; Zhang et al., 2013; Ran et al., 2013). The Huanghe has been highly managed over the last few decades, leading to a decrease of nearly 90% of its sediment load (Wang and Fu et al., 2016; Wang et al., 2007; Milliman et al., 1987) and a significant decrease in its POC delivery to the ocean. Reservoir construction dramatically affects the transport and the fate of both sediment load and POC in large rivers (Syvitski et al., 2005; Li et al., 2015). The estimated POC flux of the Huanghe is thought to have shifted from 4.5 Tg C/yr in the 1980s (Cauwet and Mackenzie, 1993) to 0.34-0.58 Tg C/yr nowadays (Tao et al., 2018) in response to both anthropogenic influence (Hu et al., 2015; Tao et al., 2018; Yu et al., 2019a) and natural variability of the regional hydrological cycle (Qu et al., 2020). These large-scale perturbations are likely to have modified the OC input from the different terrestrial pools, an alteration of the carbon cycle that remains to be addressed.

Over the last decade, POC transport in the Huanghe has been investigated for 1) determination and quantification of POC sources, based on bulk or molecular carbon isotopic composition (Tao et al., 2015; Yu et al., 2019b; Ge et al., 2020; Qu et al., 2020); 2) temporal and spatial variations in POC export and distribution among different size fractions (Ran et al., 2013; Wang 2012; 2016; Yu et al., 2019a, b, Qu et al., 2020); 3) impact of anthropogenic activities (Hu et al., 2015; Tao et al., 2018; Yu et al., 2019a); and 4) burial efficiency and preservation in the ocean (Sun et al., 2018; Tao et al., 2016; Ge et al., 2020). However, all these studies rely on suspended sediment samples collected near the channel surface or at a single, intermediate depth in the river channel, further assuming a homogeneous distribution of sediment characteristics in the water column, both vertically and laterally. However, it is now well recognized that suspended sediments present physical, mineralogical, chemical, and isotopic heterogeneities in river cross-sections due to hydrodynamic sorting and tributary mixing (Galy et al., 2008b; Garzanti et al., 2010; Bouchez et al., 2010, 2011a). This is

also true for POC, whose age and composition vary within cross-sections (*e.g.*, Bouchez et al., 2014; Baronas et al., 2020) and between sediment size fractions separated in the laboratory (Yu et al., 2019b; Ge et al., 2020). Such heterogeneity warrants a re-evaluation of POC transport in the Huanghe, accounting for the variability in suspended sediment characteristics over the channel cross-section.

In this study, we take advantage of in-river hydrodynamic sorting to access the full range of suspended sediment size fractions by collecting suspended particulate matter (SPM) samples along several river depth profiles distributed across a channel transect (*e.g.*, Bouchez et al., 2014; Freymond et al., 2018; Baronas et al., 2020). We apply this sampling scheme to a cross-section of the Huanghe located 200 km upstream from the river mouth and report SPM OC content, stable isotope composition, and radiocarbon activity as well as total nitrogen, major element composition (aluminum and silicon), and particle size distribution. Based on these novel samples and data sets, this study aims at 1) determining the transport mode of POC in the Huanghe; 2) tracing and quantifying the sources of riverine POC; and 3) providing depth-integrated estimates of POC fluxes in the most turbid large river system.

2. Study area

The Huanghe originates from the north-eastern Qinghai-Tibet Plateau (QTP) and runs through the Chinese Loess Plateau (CLP) and the North China Plain (NCP) to the Bohai Sea (Figure 1a). It is 5,464 km long and drains a basin area of 79.5×10^4 km^2. The Huanghe drainage basin can be subdivided into three main geomorphic units: 1) the high relief upper reaches spanning from the source region (elevation of 4,500 m) to the city of Toudaoguai (located 3,472 km downstream at an elevation of 1,000 m); 2) the middle reaches with a channel length of 1,206 km, ending at Huayuankou (elevation of 110 m) and presenting relatively gentle slopes; and 3) the lower reaches where the river flows eastwards across a fluvial plain over a length of 786 km. These three sections represent 53.8%, 43.3%, and 2.9% of the whole Huanghe basin area, respectively (Wang et al., 2007; YRCC, 2016). Most second-order tributaries drain the CLP region and feed the main channel in the middle reaches, with the Dawenhe River being the only tributary of the lower reaches, with negligible water and sediment supply due to upstream trapping in lakes and reservoirs. Additionally, it is worth noting that more than 50% of the water discharge at the mouth comes from the QTP, whereas over 90% of the sediment load originates from the CLP (Wang et al., 2010, 2017; Pan et al., 2016).

The CLP is thus the principal source area of sediment to the Huanghe (Shi and Shao, 2000; Guo et al., 2002; Wang and Fu et al., 2016).

The Huanghe mostly drains the North China craton, and its basin is bounded by several mountain belts. The watershed encompasses 46% of sedimentary rock outcrops (mainly siliciclastic rocks with minor carbonates), and about 45% of unconsolidated sediments (mainly Quaternary loess deposits). The remaining outcrops include metamorphic, plutonic, and volcanic rocks formed from the Archean to the Tertiary (Figure S1). Although river incision is strong in the QTP, a substantial part of the corresponding eroded material is not effectively transferred to the lower reaches due to deposition in the CLP and the western Mu-Us desert, a situation that has prevailed since at least the middle Pleistocene (Nie et al., 2015; Licht et al., 2016; Pan et al., 2016). In addition, recent anthropogenic disturbance such as constructions of large dams in the upper reaches has profoundly modified the export of solid materials (Wang et al., 2007). Huanghe then flows through the CLP that has acted as the major supplier of sediment to the system since at least the Calabrian Pleistocene (Stevens et al., 2013; Bird et al., 2015). There, the easily erodible loess-paleosol formation has accumulated since 2.58 Ma (Guo et al., 2002), over a thickness ranging from a few meters to more than 500 m, with an average of 100 m. The loess-paleosol formation and underlying Cretaceous sedimentary rocks are actively incised by the main stem and its tributaries (Shi and Shao, 2000; Guo et al., 2002; Wang and Fu et al., 2016). Notably, the Ordos Basin geographically underlying the CLP is enriched in oil and gas (Guo et al., 2014). In the lower reaches, the river drains Quaternary fluvial deposits and sedimentary rocks.

The Huanghe drainage basin encompasses the entire arid and semi-arid region of northern China in the upper and middle reaches and is characterized by more humid climate conditions in the lower reaches. Annual average precipitation (over the period 1950 - 2000) in the upper, middle and lower reaches regions is 368 mm, 530 mm, and 670 mm, respectively (Wang et al., 2007). As a result of the East Asian summer and winter monsoon circulations, the rainy season (June to September) contributes 85% of the annual precipitation (Wang et al., 2007). During the rainy season, frequent storm events lead to concentrated flows (relatively high discharge) in vulnerable gully-hill systems, the dominant regional geomorphic landscape, and actively participates in soil erosion in the CLP (Shi and Shao, 2000; He et al., 2004; Qu et al., 2020). The present-day (2002 to 2016) suspended sediment flux delivered by the Huanghe to the sea is about 0.12 Gt/yr, which implies a nearly 90% decrease in sediment export compared to

the widely cited estimate of 1.08 Gt/yr (average value between 1950 to 1980, Milliman and Farnsworth, 2011). This massive decrease in sediment export mostly results from human perturbations, including soil conservation practices in the CLP and retention in large reservoirs, rather than the climatic variations such as the decreasing precipitation observed in the region over the last decades (Wang et al., 2007; Ran et al., 2013; Wang and Fu et al., 2016). A practice for water and sediment regulation (WSR) has been implemented through the construction of the Xiaolangdi Reservoir since 2002, aiming to mitigate water and sediment imbalances in the lower reaches. This regulation practice has been modifying the flux of sediment delivered to the lower reaches and estuary, making the Huanghe a highly human-regulated river system. However, no WSR was carried out in 2016, our sampling year, indicating that the collected SPM samples are much less affected by large dams and thus are representative of the fluvial transport of terrestrial materials eroded from the CLP.

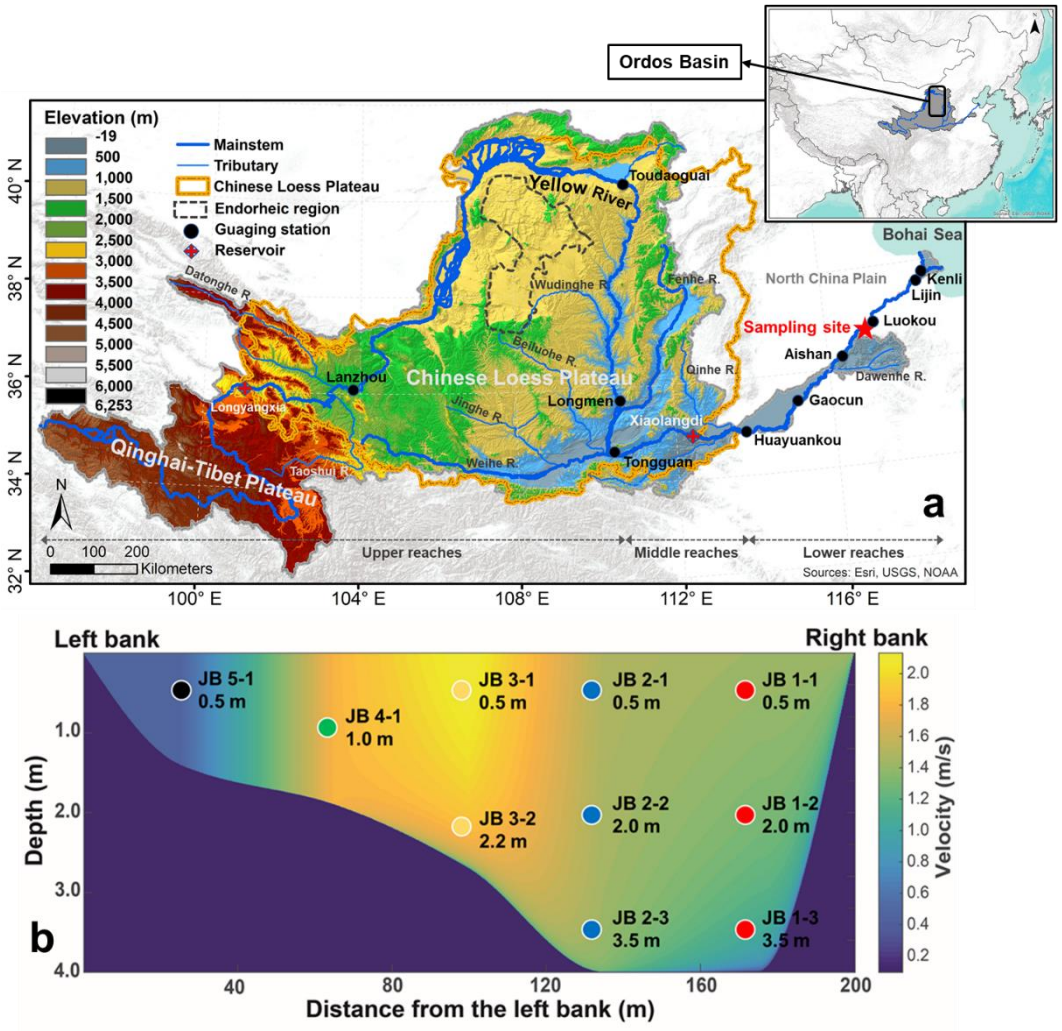

Fig. 1 (a) Elevation map of the Huanghe drainage basin showing the main reservoirs and gauging stations along the main stem as well as our sampling site (36.75°N,

117.02ºE, near the Luokou gauging station); and (b) channel cross-section sampled for this study showing the depth and lateral distribution of suspended particulate matter (SPM) samples and modeled velocity distribution based on the "law of the wall" using the point velocity data measured by a current meter.

3. Sampling and analytical methods

3.1 Sampling

Detailed sampling of a cross-section of the Huanghe was carried out on the 17th of July, 2016, during the flood season. Samples were collected along five depth profiles near the Luokou hydrological station, 250 km upstream of the river mouth (Figure 1). This sampling strategy allows for accessing the full range of suspended sediment particle size (Bouchez et al., 2014). The cross-section is 200-meters wide at the surface and 4 meters deep at most (Figure 1). We used a 10-liter, point-sediment NISKIN sampler attached to a current velocity meter, to collect river water samples and measure the water velocity simultaneously. Subsequently, two river samples were collected at the surface near the right bank in May and June 2017 before the flooding season, to retrieve fine suspended particulate matter. For each sample, approximately 30 liters of river water were collected and were then filtered through pre-weighed 0.22-µm porosity cellulose acetate membrane filters within 24 hours. After rinsing the filters with filtered water, all sediment samples were transferred into centrifuge tubes and freeze-dried before weighing and analysis.

3.2 Physical and geochemical analysis

Apart from a 50-mg aliquot of SPM samples preserved for particle size analysis, samples were finely ground using an agate mortar and pestle for chemical and isotopic analyses. The particle size distribution of the unground aliquots was measured using a Laser Diffraction Particle Size Analyzer (Beckman Coulter LS-12 320) at the École Normale Supérieure (ENS), Paris, France. Before analysis, unground SPM aliquots were dispersed in deionized water and then in sodium hexametaphosphate in an ultrasonic bath. For each sample, we measured three replicates and report the average median particle size (D50, µm) with an uncertainty better than 2% (Table 1). The chemical composition of SPM samples was measured on ground aliquots at the Centre de Recherches Pétrographiques et Géochimiques (CRPG), Vandoeuvre-lès-Nancy, France, using ICP-OES for major elements with typical uncertainties of 3% (Carignan

et al., 2001).

For particulate organic carbon content (POC%, wt.), stable carbon isotope $\delta^{13}C$ (in $‰_{VPDB}$, *i.e.*, in ‰ relative to Vienna Pee Dee Belemnite) and radiocarbon isotope $\Delta^{14}C$ (expressed as fraction modern, Fm), ground homogenized samples were fumigated using 12M HCl fumes in a closed Teflon tank at 60 °C for 48 hours to remove the carbonate fraction, and were then dried under vacuum prior to analysis. Total nitrogen content (TN%, wt.) was measured on non-acidified samples (Komada et al., 2008). Triplicate analysis on POC% and $\delta^{13}C$ of POC (acidified aliquots) as well as TN% (non-acidified aliquots) were carried out on an Organic Elemental Analyzer (OEA) coupled with Isotope Ratio Mass Spectrometry (IRMS, Thermo Scientific Flash 2000) under continuous flow mode at Géosciences Paris Saclay (GEOPS), Orsay, France. Uncertainties on POC%, $\delta^{13}C$, and TN%, based on replicate measurements (1σ, n=3), are less than 0.02%, 0.06‰, and 0.02‰, respectively. The ^{14}C activity of POC was measured on a new compact accelerator mass spectrometry (AMS), *ECHo*MICADAS (Hatte et al., 2016), using a gas ion source interface system at the Laboratoire des Sciences du Climat et de l'Environnement (LSCE), Gif-sur-Yvette, France, with an absolute uncertainty of ±0.5% or better.

3.3 POC source apportionment

To quantify the contribution and associated uncertainties of various sources to POC transported in the Huanghe, a Bayesian Markov chain Monte Carlo based on a three-end member mixing scheme (burn-in of 1,000 steps, data thinning of 100, and iterations of 5,000,000) was adopted (Andersson et al., 2015). This approach assumes that the uncertainty on each end member contribution can be represented by a normal distribution. The mixing model was constructed on the dual stable and radioactive isotope of the riverine POC pool ($\delta^{13}C$ and $\Delta^{14}C$) and of the three potential source pools (section 5.2) by the following equations:

$$\text{Isotope\_ratio}_{\text{sample}} = \sum_{\text{source}} (f_{\text{source}} * \text{Isotope\_ratio}_{\text{source}})$$

$$\sum_{\text{source}} f_{\text{source}} = 1$$

where $\text{Isotope\_ratio}_{\text{sample}}$ is either the $\delta^{13}C$ or $\Delta^{14}C$ value of the sample, $\text{Isotope\_ratio}_{\text{source}}$ is either the $\delta^{13}C$ or $\Delta^{14}C$ value of different possible sources of POC and f_{source} the relative contribution of each source of POC.

3.4 Depth-integrated fluxes

Instantaneous depth-integrated fluxes of SPM and POC sources were calculated for the cross-section using a method developed by Bouchez et al. (2011a, b). This method is based on the systematic variation of SPM concentration in the water column (Figure 2) applying a Rouse-based model (Rouse, 1950). We first constructed a bathymetric profile of the river cross-section based on the depth information collected in the field and then modeled the velocity distribution across the transect (Figure 1b) using fits of the so-called "law of the wameasureeasured water velocity profiles, based on locally measured water velocity at each sampling point. Afterward, the concentration of total SPM and various particle size fractions could be estimated by applying the so-called Rouse model (Rouse, 1950) to each particle size fraction separately (Bouchez et al., 2011a), resulting in a map of the particle size distribution in the river cross-section (Figure S2). The aluminum to silicon ratio (Al/Si mass ratio) is inversely related to the particle size of river SPM in the Ganges-Brahmaputra, the Amazon, and the Mackenzie Rivers (Galy et al., 2007; Bouchez et al., 2014; Hilton et al., 2015). Such a linear relationship between D50 and Al/Si was also observed in our dataset, allowing for computing the spatial distribution of POC content in the cross-section, based on the linear relationship between POC and Al/Si (Figure 3). Finally, combining modeled water velocity, SPM concentration, and POC distribution we calculated a depth-integrated, instantaneous POC flux for the whole river channel (Figure S2, detail in supplementary material).

4. Results

We report the first isotopic dataset of POC samples collected along several depth profiles distributed over a cross-section of the Huanghe (Table 1). SPM concentrations range from 679 to 2,459 mg/L (avg. 1,286 mg/L) and show an obvious increase from the surface to the bottom and from the right bank to the left bank (Figure 1b and 2a). The SPM transported at the surface (*i.e.*, samples collected 0.5 m below the surface) shows a decreasing concentration when the total water column deepens. The spatial distribution of the D50, *i.e.* the median particle size (19.5-86.0 µm, Figure 2b), shows that the finest SPM is transported on the right bank and at the surface, while the coarsest SPM is found at the bottom of the middle profile (sample JB2-3). Two types of depth profiles can be distinguished based on particle size distributions (Figure S3) and the relationship between D50 and water depth (Figure 2b). On the one hand, the JB1 and

JB4 profiles show a well-marked, bi-modal distribution of particle size (Figure S3) together with relatively low and consistent D50 (Figure 2b). On the other hand, the JB2, JB3, and JB5 profiles show a more unimodal distribution of particle size (Figure S3) and a unique D50 - sampling depth relationship (Figure 2b). Interestingly, these two groups can also be distinguished in terms of relationships between POC% and $\delta^{13}C$ with water depth (Figures 2d and 2f). As expected, the Al/Si ratio is well-related to the particle size, with the middle profile varying from 0.17 (sample JB2-3) to 0.26 (sample JB2-1), covering the full range of Al/Si measured in the whole cross-section (avg, 0.21 ± 0.03, Figure 2c). The relatively low Al/Si ratios are comparable to that of the middle Huanghe (Qu et al., 2020) and other large turbid river systems such as the Ganges-Brahmaputra (Galy et al., 2008b), Salween, and Irrawaddy (Tipper et al., 2021).

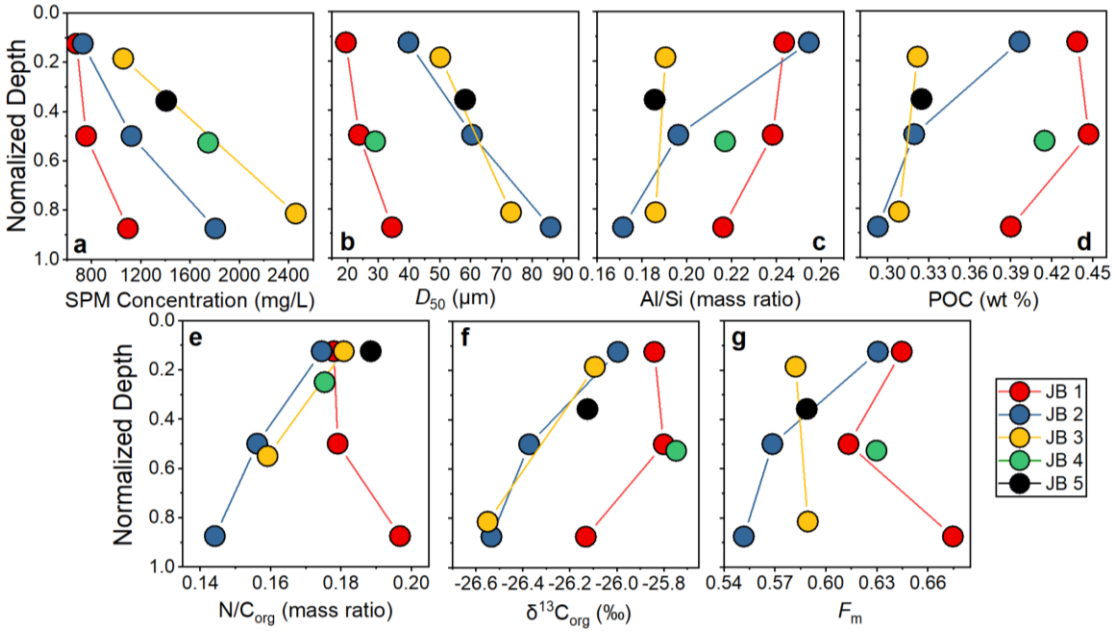

Fig. 2 Variation of physical and chemical parameters in the river cross-section. (a) SPM concentration; (b) particle size distribution D50; (c) Al/Si mass ratio; (d) POC content (%); (e) N/ C_{org} mass ratio; (f) stable carbon isotope ratio $\delta^{13}C_{org}$ (‰); (g) radiocarbon activity F_m.

SPM in the Huanghe is characterized by low TN and POC content (wt.%), ranging from 0.04% to 0.08% (avg., 0.06 ± 0.01%) and from 0.29% to 0.42% (avg., 0.37 ± 0.06%), respectively (Figure 4d; Table 1). POC content generally decreases from the surface to the river bed, with quantitative differences from one profile to another (Figure 2d). Notably, the JB1 profile shows the highest POC% and TN%. In addition,

the ratio of TN% to POC%: N/C_{org} increases along the JB1 profile (from top to bottom), while it decreases along the JB2 and JB3 profiles (Figure 2e). The $\delta^{13}C$ of POC varies over a narrow range from −26.55‰ to −25.75‰ (avg., −26.12 ± 0.29‰, Figure 2f) and becomes lighter with depth, showing that fine SPM has higher $\delta^{13}C$ than coarse SPM. These values are lower than previously reported for upstream sites: −24.7 ± 0.4‰ at Toudaoguai, −24.9 ± 0.6‰ at Longmen, and −23.8 ± 0.6‰ at Lijin (Qu et al., 2020, Hu et al., 2015; Tao et al., 2015; Yu et al., 2019a; Ge et al., 2020). The radiocarbon activity of POC is relatively low (Figure 2g), with Fm ranging from 0.552 ($\Delta^{14}C$ = −453‰; sample JB2-3) to 0.675 ($\Delta^{14}C$ = −331‰; sample JB1-3), spanning from 3,160 to 4,780 ^{14}C yr, and the average value is 0.607 ± 0.038 ($\Delta^{14}C$ = −412‰). The variable radiocarbon activity is consistent with published values for POC collected at the river surface downstream of Toudaoguai (Qu et al., 2020). All the POC radiocarbon activity data reported so far for the Huanghe are significantly older than the median value for global rivers ($\Delta^{14}C$ = −203‰, ca. 1,800 ^{14}C yr, Marwick et al., 2015), revealing the multimillennial-age nature of POC transported by the Huanghe. The elemental and isotopic signatures of the two fine SPM samples HH 17.05 and HH 17.06 (on average POC% = 1.07%, $\delta^{13}C$ = −25.67%, F_m = 0.720; and Al/Si = 0.37) are significantly different from those of the depth profile samples (Table 1). The bedload sample has a comparatively low POC% (0.21%), $\delta^{13}C$ (−27.35%), F_m (0.099), and Al/Si ratio (0.17).

Table 1. SPM characteristics and POC properties of the river-cross-section sampling.

Sample ID	Type	Depth (m)	SPM mg/L	POC (%)	SD	$\delta^{13}C_{org}$ (‰)	SD	F_m	$\Delta^{14}C$ (‰)	^{14}C age	TN (%)	N/C_{org}	Al/Si	D50 µm
JB 1-1	SPM	0.5	679	0.44	0.02	−25.84	0.03	0.645	−360	3527	0.078	0.178	0.243	19.5
JB 1-2	SPM	2	757	0.45	0.01	−25.80	0.06	0.613	−392	3929	0.080	0.179	0.238	23.7
JB 1-3	SPM	3.5	1095	0.39	0.01	−26.13	0.04	0.675	−331	3161	0.077	0.197	0.216	34.5
JB 2-1	SPM	0.5	730	0.40	0.03	−26.00	0.01	0.631	−374	3703	0.069	0.175	0.255	39.8
JB 2-2	SPM	2	1124	0.32	0.01	−26.37	0.06	0.569	−436	4537	0.050	0.156	0.196	60.4
JB 2-3	SPM	3.5	1806	0.29	0.01	−26.53	0.06	0.552	−453	4779	0.042	0.144	0.172	86.0
JB 3-1	SPM	0.5	1058	0.32	0.02	−26.09	0.03	0.582	−422	4346	0.058	0.181	0.190	50.1
JB 3-2	SPM	2.2	2459	0.31	0.02	−26.55	0.04	0.589	−415	4247	0.049	0.159	0.186	73.1
JB 4-1	SPM	1	1747	0.41	0.02	−25.75	0.06	0.630	−375	3714	0.073	0.175	0.217	29.0
JB 5-1	SPM	0.5	1406	0.32	0.01	−26.12	0.05	0.589	−416	4256	0.061	0.188	0.186	58.2
HH 17.05	SPM	0	83	0.92	0.00	−25.73	0.14	0.711	−295	2740	0.184	0.200	0.358	5.2
HH 17.06	SPM	0	54	1.21	0.01	−25.60	0.07	0.729	−277	2539	0.261	0.215	0.377	4.3
HH	Bedload			0.21	0.03	−27.35	0.05	0.099	−901	18539	0.019	0.087	0.175	44.4

5. Discussion

We observe significant heterogeneities of elemental and isotopic carbon composition as well as inorganic chemistry over the studied river cross-section. The possible

mechanisms behind these variations are assessed, with a detailed interpretation of the low POC loading. Then, sources of riverine POC are determined and quantified, confirming that the erosion to the loess-paleosol sequence of the CLP is an important mechanism supplying aged and refractory biospheric OC to the fluvial transport. Finally, we assess the POC load and its variability over the transect profile, inferring the importance of the supply of POC from the river bottom in the Huanghe.

5.1 Transportation mode of POC

5.1.1 POC loading and its controls

The Huanghe is characterized by a high SPM load with relatively low POC% (avg. 0.37 ± 0.06%). Since the CLP is the dominant sediment source to the Huanghe, these features are largely inherited from the nature of the loess deposits, which are prone to erosion of OC-poor material (Huang and Ren, 2006; He et al., 2006; Ning et al., 2006; Wang and Fu, 2016). In the cross-section, POC content generally increases with decreasing particle size (Figure S4). The two clay-sized HH - SPM samples show a relative enrichment of POC (Table 1). This pattern is consistent with the POC variability among manually separated size fractions of the Huanghe sediments (Yu et al., 2019b), explained by a larger specific surface area of minerals in the finer fractions (Keil et al., 1997; Blair and Aller, 2012). However, many studies show that OC adsorption onto the mineral surface is not the only control on POC loading (Curry et al., 2007; Galy et al., 2008b; Blair and Aller, 2012; Bouchez et al., 2014; Qu et al., 2020).

The Al/Si ratio varies as an inverse linear function of the median particle sizes D50 (R^2=0.72, Figure 3a), while it positively correlates with POC% (R^2=0.81, Figure 3b). Those patterns support the widely observed feature that fine particles tend to be rich in clay and POC compared to coarse particles that are generally quartz-enriched and POC-poor (Galy et al., 2008b; Bouchez et al., 2014; Hilton et al., 2015). POC loading can be characterized by the slope in the Al/Si-POC diagram (Galy et al., 2008b). As shown in Figure 4, Al/Si ratio is comparatively low in Huanghe SPM, a feature largely inherited from the quartz-rich and clay-poor nature of loess deposits (Jahn et al., 2001). In loess-paleosol deposits, OC is mostly preserved and stabilized by forming organo-aggregates with kaolinite and through adsorption onto iron oxides (Wang et al., 2013). For a given Al/Si ratio, POC% in the cross-section is similar to that of the middle Huanghe (Qu et al., 2020), indicating the relatively invariant transport mode of POC between the middle and lower reaches. However, POC loading in the Huanghe is small compared to that of

the Amazon (Bouchez et al., 2014), where POC loading is higher during the high water stage compared to the rising water stage, possibly due to the erosion of discrete organic debris from river flanks. Such a process could be invoked to explain the diverse POC loading between JB1 and JB2 depth profiles (Figure 3). In particular, this diversity in POC loading in a single cross-section might indicate the delivery of recent OC_{bio} near the right bank, this assumption is supported by the comparatively younger ages of POC in profile JB1.

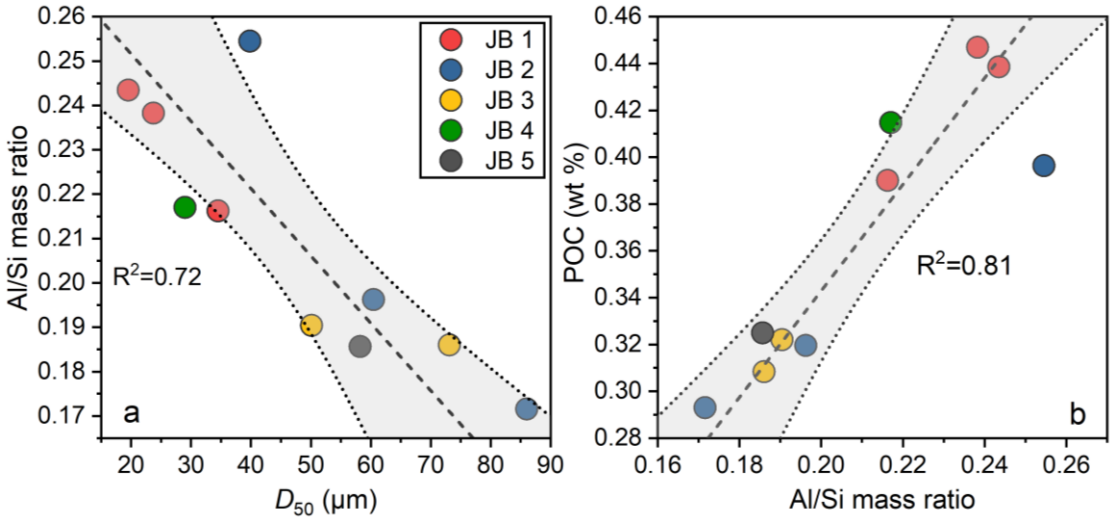

Fig. 3 Relationships between (a) particle size D50 and Al/Si mass ratio; (b) Al/Si mass ratio and POC content for the Luokou cross-section on the Huanghe. The grey shade represents the 95% confidence area of the linear best-fit (black dashed line), the upper and lower bound are marked by grey dotted lines.

The inferred POC loading in the Al/Si-POC diagram might help to decipher the possible POC components and to evaluate the likelihood of POC preservation in the estuary. The Ganges-Brahmaputra fluvial system delivers millennial-aged OC_{bio} to the Bengal Fan with an almost complete burial efficiency (Galy et al., 2007), and the Huanghe POC has equally high preservation for aged OC_{bio} originated from loess deposits (Tao et al., 2016). Given that modern OC (recently photosynthesized in terrestrial or aquatic ecosystems) can be readily oxidized within catchments (Mayorga et al., 2005), the relatively low POC loading observed at the mouth for the Ganges-Brahmaputra and the Huanghe (Figure 4) suggests a major component of aged OC_{bio} and OC_{petro}. In addition to the low reactivity of these OC fractions, the high sediment accumulation rates in the Huanhge coastal domain further inhibit their oxidation (Blair

and Aller, 2012). As a consequence, the case of the Huanghe differs drastically from that of the Amazon, where higher POC loading is observed, with a larger contribution of young, labile OC_{bio} either as discrete organic matter or associated with mineral surfaces, leading to low POC burial efficiency in the ocean (Bouchez et al., 2014; Blair and Aller, 2012).

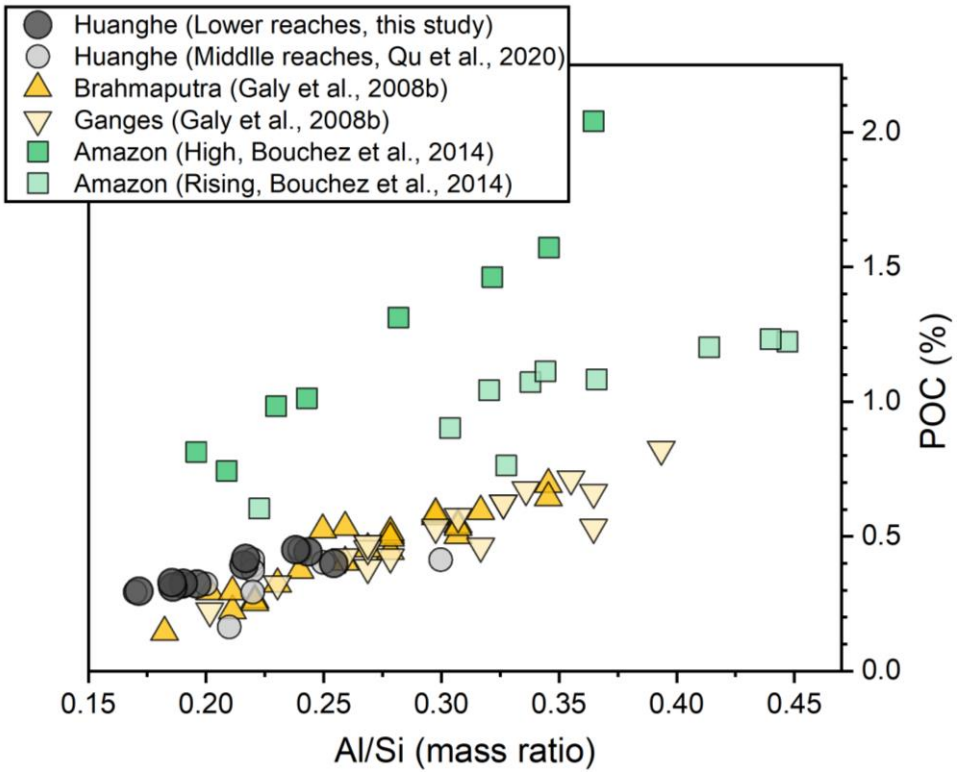

Fig. 4 POC content in river SPM of large rivers as a function of the Al/Si ratio. The POC loading is estimated from the slope of the relationship between POC content and the Al/Si ratio of each fluvial system (Galy et al., 2008b). All SPM samples were collected along depth profiles except for the middle Huanghe (Qu et al., 2020).

5.1.2 Chemical heterogeneity within the transect

There is clear lateral and vertical variability of POC content and SPM inorganic chemistry across the cross-section. Elemental (POC%) and isotopic POC signatures (^{13}C and ^{14}C) are inversely related to the particle size distribution (D50) (Figure S4). For each vertical depth profile, clay-rich fine particles are transported near the channel surface, and quartz-rich coarse particles flow near the river bottom. Accordingly, the Al/Si ratio, POC content and POC radiocarbon activity generally decrease with depth. These patterns are observed in other large fluvial systems, *e.g.*, Ganges and Brahmaputra, Amazon and Mackenzie (Galy et al., 2008b; Bouchez et al., 2014, Hilton et al., 2015), showing that hydrodynamic sorting is the primary control on suspended

sediment OC content, segregating inorganic and organic material according to their particle size (Bouchez et al., 2011a, 2014).

At the sampling site, lateral variability at the channel surface shows that POC-rich fine particles are preferentially transported near the right bank (Figure 2 and Figure S2). The channel geometry is thus examined as a potential factor creating lateral heterogeneity, through bank erosion and bedload resuspension.

The lower Huanghe has a relatively shallow depth (< 5.0 m) with generally deeper bathymetry near the right bank (YRCC, 2016), indicating preferential erosion of the right bank and potential deposition near the left bank. Continuous erosion of the right bank would provide solid material to the river, especially during the flood season. Such preferential erosion would make OC from the alluvial plain a potential source of POC in the lower reaches. This mechanism provides a possible explanation for the opposite trends displayed by JB1 and JB2 samples in $\Delta^{14}C$ vs. $\delta^{13}C$ space (Figure 5). The youngest POC was found at the bottom of the JB-1 profile. Meanwhile, the JB-1 samples have comparatively higher N/C_{org} ratios and N% consistent with discrete input of organic matter (*e.g.*, plant debris) from the bank in addition to rock-derived detrital clastic material in the coarse fractions (> 32 μm, Yu et al., 2019b). This would also explain the higher POC loading of the JB1 profile (section 5.1.1). Local bank erosion could be a significant erosion mechanism in river systems with low SPM concentrations, as shown for Arctic rivers (Guo et al, 2007).

The resuspension of bed sediments is also a possible mechanism to explain the lateral heterogeneity in POC content in the study cross-section of the Huanghe. Indeed, the scouring of channel bed sediment at high water flow may also shift POC to more negative radiocarbon and stable isotope signatures. Our sample set collected in July 2016 during flooding (water flow velocity up to 2.1 m/s, Figure 1) supports this hypothesis. Indeed, the increase in D50 of surface SPM samples from right to the left bank, that is with total channel depth decrease, is consistent with bed sediment resuspension. Such a scenario is also supported by the three-fold increase in sediment flux from Huayuankou to Lijin in July 2016 although the water discharge remained relatively constant between the two stations. The strong river bed scouring leads to resuspension of bed sediment that is very depleted in POC and in particular in ^{13}C and ^{14}C, thereby exerting a strong control on suspended POC. Interplayed by the previously mentioned processes, riverine POC heterogeneity occurs vertically and laterally over the cross-section.

5.2 POC provenance: the significance of loess-paleosol-derived OC

5.2.1 Physical erosion of the loess-paleosol sequence

Over decennial to centennial time scales, the POC export of the Huanghe is mainly controlled by physical erosion rates, especially by those in the CLP. Throughout the Quaternary, the erosion rate in the Huanghe basin has been mainly driven by climate shifts until human activities started and profoundly impacted sediment fluxes in the mid-Holocene (He et al., 2006). To determine the possible terrestrial OC components in riverine POC, we compiled published POC carbon isotope data for sediments collected in the lower reaches from 2011 to 2016 (Figure 5-6). Even though the Huanghe has experienced a 90% decrease in annual sediment load since the 1950s (Wang et al., 2015), the radiocarbon age of delivered POC is considerably old (avg 5,100 ± 1,700 ^{14}C yr, n=29), indicating a minor fraction of modern photosynthesized OC. This relatively ^{14}C-depleted POC suggests the significant contribution of OC originated from deep soil horizons. Given the fact that loess is easily erodible, the negative trend between ^{13}C and Fm for POC samples collected over the 2011-2016 period (Figure 5a) suggests that deep horizons of the loess-paleosol sequence are a plausible candidate for the ^{14}C-depleted end member. Besides, there is no doubt that the erosion of recently photosynthesized and possibly degraded OC_{bio} from the overlying topsoils (< 10 cm) contributes to riverine POC (Tao et al., 2015).

As such, the variable contribution of aged and radiocarbon-free OC from deep horizons of the loess-paleosol sequences has a significant impact on the elemental and isotopic signature of POC in the lower Huanghe. Erosion of loess-paleosol can also explain the decreasing POC% with increasing SPM concentration at different sites of the main channel (Ran et al., 2013; Qu et al., 2020) and the negative relationship between SPM concentration and corresponding POC Fm at Luokou (Figure 6) as the deep horizons of the loess-paleosol sequences are OC-poor, and mostly host OC that is highly degraded and refractory (Liu et al., 2012; Wang et al., 2013; Cheng et al., 2020). However, δ^{13}C of POC slightly increases with increasing SPM concentration, which might indicate the strengthened supply of soil OC from shallow depth as inferred from the δ^{13}C variation within the Xifeng loess-paleosol sequence (Figure 5a).

The N/C_{org} ratio provides additional evidence for the contribution of loess-paleosol material to Huanghe POC (Figure S5). Indeed, the N/C_{org} ratios of SPM collected in the lower reaches ranges from 0.10 to 0.23 (this study, Ran et al., 2013; Yu et al., 2019a),

while topsoils of the CLP are characterized by N/C_{org} lower than 0.14 (Liu and Liu, 2017) and sedimentary rocks typically have very low N/C_{org} (Hilton et al., 2015). Soil OC input from the North China Plain is also unlikely given its N/C_{org} of 0.10-0.13 (Shi et al., 2017). Therefore, all these possible sources cannot explain the high N/C_{org} signatures of riverine SPM. In addition, the high turbidity of the Huanghe (> 600 mg/L) during the sampling season prevents significant input from *in-situ* primary production (N/C_{org} > 0.13) (Zhang et al., 2013; Hu et al., 2015). As a consequence, only soil OC from deep loess-paleosol horizons appears as a plausible supplier to downstream Huanghe POC, as high N/C_{org} ratios are reported for different loess-paleosol sequences (Figure S5, Ning et al., 2006).

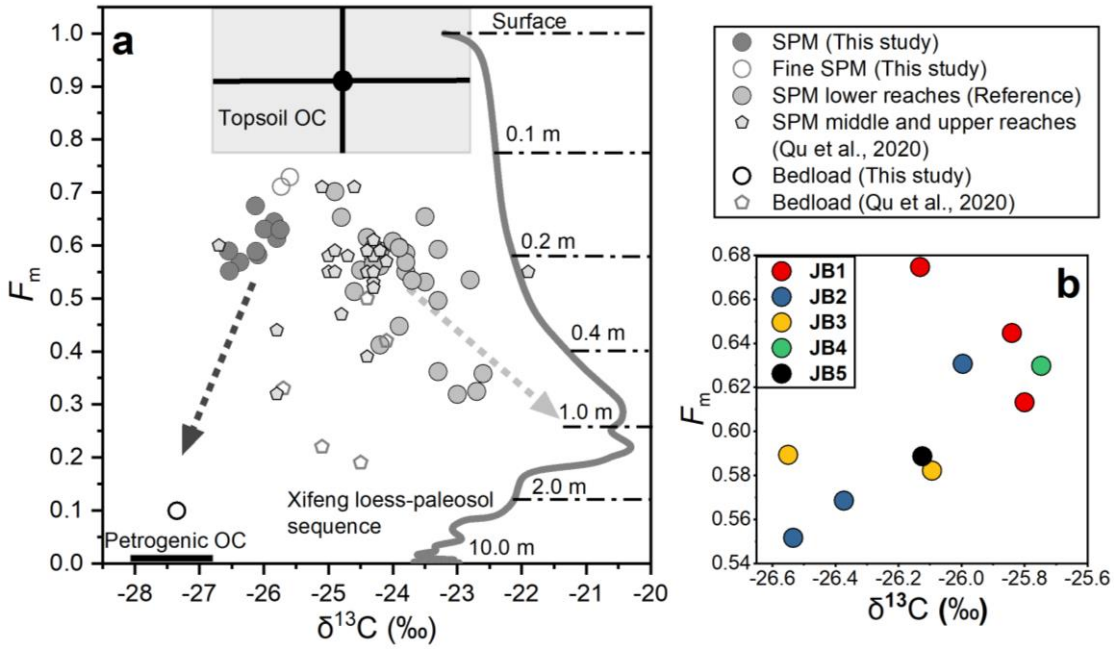

*Fig. 5 (a) Cross-plot of Fm and $\delta^{13}C$ used to infer the provenance of the Huanghe POC, using a compilation of POC data collected over the 2011-2016 period in the lower Huanghe, including samples from this study and previous studies at Huayuankou, Lijin, and Kenli (Hu et al., 2015; Tao et al., 2015; Yu et al., 2019a; and Ge et al., 2020); SPM and bedload collected by Qu et al., 2020 at Toudaoguai (most downstream location of the upper reaches) and Longmen in the middle reaches (Table S1). The grey curve corresponds to $\delta^{13}C_{org}$ of the top 10 m of the Xifeng loess-paleosol (Ning et al., 2006), and the corresponding Fm was calculated from ^{10}Be-derived ages following 'Age = −8033*ln(Fm)'. The soil depth is marked above the dot-dash line (Zhou et al., 2010). Topsoil OC represents OC from the upper 10 cm of the loess-paleosol sequence. (b) Cross-plot of POC Fm and $\delta^{13}C$ for the river samples collected in this study at the*

Luokou cross-section. The dark grey arrow represents the trend of dual carbon isotopic signatures over the cross-section obtained in this study, while the light grey arrow represents the trend described by a time series of surface SPM samples over the period 2011-2016, as compiled from studies cited above.

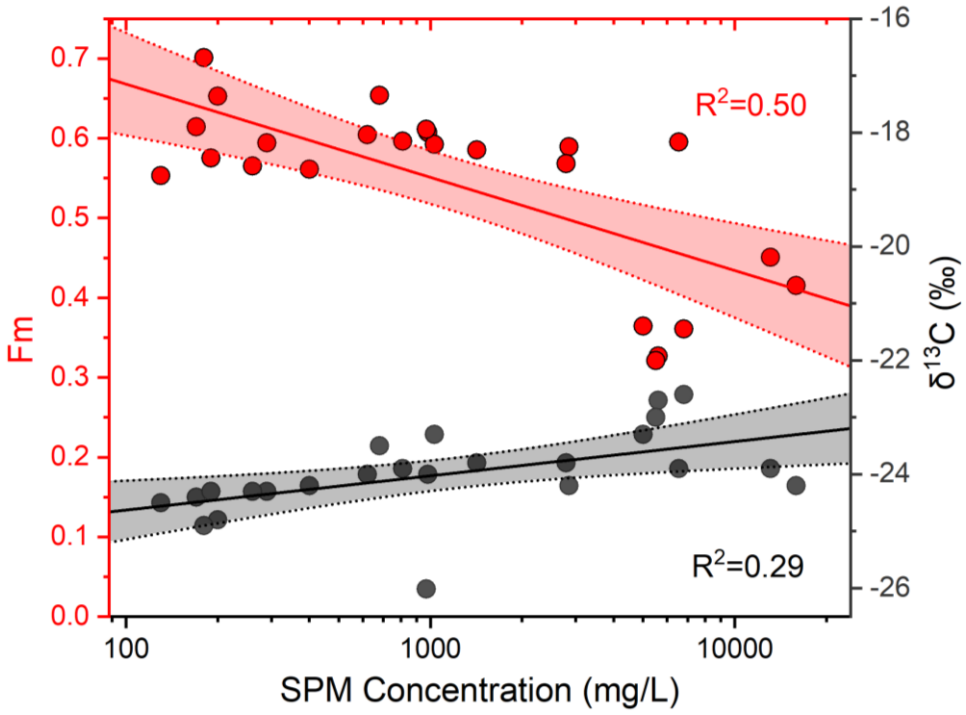

Fig. 6 $\Delta^{14}C$ (expressed as Fm; red circles) and $\delta^{13}C$ (black circles) of POC vs. SPM concentration for surface samples from the Huanghe collected from 2011 to 2016 (average SPM concentration of surface samples in this study and from Hu et al. (2015); Tao et al. (2015); Yu et al. (2019a); and Ge et al. (2020)). Paired dual carbon isotope data corresponds to the group 'SPM lower reaches' in Figure 5. Straight lines correspond to best-fit logarithmic curves, and shaded areas represent the 95% confidence interval.

Geomorphic processes in the CLP region support the erosion of deep soil horizons. The transfer of OC from the deep horizons takes place through erosion in gullies. Gully erosion is thought to be responsible for more than 80% of the total sediment yield in the CLP (He et al., 2006). Gullies are densely distributed and cover about 42% of the total area of the CLP and up to 60% in hilly regions (Huang and Ren, 2006; He et al., 2006). Nowadays, the well-developed gully geomorphic system in loess is characterized by gullies with a depth of about 10 m on average and represents the most active vertical and regressive erosion of loess (Huang and Ren, 2006). This incision process erodes all types of unconsolidated materials, including the loess-paleosol

sequence, underlaying red clays, and colluvial deposits in the form of creeps, falls, and slides in the watershed (Zhu, 2012). All these observations suggest that gully erosion strongly impacts the composition of riverine POC. As gully erosion is sensitive to climate change and anthropogenic activities, soil dynamics in the Huanghe basin have been altered since the mid-Holocene. In recent years, soil and water conservation and environmental rehabilitation campaigns (Wang et al., 2007) largely contributed to the reduction of SPM export by the Huanghe with a transfer to the estuary of 10.6 Mt in 2016, which represents a few percent of the annual sediment flux measured in 2013 (172.8 Mt) and less than one percent of the flux of the 1950s (*ca*. 1,340 Mt; Wang et al., 2015). Such modifications have drastically affected POC export by the Huanghe.

5.2.2 POC source determination and end member apportionment

Considering the SPM geochemistry and the basin characteristics, three terrestrial sources can be identified as necessary to explain the composition of the Huanghe POC at the Luokou cross-section. As discussed in section 5.2.1 and shown in Figure 5a, two sources are (a) the topsoil-derived OC (OC_{ts}) and (b) the loess-paleosol sequence OC (OC_{lps}) excluding topsoil. In addition, at the Luokou cross-section, bedload OC shows lower Fm and $\delta^{13}C$ compared to that of SPM, suggesting a significant contribution for (c) rock-derived OC from erosion in the middle reach (OC_{petro}).

As topsoil typically contains recently photosynthesized OC_{bio}, we used a $\delta^{13}C$ value of −24.8 ± 1.9‰ (n=166) according to the subsurface soil OC values measured across the Huanghe basin (Rao et al., 2017). Over the sampled cross-section, the depleted ^{13}C values indicate the dominant and almost exclusive input of C3 plant-derived material to the Huanghe POC in the lower reaches. Based on ^{14}C (Liu et al., 2012) and ^{10}Be (Zhou et al., 2010) dating of < 10 cm-deep soil horizons in the Huanghe Basin, the average age of topsoil was chosen as being younger than 2,000 yr (*i.e.*, $\Delta^{14}C > -220‰$). As the topsoil end member includes modern biospheric material ($\Delta^{14}C$ around 40‰, Hua et al., 2013), we assigned a $\Delta^{14}C$ value of −90 ± 130‰ (Fm = 0.91 ± 0.13) to this endmember. This range also includes the range of $\Delta^{14}C$ values of pre-aged soil OC indicated by the long-chain n-$C_{24+26+28}$ alkanols of the Huanghe POC reported by Tao et al. (2015) and Yu et al. (2019a). Their results show consistent POC $\Delta^{14}C$ values in the lower reaches of −204 ± 20‰ (Fm = 0.80 ± 0.03, n=7) from June 2015 to May 2016 and −219 ± 33‰ (Fm = 0.79 ± 0.04, n=4) at Kenli and of −198±15‰ (Fm = 0.81 ± 0.02, n=6) from June 2015 to April 2016 at Huayuankou.

The second end member should be characterized by aged and refractory OC from the loess-paleosol sequence excluding topsoil (upper 10 m) of the CLP. Radiocarbon dating has an upper age limit of around 50,000 yr, age above which F_m is equal to 0. However, radiocarbon-free OC spanning from 50,000 to 100,000 yr must still be considered as OC_{bio} in the long-term carbon cycle. Here, we name this ignored OC as the "dormant" OC, without which the OC_{bio} (*i.e.*, less than 100,000 yr old) would be underestimated to some extent because the radiocarbon-free OC is misinterpreted as having a petrogenic origin. To consider this "dormant" OC, a $\delta^{13}C$ values of −22.7 ± 1.0‰ and a $\Delta^{14}C$ values of −610 ± 390‰ (Fm, 0.39 ± 0.39) were adopted based on loess-paleosol sequence average. Although the radiocarbon-free OC older than 100,000 yr overlaps with this endmember, such old (and deep) soil organic carbon is probably not mobilized as modern gully erosion mainly concerns the upper 10 m of the loess-paleosol sequences.

Regarding OC_{petro}, rock-derived OC from the QTP and the CLP, as well as kerogen from oil-gas fields from the Ordos Basin, were all considered to be possible contributors. The $\delta^{13}C$ of OC_{petro} greatly varies between the QTP (−21.2 ± 1.2‰, n=11, Liu et al., 2007) and the CLP (−26.8 ± 0.5‰, n=8, Qu et al., 2020). However, most of the sediments eroded from the QTP are not transferred to the lower reaches as they remain trapped in the CLP and the western Mu Us desert (Nie et al., 2015; Licht et al., 2016; Pan et al., 2016). In addition, the construction of large dams in the upper reaches has considerably reduced the transfer of solid materials downstream (Wang et al., 2007). Therefore, rock-derived OC inherited from the denudation of the QTP region is not further considered. Kerogen from the oil-gas fields of the Ordos Basin in the CLP region (Figure 1) has $\delta^{13}C$ values of −29.2 ± 0.9‰ (n=10, Guo et al., 2014). Taking these constraints together, we consider a $\delta^{13}C$ value of −28.1 ± 1.5‰ for the OC_{petro} end member, and a $\Delta^{14}C$ value of −1000‰ (F_m = 0) by definition.

A three endmembers Bayesian Monte-Carlo simulation model based on the mass balance of carbon isotopes ($\delta^{13}C$ and $\Delta^{14}C$) has been used to reconstruct source apportionment (Section 3.3). Modeling results are shown in Figure 7 as relative contributions from OC_{ts}, OC_{lps}, and OC_{petro} (Table S2). The contribution of OC_{petro} to total OC varies between 21% and 33% in the cross-section, which is higher than that in the two fine SPM samples (17% on average) and much smaller than in the bedload (78 ± 10%). The inferred OC_{petro} concentration is remarkably uniform in the cross-section, representing 0.10 ± 0.01% of SPM. This result is consistent with the OC contents of

midstream sedimentary rocks at 0.09 ± 0.08% (Qu et al., 2020). In addition, these findings imply that OC_{petro} concentration does not depend on particle size and confirm previous findings of OC_{petro} being present in a range of clastic particles or as discrete particles (Galy et al., 2008a; Bouchez et al., 2014). In other words, the rock-derived OC has a relatively invariant contribution with depth (Galy et al., 2008a; Bouchez et al., 2014), meaning that biospheric OC exerts a first-order control on POC content and isotopic variations throughout the cross-section.

At the study cross-section, OC_{ts} and OC_{lps} contribute 50%-60% and 17%-23% to the total POC, respectively. The sum of these two components can be considered as OC_{bio}, which varies between 67% and 77% The corresponding OC_{bio} content of sediment is quite variable, ranging from 0.20% (sample JB2-3) to 0.34% (sample JB1-1), and generally decreases from the river surface to the bottom. Given the rather invariant OC_{petro} concentration in the sediment, there are thus marked heterogeneities of POC provenance in the cross-section. For instance, POC transported close to the right bank and in the finer SPM samples show a higher contribution from OC_{bio} with a relatively lower relative contribution of OC_{petro}. From the knowledge of the relative contributions of OC_{ts} and OC_{lps} and their respective ^{14}C activity, can also estimate the Fm values for the bulk OC_{bio} from mass balance. The modeled radiocarbon activity of OC_{bio} is relatively homogeneous with an average $\Delta^{14}C$ value of −178 ± 11‰ (1,510 ± 110 ^{14}C yr) whereas there is a great variance in the bulk ^{14}C content. In summary, our results support the first-order control of OC_{bio} abundance on POC radiocarbon in the Huanghe.

Applying the same mixing model to previously published Huanghe POC data (2011-2016, Table S1) shows (1) dominance of the OC_{bio} contribution to POC, (2) variable relative mixing proportions of OC_{ts} and OC_{lps}; (3) a wide range of ^{14}C age for OC_{bio} (from 1,040 to 8,050 yr). In particular, OC_{ts} and OC_{lps} contributed 20%-30% and 46%-68% to POC collected in 2013 (Hu et al., 2015), leading to 75%-89% of OC_{bio}. Yu et al. (2019a) estimated that OC_{bio} contributed 63%-81% to the lower Huanghe POC (2015-2016) using a different mixing model. Using their data in our mixing model results an OC_{bio} contribution of 77%-87%, consisting of 39%-53% for OC_{ts} and 30%-47% for OC_{lps}. This difference mainly results from the fact that "dormant" OC_{bio} from loess-paleosol sequences was not considered in Yu et al. (2019a)'s study, and from the different isotopic signatures chosen for the POC endmembers. However, both estimates ignore the possible presence of rock-derived OC in soils. In any case, our results suggest

that the Huanghe transports more OC_{bio}-derived POC than previously thought, with more aged, soil-derived OC.

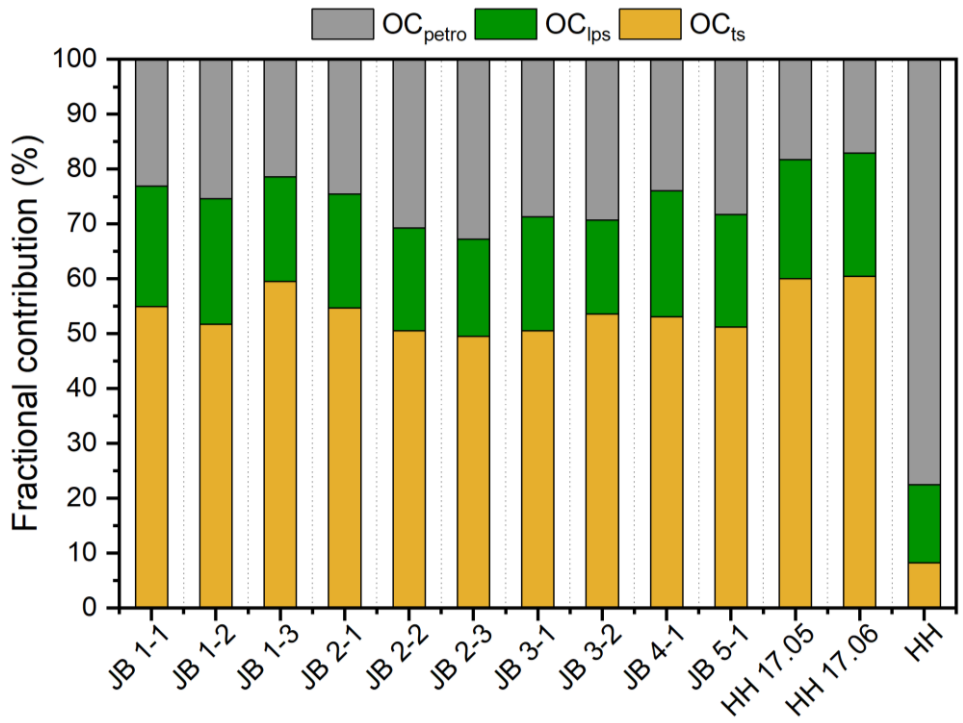

Fig. 7 Relative contributions of the three different sources of POC at the Luokou cross-section on the Huanghe as inferred from our mixing model.

It is worth noticing that the OC_{lps} fraction is significantly higher in 2013 than in 2016. As most Huanghe sediments are derived from the CLP, the higher physical erosion in the CLP likely enhances the mobilization of aged and "dormant" OC_{bio} into the river system. This relatively refractory OC_{bio} fraction is nearly stabilized and mostly preserved by kaolinite and iron oxides (Wang et al., 2013). As a consequence, the decrease in sediment supply from the CLP initiated a few decades ago (Wang and Fu et al., 2016), which is likely to continue in the future, will probably lead to the reduction of the contribution of OC_{lps} to total POC export from the Huanghe. This might have an impact on the burial efficiency of riverine POC on the continental margins, as OC_{ts} is more labile than OC_{lps} and thus a more prone remineralization process before burial. Moreover, a decreasing erosion rate in the Huanghe basin will potentially favor oxidation of all POC components before burial, because of the lower sediment accumulation rate (Blair and Aller, 2012). Overall, CO_2 degassing should mitigate to play a more important role in the carbon cycling of the Huanghe basin as a response to the weakening terrestrial physical erosion.

5.3 Instantaneous fluxes

In the Huanghe, POC content varies both vertically and laterally throughout the cross-section (Figure 2). This spatial variability of both physical and chemical SPM characteristics must be modeled in the whole cross-section when estimating integrated instantaneous POC flux and concentration (Section 3.4).

At the sampling time (July 2016), the Huanghe transported 1,075 kg/s of SPM for a water discharge of 731 m^3/s, such that the cross-section integrated SPM concentration (SPM_{int}) was 1,472 mg/L, a value relatively close to the average concentration of our 10 samples (1,286 mg/L). The Luokou gauging station records a monthly SPM load of 1,826 kg/s in July 2016, and the daily average SPM load of 1,096 kg/s for the daily average water discharge of 643 m^3/s on the 16^{th} and 17^{th} of July 2016 (method: three water samples were collected at 0.5 m below the channel surface in the transect profile, data available at http://www.yrcc.gov.cn). Even though the calculation neglects the vertical heterogeneity within this relatively shallow river (< 5.0 m), estimates give similar results.

We obtain an instantaneous POC flux of 3.69 kg/s, corresponding to a cross-section integrated average POC content (POC_{int}%) of 0.34% when dividing this instantaneous POC flux by the instantaneous SPM load. Given the relatively homogenous distribution of OC_{petro}, the instantaneous flux of OC_{petro} was calculated by multiplying the average OC_{petro} content by the instantaneous cross-section integrated SPM flux, yielding 1.07 ± 0.11 kg/s. The instantaneous OC_{bio} flux was then calculated by subtracting the instantaneous flux of OC_{petro} from the instantaneous POC flux, yielding 2.61 ± 0.26 kg/s. Assuming that our SPM samples are representative in terms of POC content exported in July 2016, and taking the SPM flux of the gauging station for July, then the estimated fluxes of POC, OC_{bio}, and OC_{petro} for the flood period of July 2016 are 6.1, 4.3, and 1.8 kg/s, respectively. Taking POC_{int} content for estimating the annual POC flux gives a value of 1.1 kg/s consisting of 0.8 and 0.3 kg/s for OC_{bio} and OC_{petro} fluxes, respectively. Note that these numbers are lower estimates because POC content in Huanghe SPM collected during flood periods is generally the lowest (Ran et al., 2013).

The above numbers present a sharp decrease compared to the estimated POC and OC_{bio} fluxes transported by the Huanghe over the period 2008 to 2013. Galy et al. (2015) estimated an OC_{petro} flux of 1.9 kg/s and an OC_{bio} flux of 11.4 kg/s from 2008 to 2012 (SPM flux: 3,655 kg/s, YRCC 2016), while Tao et al. (2018) reported an OC_{petro} flux

of 5.8 kg/s and a similar OC_{bio} flux of 12.6 kg/s from June 2012 to May 2013 (SPM flux: 5,723 kg/s, YRCC 2016). The dramatic decrease in sediment load exerts a first-order control on the POC reduction. In addition, previous estimates of POC flux in the Huanghe might be biased as these estimates neglect the variability over the cross-section (*e.g.*, Hu et al., 2015; Ran et al., 2013; Tao et al., 2015). SPM samples analyzed so far for the Huanghe were generally collected within the first 0.5 m below the surface, meaning that previous POC estimates did not consider the observed vertical and lateral POC heterogeneities and have thus misestimated POC sources and fluxes. Those estimates were calculated by multiplying an individual surface POC content by the corresponding monthly or weekly suspended sediment load, as provided by hydrological stations. Such estimates can be problematic because POC content in SPM generally decreases from top to bottom (Figure 2), resulting in biased surface-based estimates of fluxes (Bouchez et al., 2014). Using our cross-section data, we can estimate the variability in POC flux estimates by multiplying depth-integrated sediment flux by the POC content of every single sample. Such calculation shows different POC fluxes ranging from −15% to +30% compared to the depth-integrated estimate, which is mostly influenced by the variable POC content. Considering SPM collected at the channel surface, POC flux estimates using samples JB 1-1 and JB 2-1 are 28% and 15% higher, respectively, and are 6% and 5% lower using samples JB 3-1 and JB 5-1, respectively, than the depth-integrated estimate. This simple sensitivity analysis shows that channel surface sampling of SPM alone does not necessarily result in an overestimation of POC flux because of lateral heterogeneity, even though the POC content of SPM is generally higher at the surface than at the bottom (Figure 2). "Local" POC loads can also be calculated throughout the cross-section using the local water velocity, SPM concentration, and POC content (Figure 8). In general, in the Huanghe more POC is transported near the river bottom and on the left side of the channel (except for profile JB 5). For instance, there is a nearly two-fold increase in POC export from the surface to the bottom for the JB 2 and JB 3 profiles. The maximum local bulk POC export (sample JB 3-2), OC_{bio} (sample JB 3-2), and OC_{petro} (sample JB 4-1) are over 6 times higher than the corresponding minimum values (sample JB 5-1). The POC load spatial pattern is almost the reverse of the POC% variation over the cross-section, indicating the high potential of POC load transferred in high turbidity flows and the importance of the river dynamics in POC delivery. It could be anticipated that during the low-water season, when water velocity is slower, near-bottom SPM is deposited on

the channel bed, withdrawing a high flux of POC from the river export, a topic that should be further examined in further research.

Interestingly, anthropogenic activities may have antagonistic effects on POC export. Activities such as deforestation, agriculture, or mining have considerably enhanced the sediment yield from the CLP since the mid-Holocene (He et al., 2006) while the construction of large dams, soil and water conservation measures, and afforestation has considerably reduced the sediment yield since the 1950s (Wang and Fu et al., 2016; Wang et al., 2007; Syvitski et al., 2005). Yet the Huanghe exports substantial OC_{bio} and OC_{petro} with a significantly higher burial efficiency (~42% on average; Sun et al., 2018) than other large fluvial systems entering passive continental margins, such as the Changjiang, Amazon, and Mississippi (Blair and Aller, 2012). It is reported that aged soil OC is nearly fully preserved in continental margins and that OC_{petro} has a *ca.* 70% burial efficiency (Tao et al., 2016). However, the contribution of the Huanghe OC burial to the global C sink is likely to be lower in the future as the consequence of 1) sharp decrease in SPM and POC export due to weakened physical erosion in the CLP; 2) reduced sediment accumulation rate favoring OC remineralization in estuaries (Blair and Aller, 2012; Walling and Fan, 2003; Milliman and Farnsworth, 2011; Galy et al., 2015).

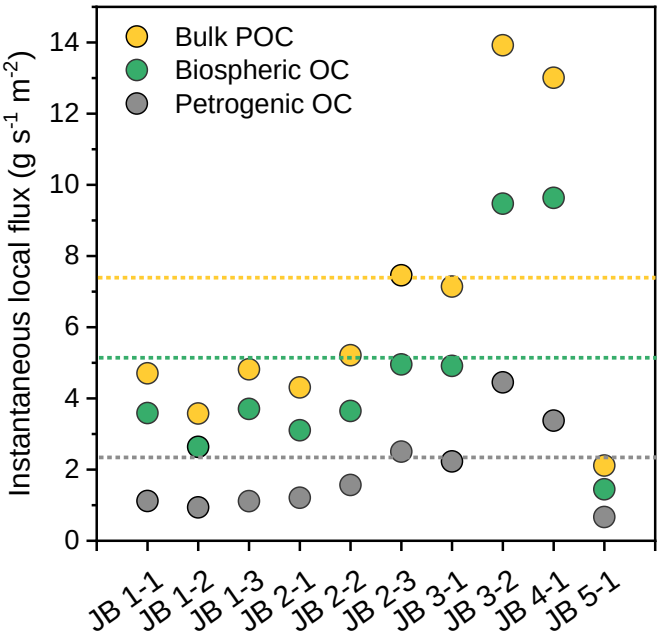

Fig. 8 Estimates of instantaneous "local" flux of bulk POC and two components (OC_{bio} and OC_{petro}), calculated for each sample of the cross-section. The three dotted lines marked in orange, green, and grey represent the corresponding instantaneous, cross-section integrated fluxes.

6. Conclusions

In this contribution, we present the first detailed study of particulate organic carbon (POC) over a complete river cross-section of the Huanghe, providing new perspectives on the transport mode, source, and instantaneous fluxes of POC in this turbid large river.

At the scale of a cross-section, physical and chemical properties of SPM are heterogeneous both vertically and laterally, a feature that is mainly controlled by bathymetry and hydrodynamic sorting. Resuspension of bed sediment and local erosion of the right bank together impact the suspended POC composition during the considered flooding period. This spatial heterogeneity shows that near-bottom SPM plays a dominant role in the delivery of OC_{bio} (topsoil and deep soil OC combined) and OC_{petro}. Despite a relatively shallow river depth (< 5.0 m) and narrow width (< 200 m), the heterogeneity of POC transport over a cross-section needs to be considered in constraining POC transport mode and estimating POC fluxes,

Despite its millennial age, POC in the Huanghe is dominated by OC_{bio} with a contribution of 67% to 79%. OC_{petro} content in SPM is relatively homogeneous (0.08% - 0.11%) over the cross-section, indicating that the variability in bulk POC $\Delta^{14}C$ is mainly controlled by the variability in OC_{bio} content, especially in the finest SPM fraction. OC_{bio} ages deduced from the application of our mixing model to literature data (record period 2011-2016) are highly variable, ranging from 1,040 to 8,050 ^{14}C yr. We interpret this feature as resulting from the erosion of deep horizons by gully systems in the loess-paleosol sequences containing ^{14}C-dead OC_{bio}. Enhanced erosion of deep loess-paleosol horizons mobilizes aged and refractory OC to the ocean with high burial efficiency on the passive margin. However, the construction of large dams has drastically affected the sediment load of the Huanghe system and retains substantial quantities of sediments that previously ended in the ocean. Future work is needed to further quantify how these anthropogenic modifications alter POC composition and transport mode, by conducting comprehensive cross-section sampling campaigns over extended time series upstream and downstream from dams.

Acknowledgments

This study was financially supported by the Agence Nationale de la Recherche (ANR) SEDIMAN (Grant ANR-15-CE01-0012), the National Natural Science Foundation of China (NSFC), grants 41561134017, 41625012, and the China Scholarship Council (CSC) to Yutian Ke (No.201706180008). We thank Yulong Liu and Shengliu Yuan for

their help during the sampling and, François Thil and Nadine Tissenerat for invaluable help when running the ECHoMICADAS.

Reference

Andersson, A., Deng, J., Du, K., Zheng, M., Yan, C., Sköld, M., & Gustafsson, Ö. (2015). Regionally-Varying Combustion Sources of the January 2013 Severe Haze Events over Eastern China. Environmental Science & Technology, 49(4), 2038–2043.

Baronas, J. J., Stevenson, E. I., Hackney, C. R., Darby, S. E., Bickle, M. J., Hilton, R. G., et al. (2020). Integrating suspended sediment flux in large alluvial river channels : application of a synoptic Rouse-based model to the Irrawaddy and Salween rivers. Journal of Geophysical Research, 125(9).

Bianchi, T. S. (2011). The role of terrestrially derived organic carbon in the coastal ocean: A changing paradigm and the priming effect. Proceedings of the National Academy of Sciences of the United States of America, 108(49), 19473–19481.

Bird, A., Stevens, T., Rittner, M., Vermeesch, P., Carter, A., Andò, S., et al. (2015). Quaternary dust source variation across the Chinese Loess Plateau. Palaeogeography, Palaeoclimatology, Palaeoecology, 435(435), 254–264.

Blair, N. E., & Aller, R. C. (2012). The fate of terrestrial organic carbon in the marine environment. Annual Review of Marine Science, 4(1), 401–423.

Blair, N. E., Leithold, E. L., Brackley, H., Trustrum, N., Page, M., & Childress, L. (2010). Terrestrial sources and export of particulate organic carbon in the Waipaoa sedimentary system: Problems, progress and processes. Marine Geology, 270(1), 108–118.

Bouchez, J., Galy, V., Hilton, R. G., Gaillardet, J., Moreira-Turcq, P., Pérez, M. A., et al. (2014). Source, transport and fluxes of Amazon River particulate organic carbon: Insights from river sediment depth-profiles. Geochimica et Cosmochimica Acta, 133, 280–298.

Bouchez, J., Gaillardet, J., France-Lanord, C., Maurice, L., & Dutra-maia, P. (2011a). Grain size control of river suspended sediment geochemistry: Clues from Amazon River depth profiles. Geochemistry Geophysics Geosystems, 12(3).

Bouchez, J., Lupker, M., Gaillardet, J., France-Lanord, C., & Maurice, L. (2011b). How important is it to integrate riverine suspended sediment chemical composition with

depth? Clues from Amazon River depth-profiles. Geochimica et Cosmochimica Acta, 75(22), 6955–6970.

Carignan, J., Hild, P., Mevelle, G., Morel, J., & Yeghicheyan, D. (2001). Routine Analyses of Trace Elements in Geological Samples using Flow Injection and Low Pressure On-Line Liquid Chromatography Coupled to ICP-MS: A Study of Geochemical Reference Materials BR, DR-N, UB-N, AN-G and GH. Geostandards and Geoanalytical Research, 25, 187-198.

Cauwet, G., & Mackenzie, F. T. (1993). Carbon inputs and distribution in estuaries of turbid rivers: the Yang Tze and Yellow rivers (China). Marine Chemistry, 43, 235-246.

Cheng, P., Burr, G. S., Zhou, W., Chen, N., Hou, Y., Du, H., et al. (2020). The deficiency of organic matter 14C dating in Chinese Loess-paleosol sample. Quaternary Geochronology, 56, 101051.

Curry, K. J., Bennett, R. H., Mayer, L. M., Curry, A., Abril, M., Biesiot, P. M., & Hulbert, M. H. (2007). Direct Visualization of Clay Microfabric Signatures Driving Organic Matter Preservation in Fine-grained Sediment. Geochimica et Cosmochimica Acta, 71(7), 1709-1720. https://doi.org/10.1016/J.GCA.2007.01.009

Dellinger, M., Gaillardet, J., Bouchez, J., Calmels, D., Galy, V., Hilton, R. G., et al. (2014). Lithium isotopes in large rivers reveal the cannibalistic nature of modern continental weathering and erosion. Earth and Planetary Science Letters, 401, 359–372.

Freymond, C. V, Lupker, M., Peterse, F., Haghipour, N., Wacker, L., Filip, F., et al. (2018). Constraining Instantaneous Fluxes and Integrated Compositions of Fluvially Discharged Organic Matter. Geochemistry Geophysics Geosystems, 19(8), 2453–2462.

Gaillardet, J., Dupré, B., & Allègre, C. J. (1999). Geochemistry of large river suspended sediments: silicate weathering or recycling tracer? Geochimica et Cosmochimica Acta, 63(23), 4037–4051. https://doi.org/10.1016/S0016-7037(99)00307-5

Galy, V., & Eglinton, T. (2011). Protracted storage of biospheric carbon in the Ganges-Brahmaputra basin. Nature Geoscience, 4(12), 843–847.

Galy, V., Beyssac, O., France-Lanord, C., & Eglinton, T. (2008a). Recycling of Graphite During Himalayan Erosion: A Geological Stabilization of Carbon in the Crust. Science, 322(5903), 943–945.

Galy, V., France-Lanord, C., & Lartiges, B. (2008b). Loading and fate of particulate organic carbon from the Himalaya to the Ganga–Brahmaputra delta. Geochimica et Cosmochimica Acta, 72(7), 1767–1787.

Galy, V., France-Lanord, C., Beyssac, O., Faure, P., Kudrass, H., & Palhol, F. (2007). Efficient organic carbon burial in the Bengal fan sustained by the Himalayan erosional system. Nature, 450(7168), 407–410.

Galy, V., Peucker-Ehrenbrink, B., & Eglinton, T. I. (2015). Global carbon export from the terrestrial biosphere controlled by erosion. Nature, 521(7551), 204–207.

Garzanti, E., Andò, S., France-Lanord, C., Vezzoli, G., Censi, P., Galy, V., & Najman, Y. (2010). Mineralogical and chemical variability of fluvial sediments 1. Bedload sand (Ganga–Brahmaputra, Bangladesh). Earth and Planetary Science Letters, 299(3), 368–381.

Ge, T., Xue, Y., Jiang, X., Zou, L., & Wang, X. (2020). Sources and radiocarbon ages of organic carbon in different grain size fractions of Yellow River-transported particles and coastal sediments. Chemical Geology, 534, 119452.

Gu, Z., Duan, X., Shi, Y., Li, Y., & Pan, X. (2018). Spatiotemporal variation in vegetation coverage and its response to climatic factors in the Red River Basin, China. Ecological Indicators, 93, 54–64.

Guo, H., Jia, W., Peng, P., Lei, Y., Luo, X., Cheng, M., et al. (2014). The composition and its impact on the methane sorption of lacustrine shales from the Upper Triassic Yanchang Formation, Ordos Basin, China. Marine and Petroleum Geology, 57, 509–520.

Guo, K., Zou, T., Jiang, D., Tang, C., & Zhang, H. (2017). Variability of Yellow River turbid plume detected with satellite remote sensing during water-sediment regulation. In Continental Shelf Research (Vol. 135, pp. 74–85).

Guo, L., Ping, C. L., & Macdonald, R. W. (2007). Mobilization pathways of organic carbon from permafrost to arctic rivers in a changing climate. Geophysical Research Letters, 34(13). https://doi.org/10.1029/2007GL030689

Guo, Z. T., Ruddiman, W. F., Hao, Q. Z., Wu, H. B., Qiao, Y. S., Zhu, R. X., et al. (2002). Onset of Asian desertification by 22 Myr ago inferred from loess deposits in China. Nature, 416(6877), 159–163.

Hatte, C., Tisnerat-Laborde, N., Ayrault, S., Balesdent, J., Chapon, V., Bourguignon, J., ... and Moulin, C., 2016. Echomicadas, a new tool to analyse carbon 14. Biofutur (Paris), 26-57.

Hay, W. W. (1998). Detrital sediment fluxes from continents to oceans. Chemical Geology, 145(3), 287–323.

He, X., Zhou, J., Zhang, X., & Tang, K. (2006). Soil erosion response to climatic change and human activity during the Quaternary on the Loess Plateau, China. Regional Environmental Change, 6(1), 62–70. https://doi.org/10.1007/S10113-005-0004-7

Hemingway, J. D., Hilton, R. G., Hovius, N., Eglinton, T. I., Haghipour, N., Wacker, L., et al. (2018). Microbial oxidation of lithospheric organic carbon in rapidly eroding tropical mountain soils. Science, 360(6385), 209–212.

Hemingway, J. D., Rothman, D. H., Grant, K. E., Rosengard, S. Z., Eglinton, T. I., Derry, L. A., & Galy, V. V. (2019). Mineral protection regulates long-term global preservation of natural organic carbon. Nature, 570(7760), 228–231.

Hilton, R. G., Gaillardet, J., Calmels, D., & Birck, J.-L. (2014). Geological respiration of a mountain belt revealed by the trace element rhenium. Earth and Planetary Science Letters, 403, 27–36.

Hilton, R. G., Galy, A., Hovius, N., Horng, M.-J., & Chen, H. (2011). Efficient transport of fossil organic carbon to the ocean by steep mountain rivers: An orogenic carbon sequestration mechanism. Geology, 39(1), 71–74.

Hilton, R. G., Galy, V., Gaillardet, J., Dellinger, M., Bryant, C., O'Regan, M., et al. (2015). Erosion of organic carbon in the Arctic as a geological carbon dioxide sink. Nature, 524(7563), 84–87.

Hu, B., Li, J., Bi, N., Wang, H., Wei, H., Zhao, J., et al. (2015). Effect of human-controlled hydrological regime on the source, transport, and flux of particulate organic carbon from the lower Huanghe (Yellow River). Earth Surface Processes and Landforms, 40(8), 1029–1042.

Hua, Q., Barbetti, M., & Rakowski, A. Z. (2013). Atmospheric Radiocarbon for the Period 1950–2010. Radiocarbon, 55(4), 2059–2072.

Huang, C. C., & Ren, Z. (2006). Fluvial erosion and the formation of gully systems over the chinese loess plateau. WSEAS Transactions on Environment and Development, 2(2), 141-145.

Jahn, B., Gallet, S., & Han, J. (2001). Geochemistry of the Xining, Xifeng and Jixian sections, Loess Plateau of China: eolian dust provenance and paleosol evolution during the last 140 ka. Chemical Geology, 178(1), 71–94. https://doi.org/10.1016/S0009-2541(00)00430-7

Keil, R. G., Mayer, L. M., Quay, P. D., Richey, J. E., & Hedges, J. I. (1997). Loss of

organic matter from riverine particles in deltas. Geochimica et Cosmochimica Acta, 61(7), 1507–1511.

Li, G., Wang, X. T., Yang, Z., Mao, C., West, A. J., & Ji, J. (2015). Dam-triggered organic carbon sequestration makes the Changjiang (Yangtze) river basin (China) a significant carbon sink. Journal of Geophysical Research: Biogeosciences, 120(1), 39-53.

Licht, A., Pullen, A., Kapp, P., Abell, J., & Giesler, N. (2016). Eolian cannibalism: Reworked loess and fluvial sediment as the main sources of the Chinese Loess Plateau. Geological Society of America Bulletin, 128, 944–956.

Liu, G., Xu, W., Zhang, Q., & Xia, Z. (2012). Holocene Soil Chronofunctions, Luochuan, Chinese Loess Plateau. Radiometric Dating, 41.

Liu, J., & Liu, W. (2017). Soil nitrogen isotopic composition of the Xifeng loess-paleosol sequence and its potential for use as a paleoenvironmental proxy. Quaternary International, 440, 35–41.

Liu, W., Yang, H., Ning, Y., & An, Z. (2007). Contribution of inherent organic carbon to the bulk δ13C signal in loess deposits from the arid western Chinese Loess Plateau. Organic Geochemistry, 38(9), 1571–1579.

Ludwig, W., Probst, J.-L., & Kempe, S. (1996). Predicting the oceanic input of organic carbon by continental erosion. Global Biogeochemical Cycles, 10(1), 23–41.

Mayorga, E., Aufdenkampe, A. K., Masiello, C. A., Krusche, A. V, Hedges, J. I., Quay, P. D., et al. (2005). Young organic matter as a source of carbon dioxide outgassing from Amazonian rivers. Nature, 436(7050), 538–541.

Milliman, J. D., & Farnsworth, K. L. (2011). River discharge to the coastal ocean: a global synthesis. Cambridge University Press.

Milliman, J. D., Yun-Shan, Q., Mei-E, R., & Saito, Y. (1987). Man's Influence on the Erosion and Transport of Sediment by Asian Rivers: The Yellow River (Huanghe) Example. The Journal of Geology, 95(6), 751–762.

Ning, Y., Liu, W., & An, Z. (2006). Variation of soil $\delta^{13}C$ values in Xifeng loess-paleosol sequence and its paleoenvironmental implication. Chinese Science Bulletin, 51(11), 1350-1354.

Pan, B., Pang, H., Gao, H., Garzanti, E., Zou, Y., Liu, X., et al. (2016). Heavy-mineral analysis and provenance of Yellow River sediments around the China Loess Plateau. Journal of Asian Earth Sciences, 127(127), 1–11.

Qu, Y., Jin, Z., Wang, J., Wang, Y., Xiao, J., Gou, L., et al. (2020). The sources and

seasonal fluxes of particulate organic carbon in the Yellow River. Earth Surface Processes and Landforms, 45(9), 2004–2019.

Ran, L., Lu, X. X., & Xin, Z. (2014). Erosion-induced massive organic carbon burial and carbon emission in the Yellow River basin, China. Biogeosciences, 11(4), 945–959.

Ran, L., Lu, X. X., Sun, H., Han, J., Li, R., & Zhang, J. (2013). Spatial and seasonal variability of organic carbon transport in the Yellow River, China. Journal of Hydrology, 498, 76–88. https://doi.org/10.1016/J.JHYDROL.2013.06.018

Rao, Z., Guo, W., Cao, J., Shi, F., Jiang, H., & Li, C. (2017). Relationship between the stable carbon isotopic composition of modern plants and surface soils and climate: A global review. Earth-Science Reviews, 165(165), 110–119.

Shi, H., & Shao, M. (2000). Soil and water loss from the Loess Plateau in China. Journal of Arid Environments, 45(1), 9–20.

Stevens, T., Carter, A., Watson, T. P., Vermeesch, P., Andò, S., Bird, A. F., et al. (2013). Genetic linkage between the Yellow River, the Mu Us desert and the Chinese Loess Plateau. Quaternary Science Reviews, 78, 355–368.

Sun, D., Tang, J., He, Y., Liao, W., & Sun, Y. (2018). Sources, distributions, and burial efficiency of terrigenous organic matter in surface sediments from the Yellow River mouth, northeast China. Organic Geochemistry, 118, 89–102.

Syvitski, J. P. M., Vörösmarty, C. J., Kettner, A. J., & Green, P. (2005). Impact of Humans on the Flux of Terrestrial Sediment to the Global Coastal Ocean. Science, 308(5720), 376–380.

Tao, S., Eglinton, T. I., Montluçon, D. B., McIntyre, C., & Zhao, M. (2015). Pre-aged soil organic carbon as a major component of the Yellow River suspended load: Regional significance and global relevance. Earth and Planetary Science Letters, 414, 77–86.

Tao, S., Eglinton, T. I., Montluçon, D. B., McIntyre, C., & Zhao, M. (2016). Diverse origins and pre-depositional histories of organic matter in contemporary Chinese marginal sea sediments. Geochimica et Cosmochimica Acta, 191(2016), 70–88. https://doi.org/10.1016/J.GCA.2016.07.019

Tao, S., Eglinton, T. I., Zhang, L., Yi, Z., Montluçon, D. B., McIntyre, C., ... & Zhao, M. (2018). Temporal variability in composition and fluxes of Yellow River particulate organic matter. Limnology and Oceanography, 63(S1), S119-S141. https://doi.org/10.1002/LNO.10727

Walling, D. E., & Fang, D. (2003). Recent trends in the suspended sediment loads of the world's rivers. Global and planetary change, 39(1-2), 111-126.

Wang, C., Li, F., Shi, H., Jin, Z., Sun, X., Zhang, F., et al. (2013). The significant role of inorganic matters in preservation and stability of soil organic carbon in the Baoji and Luochuan loess/paleosol profiles, Central China. Catena, 109, 186–194. https://doi.org/10.1016/J.CATENA.2013.04.001

Wang, G., Feng, X., Han, J., Zhou, L., Tan, W., & Su, F. (2008). Paleovegetation reconstruction using δ 13 C of Soil Organic Matter. Biogeosciences, 5(5), 1325–1337.

Wang, H., Bi, N., Saito, Y., Wang, Y., Sun, X., Zhang, J., & Yang, Z. (2010). Recent changes in sediment delivery by the Huanghe (Yellow River) to the sea: Causes and environmental implications in its estuary. Journal of Hydrology, 391(3), 302–313.

Wang, H., Wu, X., Bi, N., Li, S., Yuan, P., Wang, A., ... & Nittrouer, J. (2017). Impacts of the dam-orientated water-sediment regulation scheme on the lower reaches and delta of the Yellow River (Huanghe): A review. Global and Planetary Change, 157, 93-113.

Wang, H., Yang, Z., Saito, Y., Liu, J. P., Sun, X., & Wang, Y. (2007). Stepwise decreases of the Huanghe (Yellow River) sediment load (1950–2005): Impacts of climate change and human activities. Global and Planetary Change, 57(3), 331–354.

Wang, S., Fu, B., Piao, S., Lü, Y., Ciais, P., Feng, X., & Wang, Y. (2016). Reduced sediment transport in the Yellow River due to anthropogenic changes. Nature Geoscience, 9(1), 38–41.

Wang, X., Xu, C., Druffel, E. M., Xue, Y., & Qi, Y. (2016). Two black carbon pools transported by the Changjiang and Huanghe Rivers in China. Global Biogeochemical Cycles, 30(12), 1778–1790.

Weiguo, L., Xiahong, F., Youfeng, N., Qingle, Z., Yunning, C., & Zhisheng, A. N. (2005). δ13C variation of C3 and C4 plants across an Asian monsoon rainfall gradient in arid northwestern China. Global Change Biology, 11(7), 1094–1100.

Xiubin, H., Tang, K., & Zhang, X. (2004). Soil Erosion Dynamics on the Chinese Loess Plateau in the Last 10,000 Years. Mountain Research and Development, 24(4), 342–347.

Yu, M., Eglinton, T. I., Haghipour, N., Montluçon, D. B., Wacker, L., Hou, P., et al. (2019a). Impacts of Natural and Human-Induced Hydrological Variability on Particulate Organic Carbon Dynamics in the Yellow River. Environmental Science

& Technology, 53(3), 1119–1129.

Yu, M., Eglinton, T. I., Haghipour, N., Montluçon, D. B., Wacker, L., Wang, Z., et al. (2019b). Molecular isotopic insights into hydrodynamic controls on fluvial suspended particulate organic matter transport. Geochimica et Cosmochimica Acta, 262, 78–91.

Zhang, L. J., Wang, L., Cai, W.-J., Liu, D. M., & Yu, Z. G. (2013). Impact of human activities on organic carbon transport in the Yellow River. Biogeosciences, 10(4), 2513–2524.

Zhu, T. (2012). Gully and tunnel erosion in the hilly Loess Plateau region, China. Geomorphology, 153, 144–155.

Supplementary Materials

Transport of particulate organic carbon in the Huanghe: insights from lateral and vertical heterogeneity in a river cross-section

Yutian Ke[1], Damien Calmels[1], Julien Bouchez[2], Marc Massault[1], Benjamin Chetelat[3], Aurélie Noret[1], Hongming Cai[2], Jiubin Chen[3], Jérôme Gaillardet[2], Cécile Quantin[1]

[1] GEOPS, Université Paris-Saclay-CNRS, 91405 Orsay, France

[2] Université de Paris, Institut de Physique du Globe de Paris, CNRS, 75005 Paris, France

[3] School of Earth System Science, Institute of Surface-Earth System Science, Tianjin University, 300072 Tianjin, China

Figure S1-5

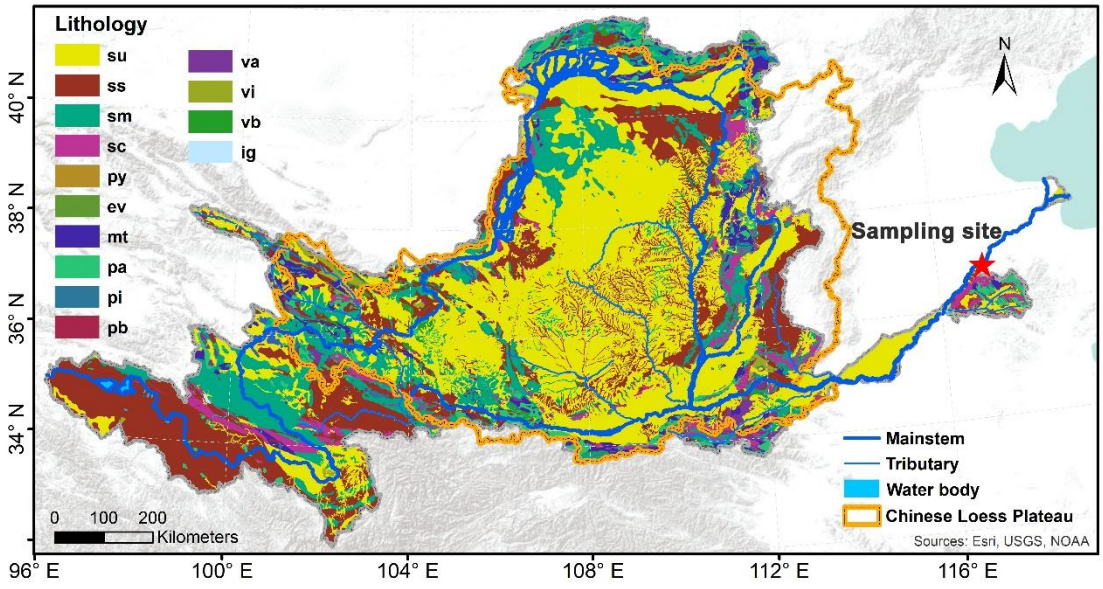

Fig. S1 Lithological map of the Yellow River Basin (data extracted from the GLiM v1.1 database by Hartmann and Mossdorf, 2012). Except for no data (ND) and water body (wb), the lithology is as follows. su: Unconsolidated Sediments; ss: Siliciclastic Sedimentary Rocks; sm: Mixed Sedimentary Rocks; sc: Carbonate Sedimentary Rocks; py: Pyroclastics; ev: Evaporites; mt: Metamorphic Rocks; pa: Acid Plutonic Rocks; pi: Intermediate Plutonic Rocks; pb: Basic Plutonic Rocks; va: Acid Volcanic Rocks; vi: Intermediate Volcanic Rocks; vb: Basic Volcanic Rocks; ig: Ice and Glaciers.

Sediment and POC flux estimation methods

We used water flow velocity profiles to "map" the flow velocity distribution across the river section. After constructing a bathymetric profile of the river cross-section based on the depth profiles, the flow velocity distribution across the river transect was modeled by the so-called velocity-defect law (Garcia, 2008) (Equation 1) which assumed that the maximum flow velocity u_{max} takes place at the water surface *i.e.* at z = H.

$$\frac{u_{max}-u}{u*} = -\frac{1}{\kappa} ln \frac{z}{H} \qquad (1)$$

where z is the height above the river bed, H is the channel depth, u^* is the bottom shear velocity and κ is the von Karman's constant equal to 0.41.

Each velocity profile is fitted with the velocity-defect law and a pair of u_{max} and u* values are estimated. Values of these two parameters are then linearly interpolated between profiles to model the water velocity distribution across the river section. For profiles where only one velocity data was measured, we assumed that the velocity was constant with depth.

Variation of SPM concentrations with depth in large rivers can be described by a Rouse profile (*e.g.*, Bouchez et al., 2011) where the Rouse model (Rouse, 1950) assumes that downward flux of sinking SPM is in equilibrium with the upward flux of SPM re-suspended from the river bed due to turbulent flow. This model can be described by the following equation:

$$\frac{C(z)}{C(a)} = \left(\frac{H-z}{z} \times \frac{a}{H-a}\right)^{Z_R} \quad (2)$$

where *C* is the SPM concentration, *z* is the height above the river bed, *a* is a reference height above the river bed, *H* is the channel depth, Z_R is the Rouse number. The surface sampling point was chosen as the reference height *a* in the Rouse equation. For each profile, the variation of the SPM concentration with depth is "fitted" by the Rouse equation which allows to determine the value of the Rouse number and then, to calculate the near-bottom sediment concentration. The Rouse equation is then used to model the distribution of the SPM concentration (Figure S2a) over the whole river cross-section using a linear, lateral interpolation of the Rouse numbers and near-bottom concentration between profiles, and extrapolating from the lateral profiles to the corresponding river banks.

The Rouse equation can also be used to model the variations of the concentrations with depth for each class of grain size. For a given depth profile, each class of grain

size shows a different "Rouse profile". Fine particles show a more uniform distribution of concentration with depth ('vertical profile') characterized by a small Rouse number whereas coarse particles are concentrated near the bottom of the river and their concentration profile is characterized by a larger Rouse number. The calculation of the different classes of grain sizes allows for modeling the spatial distribution of D50 across the whole river transect (Figure S2b). Based on the relationships between D50 and Al/Si and between Al/Si and POC content, it is then possible to model the distribution of the Al/Si ratios and the POC content (Figure S2c) over the river section.

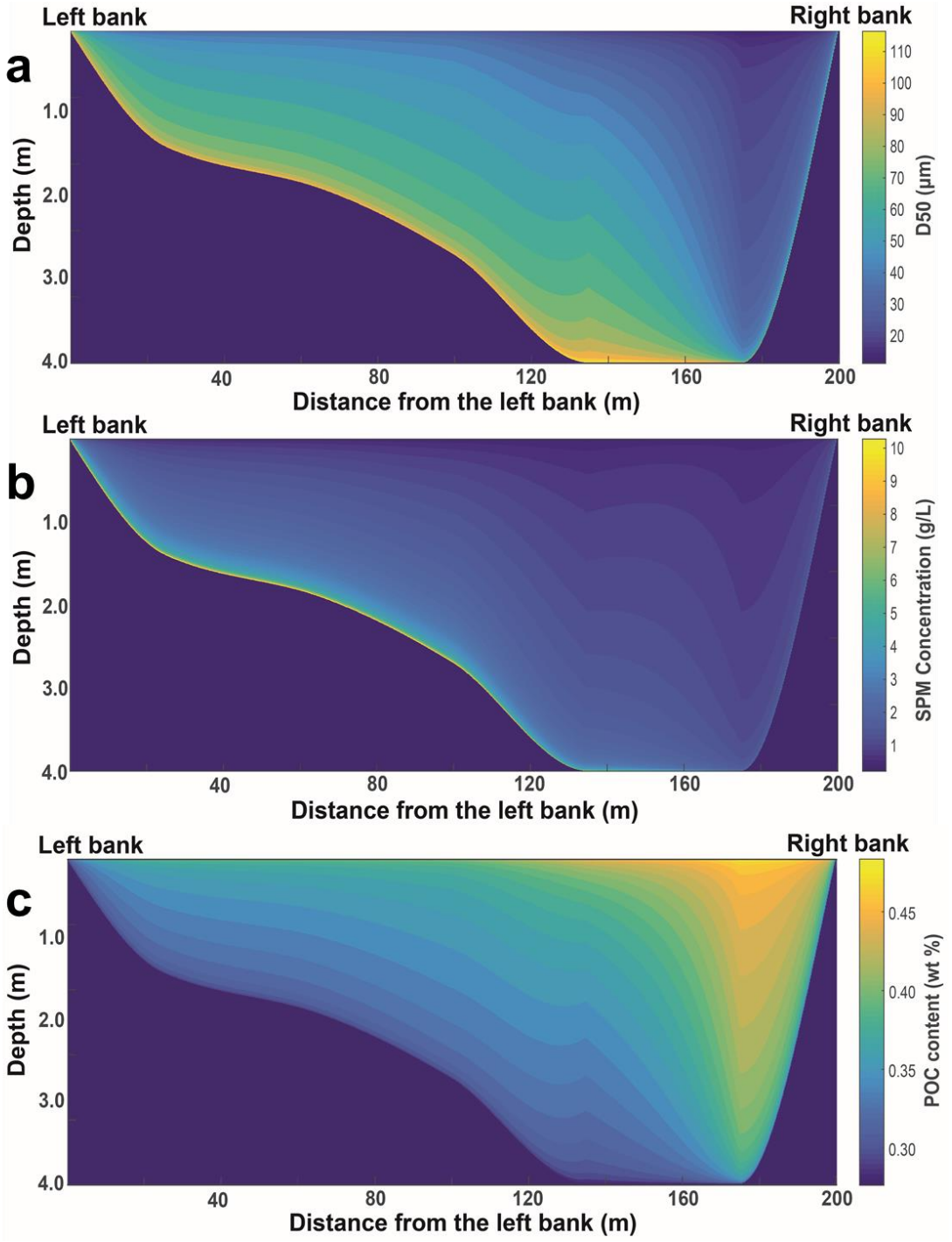

Fig. S2 Modeled spatial distribution of (a) particle size (D50), (b) SPM concentration, and (c) POC content (%) over the channel cross-section at Luokou.

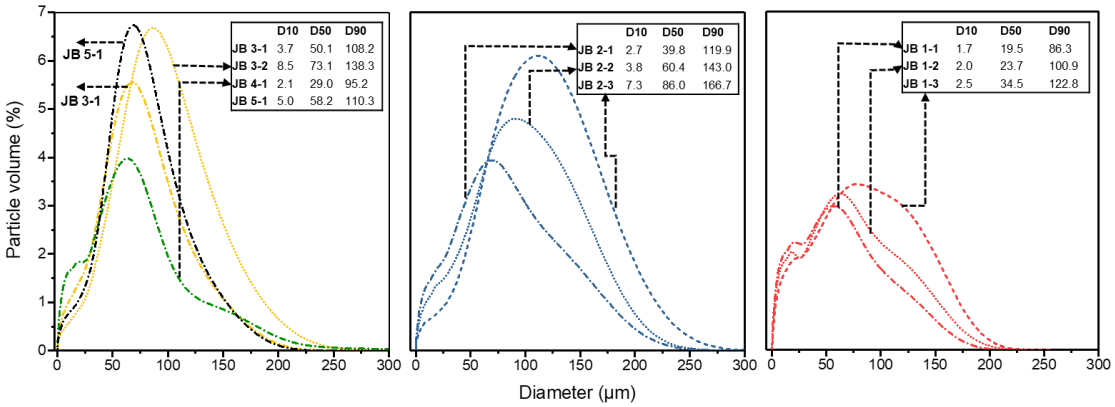

Fig. S3 Particle size distribution of SPM over the channel cross-section at Luokou. Particle size parameters including D10, D50, and D90 are given in the insets.

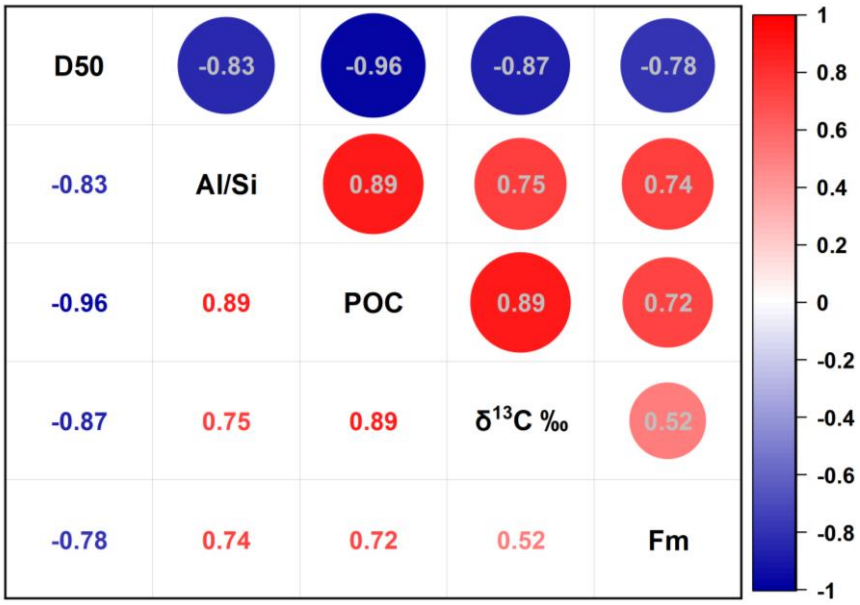

Fig. S4 Spearman correlation plot of physical and chemical parameters of SPM in the river cross-section. The size of circles is consistent with the color bar, representing the correlation value.

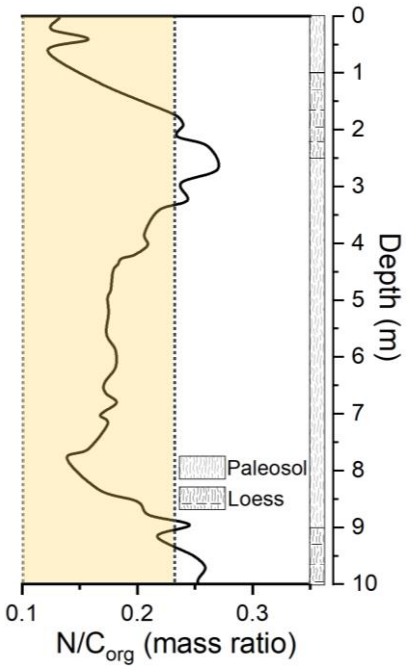

Fig. S5 N/C_{org} variations in the Xifeng loess-paleosol sequence with depth (< 10 m), the orange-shaded area constrained by two dotted lines is the range of N/C_{org} (0.10 - 0.23) in SPM (suspended particulate matter) collected from the lower reaches of the Yellow River (data compiled from this study, Yu et al. (2019b), Ran et al. (2013)). N/C_{org} values with the loess-paleosol sequence are from Ning et al. (2006).

Table. S1 Elemental and isotopic parameters of POC in the Yellow River, provenance modeling results are included.

Code	Location	Type	Sample date	TSM (mg/L)	POC (%)	$\delta^{13}C$ (‰)	$\Delta^{14}C$ (‰)	Fm	^{14}C age	OC_{ts}	SD	OC_{lps}	SD	OC_{petro}	SD	Fm_{bio}	OC_{bio} age	Reference
JB 1-1	Luokou	SPM	07/17/2016	678.8	0.44	-25.8	-360	0.65	3527	0.55	0.18	0.22	0.15	0.23	0.11	0.84	1423	This study
JB 1-2	Luokou	SPM	07/17/2016	756.6	0.45	-25.8	-392	0.61	3929	0.52	0.18	0.23	0.16	0.25	0.11	0.82	1620	This study
JB 1-3	Luokou	SPM	07/17/2016	1095.1	0.39	-26.1	-331	0.68	3161	0.60	0.17	0.19	0.14	0.21	0.10	0.85	1264	This study
JB 2-1	Luokou	SPM	07/17/2016	729.6	0.40	-26.0	-374	0.63	3703	0.55	0.17	0.21	0.15	0.25	0.11	0.84	1388	This study
JB 2-2	Luokou	SPM	07/17/2016	1124.5	0.32	-26.4	-436	0.57	4537	0.51	0.16	0.19	0.14	0.31	0.11	0.82	1549	This study
JB 2-3	Luokou	SPM	07/17/2016	1805.7	0.29	-26.5	-453	0.55	4779	0.50	0.15	0.18	0.13	0.33	0.11	0.82	1556	This study
JB 3-1	Luokou	SPM	07/17/2016	1058.0	0.32	-26.1	-422	0.58	4346	0.50	0.17	0.21	0.15	0.29	0.11	0.82	1597	This study
JB 3-2	Luokou	SPM	07/17/2016	2458.7	0.31	-26.6	-415	0.59	4247	0.54	0.15	0.17	0.13	0.29	0.11	0.83	1501	This study
JB 4-1	Luokou	SPM	07/17/2016	1747.3	0.41	-25.7	-375	0.63	3714	0.53	0.18	0.23	0.16	0.24	0.11	0.83	1507	This study
JB 5-1	Luokou	SPM	07/17/2016	1406.1	0.32	-26.1	-416	0.59	4256	0.51	0.16	0.20	0.14	0.28	0.11	0.82	1613	This study
HH 17.05	Luokou	SPM	05/2017	82.6	0.92	-25.7	-295	0.71	2740	0.60	0.18	0.22	0.16	0.18	0.10	0.87	1146	This study
HH 17.06	Luokou	SPM	06/2017	54.2	1.21	-25.6	-277	0.73	2539	0.60	0.19	0.23	0.17	0.17	0.10	0.88	1043	This study
Lijin	Lijin	SPM	06/26/2013	6800	0.35	-22.6	-642	0.36	8249	0.22	0.15	0.67	0.18	0.11	0.09	0.40	7318	Hu et al. (2015)
Lijin	Lijin	SPM	06/30/2013	5000	0.40	-23.3	-638	0.36	8169	0.23	0.15	0.60	0.19	0.16	0.12	0.43	6726	Hu et al. (2015)
Lijin	Lijin	SPM	07/02/2013	5600	0.43	-22.7	-676	0.32	9041	0.20	0.15	0.68	0.17	0.12	0.10	0.37	8051	Hu et al. (2015)
Lijin	Lijin	SPM	07/06/2013	5500	0.46	-23.0	-681	0.32	9181	0.21	0.14	0.65	0.17	0.14	0.11	0.37	7978	Hu et al. (2015)
Lijin	Lijin	SPM	07/10/2013	15900	0.47	-24.2	-588	0.41	7119	0.29	0.16	0.46	0.20	0.25	0.14	0.55	4784	Hu et al. (2015)
Lijin	Lijin	SPM	07/12/2013	13100	0.55	-23.9	-553	0.45	6459	0.30	0.17	0.48	0.21	0.21	0.13	0.57	4543	Hu et al. (2015)
Lijin	Lijin	SPM	06/22/2014		0.28	-23.8	-454	0.55	4799	0.37	0.20	0.45	0.22	0.18	0.11	0.67	3220	Ge et al. (2020)
Lijin	Lijin	SPM	07/01/2014		0.29	-22.8	-469	0.54	5023	0.33	0.21	0.55	0.24	0.12	0.09	0.61	4005	Ge et al. (2020)
Lijin	Lijin	SPM	07/04/2014		0.27	-23.5	-473	0.53	5083	0.35	0.20	0.49	0.22	0.16	0.11	0.63	3662	Ge et al. (2020)
HYK	Huayuankou	SPM	07/05/2014		0.30	-23.7	-470	0.53	5038	0.36	0.20	0.47	0.22	0.18	0.11	0.65	3486	Ge et al. (2020)
HYK	Huayuankou	SPM	07/06/2014		0.32	-23.3	-508	0.50	5635	0.32	0.19	0.53	0.22	0.15	0.11	0.59	4296	Ge et al. (2020)
HYK	Huayuankou	SPM	07/09/2014		0.29	-24.6	-491	0.51	5363	0.37	0.18	0.37	0.20	0.25	0.12	0.69	3028	Ge et al. (2020)
HYK	Huayuankou	SPM	(05-06)/2015		0.25	-24.1	-425	0.58	4380	0.40	0.20	0.41	0.22	0.19	0.11	0.71	2704	Xue et al. (2017)
Jinan	Jinan	SPM	(05-		0.29	-23.8	-471	0.53	5060	0.36	0.19	0.46	0.22	0.18	0.11	0.65	3427	Xue et al. (2017)

			06)/2016														
Lijin	Lijin	SPM	06/28/2011	1420	0.4	-23.8	-419	0.59	4303	0.40	0.21	0.43	0.22	0.17	0.10	0.70	2818	Tao et al. (2015)
Lijin	Lijin	SPM	09/22/2011	2850	0.33	-24.2	-415	0.59	4248	0.41	0.20	0.39	0.21	0.19	0.11	0.73	2542	Tao et al. (2015)
Lijin	Lijin	SPM	11/17/2011	620	0.45	-24.0	-400	0.60	4044	0.42	0.21	0.41	0.22	0.17	0.10	0.73	2510	Tao et al. (2015)
Lijin	Lijin	SPM	01/13/2012	810	0.32	-23.9	-408	0.60	4151	0.41	0.21	0.42	0.22	0.17	0.10	0.72	2644	Tao et al. (2015)
Lijin	Lijin	SPM	04/22/2012	400	0.47	-24.2	-443	0.56	4641	0.39	0.20	0.40	0.21	0.20	0.11	0.70	2825	Tao et al. (2015)
Lijin	Lijin	SPM	06/19/2012	980	0.27	-24.0	-397	0.61	4003	0.42	0.21	0.41	0.22	0.17	0.10	0.73	2476	Tao et al. (2015)
Lijin	Lijin	SPM	06/27/2012	2790	0.32	-23.8	-436	0.57	4540	0.38	0.20	0.44	0.22	0.17	0.11	0.69	3012	Tao et al. (2015)
HYK	Huayuankou	SPM	06/09/2015	200	0.26	-24.8	-352	0.65	3422	0.49	0.21	0.32	0.20	0.19	0.10	0.81	1704	Yu et al. (2019a)
HYK	Huayuankou	SPM	11/12/2015	130	0.27	-24.5	-451	0.55	4754	0.40	0.19	0.37	0.20	0.23	0.12	0.71	2696	Yu et al. (2019a)
HYK	Huayuankou	SPM	01/07/2016	170	0.34	-24.4	-390	0.61	3907	0.44	0.21	0.37	0.21	0.19	0.11	0.76	2194	Yu et al. (2019a)
HYK	Huayuankou	SPM	04/24/2016	290	0.25	-24.3	-410	0.59	4174	0.42	0.20	0.38	0.21	0.20	0.11	0.74	2428	Yu et al. (2019a)
Kenli	Kenli	SPM	04/06/2015	1030	0.16	-23.3	-412	0.59	4203	0.39	0.22	0.47	0.24	0.14	0.10	0.69	3006	Yu et al. (2019a)
Kenli	Kenli	SPM	07/09/2015	6540	0.27	-23.9	-409	0.60	4162	0.41	0.21	0.42	0.22	0.17	0.10	0.72	2651	Yu et al. (2019a)
Kenli	Kenli	SPM	08/04/2015	680	0.29	-23.5	-351	0.65	3410	0.44	0.23	0.43	0.24	0.13	0.09	0.76	2250	Yu et al. (2019a)
Kenli	Kenli	SPM	11/24/2015	190	0.12	-24.3	-429	0.58	4438	0.41	0.20	0.39	0.21	0.20	0.11	0.72	2617	Yu et al. (2019a)
Kenli	Kenli	SPM	01/21/2016	260	0.35	-24.3	-439	0.57	4579	0.40	0.20	0.39	0.21	0.21	0.11	0.71	2711	Yu et al. (2019a)
Kenli	Kenli	SPM	07/05/2016	180	0.75	-24.9	-304	0.70	2847	0.53	0.21	0.30	0.20	0.17	0.10	0.85	1337	Yu et al. (2019a)
TGD13-13	Toudaoguai	SPM	03/23/2013	1100	0.49	-25.0	-424	0.58	4376									Qu et al. (2020)
TDG13-25	Toudaoguai	SPM	06/05/2013	2230	0.44	-24.9	-414	0.59	4238									Qu et al. (2020)
TDG13-29	Toudaoguai	SPM	06/30/2013	1180	1.06	-25.8	-563	0.44	6595									Qu et al. (2020)
TDG13-34	Toudaoguai	SPM	07/26/2013	1250	0.46	-24.4	-454	0.55	4802									Qu et al. (2020)
TDG13-35	Toudaoguai	SPM	08/02/2013	1280	0.46	-24.1	-434	0.57	4516									Qu et al. (2020)
TDG13-39	Toudaoguai	SPM	08/30/2013	2680	0.39	-24.3	-474	0.53	5100									Qu et al. (2020)
TDG13-40	Toudaoguai	SPM	09/06/2013	1990	0.47	-25.0	-454	0.55	4802									Qu et al. (2020)
TDG13-42	Toudaoguai	SPM	09/20/2013	1440	0.45	-24.3	-395	0.61	3971									Qu et al. (2020)
TDG13-44	Toudaoguai	SPM	10/04/2013	1270	0.49	-24.3	-424	0.58	4376									Qu et al. (2020)
TDG13-46	Toudaoguai	SPM	10/18/2013	1050	0.52	-24.4	-414	0.59	4238									Qu et al. (2020)
LM13-5	Longmen	SPM	02/02/2013	310	1.12	-25.8	-682	0.32	9153									Qu et al. (2020)

LM13-9	Longmen	SPM	03/02/2013	310	1.33	-21.9	-454	0.55	4802	Qu et al. (2020)
LM13-13	Longmen	SPM	03/30/2013	6030	0.61	-24.7	-424	0.58	4376	Qu et al. (2020)
LM13-22	Longmen	SPM	06/01/2013	150	1.88	-26.7	-405	0.60	4103	Qu et al. (2020)
LM13-28	Longmen	SPM	07/08/2013	1870	0.50	-24.8	-534	0.47	6065	Qu et al. (2020)
LM13-29	Longmen	SPM	07/12/2013	31160	0.16	-24.4	-613	0.39	7564	Qu et al. (2020)
LM13-31	Longmen	SPM	07/22/2013	13230	0.42	-24.7	-424	0.58	4376	Qu et al. (2020)
LM13-32	Longmen	SPM	07/23/2013	68160	0.37	-25.1	-295	0.71	2751	Qu et al. (2020)
LM13-33	Longmen	SPM	07/24/2013	3600	0.43	-24.3	-484	0.52	5253	Qu et al. (2020)
LM13-34	Longmen	SPM	07/25/2013	68990	0.41	-24.6	-295	0.71	2751	Qu et al. (2020)
LM13-37	Longmen	SPM	08/12/2013	14940	0.29	-24.3	-454	0.55	4802	Qu et al. (2020)
LM13-41	Longmen	SPM	09/04/2013	3480	0.45	-24.2	-414	0.59	4238	Qu et al. (2020)
LM13-43	Longmen	SPM	09/11/2013	4680	0.39	-24.9	-454	0.55	4802	Qu et al. (2020)
2017 TDG-1	Toudaoguai	Bedload	09/2017		0.17	-23.5	-583	0.42	6969	Qu et al. (2020)
2017 LM	Longmen	Bedload	09/2017		0.10	-24.5	-812	0.19	13341	Qu et al. (2020)
2017 TG	Tongguan	Bedload	09/2017		0.17	-25.7	-673	0.33	8906	Qu et al. (2020)
2016 LM	Longmen	Bedload	09/2016		0.07	-25.1	-782	0.22	12163	Qu et al. (2020)
2016 TDG	Toudaoguai	Bedload	09/2016		0.17	-24.4	-504	0.50	5568	Qu et al. (2020)

Table S2. Relative contributions of the three different sources of POC at the Luokou cross-section on the Huanghe as inferred from our mixing model.

Sample ID	Fractional proportions						OC content (%)			
	OC_{ts}	**SD**	**OC_{lps}**	**SD**	**OC_{petro}**	**SD**	**OC_{bio}**	**SD**	**OC_{petro}**	**SD**
JB 1-1	0.55	0.18	0.22	0.15	0.23	0.11	0.34	0.10	0.10	0.05
JB 1-2	0.52	0.18	0.23	0.16	0.25	0.11	0.33	0.11	0.11	0.05
JB 1-3	0.60	0.17	0.19	0.14	0.21	0.10	0.31	0.09	0.08	0.04
JB 2-1	0.55	0.17	0.21	0.15	0.25	0.11	0.30	0.09	0.10	0.04
JB 2-2	0.51	0.16	0.19	0.14	0.31	0.11	0.22	0.07	0.10	0.04
JB 2-3	0.50	0.15	0.18	0.13	0.33	0.11	0.20	0.06	0.10	0.03
JB 3-1	0.50	0.17	0.21	0.15	0.29	0.11	0.23	0.07	0.09	0.04
JB 3-2	0.54	0.15	0.17	0.13	0.29	0.11	0.22	0.06	0.09	0.03
JB 4-1	0.53	0.18	0.23	0.16	0.24	0.11	0.32	0.10	0.10	0.05
JB 5-1	0.51	0.16	0.20	0.14	0.28	0.11	0.23	0.07	0.09	0.04
HH 17.05	0.60	0.18	0.22	0.16	0.18	0.10	0.75	0.22	0.17	0.09
HH 17.06	0.60	0.19	0.23	0.17	0.17	0.10	1.00	0.31	0.21	0.12
HH	0.08	0.05	0.14	0.10	0.78	0.10	0.05	0.02	0.17	0.02

Chapter 4

Enhanced Organic Carbon Sequestration induced by Massive Dam-building in the Changjiang River Basin, a Preliminary Investigation on Cascade Mega Reservoirs

Yutian Ke[1], Damien Calmels[1], Julien Bouchez[2], Aurélie Noret[1], Marc Massault[1], Benjamin Chetelat[3], Hongming Cai[3], Jiubin Chen[3], Cécile Quantin[1], Jérôme Gaillardet[2]

[1] GEOPS, Université Paris-Saclay-CNRS, 91405 Orsay, France,

[2] Université de Paris, Institut de Physique du Globe de Paris, CNRS, 75005 Paris, France

[3] School of Earth System Science, Institute of Surface-Earth System Science, Tianjin University, 300072 Tianjin, China

Abstract

Artificial reservoirs strongly impact the natural delivery of suspended particulate matter (SPM) by rivers to the ocean and consequently alter the global carbon cycle, trapping a large amount of particulate organic carbon (POC) for decades to centuries. In the upper Changjiang (CJ) River basin, the development of cascade mega-reservoirs (CMRs) along the Jinshajiang River represents a recent new developed perturbation of SPM and POC delivery, in addition to the Three Gorges Dam (TGD). Here we examine the composition, transport, and fate of riverine POC in the CJ River Basin as well as the POC sequestration in those large reservoirs. We report the elemental and isotopic composition of POC (radiocarbon and stable carbon isotopic compositions) as well as the inorganic chemistry of SPM samples collected with transect depth profiles and times series of near-surface SPM sampled in the upper and lower CJ from July 2016 to September 2017. A binary mixing model (petrogenic POC [POC_{petro}] and biospheric POC [POC_{bio}]) and a MIXSIAR model (rock-derived OC, modern plant OC, and aged soil OC) were applied to quantitatively apportion the different sources of POC in the

CJ. Lower POC contents and less pronounced radiocarbon activities were observed in the upper reaches of the CJ. Results reveal that 1) the distinct seasonal variation of elemental and isotopic behavior of POC; 2) fractional POC from thawing permafrost on the Qinghai-Tibet Plateau indicated by the significant old biospheric POC (3,600 ^{14}C years); 3) the intensive physical erosion mobilizes substantial rock-derived organic carbon into rivers; 4) the instantaneous massive POC transport induced by storm events in a small catchment. Based on our depth-integrated POC data and historic hydrologic dataset, we demonstrate that the temporal POC sequestration within the CJ basin is even enhanced under the current mass dam-building and the intensified physical erosion. We estimate sequestration of about 6.6 megatons (Mt) POC in reservoirs behind dams every year under the current intensified physical erosion rate, with annual sequestration of from 3.5 to 5.8 Mt POC_{bio}. The POC sequestration in the TGD has been greatly alleviated, a decrease of from 1.58 to 0.45 Mt every year since the operation of CMRs, where annually sequester 0.61 Mt POC, indicating a shift of POC burial site upper forward of the TGD and the East China Sea margin. Rapid burial of terrestrial POC delivered by a mountainous river in reservoirs could have significant high preservation by helping POC escape from mineralization along the long pathway and deposition in the estuary. With the remarkable decline in sediment load and increase in POCbio fractions after retainment of reservoirs, the POC flux and composition variations have significant implications for carbon cycle processes downstream of reservoirs and in the estuary.

Keyword: Jinshajiang, Changjiang, cascade reservoirs, POC, burial efficiency

1. Introduction

As the connection between the continent and ocean, rivers deliver eroded terrestrial materials as suspended particulate matter (SPM) carrying particulate organic carbon (POC) to estuaries, playing an important role in the global carbon cycle (Ludwig et al., 1996; Berner, 2004; Blair and Aller, 2012; Galy et al., 2007; Hilton and West, 2020). Riverine POC is derived from either the “modern” biosphere (modern plants, soils, and autochthonous organisms with radiocarbon-enriched OC: POC_{bio}) or sedimentary rocks (radiocarbon-dead recycled OC, *i.e.*, petrogenic OC: POC_{petro}) (Blair et al., 2003; 2004; Galy et al., 2007; Hilton et al., 2008; Aufdenkampe et al., 2011). Depending on their fate (degradation or burial), these two POC components may have antagonist impacts

on the carbon cycle and therefore antagonist feedbacks on the Earth's climate. While the degradation of POC_{bio} is considered either as a net source of CO_2 to the atmosphere (decadal to millennial timescale; Mayorga et al., 2005) or as having no impact on the carbon cycle (geological timescale: > 100,000 years), the oxidation of POC_{petro} represents a net source of CO_2 at all timescales (Hilton et al., 2014, Petsch et al., 2000; Bouchez et al., 2010;). On the contrary, POC burial can be viewed either as a net sink of CO_2 at both short and long timescales (POC_{bio} burial) or as having no impact on the carbon cycle (POC_{petro} re-burial) (Berner, 1982; Galy et al., 2015; France-Lanord and Derry, 1997; Mayorga et al., 2005; Galy et al., 2008a; Hilton et al., 2011). Globally, rivers export ~200 megatonnes per year (Mt/yr) of POC (110-230 MtC/yr as POC_{bio} and 20-100 MtC/yr as POC_{petro}) to continental margins (Galy et al., 2015; Ludwig et al., 1996), where ~55%–80% of this exported terrestrial POC is remineralized (Burdige, 2005).

Large river systems that deliver terrestrial POC to tectonically passive margins (*e.g.*, Changjiang, Amazon, or Mississippi) have relatively low OC preservation efficiency (~20%-30%) (Blair and Aller, 2012; Wu et al., 2013), owing to the relatively low sedimentation rate and prolonged particle residence time in refluxing deltaic muds (Blair and Aller, 2012; Burdige, 2005). In contrast, river systems delivering POC to active continental margins have high preservation efficiency due to rapid burial driven by high suspended sediment export yields and therefore high sedimentation rates. This is observed for both large rivers such as the Ganges-Brahmaputra (Galy et al., 2007; 2008a) and small mountainous rivers with short-distance and rapid export, *e.g.*, rivers in Taiwan (Hilton et al., 2011; Blair and Aller, 2012). Whether riverine POC could be efficiently preserved therefore depends on its intrinsic reactivity to successive transportation-reaction steps during its "journey" and sedimentation rates on the margin (Blair and Aller, 2012).

Nowadays, only 23% of the large rivers with a length of more than 1,000 km flow uninterrupted to the ocean. The remaining 77% are impacted by human activities, especially by the construction of artificial reservoirs that lead to a dramatic decrease in suspended sediment export to continental margins worldwide (*e.g.*, Mississippi, Huanghe, Changjiang, Zambezi, etc.; Grill et al., 2019; Milliman and Farnsworth, 2011). Most suspended sediments are retained in the reservoirs instead of entering the estuary (Battin et al., 2009; Maavara et al., 2017). However, the drastic decrease of

POC export to continental margins does not mean that the fluvial system is less efficient in the long-term carbon cycle regulation. As a matter of fact, POC is still efficiently buried, but on the continent upstream of the dams rather than in the ocean. High sedimentation rates behind dams should prevent POC from being oxidized due to limited exposure time to oxygenated waters (Mendonça et al., 2012; 2017, Dean et al., 1998; Tranvik et al., 2009). This overall effect remains to be further constrained.

The CJ river is an emblematic example of large fluvial systems under strong anthropogenic pressure. With approximately 50,000 dams in operation within its basin, the CJ river has been regulated for more than 50 years (Yang et al., 2018). Since the operation of the Three Gorges Dam in the middle reaches (TGD, total storage capacity 39.3 km^3), sediment load at the river mouth experienced a 75% decrease (Yang et al., 2005; 2018), which led to a dramatic decrease in sediment accumulation rate on the East China Sea margin. The upper reaches of the CJ also experience strong perturbation with the implementation of a series of 4 cascade dams along the Jinshajiang (JSJ) river (Figure 1), which are either in operation or under construction (Yang et al., 2005; Li et al., 2018). The final storage capacity of those 4 CMRs will be ~52 km^3. The JSJ drains a tectonically active and high-elevation region, the Qinghai-Tibet Plateau (QTP), which is characterized by relatively high erosion rates (Li et al., 2018). Massive and rapid burial of POC in those successive mega-reservoirs can thus be hypothesized. It is essential to investigate the sources and composition of POC to understand its fate either in artificial reservoirs or on continental margins. While the effect of the TGD dam on the composition and structure of POC has been partly investigated (Wu et al., 2007; 2018; Bao et al., 2014; Li et al., 2015; Liu et al., 2019), very few studies were carried out on the composition and flux of POC in the Jinshajiang (Wu et al., 2018).

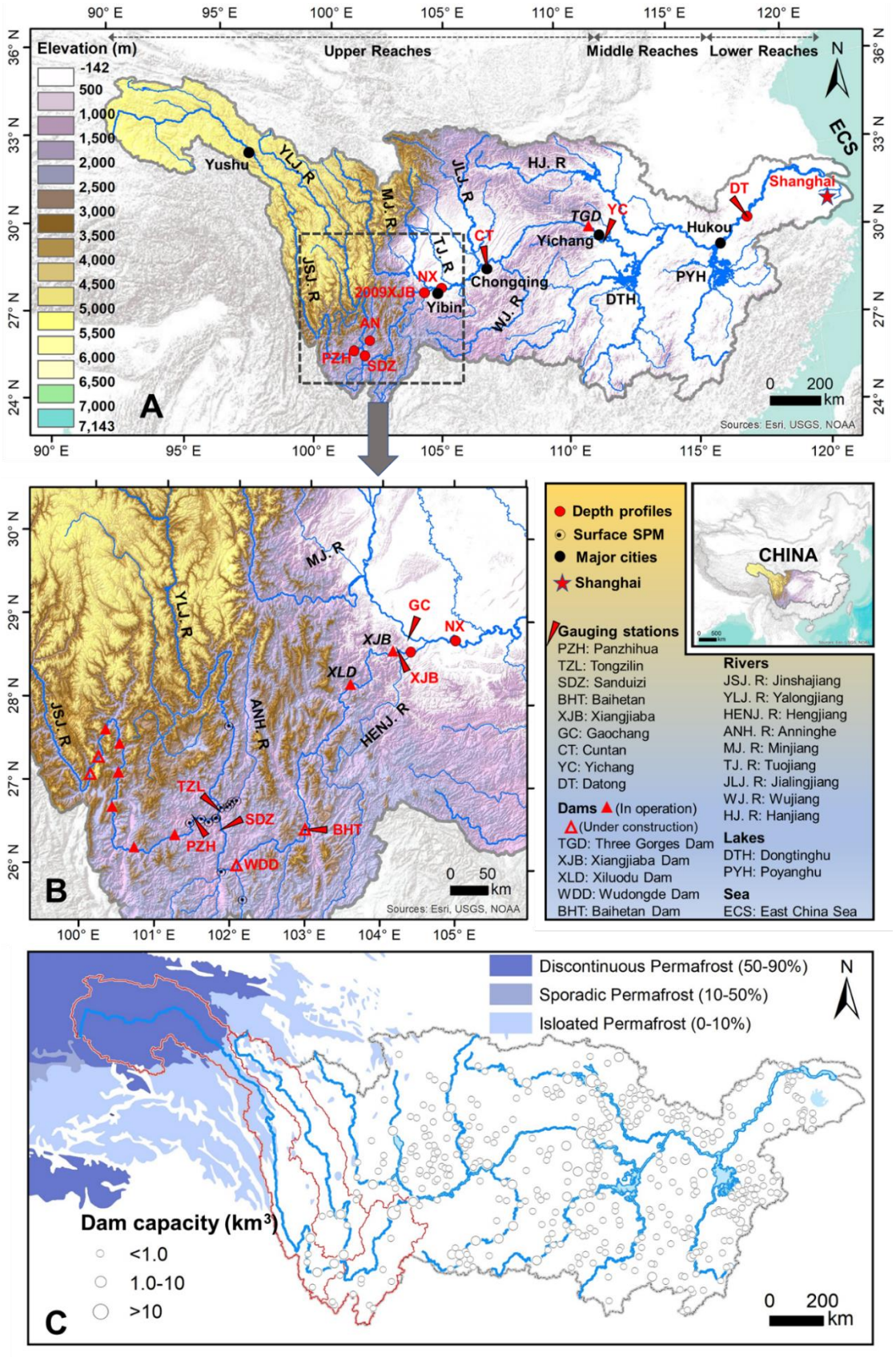

Fig. 1 The Changjiang River basin and sampling locations. A, topographic map with the main channel and major tributaries of the Changjiang. Topographic data are from

the Shuttle Radar Topographic Mission (SRTM) digital elevation model (DEM) at 30 × 30 m resolution, overlying on an online Esri global terrain map. B, topographic map of the upper Changjiang, with a focus on the sampling sites in the Jinshajiang basin. C, distribution map of dams (before 2016) in the basin, and permafrost extent in the source region, the red lines denote the boundary of three subbasins of the Jinshajiang River basin, which are the Yalong River basin, the upstream regions of PZH (Jinshajiang before its confluence with the Yalong), and the lower reaches regions downstream of PZH. Dam distribution has been extracted from the GRanD dataset compiled by Lehner et al. (2011). Permafrost distribution is from Brown et al. (1997).

In this study, we characterized the inherent elemental and dual isotopic composition of fluvial POC in the CJ River system from source to sink under varying hydrological conditions. We focus on the influence of dams on POC export, with a special focus on the Jinshajiang where POC sources and fluxes are poorly constrained. Assessments of POC sources, composition, and metabolic processes are based on SPM samples collected with multiple depth profiles together with bank sediments or bedload collected from the main channel and tributaries in the mid-lower region of the JSJ. Monthly time series and depth profiles were collected after the confluence of JSJ and Minjiang (MJ) with CJ to examine the seasonal variation and the dam-induced alteration of POC export. Lastly, depth profiles were collected at the tidal limit of the CJ to further reveal the properties of POC that would be eventually delivered into the East China Sea since the operation of dams in the Jinshajiang.

2. Materials and Methods

2.1 Study area

The Changjiang (CJ) River is the third-longest river in the world. It flows 6,387 km eastward from Jari Hill (Tanggula Mountain) in the Qinghai-Tibet Plateau (QTP) to the East China Sea, draining an area of 1.8×10^6 km^2 (~ 20% of mainland China). There are contrasting tectonic settings, topography gradients, and climates between its upper and mid-lower reaches. The upper reaches range from the source region to Yichang, accounting for 55% of the total drainage area. The Three Gorges Dam is located upstream of Yichang, regulating water and sediment discharge to the mid-lower reaches. The section between Yushu and Yibin corresponds to the Jinshajiang River that is 3,481

km long and drains an area of 50.2×10^4 km^2 (Figure 1A). The 4 CMRs in the lower JSJ (from Panzhihua to Yibin, Figure 1B) are either under construction or in operation and include the Baihetan, Xiluodu, Wudongde, and Xiangjiaba reservoirs that have a storage capacity of 20.6 km^3, 12.7 km^3, 7.4 km^3, and 5.2 km^3, respectively. There are also eight cascade dams either in operation or under construction in the middle JSJ upstream of Panzhihua. The largest tributary of JSJ is the Yalong River. After the city of Yibin, the Minjiang, Tuojiang, Jialingjiang, and Wujiang rivers join to form the CJ. The middle reaches of CJ lie within Yichang and Hukou city (Figure 1A), connecting the Hanjiang river and two big lake systems, namely the Dongtinghu and the Poyanghu lakes. The section downstream of Hukou till the river mouth represents the lower reaches. The CJ basin has contrasted topography, while the upper reaches are characterized by high relief, steep slopes and a sharp decrease in elevation of riverbed (3,300 m drop) from the spring to Yibin, the mid-lower reaches drain gentle hill, floodplains, and lakes. The CJ drainage basin consists of various tectonic settings, from the active uplifting Longmenshan region in the upper reaches to the stable Yangtze Craton in the middle and lower reaches. The upper reaches undergo frequent earthquakes that trigger landslides and rockfalls, providing materials to rivers (Jin et al., 2016; Wang et al., 2019). Besides, there is abundant permafrost in the QTP region (Figure 1C).

The drainage basin is dominated by sedimentary rocks, covering around 72% of the total area and up to 80% in the upper reaches (extracted from the GLiM v1.1 database by Hartmann and Mossdorf, 2012), the lithologies are characterized by silicates, carbonates, and alluvial deposits from Precambrian to Quaternary in age (Figure S1). Metamorphic and plutonic rocks are sporadically distributed. In the JSJ drainage basin, siliciclastic sedimentary rocks are widely distributed (~47%), while the carbonate sedimentary rocks (14%) are mainly located in the source region and the southern part. In the mid-lower reaches, fluvial unconsolidated sediments cover ~42% of the watershed.

Concerning climate, the CJ River basin is strongly affected by the humid sub-tropical Asian monsoon. While the upper basin is subject to the Indian Summer Monsoon, the mid-lower region is dominated by the East Asian Summer Monsoon. Nowadays, more than 70% of annual water discharge occurs from May to October with a peak discharge in July. The mean annual precipitation is estimated at 1,037 mm/yr for

the entire river basin and varies spatially, showing a westward decreasing trend from more than 2,000 mm/yr in the eastern Yangtze Plains to less than 400 mm/yr in the western QTP (the WorldClim 2 database by Fick and Hijmans, 2017).

2.2 Sampling

From August 2016 to September 2017, we have been systematically collecting SPM samples in the CJ river basin, with a special focus on its uppers reaches (Figure 1). Sediments were collected during the flooding season except for the monthly time series. In August 2016, a cross-section sampling with three depth profiles (three samples in each depth profile) was carried out at NX (in Yibin city), after the confluence of Minjiang with JSJ (Figure 1). We also collected surface samples (0.5m below the surface) at NX every month from August 2016 until July 2017 (except for January 2017). In August 2017, a cross-section sampling was performed at Datong, the tidal limit of CJ, where 17 samples were collected with three depth profiles. In September 2017, a field trip was conducted in the JSJ river basin during which depth profiles were collected upstream from the confluence with the Yalong river (1 depth profile), 100km downstream of the confluence with the Yalong (cross-section with two depth profiles) and in the Anning river (a tributary of the Yalong river) just after a strong storm event that generated many landslides and road-cut and one day later at the same place. Surface samples were also collected from the Yalong river and other tributaries as well as bank sediments and bedload. Between 10 and 30 liters of river water were collected for each sample, using a 10-liter point-sediment sampler binding together with a current velocity meter. When possible, we also used ADCP (Acoustic Doppler Current Profiler) to acquire the flow velocity and bathymetric profiles. All collected water samples were filtered through 0.22-micrometer Teflon (PTFE) membrane filters within 24 hours. After rinsing the filters with filtered water, all suspended particulate matter was transferred into 50-milliliter centrifuge tubes and was freeze-dried at -20 °C before weighing.

2.3 Analytical methods

Aliquots of sediment samples were ground using an agate mortar and pestle for chemical and isotopic analysis. Not-ground aliquots of SPM were dispersed in deionized water and pretreated with sodium hexametaphosphate (SHMP) solution in an ultrasonic bath before measuring the particle size distribution on a Laser Diffraction Particle Size Analyzer (Beckman Coulter LS-12 320) at the École Normale Supérieure

(ENS), Paris, France. For each sample, we made three sub-measurement and used D90 (the proportion of particles with diameters below this value is 90%, μm) with an uncertainty better than 2%. Organic carbon content (OC_{total}, wt%), $\delta^{13}C$ (in ‰ VPDB) and radiocarbon isotope $\Delta^{14}C$ (expressed as fraction modern, Fm) of POC were obtained from ground homogenized SPM samples after acidification with 12M HCl fumes in a closed Teflon tank at 60 °C for 48 hours (to remove any trace of carbonate) and drying under vacuum. (Komada et al., 2008). Triplicate analysis of POC content and $\delta^{13}C$ were performed on fumed samples (sealed in tin capsule) using Elemental Analyser (EA) coupled with Isotope Ratio Mass Spectrometry (IRMS, Thermo Scientific Flash 2000) at the Laboratoire Géosciences Paris Saclay (GEOPS), Orsay, France. Associated uncertainties (1σ, n=3) are better than 0.05% and 0.1‰, respectively (Table. 1). Prior to radiocarbon analysis, samples are fumigated into pyrex tubes and then transferred into quartz tubes with suitable amounts of CuO and silver wool. Both quartz tubes and CuO have been heated at 550 °C for 24 hours before use. Sample-loaded quartz tubes are then purged under vacuum and sealed before being combusted for 12h at 850 °C. The combustion process fully converts POC as CO_2 gas. Combusted quartz tubes are cracked in a vacuum line to recover and purify CO_2 through successive liquid nitrogen (LN2) and LN2+ethanol (-110°C) traps. The CO_2 is then transferred into mini pyrex tubes (pre-combusted under a 500 °C furnace environment), which are eventually sealed. Sealed CO_2 samples are introduced into a new compact accelerator mass spectrometry (AMS), *ECHo*MICADAS, using a gas ion source interface system at the Laboratoire des Sciences du Climat et de l'Environnement (LSCE), Gif Sur Yvette, France, to measure Fm with a typical uncertainty of ±5‰ in this study. The chemical composition of SPM samples was measured at the Centre de Recherches Pétrographiques et Géochimiques (CRPG), Vandoeuvre-lès-Nancy, France, using ICP-OES for major elements with typical uncertainty of 3%.

2.4 Calculation methods for POC sources apportionment

Contributions of the various sources of POC transported by the CJ River were estimated using two different approaches, a binary mixing model (Galy et al., 2008a) and a Bayesian dual-isotope mixing model using the package “MixSIAR GUI” under the *R* statistic computing environment (Parnell et al., 2010).

The binary mixing model was applied to estimate POC_{petro} and POC_{bio} using Fm and POC% as follows:

$$\mathrm{F}_m \times POC = \mathrm{F}_{m_{bio}} \times POC_{bio} + \mathrm{F}_{m_{petro}} \times POC_{petro}$$

$$POC = POC_{bio} + POC_{petro}$$

Where Fm_{bio} and Fm_{petro} are the Fm of biospheric and petrogenic fractions of POC, respectively. As POC_{petro} is radiocarbon-dead, a linear equation can be written between POC and Fm × POC (modern OC):

$$\mathrm{F}_m \times POC = \mathrm{F}_{m_{bio}} \times (POC - POC_{petro})$$

Thus, based on the observed linear fit, Fm_{bio} equals the slope of the regression equation, and POC_{petro} can be calculated using the Y-intercept, POC_{bio} can be obtained by subtracting POC_{petro} from POC.

The MIXSIAR model was built using stable and radioactive isotopic values ($\delta^{13}C$ and $\Delta^{14}C$) of expected POC pools contributing to riverine SPM. Three or four potential POC sources were used, depending on the study watershed. The model can be illustrated by the following equations based on isotopic mass balance:

$$\mathrm{Isotope}_{\mathrm{sample}} = \sum_{\mathrm{source}} (f_{\mathrm{m}_{\mathrm{source}}} * \mathrm{Isotope}_{\mathrm{source}})$$

$$\sum_{\mathrm{source}} f_{\mathrm{m}_{\mathrm{source}}} = 1$$

where $\mathrm{Isotope}_{\mathrm{sample}}$ and $\mathrm{Isotope}_{\mathrm{source}}$ are the $\delta^{13}C$ or $\Delta^{14}C$ value of the sample and endmembers, respectively, and $f_{\mathrm{m}_{\mathrm{source}}}$, the contributing fraction of each source.

A burn-in of 1,000,000 iterations coupled with three parallel Markov chains Monte Carlo (MCMC) with a length of 500,000 for each chain was used. We performed the simulation for each POC sample to avoid the automatically incorporated uncertainty within the applied POC data by the model. Additionally, uninformative prior was applied in the mixing model as we consider that every possible set of proportions has equal probability (Stock et al., 2018).

2.5 Calculation method of instantaneous depth-integrated fluxes

Instantaneous depth-integrated fluxes of SPM and POC are calculated over river cross-section using a method developed by Lupker et al. (2011) and Bouchez et al. (2011a, b). This method uses the SPM concentration variation law in different size fractions separated by hydrodynamics sorting along depth profiles, based on the Rouse model (Rouse, 1950). At NX, owing to the absence of ADCP, a current velocity meter was used in the field which allowed to reconstruct the cross-section flow velocity based on

a manually built bathymetric profile. The distribution of both total SPM concentration and different particle sizes concentrations can therefore be estimated, just like the total instantaneous SPM flux. As Al/Si ratio is an efficient proxy for particle size (D90 in this study), the SPM Al/Si (mass ratio) profile was modeled based on the pre-modeled D90 profile. Subsequently, the POC profile over the cross-section based on the Al/Si profile was modeled. Finally, we can obtain the instantaneous POC flux and depth-integrated average POC content (POC_{int}).

3. Results

3.1 POC content

In general, trends of decreasing POC content with increasing sampling depth present in the Changjiang (CJ) River Basin for vertical depth profiles (Figure 2), as observed elsewhere in other large fluvial systems (Galy et al., 2008b; Bouchez et al., 2014; Hilton et al., 2015). Even though some depth profiles have relatively invariant POC content in SPM along the water column, they all show relatively enriched POC at the river surface and depleted POC at the bottom. When several depth profiles have been collected along a cross-section (DT, NX, and PZH samples), lateral heterogeneity of elemental POC abundancy within delivered SPM is always observed (Figure 2, Table. 1).

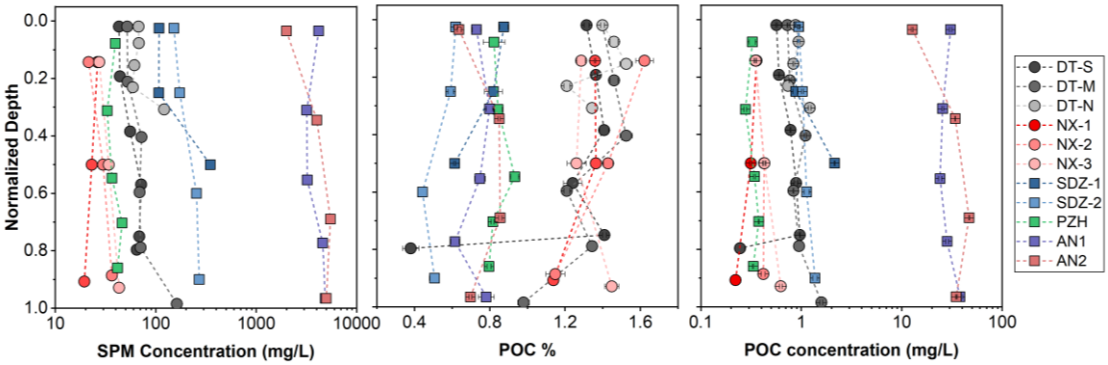

Fig. 2 Variations of SPM and POC with depth profiles. The normalized depth is calculated by normalizing the sampling depth to the maximum depth of transect of individual depth profiles. SPM samples collected at the main channel of CJ and within the JSJ river basin are represented by circles and squares, respectively.

In the upper CJ, SPM transported by the JSJ river upstream of its confluence with the Yalong (at PZH) show relatively homogeneous POC content at 0.84 ± 0.05% (n=5, ADCP profile based average: POC_{int} 0.96%), a value that decreases to 0.64 ± 0.16% (n=7, POC_{int} 0.73%) at SDZ after the confluence. This small decrease in POC content is accompanied by the increase in SPM concentration (ADCP profile based average) by a factor of 6 from ~39 mg/L to ~230 mg/L. The Yalong River is a quite turbid river system having SPM with a POC content of 1.61% (based on one single surface data) before its confluence with the Anning (AN), and 0.73% after the confluence (based one single surface data). Two depth profiles collected in the AN river after a storm event (the first AN1, right after the storm, and the second AN2, 24h later) document the delivery of SPM in a very turbid condition with SPM content over 4,000 mg/L. POC content in AN1 and AN2 samples is relatively constant at 0.73 ± 0.07% (n=5, POC_{int} 0.73%) and 0.76 ± 0.11% (n=4, POC_{int} 0.85%), respectively. Tributaries of the AN river sampled right after the storm event have high SPM concentrations of 3,600 ± 1,800 mg/L (n=4) and low POC content in SPM at 0.43 ± 0.10%. After the confluence between the JSJ and the Minjiang (NX), POC content of SPM from the cross-section averages 1.34 ± 0.15% (n=9, POC_{int} 1.41%) while the average SPM concentration is 29 ± 7.7 mg/L. These values greatly differ from SDZ values (upstream) presented above (POC=0.64% and [SPM]=230 mg/L). Moreover, the time series of surface samples collected at NX always shows high POC content in SPM (1.91± 0.47%, n=11; annual weighted average 1.54%) and relatively low SPM concentration from 8.6 mg/L to 91.5 mg/L. In the JSJ River basin, bank sediments and bedload are POC-depleted with contents of 0.18 ± 0.01% (n=4) in the main channel, and of 0.25 ± 0.15% (n=14) in Yalong tributaries. Further downstream, the CJ at DT also shows relatively low concentration of SPM (70.7 ± 29.1 mg/L, n=17) that contain on average 1.25 ± 0.27% of POC (n=17, POC_{int} 1.07%). Those values are similar to the ones reported by Wang et al. (2012) and Li et al. (2015). Meanwhile, seasonal variations of SPM concentration and POC content (see Method in Supplementary material) are observed at both NX (upper reaches) and DT (lower reaches). At NX, SPM concentration is significantly lower with relatively higher POC content in dry seasons (October 2016 – March 2017) compared to that in wet seasons (August 2016 – September 2016 and April 2017 – July 2017), however, the differences are weakened at DT, suggesting the transport of substantial SPM and POC in dry seasons in lower reaches (Figure 3). In terms of POC concentration, DT is obviously higher than NX, besides, it is remarkably higher in wet

seasons at NX while slightly higher at DT compared to that in dry seasons. In general, POC content increases when SPM concentration decreases within the entire CJ basin (Figure 4).

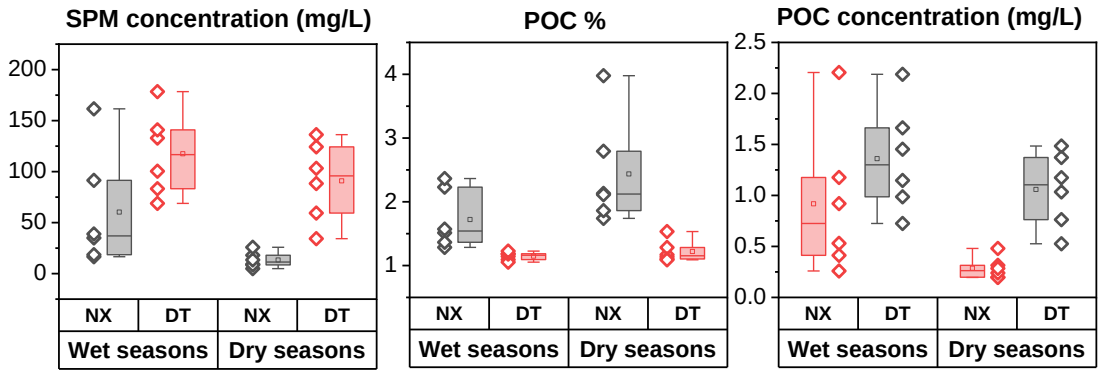

Fig. 3 Comparison of POC and SPM properties between wet and dry seasons at Nanxi and Datong. Squares are the data distribution of corresponding parameters.

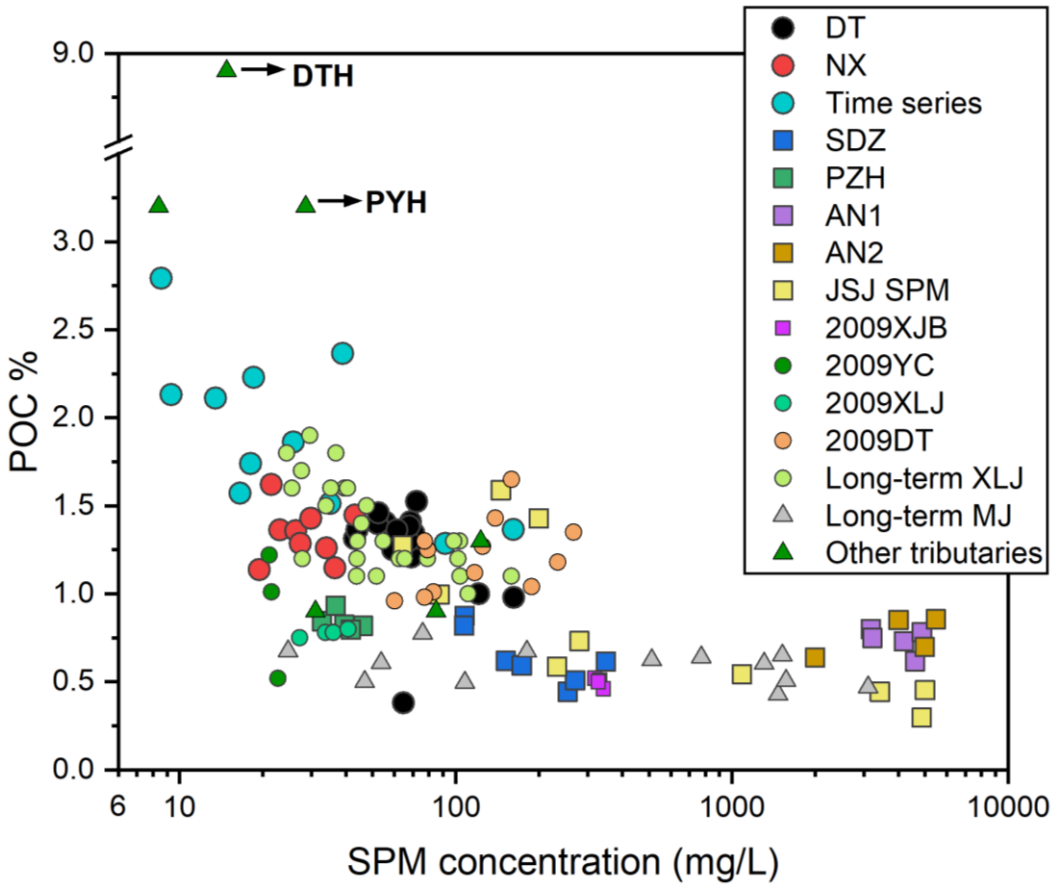

Fig. 4 Relationship between SPM concentration and POC content for all the samples collected so far (this study and in the literature) in the Changjiang River basin. Circles denote samples collected in the Changjiang mainstem, while squares are samples collected at the Jinshajiang River basin, and triangles are samples from lakes and major tributaries of the Changjiang. 2009XJB, 2009YC, 2009XLJ are depth profiles collected in 2009 (Wu et al., 2018) at the outlet of the JSJ, at Yichang downstream of the TGD, and at Xuliujing (the mouth of Changjiang), respectively. Long-term XLJ is SPM sampled at the river surface at Xuliujing from 2003 to 2011 (Wu et al., 2018). 2009DT is the monthly collected SPM at Datong by Wang et al., (2012). Long-term MJ denotes SPM collected at the main channel of Minjiang from 2009 to 2011 (Wang et al., 2019). Other tributaries include SPM from Jialingjiang, Hanjiang, Dongtinghu (DTH), and Poyanghu (PYH, Wu et al., 2018), hereinafter.

Table. 1 Sediment inorganic characteristics, elemental and isotopic organic carbon values.

Code	Sample ID	Depth (meter)	Profile	Location	SPM mg/L	POC mg/L	OC_{total} %	SD	$\delta^{13}C$ (‰)	SD	Fm OC	SD	$\Delta^{14}C$ (‰)	Al/Si mass ratio	D90 (μm)
Suspended particulate matter															
CJ-D1701	DT-S1	0.5	DT-S	Datong	43.0	0.56	1.31	0.01	-26.68	0.03	0.721	0.008	-284	0.350	37.0
CJ-D1702	DT-S2	5	DT-S	Datong	43.9	0.60	1.36	0.01	-27.16	0.01	0.731	0.007	-275	0.347	33.8
CJ-D1703	DT-S3	10	DT-S	Datong	55.5	0.78	1.41	0.03	-26.68	0.13	0.723	0.008	-282	0.324	45.7
CJ-D1704	DT-S4	14.8	DT-S	Datong	71.5	0.89	1.24	0.05	-27.03	0.06	0.707	0.008	-299	0.311	54.2
CJ-D1705	DT-S5	19.5	DT-S	Datong	68.5	0.96	1.41	0.01	-26.37	0.09	0.726	0.008	-279	0.333	45.3
CJ-D1706	DT-S6	20.7	DT-S	Datong	64.6	0.25	0.38	0.04	-26.35	0.02	0.577	0.018	-428	0.181	229.0
CJ-D1707	DT-M1	0.5	DT-M	Datong	52.0	0.73	1.40	0.01	-26.60	0.06	0.736	0.008	-270	0.344	40.8
CJ-D1708	DT-M2	5.5	DT-M	Datong	52.4	0.77	1.46	0.02	-26.83	0.05	0.739	0.007	-267	0.337	42.1
CJ-D1709	DT-M3	10.5	DT-M	Datong	72.1	1.10	1.52	0.03	-26.36	0.04	0.747	0.009	-259	0.325	50.1
CJ-D1710	DT-M4	15.5	DT-M	Datong	69.0	0.83	1.21	0.02	-26.94	0.05	0.741	0.008	-265	0.293	86.5
CJ-D1711	DT-M5	20.5	DT-M	Datong	70.5	0.95	1.34		-26.88		0.724	0.010	-282	0.317	54.4
CJ-D1712	DT-M6	25.6	DT-M	Datong	162.0	1.59	0.98	0.03	-26.34	0.03	0.734	0.008	-272	0.248	249.2
CJ-D1713	DT-N1	0.5	DT-N	Datong	67.4	0.88	1.30	0.01	-26.59	0.05	0.708	0.010	-298	0.333	44.8
CJ-D1714	DT-N2	2	DT-N	Datong	67.8	0.94	1.38	0.04	-26.80	0.02	0.744	0.009	-262	0.341	42.7
CJ-D1715	DT-N3	4	DT-N	Datong	61.2	0.83	1.36	0.03	-26.73	0.05	0.755	0.008	-251	0.337	42.2
CJ-D1716	DT-N4	6	DT-N	Datong	59.0	0.74	1.25		-26.19		0.714	0.008	-292	0.276	103.4
CJ-D1717	DT-N5	8	DT-N	Datong	121.0	1.21	1.00	0.03	-26.42	0.05	0.676	0.010	-330	0.254	137.6
CJ-D1601	NX-1-1	6.35	NX-1	Yibin	19.4	0.22	1.14		-26.03		0.656	0.005	-349	0.323	52.5
CJ-D1602	NX-1-2	3.5	NX-1	Yibin	23.0	0.31	1.36	0.03	-25.91	0.08	0.690	0.005	-315	0.323	46.4
CJ-D1603	NX-1-3	1	NX-1	Yibin	26.3	0.36	1.36	0.00	-26.09	0.05	0.652	0.005	-354	0.304	50.7
CJ-D1604	NX 2-1	6.2	NX-2	Yibin	36.5	0.42	1.15	0.05	-25.84	0.09	0.627	0.005	-378	0.297	124.4
CJ-D1605	NX 2-2	3.5	NX-2	Yibin	29.8	0.43	1.43	0.03	-25.67	0.05	0.693	0.006	-313	0.329	54.5
CJ-D1606	NX 2-3	1	NX-2	Yibin	21.5	0.35	1.62	0.05	-25.76	0.05	0.655	0.006	-350	0.326	57.6
CJ-D1607	NX-3-1	6.5	NX-3	Yibin	43.1	0.62	1.45	0.04	-25.93	0.06	0.750	0.006	-256	0.300	131.8

CJ-D1608	NX-3-2	3.5	NX-3	Yibin	34.0	0.43	1.26	0.05	-25.94	0.05	0.648	0.005	-357	0.279	105.9
CJ-D1609	NX-3-3	1	NX-3	Yibin	27.3	0.35	1.29	0.02	-25.67	0.06	0.640	0.006	-365	0.317	79.2
CJ-D1718	PZH-A	0.5	SDZ-1	Sanduzi	107.7	0.94	0.87	0.02	-25.73	0.07	0.581	0.005	-423	0.346	124.5
CJ-D1719	PZH-B	5	SDZ-1	Sanduzi	107.2	0.88	0.82	0.05	-25.89	0.00	0.642	0.005	-363	0.330	148.1
CJ-D1720	PZH-C	10	SDZ-1	Sanduzi	349.1	2.14	0.61	0.00	-26.56	0.12	0.534	0.005	-470	0.271	423.9
CJ-D1721	PZH-D	0.5	SDZ-2	Sanduzi	151.6	0.94	0.62	0.01	-26.06	0.06	0.633	0.005	-372	0.309	202.2
CJ-D1722	PZH-E	5	SDZ-2	Sanduzi	173.2	1.03	0.59	0.01	-26.05	0.07	0.612	0.005	-393	0.294	341.5
CJ-D1723	PZH-F	12	SDZ-2	Sanduzi	254.5	1.13	0.44	0.03	-26.02	0.05	0.582	0.005	-423	0.286	367.8
CJ-D1724	PZH-G	18	SDZ-2	Sanduzi	270.5	1.37	0.51	0.03	-26.06	0.03	0.582	0.005	-423	0.281	405.2
CJ-D1725	JSJ-A	0.5	PZH	Panzihua	39.6	0.33	0.82	0.06	-25.98	0.05	0.543	0.005	-461	0.410	32.7
CJ-D1726	JSJ-B	2	PZH	Panzihua	32.8	0.28	0.84	0.02	-26.08	0.12				0.416	23.0
CJ-D1727	JSJ-C	3.5	PZH	Panzihua	36.7	0.34	0.93	0.02	-26.05	0.09	0.565	0.005	-440	0.414	85.4
CJ-D1728	JSJ-D	4.5	PZH	Panzihua	46.2	0.38	0.82	0.01	-25.96	0.02	0.534	0.005	-471	0.383	39.9
CJ-D1729	JSJ-E	5.5	PZH	Panzihua	41.7	0.33	0.80	0.01	-26.52	0.10	0.504	0.005	-500	0.361	130.5
CJ-D1730	AN-A	0.5	AN1	Anning	4191.1	30.57	0.73	0.02	-25.69	0.04	0.858	0.006	-149	0.360	146.7
CJ-D1731	AN-B	4.5	AN1	Anning	3186.3	25.46	0.80	0.02	-25.10	0.04				0.398	79.7
CJ-D1732	AN-C	8.03	AN1	Anning	3220.3	24.07	0.75	0.03	-25.37	0.03	0.870	0.006	-137	0.373	79.3
CJ-D1733	AN-D	11.2	AN1	Anning	4591.8	28.26	0.62	0.02	-25.81	0.06				0.327	215.0
CJ-D1734	AN-E	14	AN1	Anning	4874.6	38.08	0.78	0.04	-26.51	0.04	0.873	0.006	-135	0.318	257.5
CJ-D1735	AN-A2	0.5	AN2	Anning	1999.5	12.73	0.64	0.01	-25.17	0.04	0.676	0.005	-329	0.425	20.9
CJ-D1736	AN-B2	5	AN2	Anning	4005.6	34.04	0.85	0.01	-25.64	0.01	0.788	0.006	-218	0.371	39.6
CJ-D1737	AN-C2	10	AN2	Anning	5471.5	46.79	0.86	0.01	-25.73	0.01	0.781	0.006	-225	0.343	47.9
CJ-D1738	AN-D2	14	AN2	Anning	4986.0	34.77	0.70	0.01	-25.69	0.06	0.770	0.006	-236	0.327	77.6
CJ-T1609	NX 16.09	0.5	Time series	Yibin	35.1	0.07	1.51		-25.89		0.532	0.004	-472	0.376	
CJ-T1610	NX 16.10	0.5	Time series	Yibin	16.5	0.20	1.57		-25.97		0.510	0.006	-494	0.366	
CJ-T1611	NX 16.11	0.5	Time series	Yibin	18.1	0.25	1.74		-26.48		0.534	0.004	-471	0.300	
CJ-T1612	NX 16.12	0.5	Time series	Yibin	9.3	0.38	2.13	0.05	-26.44	0.06	0.620	0.005	-385	0.300	
CJ-T1702	NX 17.02	0.5	Time series	Yibin	8.6	0.21	2.79	0.05	-26.50	0.05	0.614	0.005	-391	0.335	

CJ-T1703	NX 17.03	0.5	Time series	Yibin	13.5	0.31	2.11	0.03	-26.71	0.16	0.541	0.004	-463	0.290	
CJ-T1704	NX 17.04	0.5	Time series	Yibin	25.8	0.26	1.86		-26.45		0.591	0.005	-414	0.289	
CJ-T1705	NX 17.05	0.5	Time series	Yibin	18.5	1.00	2.23	0.02	-25.72	0.03	0.483	0.004	-521	0.311	51.1
CJ-T1706	NX 17.06	0.5	Time series	Yibin	161.5	0.36	1.37	0.01	-25.32	0.01	0.693	0.005	-312	0.403	25.8
CJ-T1707	NX 17.07	0.5	Time series	Yibin	38.9	0.88	2.37	0.01	-25.47	0.02	0.398	0.004	-605	0.394	59.0
CJ-S1739	JSJ Bridge	0.5	JSJ SPM				0.92		-26.42					0.438	18.4
CJ-S1740	Minya Bridge	0.5	JSJ SPM		87.3	0.87	0.99	0.01	-25.19	0.04				0.399	22.4
CJ-S1742	YLJ	0.5	JSJ SPM	Tongzilin			1.61	0.04	-24.31	0.05	0.858	0.006	-149	0.511	19.3
CJ-S1747	BSG	0.5	JSJ SPM		5000.9	22.57	0.45	0.03	-25.65	0.17				0.375	108.3
CJ-S1748	HQG	0.5	JSJ SPM		4870.9	14.41	0.30	0.01	-25.93	0.17				0.433	57.5
CJ-S1749	XHG	0.5	JSJ SPM		1086.4	5.89	0.54	0.05	-26.19	0.04				0.356	68.0
CJ-S1751	YLJ-3	0.5	JSJ SPM		280.0	2.05	0.73	0.03	-25.95	0.04				0.310	162.2
CJ-S1752	XWH	0.5	JSJ SPM		64.2	0.82	1.27	0.01	-24.84	0.10				0.443	13.7
CJ-S1753	BGH	0.5	JSJ SPM		3429.5	15.17	0.44	0.05	-26.19	0.02				0.377	260.5
CJ-S1754	WMH	0.5	JSJ SPM		199.8	2.85	1.43	0.03	-24.86	0.09				0.571	28.1
CJ-S1755	LCJ	0.5	JSJ SPM		232.6	1.36	0.59	0.01	-24.93	0.11				0.307	39.9
CJ-S1756	MGH	0.5	JSJ SPM		145.8	2.31	1.59	0.06	-25.95	0.03				0.430	29.3
Bank sediments or bedload															
CJ-S1757	YLR1						1.40	0.02	-23.95	0.05				0.323	33.7
CJ-S1758	YLR2						0.87	0.02	-24.19	0.08				0.489	217.7
CJ-S1759	GLR						0.74		-26.68					0.345	69.1
CJ-S1760	BSG-S						0.12		-27.03					0.288	215.0
CJ-S1761	BGH-BS						0.11	0.00	-29.09	0.01				0.341	392.6
CJ-S1762	ANH-BS1						0.53	0.02	-26.82	0.11				0.253	247.2
CJ-S1766	GLR-S						0.29	0.00	-25.96	0.01				0.279	233.6
CJ-S1767	XWH-BS						0.18		-25.85					0.130	134.0
CJ-S1768	ANR-S			Anning			0.26	0.01	-25.69	0.00	0.506	0.005	-498	0.259	256.5
CJ-S1769	MGH-S						0.19		-26.09					0.129	314.0
CJ-S1770	HQG-S						0.12		-26.53					0.207	256.9

CJ-S1772	XHG-S		0.08	0.00	-26.13	0.03				0.269	301.3
CJ-S1774	LCJW-S		0.36		-27.57					0.136	160.0
CJ-S1775	YLJ3-S		0.24		-26.01					0.249	178.7
CJ-S1777	NanMu-S		0.21	0.01	-26.90	0.01				0.263	306.5
CJ-S1779	JSJ-Sa		0.17		-26.48					0.198	237.1
CJ-S1780	JSJ-Sb	Panzihua	0.20		-23.53		0.401	0.004	-602	0.272	327.4
CJ-S1781	JSJ-Sc		0.19		-26.13					0.230	287.3
CJ-S1782	JSJ-Sd		0.17		-25.89					0.196	393.1
CJ-S1784	YLJ2-S		0.23		-26.84					0.252	365.6
CJ-S1787	YLRB-S	Tongzilin	0.44		-25.64		0.792	0.006	-214	0.255	172.3
CJ-S1763	ANH-BS2	Anning	0.56	0.00	-27.23	0.11	0.864	0.006	-143	0.287	249.3

3.2 Particle size and inorganic chemistry

The particle size distribution of SPM samples (as D90, *i.e.*, 90% of the SPM volume is made of particles with a diameter smaller than the D90 value) usually increases with relative water depth due to hydrodynamic sorting (Bouchez et al., 2011a). At a given site, we usually find a good inverse relationship between the D90 and the Al/Si ratio (Figure 5). This ratio is mainly governed by the balance between the clay fraction (high Al/Si) and the quartz fraction (low Al/Si) in the samples.

In the upper CJ, the JSJ river has relatively finer SPM (D90 = 62 ± 45 μm) and higher clay fraction (Al/Si = 0.40 ± 0.02) before its confluence with the Yalong river than after the confluence at SDZ (D90 = 288 ± 126 μm and Al/Si = 0.30 ± 0.02). These latter values are comparable to those found for bank sediments and bedload collected in the JSJ (D90=311 ± 66 μm and Al/Si = 0.26 ± 0.08). SPM samples collected in the Yalong basin (including the Anning river) have a highly variable particle size distribution with D90 ranging from 16 μm to 260 μm. The hydrological condition is a key parameter of D90 variation at a given site as observed in the Anning River. The AN1 samples collected just after a storm event that generated numerous landslides and road-cut, have coarser SPM (156 ± 80 μm) than AN2 samples (46 ± 24 μm) collected 24h after the storm. Note that the two depth profiles on the JSJ (at PZH and SDZ) were collected before the storm event.

In the main channel of CJ, the time-series samples collected at NX during the wet season (dry season samples have not been analyzed) have an average D90 of 54 ± 22 μm (n=4). At the same location, we do observe more variability in the 3 depth profiles collected across the river on the same date (D90 = 78 ± 34 μm, n=9). Indeed, depth profile sampling does help capture the full range of particle size of riverine SPM (Bouchez et al., 2011b). At DT (3 depth profiles along a river cross-section, n=17), the D90 of SPM samples is clearly different between the bottom-most samples (D90=205 ± 59 μm, n=3)) and samples collected at a shallower depth (D90=52 ± 19 μm, n=14).

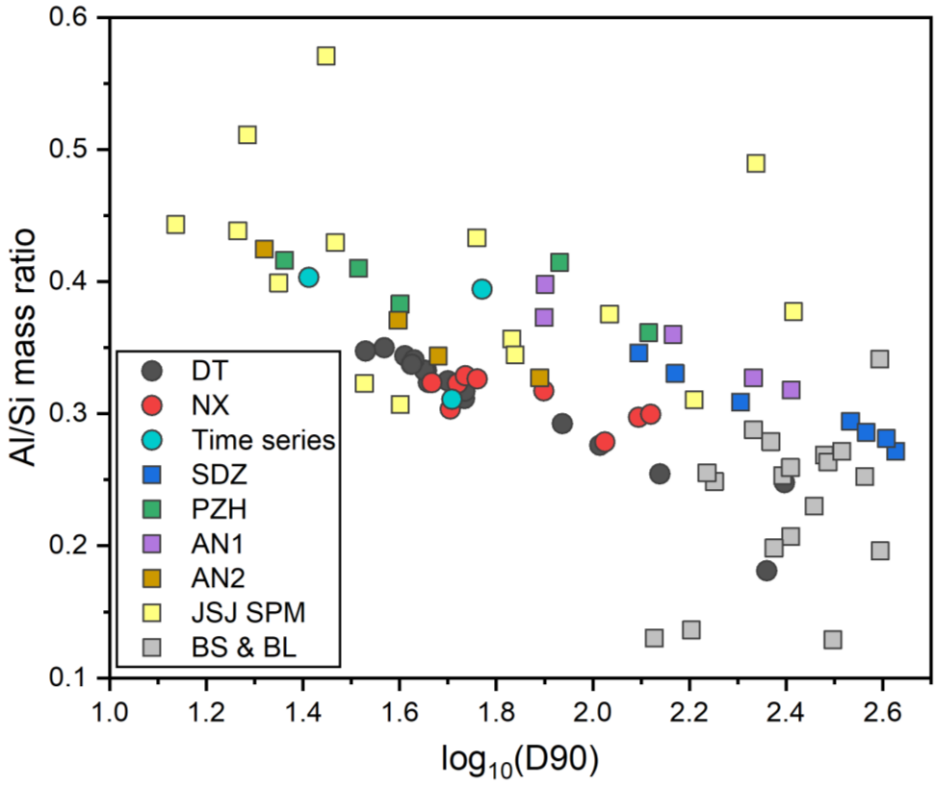

Fig. 5 Plot of sediments particle size versus its Al/Si mass ratio. Circles denote samples collected at the main channel of Changjiang, while squares are samples collected in the Jinshajiang river basin, where the suspended sediment samples collected at 0.5 m depth are denoted as JSJ SPM, and the collected bank sediment and bedload are BS and BL in short. Time series represents the monthly collected SPM at NX (hereinafter).

Al/Si (mass ratio) is an efficient chemical proxy for the particle size distribution of SPM (Galy et al., 2008b; Bouchez et al., 2011a), which has been already examined in some large fluvial systems (*e.g.*, Amazon, Ganges-Brahmaputra, Mackenzie). The CJ and JSJ samples also show an inverse relationship between Al/Si and D90 (Figure 5) with some variability from one depth profile to another. As observed elsewhere, fine clay-rich SPM are preferentially carried at the channel surface while coarse quartz-rich SPM is found near the river bed. Bank sediments and bedload generally have the lowest Al/Si ratios, indicating that they contain fewer secondary minerals such as clay and more coarse primary minerals than SPM. Notably, the correlation between particle sizes (D90) and Al/Si ratios has certain differentiation between JSJ and CJ downstream of JSJ. Putting aside SPM from tributaries, on the SPM with given particle size, a higher Al/Si ratio could be observed in JSJ. SPM at SDZ has much lower Al/Si ratios (0.302 ± 0.027) compared to SPM at PZH (0.397 ± 0.024), fitting the larger particle sizes after the confluence. With the blocking of cascade reservoirs before PZH, clay-rich SPM

was selectively delivered downwards. Even though AN1 is coarser than AN2, they have comparable Al/Si ratios of 0.355 ± 0.033 and 0.366 ± 0.043, respectively.

3.3 Dual carbon isotopes: $\delta^{13}C$ and $\Delta^{14}C$

Values of POC $\delta^{13}C$ show seasonal and spatial variation, but no systematic variation in depth profiles from top to bottom (Table 1, Figure 6A). $\delta^{13}C$ values are significantly lower in dry seasons (-26.52 ± 0.11‰, n=5) than in wet season (-25.67 ± 0.24‰, n=6), consistent with the observation made in the lower reaches (Li et al., 2015; Wang et al., 2012). Absolute $\delta^{13}C$ values are however lighter than reported ones for POC samples collected in 2009 in the upper reaches (-24.86 ± 0.35‰, n=8) (Wu et al., 2018) and in the Minjiang during the 2009-2011 wet seasons (-24.64 ± 1.20, n=27) (Wang et al., 2019). When going downstream, the depth-integrated $\delta^{13}C$ of POC in the main river channel at PZH, SDZ, NX, and DT are -26.12 ± 0.23‰, -26.05 ± 0.26‰, -25.87 ± 0.15‰, and -26.64 ± 0.28‰, respectively. A slight enrichment trend in ^{13}C could be seen when going downward in the upper reaches but the spatial variability is smaller than the standard deviation of $\delta^{13}C$ in each depth profile. However, a clear ^{13}C enrichment is observed at NX (after the confluence of the JSJ and Minjiang) during the wet season (Figure 7). In the main channel of the JSJ, POC in bank and bed sediments show relatively large $\delta^{13}C$ variations, ranging from -26.48 to -23.53‰ (average: -25.51 ± 1.34‰, n=4). In the Yalong basin, POC of SPM on one side and, bedload and bank sediments on the other side have $\delta^{13}C$ values of -25.38 ± 0.28‰ (n=13) and -26.56 ±0.90‰ (n=18), respectively. The two depth profiles collected 24 hours apart in the Anning river show similar $\delta^{13}C$ of POC (AN1: -25.70 ± 0.53‰; AN2: -25.56 ± 0.26‰) although the bottom sample of AN1 has a light ^{13}C signature at -26.51 ± 0.04‰. Depth profiles at DT show a similar pattern with a relatively heavy $\delta^{13}C$ signature at the river bottom and light $\delta^{13}C$ at the river surface.

POC radiocarbon values are reported as Fm or $\Delta^{14}C$ (‰) in this study (Table .1, Figure 6B). In depth-profiles, POC $\Delta^{14}C$ values range from -500‰ to -134‰, showing the millennial nature of POC transported in the Changjiang River system. Associated bedload samples always have the most ^{14}C-depleted OC at each location. Average $\Delta^{14}C$ of POC at depth profile location along the main CJ channel increases when going downstream with $\Delta^{14}C$ values of -451 ± 25‰, -409 ± 37‰, -337 ± 37‰ and -288 ± 41‰ at PZH, SDZ, NX, and DT, respectively. Seasonally, $\Delta^{14}C$ values range from -605‰ to -312‰ at NX with a preferable transport of more ^{14}C-depleted POC in high

variability in wet seasons when two youngest POC were observed (Figure 7). The Yalong River has comparatively younger OC in both SPM (-149‰) and bedload (-214‰). The Anning river (a tributary of the Yalong) also carries POC with relatively high ^{14}C activity both in AN1 (-140 ± 8‰) and AN2 (-252 ± 52‰) samples. The bank sediment collected at the Anning's depth sampling location contains similar young OC ($\Delta^{14}C$ = -143‰), while the bedload sample has significantly older OC ($\Delta^{14}C$ = -498‰). At PZH, SDZ, NX, and DT, POC is generally more depleted in ^{14}C in the bottom-most SPM sample. At shallower depths, POC $\Delta^{14}C$ varies to a small extent. The SDZ profile exhibits a depleting-^{14}C trend downward, while NX-3 and AN2 profiles present a reversed pattern with older POC at the surface and younger POC at the bottom.

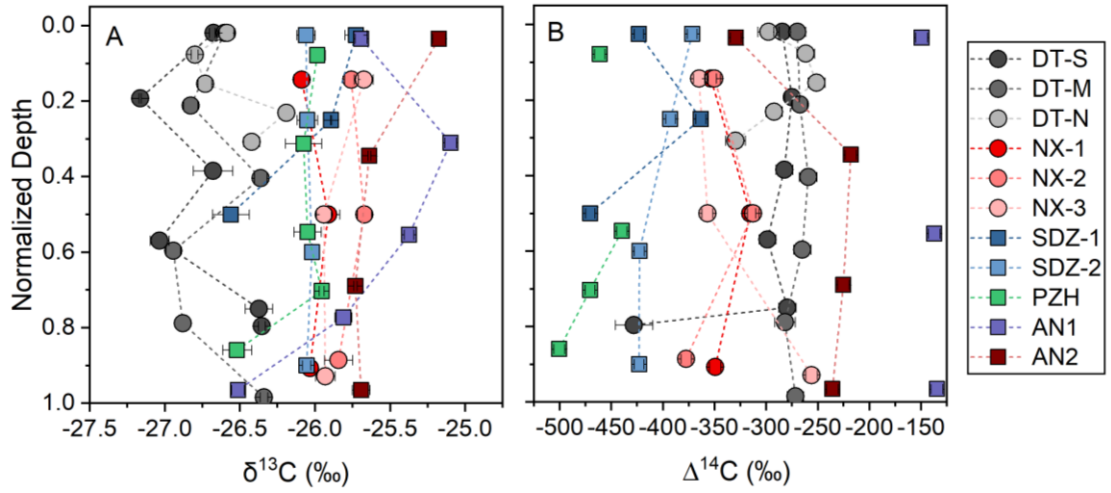

Fig. 6 Variations of dual carbon isotopic composition in POC with depth profiles. A, $\delta^{13}C$; B, $\Delta^{14}C$.

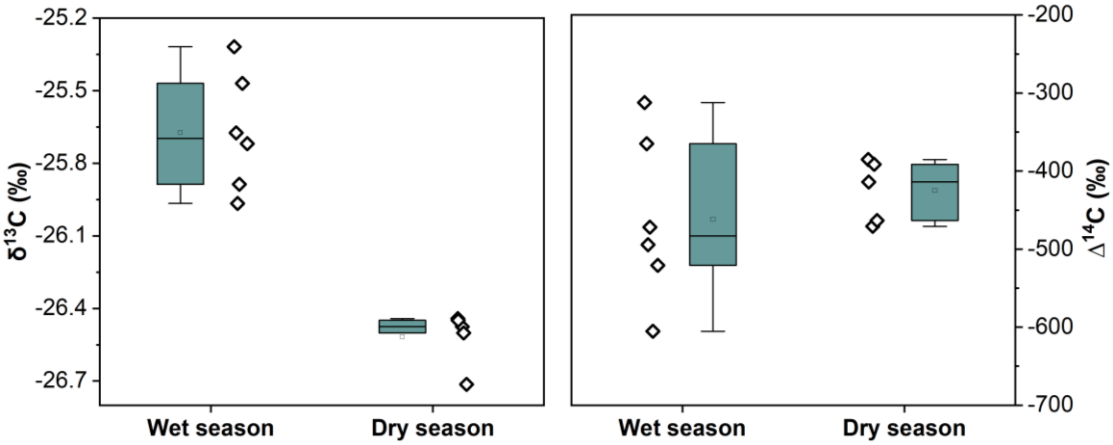

Fig. 7 Comparison of dual carbon isotopic characteristics of POC at Nanxi between wet and dry seasons. Squares are the data distribution of corresponding POC in two seasons.

4. Discussion

4.1 Temporal and spatial variation in water discharge and sediment load of the Changjiang river system

4.1.1 Annual historic records

The Changjiang is a highly regulated river system with more than 50,000 dams built since the 1950s. The total annual sediment deposition rate in reservoirs has increased from almost zero in 1950 to more than 850 Mt/yr in 2003 (Yang et al., 2005), this trend is accelerating with the ongoing construction of reservoirs, especially the CMRs in the JSJ.

Historical records of annual water discharge (Q_w) and sediment load (Q_s) over the 1953-2017 period at several gauging stations along the Changjiang (Figure 8) do not show any long-term significant change in Q_w but the abrupt decrease in Q_s after dam construction upstream. In the Jinshajiang (JSJ) River basin, the annual Q_s decreased in different degrees at the three gauging stations (PZH, BHT, and XJB), from 48.8, 161.4, and 251.2 Mt/yr during 1950-1970 (pre-dam period) to 43.87, 110.84, and 140.88 Mt/yr during 2003-2012 (post-TGD period) and further to 4.9, 93, and 1.7 Mt/yr during 2013-2017 (post-CMRs period), respectively (Figure 9). Those data show that the lower JSJ basin (after the PZH) is the main supplier of sediment to the JSJ, and also that the flux of sediment from JSJ to the CJ is nowadays almost "cut off" by reservoirs, especially the XJB and XLD CMRs (Li et al., 2018). Consequently, a ~70% decrease in annual Q_s is observed at the CT station between the post-TGD period and the post-CMRs period because the Minjiang River is still contributing to that station. As fewer sediments were exported to the TGD, Q_s at the Yichang station (downstream of TGD) decreased by another 77% to 11 Mt/yr, accounting for only 9% of the annual Qs at the mouth (DT station, 122.1 Mt/yr). The impact of anthropogenic activities (*i.e.*, dam building) is evident when comparing the sediment supply between the pre-dam period (1950-1970) and the present-day post-CMRs period with an impressive reduction of Q_s by ~99% and ~98% at XJB (whole JSJ) and Yichang (downstream of TGD), respectively. It is estimated that Q_s at Yichang will be down to 1.4 Mt/yr after the operation of all planned dams in the upper reaches (Guo et al., 2020).

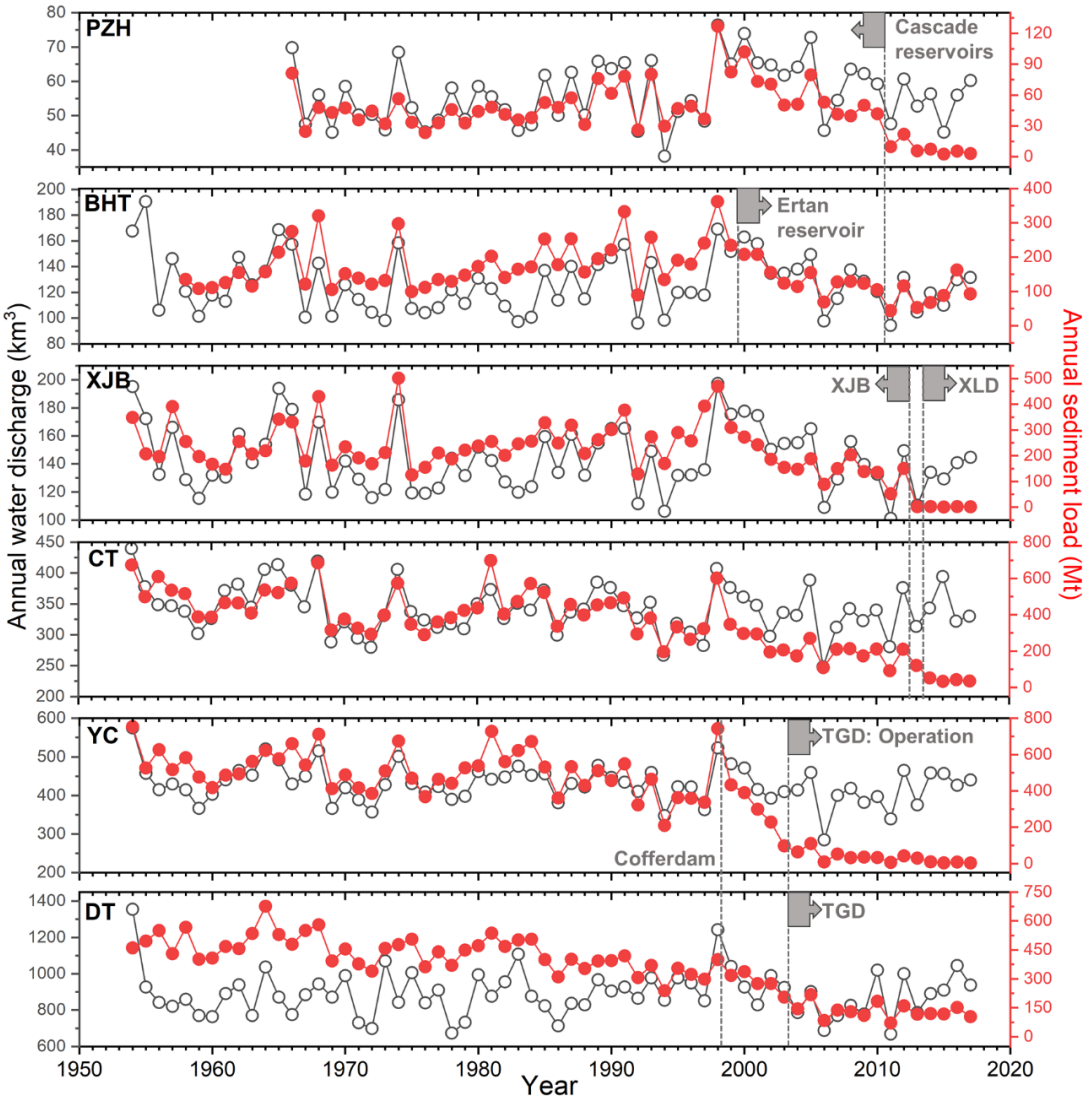

Fig. 8 Long-term annual water discharge and sediment load of the Changjiang River. Starting operation date of representative mega-reservoirs are shown with grey boxes and vertical dashed lines (Changjiang Sediment Bulletin, 2015, 2016, 2017). The gauging stations are ordered from upstream (top panel) to downstream (bottom panel) with Panzhihua (PZH), Baihetan (BHT), Xiangjiaba (XJB) along the Jinshajiang, and Cuntan (CT, after the confluence of CJ and Jialingjiang), Yichang (YC), Datong (DT) along the Changjiang mainstem.

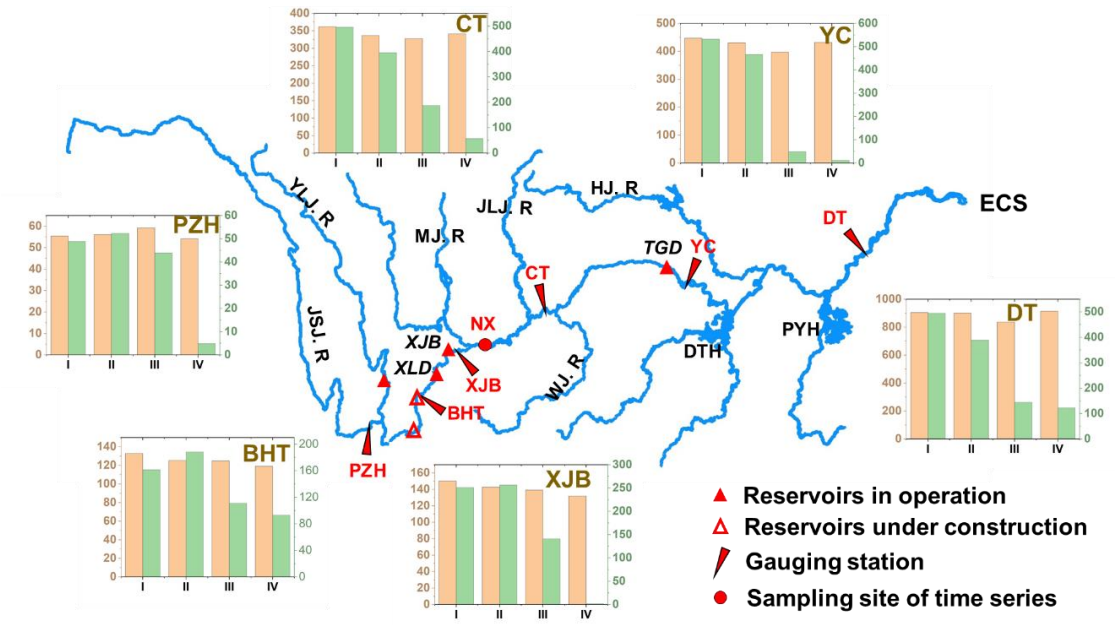

Fig. 9 Sketch map of the Changjiang showing average annual water discharge (Q_w) and sediment load (Q_s) at major gauging stations during four periods: I, 1950-1970, pre-dam period; II, 1971-2002, pre-TGD period; III, 2003-2012, post-TGD period; IV, 2013-2017, post-CMRs period. In the column plots, the left Y-axis is Q_w in km^3/yr, and the right Y-axis is Q_s in Mt/yr.

Interestingly, since the operation of the TGD and CMRs, the mid reaches of the CJ (downstream of TGD) have shifted from a sediment accumulating regime to an eroding regime (Dai et al., 2005; 2016; 2018). Indeed, Qs is now higher at DT (122 Mt/yr) than at Yichang (57 Mt/yr), while it was the reverse before dam construction (389 Mt/yr At DT and 466 Mt/yr at Yichang). This suggests that the mid reaches are now mobilizing/eroding material deposited on the riverbed before dam emplacement. Similar observations can be made between XJB and CT after the operation of the CMRs in lower JSJ. This riverbed erosion is also consistent with the bathymetric survey reported in the annual Changjiang Sediment Bulletin. Large-scale water and sediment retention by the TGD and the CMRs caused riverbed incision downstream, bed sediment coarsening, and slope steepening, leading to higher flow velocity (Lai et al., 2017; Yu et al., 2018). In the mid CJ, the role of the Dondtinghu Lake (DTH) and the Poyanghu Lake (PYH) has changed from a sink of upstream sediments to a source of sediment to the estuary. Ongoing channel incision along the CJ mainstem would further increase the elevation gradient between lakes and the river, forcing lakes to discharge

more water and sediment to the river. (Dai et al., 2018; Yang et al., 2018). Therefore, human activities profoundly impact sediment sources, characteristics, fluxes and export processes in the CJ. However, the presence of operated dams in the CJ mainstem and major tributaries alters the grain size distribution of SPM, which is known to play a key role in SPM transport mode and SPM composition (inorganic and organic). Riverine SPM is presenting an overall fining trend downstream of dams (Yang et al., 2018; Guo et al., 2020). Therefore, reservoirs would preferentially trap POC-depleted coarse particles and allow POC-enriched fine particles to flow downstream.

4.1.2 Sampling period (2016-2017) monthly records

Figure 10 shows the monthly hydrological variation during 2016-2017, Minjiang and Hengjiang together is the primary sediment contributor to Changjiang at NX, followed by Jinshajiang and Nanguanhe. The sum of the monthly Q_w and Q_s of the four rivers was used to quantify the monthly hydrological condition at NX as there is no gauging station, considering no loss of water and sediment deposition. The monthly Q_w and Q_s exhibit a seasonal pattern at each site with a higher yield in the wet seasons (May - October). During the wet season, over 90% of annual Q_s were delivered with ~70% annual Q_w in the upper reaches; while at DT station, the proportion for Q_s is ~72%, and the remaining were carried by ~35% annual Q_w during the dry seasons. The significant dominating delivery of sediments during the wet season also suggests the composition variation in different seasons, POC could have different elemental and isotopic signals. From XJB to CT, there is a factor of up to ~70 increase for monthly Q_s but a factor of a maximum of 3.6 for monthly Q_w. From Yichang to DT, the increasing trend is more drastic with a factor of up to ~180 for monthly Q_s and 2.9 for monthly Q_w. Between these two sections, the Q_s increased more drastically during wet seasons from XJB to CT and dry seasons from Yichang to DT. The observation indicates that the TGD traps sediment annually not just seasonally because all monthly Q_s reduced remarkably from CT to Yichang.

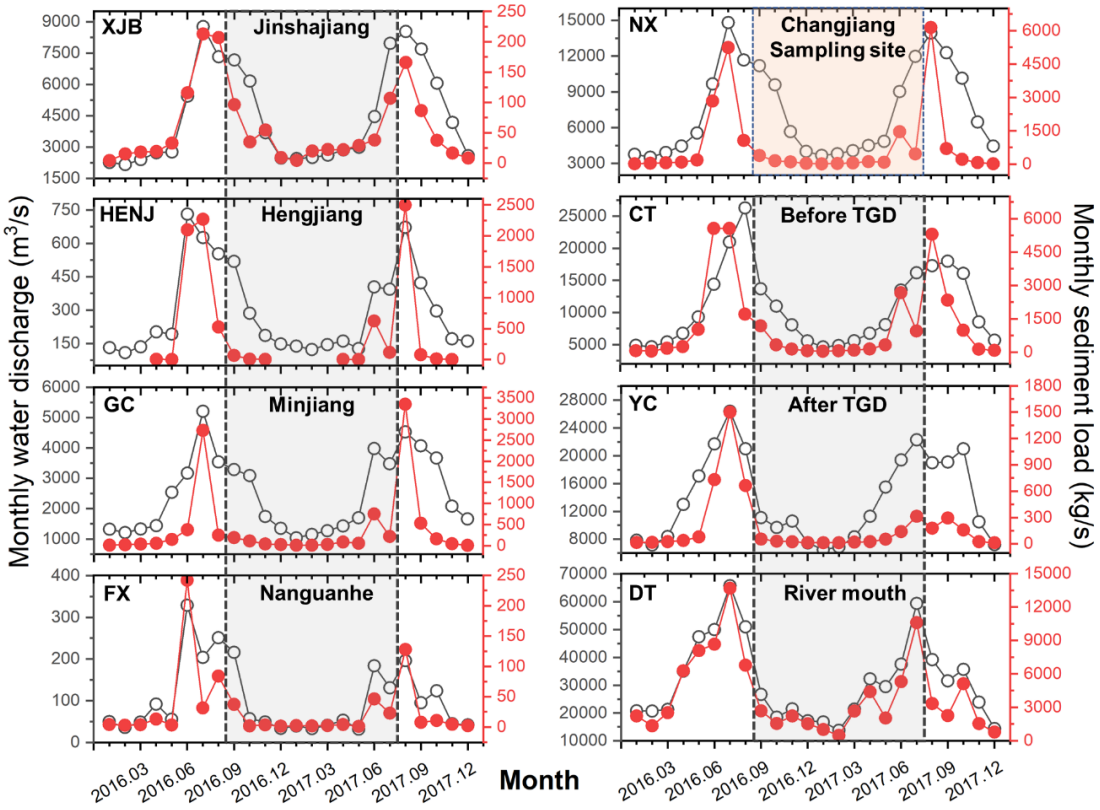

Fig. 10 Monthly water discharge and sediment load of Changjiang River basin from January 2016 to December 2017. The eight sites are Jinshajiang at Xiangjiaba (XJB), Hengjiang at Hengjiang (HENJ), Minjiang at Gaochang (GC), Nanguanhe at Fuxi (FX) and Changjiang at Nanxi, Cuntan (CT), Yichang (YC), and Datong (DT). The monthly time series SPM collection period is marked by the orange shaded area, the grey shaded areas are marked to compare the hydrological condition at NX with that at other gauging stations. All monthly hydrological data was from Changjiang Sediment Bulletin, 2016 and 2017.

4.2 Transport mode of POC in the Changjiang River system

4.2.1 Controls on SPM particle size and POC content

POC content in Changjiang River sediments is variable at both spatial (cross-section and river basin-wide) and seasonal scales. Rivers transport SPM of a large range of grain size together with POC, the finer size fraction being commonly enriched in POC because of larger mineral surface area (Galy et al., 2008b; Bouchez et al., 2014; Hilton et al., 2015). In contrast, quartz-rich coarser SPM with low Al/Si ratios are usually OC-depleted (Figure 11). As the Al/Si ratio of SPM is clearly related to particle size distribution (Figure 5), its evolution along the river channel might provide some insight into the mode of POC load and transfer (Galy et al., 2008b; Bouchez et al., 2011b;

2014). In general, vertical variation of POC content in the water column can be attributed to hydrodynamic sorting (Bouchez et al., 2011a), meaning that flow velocity heterogeneities at cross-section scale can generate lateral heterogeneities in POC content, in addition to sediment supply from bank erosion (Ke et al., submitted). In Al/Si vs. OC% space (Figure 11), two positive trends can be seen: one for samples from the upper CJ (JSJ river system) and one for the samples collected in the CJ mainstem after the confluence of JSJ and Minjiang (NX and DT samples). At a given Al/Si, SPM from the JSJ generally contains less POC than SPM from the CJ mainstem (Figure 10). Including published data, POC content in lower CJ is systematically higher than in JSJ and upper main tributaries (Figure11). However, the monthly time series collected at NX doesn't show any relationship in Al/Si vs. OC% suggesting that other factors than sorting impact POC loading. This should be attributed to CMRs dam trapping of some

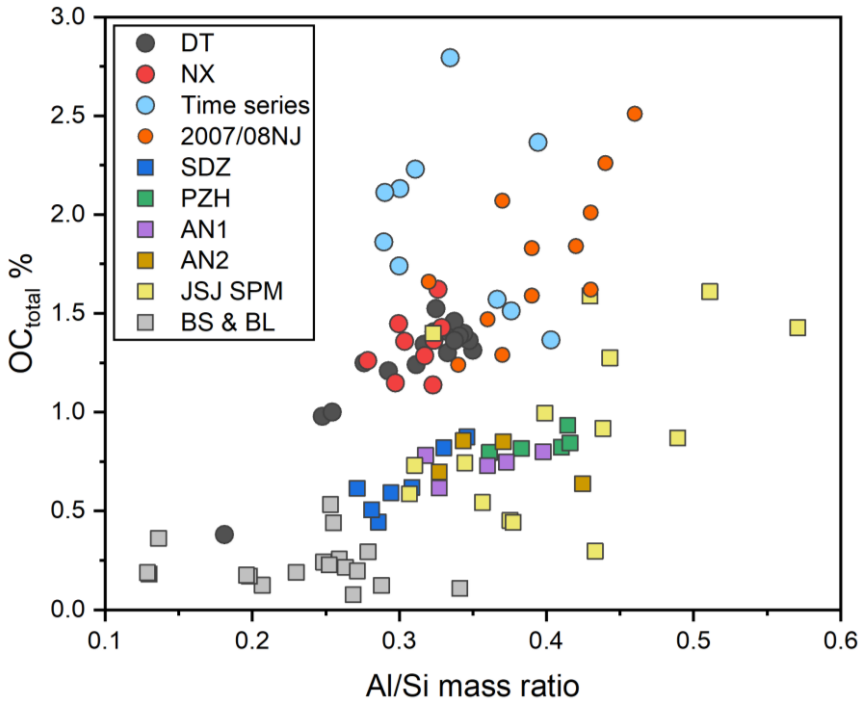

Fig. 11 Relationships between the total OC content and Al/Si mass ratio of sediments collected in the entire Changjiang River system. Circles denote samples collected at the main channel of Changjiang, while squares are samples collected in the JSJ River basin. 2007/08NJ is the monthly collected suspended sediment at Nanjing (downstream of DT) from October 2007 to September 2008 (Li et al., 2015). Sediments from the main CJ clearly have more OC% than JSJ ones at a given Al/Si ratio, indicating large-scale spatial heterogeneities in POC loading mode.

coarse fractions and external OC supply from other tributaries. Indeed, the NX time-series sampling site is located after the confluence of 4 tributaries which respective contributions to the sediment load could be seasonally driven. Anyway, systematic low Al/Si and POC-rich SPM collected in the dry season could be explained by enhanced input of soils and vegetations. In the mid CJ, aside from TGD dam trapping that alters sediment grain size and mineral compositions, the addition of young soil OC is likely. The different Al/Si-POC relations observed in Amazon and its major tributaries present mineralogical composition differentiation and discrete organic debris (Bouchez et al., 2014). Zhao et al. (2018) report that the clay fraction of JSJ contains less smectite and more chlorite than that of CJ, especially in the lower reaches. A modest variation of clay minerals may affect sediment Al/Si ratio but not POC content. As discussed in the previous section, the mid-CJ is reported to have switched from being a sediment sink to a major sediment source since TGD operation (Yang et al., 2018; Yang et al., 2019), the input of autochthonous organic matter, vegetation, and lowland soils might significantly add abundant discrete POC into the suspended load, which could be responsible for higher POC content. Meanwhile, dam construction accelerates the production of autochthonous organic matter in CJ (Wang et al., 2012; Zhang et al., 2014; Wu et al., 2018). High sediment accumulation at reservoirs reduces total SPM transfer downstream but proportionally favors the selective transport of fine OC-rich particles (Yang et al., 2018; in-situ monitoring by the Changjiang Water Resources Committee). Dam operates as an artificial concentrating process that exerts a primary control on the POC content of SPM (Wang et al., 2012; Zhang et al., 2014; Li et al., 2015; Wu et al., 2007; 2018).

4.2.2 Insights from stable carbon isotope and radiocarbon of POC

POC $\delta^{13}C$ values of SPM range from -26.94‰ to -25.10‰ in the main channel of CJ, indicating that POC mainly originates from C3 plants (Figure 12-13). We observe a slight decrease in POC $\delta^{13}C$ in the lower reaches, although there is no systematic variation if historic data from 1997 to 2010 (Wu et al., 2007; 2018) are included. That could be explained by SPM supply from tributaries, bank erosion, and resuspension of bedload. The lake systems (DTH and PYH) that contribute to the mid-CJ transfer SPM are relatively enriched in POC of more ^{14}C composition and depletion of ^{13}C (Wu et al., 2018). On the contrary, supported by the higher POC $\delta^{13}C$ values in the river bottom, resuspension of bedload with older POC in mid-lower regions should compensate for

delivery of SPM. These two processes act oppositely on the elemental and isotopic carbon (^{13}C and ^{14}C) composition of SPM. Besides, the minor difference of POC ^{13}C abundance in the vertical depth profiles as well as between bed sediments and SPM should be ascribed to the massive deposition of coarse particles in the reservoirs as well, because of the reduction of SPM chemical heterogeneity that is particle size depended.

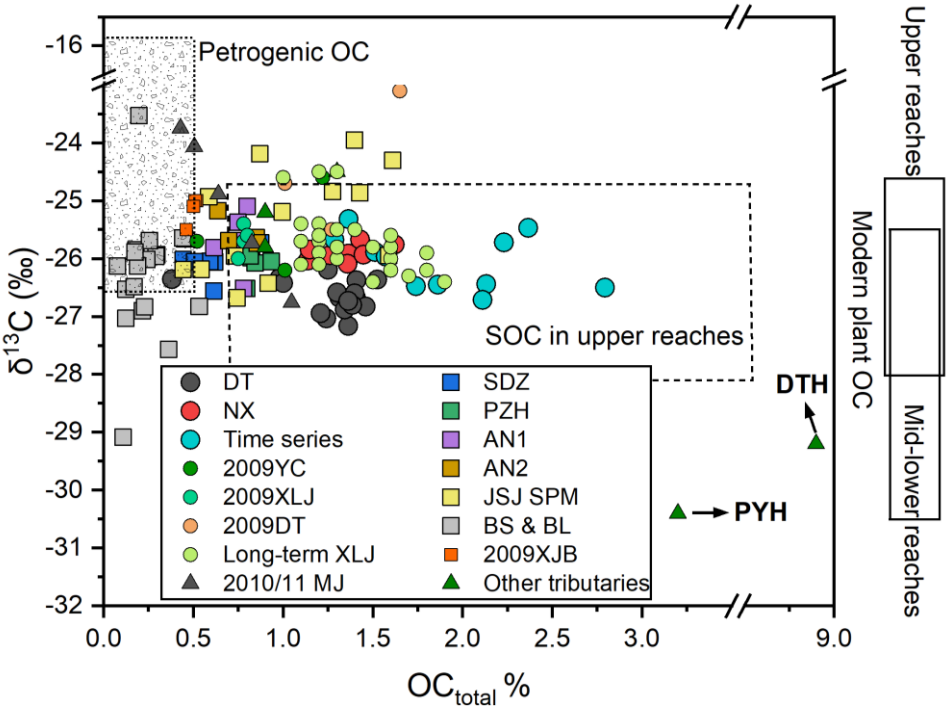

Fig. 12 Cross-plot of total organic carbon content versus $\delta^{13}C$ values for POC and its sources from Changjiang. The range of petrogenic OC and soil organic carbon in the upper reaches, and modern plant OC in the upper reaches and mid-lower reaches are marked in the plot. The modern plant OC within the basin has an OC content of 44.7 ± 2.0% with the $\delta^{13}C$ values of -26.3 ± 1.7‰ (Wang et al., 2019; Rao et al., 2017) and -28.5 ± 1.7‰ (Wu et al., 2018) for upper reaches and mid-lower reaches, respectively. The OC contents are 0.2 ± 0.3% for the petrogenic OC and are 3.1 ± 2.4% for the SOC in the upper reaches are with the $\delta^{13}C$ values -24.4 ± 1.7‰ (Galy et al., 2008b; Wang et al., 2019)) and -21.5 ± 5.7‰ (Rao et al., 2017; Wang et al., 2019), respectively.

Contrasting with the two relationships observed in OC% vs. Al/Si space (Figure 11) for JSJ samples one side and main CJ samples (NX and DT) on the other side, we observe only one negative relationship in OC% vs. D90 and Fm vs. D90 spaces for depth profiles collected in the main channel of both JSJ (SDZ) and CJ (NX and DT) (Figure S5-S6). Those negative relationships indicate that OC in coarse material is less abundant and older than in fine material, as discussed previously based on the

variability of Al/Si ratios of SPM. Even though some discrete inputs of young POC from modern plants or soils do contribute to the POC load all along the river channel, the evolution of SPM grain size and POC Fm from SDZ to NX and then to DT would be consistent with the progressive loss of the coarse and ^{14}C-depleted fraction from upstream to downstream.

However, the upper reaches are also characterized by fine particles carrying mineral-bound POC with a relatively ^{14}C-depleted signature (*e.g.*, PZH samples). This ^{14}C-depleted signature of fine material is also found in some of the NX monthly time-series samples, indicating that those fine particles escape CMRs in contrast with the coarse ones. Further downstream (at DT), the fine ^{14}C-depleted material is not found anymore with a younger ^{14}C signature in fine material. This observation could be explained by a dilution process with younger OC coming from lowland soils or autochthonous OC and vegetation debris (Figure 13) (Zhang et al., 2014; Wu et al., 2018). Indeed, the estimated soil OC (SOC) radiocarbon activity of subbasins increases when going downstream in the CJ (Figure S7), and can therefore partly explain the progressive increase in ^{14}C activity of fine SPM from the upper reaches to the lower reaches.

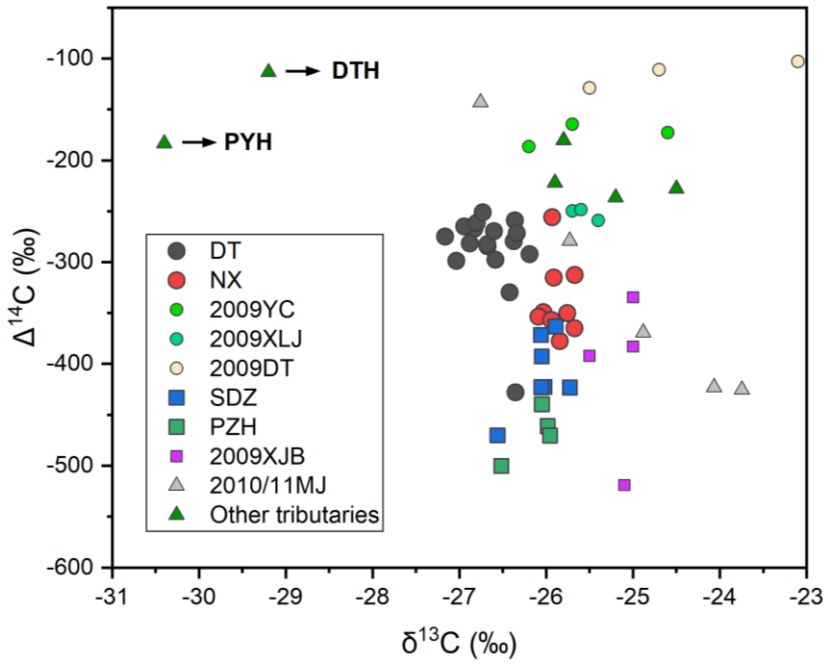

Fig. 13 Cross-plot of $\delta^{13}C$ versus $\Delta^{14}C$ values for POC in the main channel of Changjiang, data of POC from the main channel of Minjiang in 2010 and 2011 was added (Wang et al., 2019), as well as POC from Hanjiang, Dongtinghu, and Poyanghu (Wu et al., 2018).

The comparison between our sample set collected in 2017 (after CMRs operation in the JSJ) and the samples collected in 2009 (before CMRs construction) by Wu et al. (2018) reinforces our above interpretation. The OC $\delta^{13}C$ signature of 2009 samples is much heavier than our 2017 samples from the JSJ (PZH and SDZ samples) and thus closer to the rock-derived OC $\delta^{13}C$ signature (Figure 14). Since the rock-derived OC is preferentially carried by coarse material, it is also observed in JSJ revealed by the bedload (*e.g.*, Ganges-Brahmaputra, Amazon, and Mackenzie, etc.), the deposition of coarse materials in low-energy CMRs has shifted POC signature and content to values consistent with a mixture of fine soil-derived material and modern OC. In summary, reservoirs exert a strong control on both POC export fluxes and POC isotope signatures downstream.

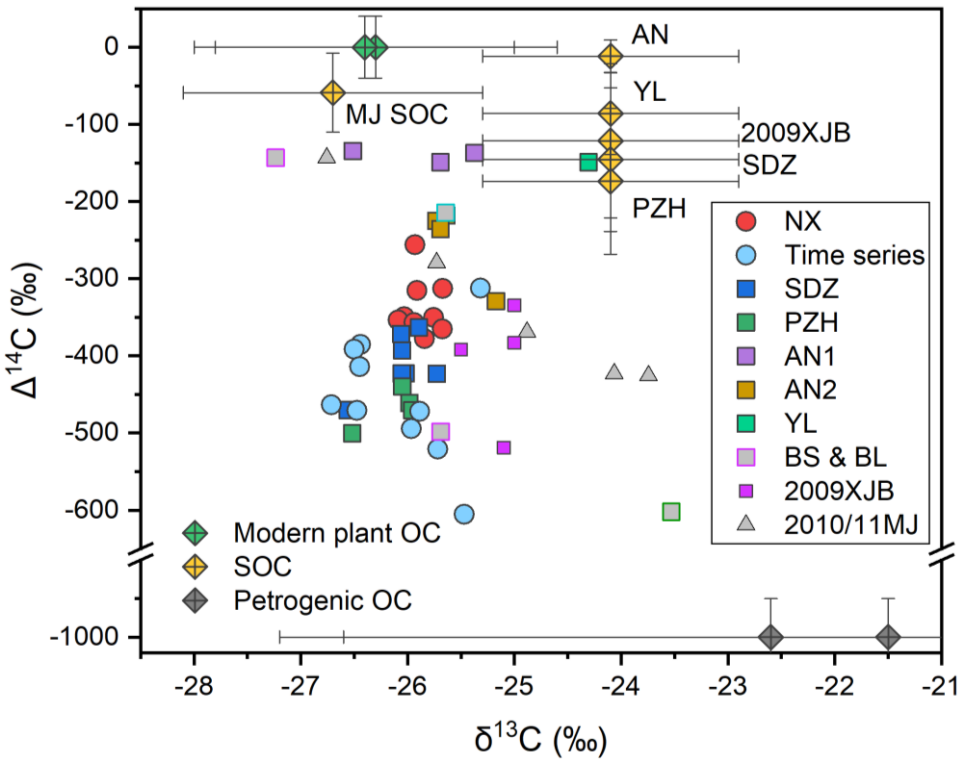

Fig. 14 Cross-plot of $\delta^{13}C$ versus $\Delta^{14}C$ values for POC and its sources for samples collected at NX and catchments upstream. Bank sediment and bedload of the corresponding depth profile were squares with a depth-profile dependent colored outline and grey fills. $\Delta^{14}C$ values of modern plant sources and petrogenic OC (sedimentary rocks OC) were assigned as 0 ± 40‰ and −1000‰ respectively. $\Delta^{14}C$ values of soil organic carbon (SOC) is site-dependent, the average value of the surface layer (depth in 30 cm) was extracted from Shi et al., 2020 using ArcGIS 10.3 (ESRI).

For the $\delta^{13}C$ of each endmember, modern plant in JSJ has a value of -26.4 ± 1.4‰ (n =33) (Rao et al., 2017), while in MJ is -26.1 ± 1.9‰ (n=54) (Wang et al., 2019), then the average value to constrain POC at NX is -26.3 ± 1.7‰ (n=87). Regarding the SOC source to POC in JSJ and its subbasins, we used a range of -24.1 ± 1.2‰ (n=75) (Rao et al., 2017), and we added the SOC of MJ -26.3 ± 1.7‰ (n=12) (Wang et al., 2019). For the petrogenic/fossil source, -22.6 ± 4.0‰ (n=12) (Galy et al., 2008b) for JSJ, and used the range of -21.5 ± 5.7‰ (n=32) with the integration of signals from MJ (-20.8 ± 4.0‰, n=20) (Wang et al., 2019) for POC at NX.

Another aspect of POC dynamics at catchment scale can be given by the analysis of POC transported by the Anning river, a tributary of the Yalong River (itself a tributary of the JSJ river), collected twice after a massive storm event (just after the storm event and 24h later). Rivers in storm events record the instantaneous fluvial process of mobilizing terrestrial materials into rivers under negligible anthropogenic interference. During the first storm, the Anning River delivers considerably young POC (~1,150 yrs), the most depleted ^{13}C and enriched ^{14}C in the bottom SPM suggests deposition of discrete OC originated from soils and modern plants. While comparatively older POC (~2,280 yrs) carried by finer SPM in the second storm, the most enriched ^{13}C and depleted ^{14}C in the river surface, which should be explained by a decreased transport of OC from biospheric debris that should be mostly be taken way in the previous mobilization. Mobilization of terrestrial organic matter by floods during storm events should be highlighted in the fluvial POC source-to-sink transport due to its massive transport of OC mixings from variable sources, especially a rapid transfer of biospheric debris, which is an important mechanism of transfer landslide deposits involving POC_{petro} and POC_{bio} in the small mountainous rivers in active tectonic regions (West et al., 2011).

4.3 Sources and fluxes of POC

4.3.1 Endmember apportionment for POC

In this study, we applied two methods to quantify the sources of POC, which are a binary mixing model (POC_{bio} vs POC_{petro}) based on bulk fraction modern (Galy et al., 2008a) and a MIXSIAR model based on dual-isotopic mass balance (Parnell et al., 2010). Bulk riverine POC could be viewed as a mixture of three major inputs: recent bio-synthesized OC (modern plants), aged soil OC, and petrogenic OC (fossil OC or

kerogen) from ancient sedimentary rocks (Blair et al., 2010; Blair and Aller, 2012). The simulation in the context of MIXSIAR could be carried out on quantification of more than three sources (Parnell et al., 2010).

In the binary mixing model, the POC content and the modern POC content (Fm × POC%) of SPM in the whole channel transect were used to construct the linear fitting (Figure 15). At PZH, NX, and DT, the transect integrated simulation resolves the heterogeneity observed among the simulation results of individual depth profiles, *i.e.*, a limited sample set can decrease the robustness of the simulation. Fm_{bio} ranges from 0.64 to 0.85 (3,600-1,300 years in terms of POC_{bio} age) in the main channel of CJ, these values are consistent with the estimates of POC_{bio} age from 1,100 years to 3,200 years for 2009 – 2010 samples by Wu et al (2018). Assuming that the POC_{petro} content obtained by the binary model (0.228%) is also valid for the time series, then a rough estimate of Fm_{bio} for the monthly time-series can be achieved, giving POC_{bio} ages from 1,470 years to 6,600 years (average 3,600 years). These values are comparable to POC_{bio} age from Huanghe (1,120-2,750 years; Tao et al., 2015) and Mackenzie (3,030-7,900 years; Hilton et al., 2015). The Anning river (a tributary of the Yalong river) just after a massive storm event delivers modern terrestrial POC_{bio} into the fluvial system with Fm_{bio} of around 1.05, indicating the rapid transfer of massive fresh POC_{bio} through landsliding. The Anning river catchment and mid-lower CJ have comparable SOC radiocarbon activity (Figure S8), where the precipitation is frequent and intensive, driving the erosion to terrestrial POC_{bio} (Figure S9). Regarding POC_{petro} composition, it is higher in the upper reaches (0.31 ± 0.12% at PZH, 0.23 ± 0.12% at NX) than in lower reaches (0.11 ± 0.03% at DT), so do the major upper tributaries (*e.g.*, Minjiang 0.13%-0.36%, Wang et al., 2019). This characteristic could be attributed to the topography as mountainous rivers have been shown to deliver SPM with high POC_{petro} contribution due to an intensive physical erosion (Blair and Aller, 2012; Hilton et al., 2010). In our study, an average POC_{petro} content of 0.14% and average Fm_{bio} of 0.76 (2,200 ^{14}C yrs) can be obtained using individual depth profiles. This latter value is significantly older than the global average for mountain forests (1,300 ^{14}C years old; Hilton., 2017), which might reflect the release of refractory SOC from the QTP permafrost-rich region. With the abundant distributed high-altitude permafrost in the QTP, the thawing process could supply old organic carbon to CJ which could be comparable to the POC aging mechanism in the large circum-Arctic permafrost rivers

(Wang et al., 2020; Guo et al., 2007; Wild et al., 2019).

Regarding the MIXSIAR model, three or four site-dependent endmembers were assigned to constrain the POC composition (detail in Table. 2 and Figure 14). The reliability of endmember parameters is essential in returning an accurate simulation, we did a site-dependent endmember determination based on the upstream area of the sampling points using multiple spatial data raster and compilations (Shi et al., 2020; Rao et al., 2017; Wang et al., 2019; Galy et al., 2008b). Due to a lack of suitable constraints for the entire basin, this model was not applied in POC from DT. The model simulations yield an uncertainty of 2% to 13% for petrogenic OC, 8%-22% for modern biomass OC, 4%-24% for SOC from the JSJ River basin and its subbasins, and 12%-22% for SOC from the Minjiang River basin. This model results in a larger POC_{petro} content (PZH 0.42%/43.5%, SDZ 0.28/37.7%, XJB/2009XJB 0.17%/33.8%, NX 0.43%/30.8%, 'POC_{petro} content/proportion') compared to that from the binary mixing, highlighting the significant export of POC_{petro} from the upper CJ (Figure 16-17). Results for fractional contribution from modern biomass and SOC might have some intersections because of the overlapped $\delta^{13}C$ and $\Delta^{14}C$ endmember values. The results show that modern plant OC contributes around 40% to the bulk POC while SOC contributes 23%, 16% at SDZ and PZH, respectively. A large proportion of modern POC load could partly be explained by autochthonous OC (Zhang et al., 2014; Wu et al., 2018), however, considering the balance of OC, a large fraction should be recently-degraded OC that resides in soils. A significant rapid transfer of modern biosphere OC could favor its preservation (Bair and Aller, 2012; Galy et al., 2008a), CMRs at lower JSJ could help it escape from metabolism by preventing a majority from longer transportation that could increase oxygen exposure time. The non-negligible proportion from JSJ SOC indicates the possible input of permafrost SOC from the QTP (Figure 1C). The presence of permafrost within the JSJ River basin is responsible for the refractory nature of SOC endmember adopted for the upstream regions of the sampling site (Table. 2). Based on the 2009XJB samples collected at XJB just before the confluence with the Minjiang (Wu et al., 2018), it can be inferred that SOC (45%) was the primary fraction of riverine POC that was delivered from the JSJ to the CJ before CMRs construction. This result suggests that the mid-lower JSJ yields substantial aged SOC to the fluvial system.

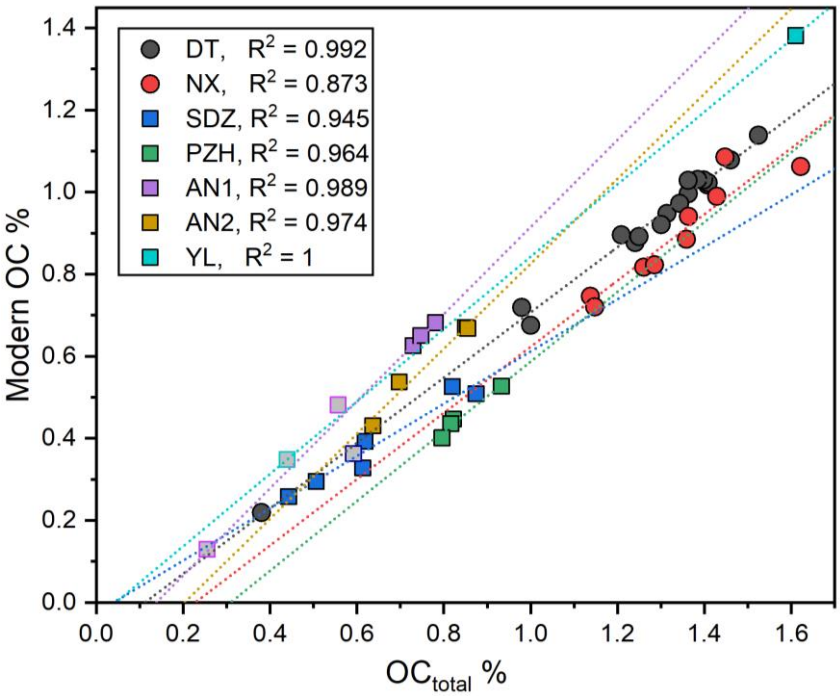

Fig. 15 The binary mixing model used to constrain the biospheric POC and petrogenic POC in SPM of depth profiles. The dot lines represent linear regression through POC samples collected in each cross-section (1 to 3 depth profiles each), bank sediments and bedload were not included in the regression fitting analysis. Regarding the Yalong (YL), only a surface collected SPM and a bedload was used to build the binary mixing. Estimation of Fm of biospheric POC and contents of petrogenic POC are listed in Table. S3.

Table. 2 Basin dependent endmember apportionment of dual carbon isotopes

Site	Parameters	Petrogenic OC	Modern plant OC	Site-based SOC	Minjiang SOC
PZH	$\delta^{13}C$ (‰)	-22.6 ± 4.0[1]	-26.4 ± 1.4[3]	-24.1 ± 1.2[3]	
	$\Delta^{14}C$(‰)	-1000	0 ± 40	-173.7 ± 94.5[4]	
SDZ	$\delta^{13}C$ (‰)	-22.6 ± 4.0[1]	-26.4 ± 1.4[3]	-24.1 ± 1.2[3]	
	$\Delta^{14}C$(‰)	-1000	0 ± 40	-145.6 ± 93.0[4]	
AN1	$\delta^{13}C$ (‰)	-22.6 ± 4.0[1]	-26.4 ± 1.4[3]	-24.1 ± 1.2[3]	
	$\Delta^{14}C$(‰)	-1000	0 ± 40	-11.7 ± 21.0[4]	
AN2	$\delta^{13}C$ (‰)	-22.6 ± 4.0[1]	-26.4 ± 1.4[3]	-24.1 ± 1.2[3]	
	$\Delta^{14}C$(‰)	-1000	0 ± 40	-11.7 ± 21.0[4]	
YL	$\delta^{13}C$ (‰)	-22.6 ± 4.0[1]	-26.4 ± 1.4[3]	-24.1 ± 1.2[3]	
	$\Delta^{14}C$(‰)	-1000	0 ± 40	-85.8 ± 52.8[4]	
2009NX	$\delta^{13}C$ (‰)	-22.6 ± 4.0[1]	-26.4 ± 1.4[3]	-24.1 ± 1.2[3]	
	$\Delta^{14}C$(‰)	-1000	0 ± 40	121.2 ± 100[4]	
NX	$\delta^{13}C$ (‰)	-21.5 ± 5.7[1, 2]	-26.3 ± 1.7[2, 3]	-24.1 ± 1.2[3]	-26.7 ± 1.4[2]
	$\Delta^{14}C$(‰)	-1000	0 ± 40	-121.2 ± 100[4]	-58.9 ± 51.3

1 [Galy et al., 2008b]; 2 [Wang et. al., 2019]; 3 [Rao et al., 2017]; 4 [Shi et al., 2020].

At NX (after the confluence with Minjiang), SOC is the dominant POC fraction with a major contribution from the Minjiang and a minor one from the JSJ. The difference in relative SOC contributions from JSJ and Minjiang is weaker in the wet season. While the SOC input from the Minjiang is 7.1-10.2 times larger than that from the JSJ in the dry season, it is only 1.7-3.4 times larger during the wet season, except in June 2017 (NX 17.06), when SOC input is slightly higher from the JSJ, 1.2 times the input from the Minjiang. This is still in line with the sediment input shown in Figure 10 that the Hengjiang contributes a significantly high amount of sediment to NX. In general, those results reveal that the JSJ only exports a small proportion of SOC (and more generally of POC) to downstream CJ since the construction of CMRs. The relative POC contributions vary significantly between wet and dry seasons, with average POC_{petro} contribution decreasing from 40.6% to 32.4% and SOC contribution from the JSJ decreasing from 14.1% to 5.9%. However, the contribution from Minjiang SOC increases from 27.8% to 46.2% between wet and dry seasons. Overall, POC_{bio} dominates the fluvial POC load in the study mountainous catchments. The two profiles collected 24h apart after a massive storm event in the Anning river show that POC from both profiles is dominated by modern plant OC and SOC, but that the one collected 24h after the storm has 10% more fractional OC contribution from the lithosphere, and 10% less from the modern biosphere than the profile collected just after the storm. This relative change in OC contribution shows that storm-induced landsliding quickly mobilizes modern biospheric OC to the fluvial system but also that this contribution decreases rapidly after the event.

Both the binary mixing and the MIXSIAR model return high POC_{petro} in the upper reaches of CJ, underlining the significance of POC_{petro} delivered from the mountainous rivers. Regarding the POC composition at PZH and NX, which are seriously impacted by upstream reservoirs, they still show substantial POC_{petro} contribution in small particles with high Al/Si ratios. It suggests that mineral protection could help refractory POC_{bio} and dead POC_{petro} passing through reservoir detainment, supporting our previous discussion based on dual carbon isotopes. Notably, permafrost collapse in the QTP (Wang et al., 2020; Gao et al., 2021) is an important process of refractory carbon release to river systems, as observed along the East Siberian margin and in the Arctic rivers (Vonk et al., 2012; 2015; Birgit et al., 2018). This process should be further investigated in the CJ river system. Millennial POC_{bio} dominates the riverine POC load

in the entire river system, meaning that the selective sedimentation of SPM fraction on land induced by reservoirs could have a significant impact on the fate of riverine POC and the global carbon cycle.

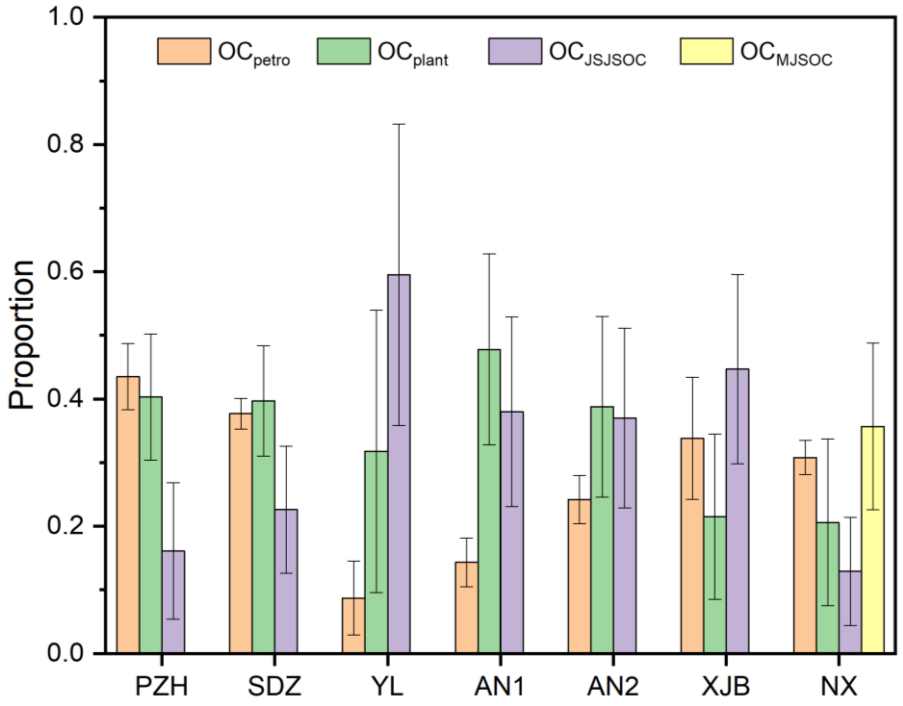

Fig. 16 Fractional contributions of different OC sources to the POC at each depth profile sampling site.

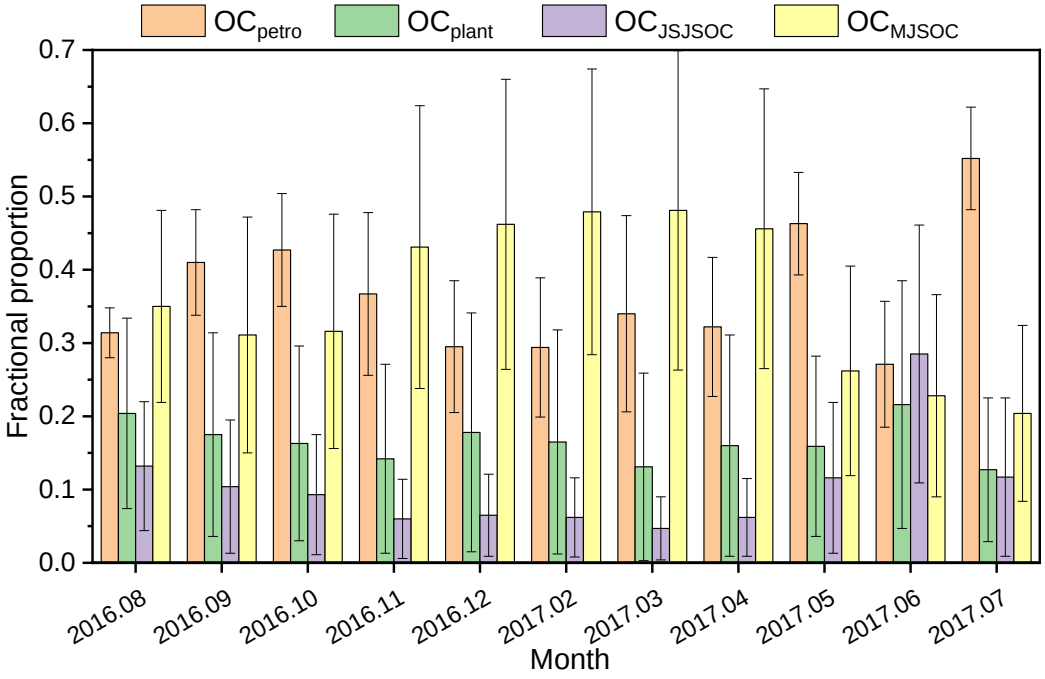

Fig. 17 Fractional contributions of different OC sources to the POC of monthly collected SPM at Nanxi. Data values are summarized in Table. S3.

4.3.2 Instantaneous flux and yield

Using ADCP or current velocity meter profile at each sampling site, we calculated instantaneous suspended sediment flux and POC flux. The instantaneous POC_{petro} flux is calculated by multiplying the instantaneous SPM flux by POC_{petro} content, which is estimated by the MIXSIAR model (the binary mixing result for DT). Subsequently, the instantaneous POC_{bio} flux is obtained by subtracting the POC_{petro} flux from the POC flux (Table. 3). Then we calculated the instantaneous POC yield through normalization to the upstream area. The topographic slope is known to exert a first-order control on physical erosion processes, but here we were not able to examine this effect due to massive interference by artificial reservoirs.

Instantaneous POC fluxes range from 1.1 kg/s at PZH to 63 kg/s at DT, with POC_{bio} fluxes from 0.63 kg/s to 54 kg/s and POC_{petro} fluxes from 0.36 kg/s to 10.3 kg/s. The storm event in the Anning basin has resulted in the mobilization of a huge amount of terrestrial material into the river, accompanied by organic matter. At the sampling date, the Anning River basin, which represents only one-150^{th} of the full CJ, has delivered a comparable amount of POC (42.7 kg/s) to DT (62.5 kg/s) and even more POC_{petro} (10.3 kg/s). This resulted in POC yield two-order magnitude larger than at DT, highlighting the important role of small catchments and land sliding process on POC export in large river systems. In addition, both POC_{bio} and POC_{petro} yields in the CJ system increase with suspended sediment yield (Figure 18), in agreement with the global observation that physical erosion rate controls the yield of POC_{bio} and POC_{petro} in small mountainous rivers and large rivers (Hilton, 2017; Galy et al., 2015; Hilton and West, 2020).

Climate parameters are major controlling parameters of radiocarbon age and turnover times of SOC in global river basins (Eglinton et al., 2021). The larger precipitation rate in the Anning River basin should be the reason for the younger SOC radiocarbon age and shorter SOC turnover time compared to other subbasins in upper CJ (Figure S7-S9), providing modern terrestrial POC into the fluvial system. At PZH and SDZ (JSJ main channel), albeit they are impacted by cascade reservoirs upstream, the latter has POC_{bio} and POC_{petro} one order of magnitude larger than that from the former, meaning that the erosion of lithogenic OC is an important process in this large mountainous river, so does in Minjiang (Wang et al., 2019), besides, the potential importance of POC contribution from Yalong for SDZ. The POC preservation in its

lower CRMs could be as efficient as the burial of Ganges-Brahmaputra POC in passive margins and small mountainous rivers such as Eel and Waopaoa etc., in active margins (Galy et al., 2008a; Blair and Aller, 2012), making the river-reservoir system an organic carbon sink over decades or millennials. If there is a high oxidation rate, the counterbalance between POC_{bio} burial and CO_2 released by POC_{petro} oxidation together could result in no net effect in geologic timescales. The topography (high elevation and steep slope) and climate (low-temperature) of the upper reaches, which are unfavorable for POC degradation (Burdige, 2011), but the terrain with a steep slope favors the erosion to terrestrial POC including POC_{bio} and POC_{petro} (Hilton, 2017) thus river-reservoirs of upper CJ is more likely to be a carbon sink.

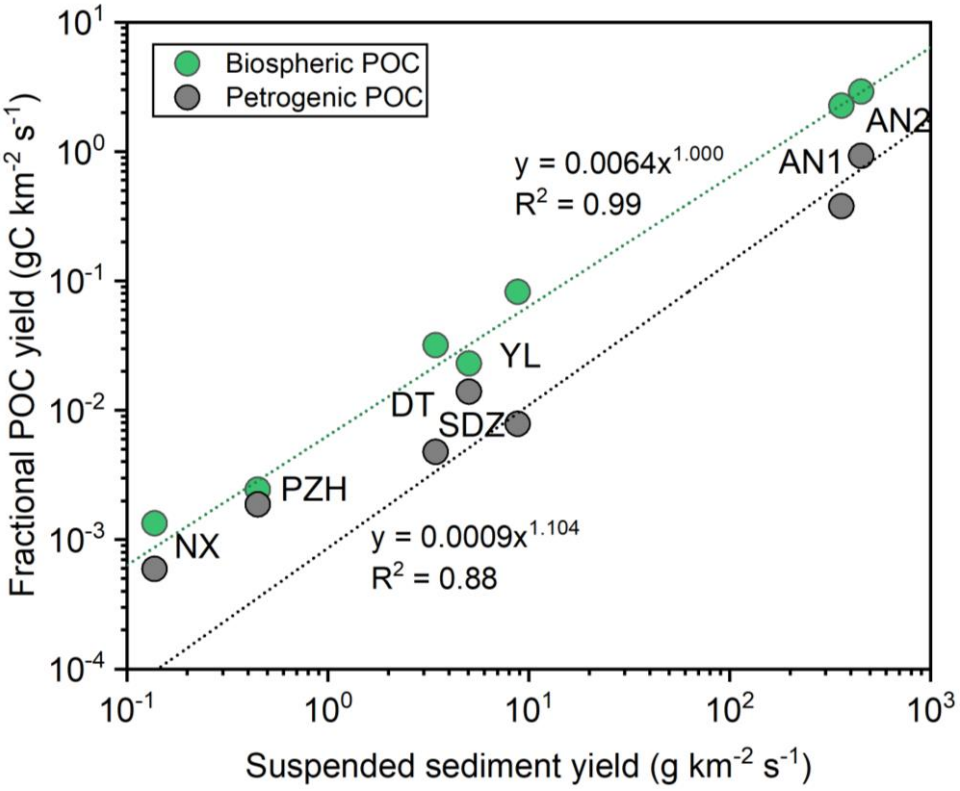

Fig. 18 Instantaneous POC_{petro} and POC_{bio} yield as a function of instantaneous suspended sediment yield in the Changjiang River basin. The nonlinear regression dot lines are fitting lines based on the power law. Data values are summarized in Table. S4

Table. 3 Instantaneous depth-integrated fluxes and yields of SPM and POC of each channel transect.

Sampling site	SPM flux kg/s	Sediment yield g/km²/s	Water discharge m³/s	Average POC %	POC flux kg/s	POC yield g/km²/s	POC_{petro} %	POC_{bio} flux kg/s	POC_{petro} flux kg/s	POC_{bio} yield g/km²/s	POC_{petro} yield g/km²/s
DT	5862	3.44	60525	1.07	62.52	0.0367	0.11	55.95	6.57	0.0328	0.0039
NX	84	0.14	3442	1.41	1.18	0.0019	0.43	0.84	0.35	0.0014	0.0006
SDZ	1959	5.04	8515	0.73	14.35	0.0369	0.29	8.94	5.41	0.0230	0.0139
PZH	116	0.45	2977	0.96	1.12	0.0043	0.42	0.63	0.49	0.0024	0.0019
AN1	4012	359.79	1000	0.73	29.46	2.6425	0.11	25.25	4.21	2.2647	0.3779
AN2	5032	451.28	1250	0.85	42.73	3.8321	0.21	32.39	10.34	2.9047	0.9274
YL[a]	1130	8.80	3690	1.03	11.58	0.0902	0.09	10.58	1.01	0.0078	0.0824

[a] Estimation is based on the daily hydrological record (SPM flux and water discharge) from the Tongzilin gauging station.

4.4 Enhanced POC deposition in artificial reservoirs

Globally, artificial reservoirs store a significant amount of OC (Mendonça et al., 2012; 2017, Dean et al., 1998; Tranvik et al., 2009), impacting the global carbon cycle. The ongoing development of mega reservoirs in the CJ river system is modifying the export of OC and therefore the exchange fluxes of C between the continent, ocean, and atmosphere in three different ways: 1) high sedimentation rates in reservoirs greatly reduces the oxygen exposure time of POC, providing a favorable burial environment for efficient POC burial (Blair and Aller, 2012; Galy et al., 2007; Mendonça et al., 2012); 2) intensification of erosion processes of banks or riverbed (Yang et al., 2005; Li et al., 2019) downstream of dams may increase the global annual export fluxes of OC at basin scale by supplying external terrestrial OC; 3) shorter pathway of POC from source to sink due to sediment interception by reservoirs would substantially prevent POC from metabolism and oxidation during longer pathway and thus increase POC preservation.

4.4.1 POC load in the TGD and the CMRs

The annual sediment accumulation load in the TGD was about 144 Mt/yr before CMRs development upstream and decreased to 46.5 Mt/yr since the CMRs in the JSJ are in operation (Changjiang sediment bulletin, 2013; 2017). The upper reaches provide SPM with an average POC content of ~1.1% of which 31% is POC_{petro} (upper band value at Fujiang, which is just upstream of the reservoir) (Wu et al., 2018). It can thus be estimated that the bulk POC load trapped in the TGD is ~1.6 MtC/yr with 0.5 MtC/yr

for POC_{petro} and 1.0 MtC/yr for POC_{bio}. The post-CMRs suspended sediment flux at NX represents 64% of that at CT. Assuming that the POC content at NX (annual average of 1.38%) can be used to roughly estimate POC exported to the TGD since CMRs are operational. We obtained a theoretical POC flux of ~0.45 MtC/yr (0.15 MtC/yr for POC_{petro} and 0.30 MtC/yr for POC_{bio}) trapped in the TGD since the operation of CMRs. Therefore, POC from upper CJ has been redistributed to dams in the upper regions of the TGD at a rate of at least 1.15 MtC/yr, especially in the cascade reservoirs along the JSJ. As for JSJ, the depth-profile integrated POC content (POC_{int}) is 0.5% near XJB in 2009 (Wu et al., 2018), the POC flux of JSJ is roughly estimated as ~0.69 MtC/yr, taking the highest possible POC_{petro} of 0.22%, then we can have a POC_{petro} flux of 0.30 MtC/yr and a conservative POC_{bio} flux of 0.39 Mt/yr. An average POC content of 3.0% in the lower reaches during the post-CMRs period is reported (Wu et al., 2020), leading to an estimated POC flux of ~0.08 MtC/yr, indicating CMRs in the lower JSJ trapped ~0.61 MtC/yr, which is responsible for ~54% of the decrease in the TGD since 2013. POC flux of JSJ represents about ~22% of the annual POC flux at NX (~0.36 MtC/yr) at present.

4.4.2 High sedimentation rate in reservoirs

Terrestrial POC is very efficiently preserved in reservoirs worldwide (Mendonça et al., 2012; 2016; Teodoru et al., 2013) because hydrodynamics is greatly reduced in the reservoir regions, resulting in enhanced sedimentation rates and remarkable stratification. The rapid sedimentation process is accompanied by limited transport of oxygen downward, suggesting restricted oxidation of POC buried in reservoirs (Blair and Aller, 2012; Mendonça et al., 2012; Leithold et al., 2016). This inhibition of POC oxidation will provide two efficient negative feedbacks on atmospheric CO_2 content. First, the rapid burial of POC_{bio} will provide an efficient carbon sink, transferring atmospheric CO_2 to the sedimentary reservoir. Secondly, high sedimentation rates behind dams will prevent POC_{petro} from being oxidized and thus from becoming a net source of CO_2 to the atmosphere. Reservoirs in CJ reached a sediment accumulation rate of over 850 Mt/yr in 2003 (Yang et al., 2005) with a total reservoir area of ~6,020 km^2 (extracted from Lehner et al., 2011, considering the maximum reservoir area). The sedimentation rate in 2003 can thus be estimated at ~1.4×10^3 t/km^2/yr. Before CMRs development, the TGD reservoir had an average sedimentation rate equivalent to all reservoirs in CJ in 2003 with a value of ~1.4×10^3 t/km^2/yr (Changjiang Sediment

Bulletin 2013). This value is nearly 8 times higher than the sediment accumulation rate on the East China Sea shelf (~0.19 × 10^3 t/km^2/yr) (Deng et al., 2006) and similar to the lower band in the Bengal Fan (~1.5 × 10^3 t/km^2/yr) (Suckow et al., 2001), where transferred terrestrial POC is almost completely preserved (Galy et al., 2007, Blair and Aller, 2012).

4.4.3 A changing sediment erosion-deposition mode after dams

Dam operation greatly reduces turbidity downstream, acting as a dilution process for SPM concentration in rivers. As a consequence, it is observed the enhanced erosion of riverbanks downstream, especially in the mid reaches of CJ (Dai et al., 2018; Li et al., 2019), and flushing of riverbed sediments (Dai et al., 2005; Yang et al., 2005; Gao et al., 2018). On the one hand, the acceleration of riverbank erosion generates a strengthened OC source to the fluvial system through mobilization of a substantial amount of previously deposited POC which could be eventually buried in the estuary. On the other hand, this process also implies that SPM (and OC) are not deposited anymore on the river banks, a process that could have helped OC from being oxidized along the flow path (Bouchez et al., 2010; Blair and Aller, 2012; Galy et al., 2008a). It is reported that the middle reaches have been acting as a net sediment source since the operation of the TGD (Dai et al., 2005; Yang et al., 2005; 2018; Yang et al., 2019). Whether this mobilization of previously deposited POC acts as a source or a sink of carbon remains unclear and will mainly depend on the difference in burial efficiency of POC between riverbed and estuary/margin. It was estimated that the riverine POC burial efficiency on the East China Sea margin was ~20%-30% (Blair and Aller, 2012; Wu et al., 2013) but the drastic decrease in sediment supply from the CJ since large dams operation may have reduced this estimate as sedimentation rates have drastically decreased as well. An observed average OC burial efficiency of ~48% was reported in lakes (Sobek et al., 2009), but the re-mineralized fraction is probably higher in shallow sediments of the riverbed (Tranvik et al., 2009). However, a comparison of those numbers suggests that the mobilization of previously deposited material would act as a net source of CO_2 to the atmosphere. Indeed, it will both favor POC_{petro} oxidation (increase in CO_2 source) and reduce POC_{bio} burial efficiency (decrease in CO_2 sink).

The consequences on the carbon cycle of enhanced bank erosion and bed scouring are reversed when considering another reservoir downstream as the final deposition site. In fact, the transfer of POC from riverbed or banks into high-preservation efficiency

reservoirs would prevent POC_{petro} from oxidation and favor POC_{bio} burial, both acting in the way. This erosion process is at play in the channel regions after XJB, downstream of CMRs, and upstream of TGD (Changjiang Sediment Bulletin, 2013-2017). Note that this enhanced CO_2 sink probably takes place in most of the CJ catchment given the huge number of dams in the basin (~50,000).

4.4.4 Perspective from intensified physical erosion, shorter flow path, and higher burial efficiency

Large rivers (LRs) deliver SPM that travel a longer pathway and go through multiple erosion-deposition cycles than small mountainous rivers (SMRs). The abundant reservoirs in the upper reaches of the CJ have cut the main channel and tributaries into multiple short and fast-speed river sections. Each isolated section operates as an active continental margin with rapid transfer of SPM and OC to high sedimentation rates and efficient burial sites (Hilton et al, 2011; Bouchez et al., 2010; Blair and Aller, 2012). Meanwhile, the high-energy bonded refractory POC found in the upper CJ provides an intrinsic advantage for the efficient preservation in reservoirs. In addition, even though the monitored SPM concentration decreases along the flow path of the CJ, sediment load increases downstream due to intensified soil erosion (Yang et al., 2005; Wang et al., 2007). This was ignored in the previous estimation of POC trapping by reservoirs (Li et al., 2015). Globally, McLennan (1993) and Syvitski et al. (2005) estimate a pre-human sediment load of 12-13 × 10^3 Mt/yr and an over 60% rise to 19-20 × 10^3 Mt/yr before worldwide massive dam construction during the past few decades. This global intensification of terrestrial erosion is linked to anthropogenic activities such as deforestation, urbanization, agriculture, mining, etc. (Milliman and Farnsworth, 2011) but was partly hidden by the building of dams that have stored large proportions of this excess sediment input (Walling, 2008; Milliman and Farnsworth, 2011).

From 1951 to the present, the total soil erosion in the CJ basin has increased from ~1,449 Mt/yr to ~2,400 Mt/yr and the riverine sediment flux from ~599 Mt/yr to ~995 Mt/yr. Over the same period, the sediment flux delivered to the estuary has decreased from ~500 Mt/yr to ~122 Mt/yr. The estimated sediment deposition in reservoirs has increased from ~440 Mt/yr in the 1980s to ~850 Mt/yr after TGD operation (Yang et al., 2005). The present-day sediment sequestration flux in reservoirs is nearly six times larger than the present-day flux of sediment delivered at the river mouth and twice the one delivered at the river mouth during the pre-dam period (494 Mt/yr). The present-

day sedimentation flux in reservoirs even exceeds the estimated sediment flux (~800 Mt/yr) that would be delivered to the estuary in a dam-free configuration (Yang et al., 2005). The increased physical erosion rate enhanced the export of POC and its burial (Galy et al., 2015; Hilton, 2017), we estimate the present-day dam-free POC flux of 800 MtC/yr based on the sediment load under an intensified physical erosion, the average POC content is ~1.0% based on the variation of POC versus SPM in global rivers calculated by Meybeck (1982). As the upper reaches provide the majority of SPM in the CJ system, we can use the upper band estimate of POC_{petro} content at NX (~0.39%, which is close to the reported 0.46% by Li et al., 2015) to calculate a rather high POC_{petro} flux of 3.2 MtC/yr but a conservative POC_{bio} flux of 4.8 MtC/yr that is exported to the estuary. Subtracting the POC flux found at DT in this study (average 1.4 MtC/yr), then the bulk POC flux entering reservoirs would be ~6.6 MtC/yr consisting of 3.1 MtC/yr of POC_{petro} and 3.5 MtC/yr of POC_{bio}. These values are comparable to the estimation by Li et al (2015) using a high averaged POC content (>2%) based on historic construction of sediment and POC flux. However, our estimate of the POC_{petro} export to reservoirs is based on a relatively low POC content. Using the POC_{petro} content of 0.11% found at DT, our calculations return a POC_{petro} flux of ~0.9 MtC/yr and a relatively high POC_{bio} flux of ~7.1 MtC/yr, while the POC_{petro} and POC_{bio} flux entering reservoirs are estimated to be 0.8 MtC/yr and 5.8 MtC/yr, respectively. The above estimations are in the circumstance of not considering the possible temporary transport of channel bed sediments that would be delivered to reservoirs. The TGD emitted a CH_4 flux of 3.1×10^{-3} MtC/yr (Yang et al, 2013) and a CO_2 flux of 0.09 MtC/yr (Li et al., 2017), the former is about three orders of magnitude while the latter is two orders of magnitude smaller than the 1.58 MtC/yr POC burial flux during the post-TGD period and about 2 orders of magnitudes smaller than the 0.45 MtC/yr POC burial flux during the post-CMRs period, indicating that the TGD is still a very efficient carbon sink even it has been weakened due to upstream dams. The sediment accumulation in reservoirs is mostly located in high-elevation, low-temperature upper reaches, which provide an unfavorable environment for POC degradation (Burdige, 2011), we thus anticipate a relatively restricted POC oxidation rate and CO_2 release compared to the massive carbon sink associated with POC burial. The above calculations suggest that dam-building has been efficiently sequestrating more terrestrial POC than in natural flow conditions, making the CJ river basin under anthropogenic pressure a more efficient carbon sink than in pre-human conditions. The

larger uncertainties on this last conclusion rely on the effective timescale over which dams can sustain such large POC trapping flux.

4.5 The changing pattern of physical erosion rate over POC export

In the CJ River basin, the SPM particle size greatly impacts the POC content, as reported for some other large river systems (*e.g.* Amazon, Ganges-Brahmaputra, Mackenzie, Huanghe, etc.) (Bouchez et al., 2014; Galy et al., 2008b; Hilton et al., 2015; Ke et al., submitted). Following the accompanying POC alteration pattern in CJ, we assume a changing presence of the correlation between physical erosion within the catchment (revealed by sediment yield) and POC yield observed in the river mouth that is reported by Galy et al. (2015). After the massive dam-building worldwide, rivers record a reduced suspended sediment yield (Milliman and Farnsworth, 2011), the assumption proposed under such conditions is that POC yield decreases, meanwhile, accompanied by an increased POC content with increased POC_{bio} fractions but decreased POC_{petro} components (Figure 19). The physical erosion rate exerts a first-order control on both POC_{bio} and POC_{petro} yields (Galy et al., 2015; Hilton et al., 2017). Yield data of the CJ is moving toward the bottom of the global compilation at a dramatic speed (Figure 19A), from a pre-TGD average sediment yield of 249 t/km^2/yr to 61 t/km^2/yr in 2017. Corresponding POC yield decreased from 2.45 tC/km^2/yr to 0.70 tC/km^2/yr. JSJ at XJB in 2009 recorded a ~44% sediment reduction (139 Mt/yr) compared to the amount under natural flow without dams (251 Mt/yr), the POC yield of the JSJ drainage basin is 1.51 tC/km^2/yr consisting of 0.51 tC/km^2/yr for POC_{petro} and 1.00 tC/km^2/yr for POC_{bio} (Figure 19B-C, Table. 4). The historic sediment yield at XJB before dam-building was ~550 t/km^2/yr, which is comparable to Ganges and Salween (Galy et al., 2015), indicating the strong erosion of terrestrial OC in JSJ. At a global scale, it is estimated that catchments with steep topography (>10^o) may account for ~70% of the global CO_2 drawdown by sedimentary burial of terrestrial POC_{bio} (Hilton, 2017; Larsen et al., 2014). Mountainous catchments of CJ such as Jinshajiang (sediment yield in the pre-dam period, 550 t/km^2/yr), Minjiang (430 t/km^2/yr), and Jialingjiang (1,090 t/km^2/yr) all have very steep topography and high physical erosion rates, which favor the intense erosion of POC_{bio} and POC_{petro} (Figure 18; Hilton, 2017; Galy et al., 2015). Fast burial of this material in reservoirs should prevent POC from being oxidized, reducing CO_2 release from POC_{petro} oxidation and increasing CO_2 sink by efficient burial of POC_{bio}. Both processes concur to limit the impact of OC erosion

on atmospheric CO_2 over decades to millennials. However, the reduced sediment export from global rivers to estuaries could potentially cause more intense erosion of the coastal margins and less efficient burial of POC in response to lower sedimentation rates (Blair and Aller, 2012; Burdige, 2005; 2011). Both processes will favor remineralization of either previously-stored POC_{petro} and POC_{bio} or incoming POC_{petro}, making the estuary a less efficient CO_2 sink or even a CO_2 source.

Due to active tectonic settings, rivers in pan-QTP regions bring a tremendous amount of continental denudated materials into the Ocean. It is reported that this area delivers a sediment flux of ~5,100 Mt/yr, accounting for ~27% of the total sediment flux in global rivers (Milliman and Farnsworth, 2011). Ganges-Brahmaputra, Salween, Irrawaddy, Mekong, Changjiang, and Huanghe originate from the QTP, and are global significant large fluvial systems that together transport an annual sediment flux of ~2,295 Mt/yr carrying ~18MtC/yr POC into the ocean (Milliman and Farnsworth, 2011; Galy et al., 2015). The POC flux includes ~3.5 MtC/yr of POC_{petro} and ~13.5 Mt/yr of POC_{bio} (Galy et al., 2015), representing ~10% of the global POC export to the estuary. The QTP region is thus a hotspot and represents an important component of the global carbon cycle. Among the seven listed large pan-QTP rivers, the Salween is the only fluvial system without artificial reservoirs, while Changjiang and Huanghe are the most regulated river systems interrupted by numerous dams (Grill et al., 2019). It would be interesting to investigate to what extent artificial reservoirs could affect the whole source-to-sink processes of carbon metabolism and burial.

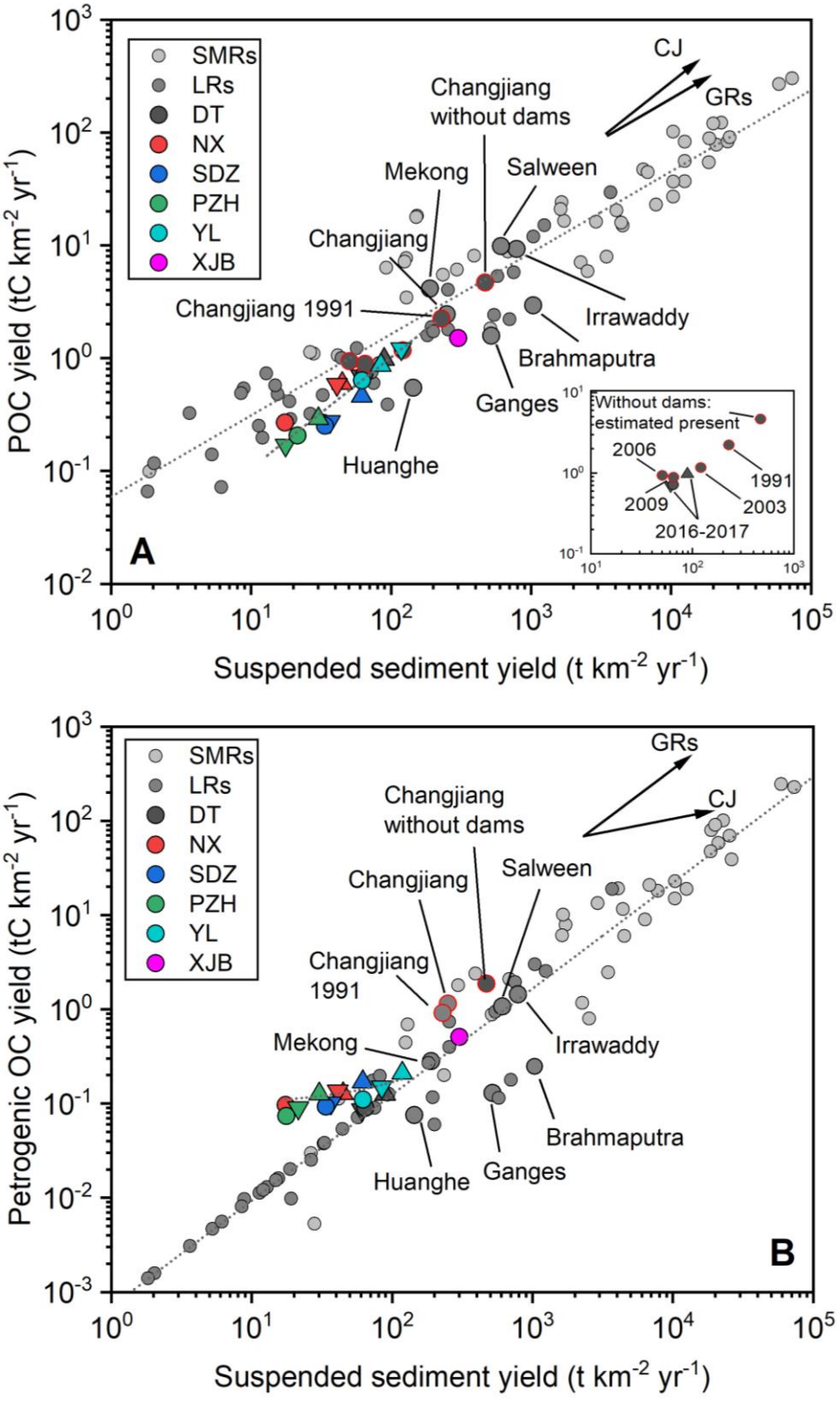
SMRs
LRs
DT
NX
SDZ
PZH
YL
XJB
CJ
GRs
Changjiang without dams
Mekong
Salween
Changjiang
Changjiang 1991
Irrawaddy
Brahmaputra
Ganges
Huanghe
Without dams: estimated present
2006
1991
2009
2003
2016-2017
A
POC yield (tC km-2 yr-1)
Suspended sediment yield (t km-2 yr-1)
SMRs
LRs
DT
NX
SDZ
PZH
YL
XJB
GRs
CJ
Changjiang without dams
Salween
Changjiang
Changjiang 1991
Mekong
Irrawaddy
Brahmaputra
Huanghe
Ganges
B
Petrogenic OC yield (tC km-2 yr-1)
Suspended sediment yield (t km-2 yr-1)

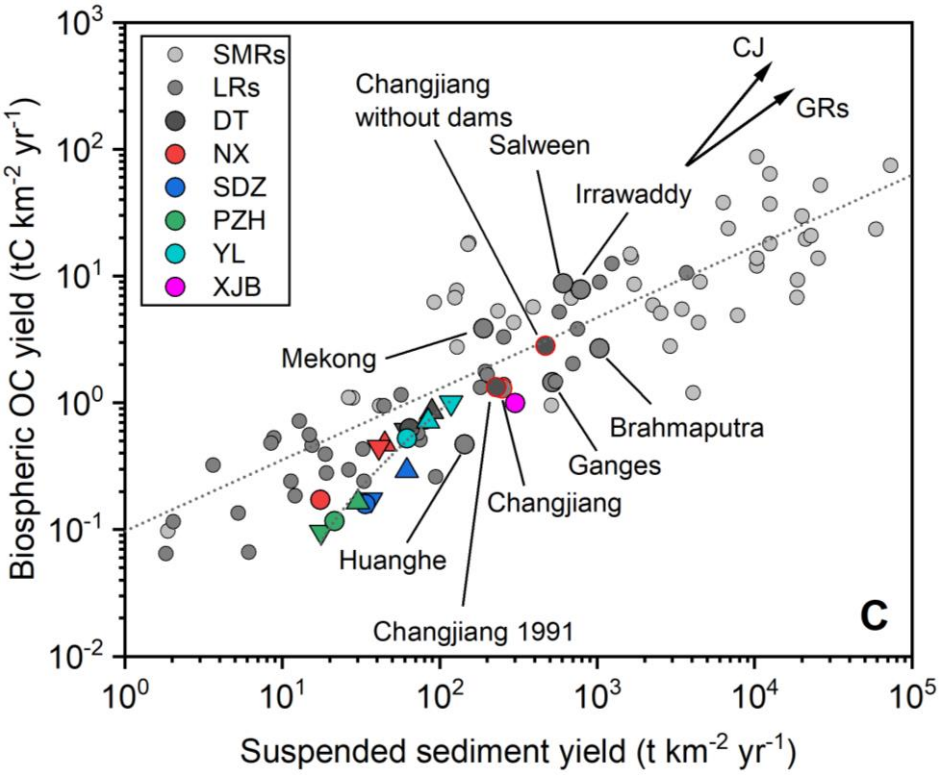

Fig. 19 Annual POC yield as a function of suspended sediment yield in the Changjiang River basin. (A) annual POC yield, (B) annual POC_{petro} yield, (C) annual POC_{bio} yield. Equilateral triangles are fluxes for 2016, inverted triangles are fluxes for 2017, and circles are fluxes for the time series sampling period. POC fluxes for global small mountainous rivers (SMRs) and large rivers (LRs) are compiled (Galy et al. 2015; Hilton, 2017) for comparison, only the largest suspended sediment yield and the corresponding POC yield were kept for rivers with the replicated data. The pan-Tibet large rivers: Ganges, Brahmaputra, Irrawaddy, Salween, Mekong, and Huanghe are marked with red outlines and tagged for comparison. 'Changjiang 1991' represents POC and suspended sediment yields in 1991 under minor dam impact, 'Changjiang without dams' is an estimation of hypothesized the current state of CJ if there are no dams but with enhanced soil erosion within the basin. Changjiang POC and sediment yield in the global compilation by Galy et al., (2015) is estimated using the long-term average before the TGD. Arrows represent the fitting of suspended sediment yield and POC yield between global rivers (GRs) and rivers in this study (CJ).

Table. 4 Summary of annual fluxes and yields of suspended sediment and POC in the Changjiang River

Year	SPM Load Mt yr^{-1}	SPM yield t yr^{-1} km^{-2}	POC Flux Mt yr^{-1}	POC yield tC yr^{-1} km^{-2}	Reference
1991	459	228.7	4.5	2.24	1
2003	206	120.8	2.0	1.17	2, 3, 4
2006	86	50.4	1.6	0.94	2, 3, 4
2009	111	65.1	1.52	0.89	5
2016	152	89.1	1.66	0.98	this study, 6
2017	104	61.0	1.19	0.70	this study, 7
Present (no dam)	800	469.1	8.0	4.69	This study

Data is either directly cited or further calculated from the following references: 1 [Cauwet and Mackenzie, 1993]; 2 [Chen et al., 2008]; 3 [Yu et al., 2011]; 4 [Li et al., 2015]; 5 [Wang et al., 2012]; 6 [Changjiang Sediment Bulletin, 2016]; 7 [Changjiang Sediment Bulletin, 2017]. "Present (no dam)" refers to the estimation of present sediment and POC yields of Changjiang without any dam-building

5. Conclusions

In this study, we examine the POC content and isotopic composition of Changjiang River sediments collected along transect depth profiles and monthly time series, with a special focus on the POC from the upper Changjiang. Using historic hydrological data, including sediment load and water discharge, we discuss the regulation of artificial reservoirs on trapping efficiency, sources, transport mode, and fluxes of POC. For the first time, the impact of cascade mega reservoirs in the lower Jinshajiang river on fluvial POC transport in Changjiang is evaluated.

The Changjiang transports POC of multi-millennial age from source to sink, showing a significantly older POC in the upper reaches (mountainous regions) than in the mid-lower reaches (plain regions). Seasonal variations of the riverine POC, show a higher POC content and ^{13}C composition, and lower ^{14}C activity during the wet season. Jinshajiang POC has a radiocarbon age of 5,010 ± 384 yrs before its confluence with the Yalong river and 4,180 ± 506 yrs after the confluence, while Changjiang POC has a radiocarbon age in the upper reaches ranging from 3,250 ± 438 yrs (depth profiles) to 4,747 ± 1,237 yrs (time-series) after the confluence with the Minjiang, and of 2,676 ± 497 yrs at the tidal limit in the lower reaches. The particle size of SPM greatly impacts the elemental and isotopic carbon signatures, with significant coarse particles deposited in artificial reservoirs, resulting in delivery of relatively fine SPM with less POC_{petro} and higher POC_{bio} of younger ^{14}C age. Strong physical erosion in mountainous regions is an important mechanism that supplies rock-derived POC_{petro} into the fluvial system

but also a massive amount of modern OC during storm events. In the Changjiang mainstem, POC_{bio} is the dominant POC fraction with varying ^{14}C age ranging from 1,300 – 3,600 yrs (Fm_{bio} 0.64 - 0.85). Meanwhile, a significant fraction of POC from soil organic carbon is confirmed. It is worth noting that permafrost thawing on the Qinghai-Tibet Plateau releases POC to the fluvial system, while recently-biosynthesized SOC contributes in the mid-lower reaches and imprint the after dam transport of riverine POC. Further studies are needed to investigate the molecular composition of riverine POC in the upper Jinshajiang to understand how the riverine POC responds to high relief permafrost thawing and its influence on the carbon cycle under the current global warming situation. In addition, we demonstrate the significance of small catchment and storm events in the terrestrial OC mobilization.

We estimate that reservoirs in the Changjiang basin receive a POC flux of approximately 6.6 MtC/yr, consisting of 0.8-3.1 MtC/yr of POC_{petro} and from 3.5 -5.8 MtC/yr of POC_{bio}. In contrast, the POC flux entering the East China Sea in 2017 was only 1.2 MtC. A significant fraction of POC that was annually buried in the Three Gorges Dam is now deposited in reservoirs upstream, especially in the cascade mega reservoirs in the lower Jinshajiang. After the operation of cascade reservoirs, POC trapped in the Three Gorges Dam decreased from ~1.58 MtC/yr to ~0.45 MtC/yr, while the two most downstream CMRs in the JSJ annually trap about 0.61 MtC/yr. Cascade reservoirs all along the JSJ have replaced the Three Gorges Dam as the largest temporal POC sink. However, even though the operation of cascade reservoirs almost completely prevents POC from Jinshajiang from traveling downstream in the Changjiang, the POC export flux to the estuary has been only slightly impacted. Although the succession of CMRs and TGD have increased particle trapping, the erosion of pre-deposited sediments in the mid-CJ channel and the net input from the two lake systems have sustained the flux of POC to the estuary. How the upper forward shift of POC burial in reservoirs affects the POC alteration and metabolism needs to be further assessed but we anticipate that this process has led to more efficient preservation of POC in a high sedimentation rate environment.

In fact, dam-building in the upper reaches of CJ has created a rapid burial environment for POC. As a consequence, mineralization rates of POC should have decreased between a free-dam configuration where POC travels long distance in oxygenated waters before entering the estuary with a relatively low (20-30%) POC

preservation rate, and a post-dam building configuration where particles travel a short distance from source to efficient preservation sink environment. This process would have made the Changjiang River a more efficient negative feedback on atmospheric CO_2 content over decades to millennials. Concerning large rivers in the pan-QTP regions, dam-building is expected to efficiently counteract the delivery of massive terrestrial eroded organic matter into the Ocean mitigating the CO_2 release by POC_{petro} mineralization. However, the burial efficiency of terrestrial POC in artificial reservoirs and estuary should be further investigated to better quantify the overall organic carbon cycle of a highly regulated large river system.

Acknowledgments

This projected was study was financially supported by the Agence Nationale de la Recherche (ANR) SEDIMAN (Grant ANR-15-CE01-0012), the National Natural Science Foundation of China (NSFC), grants 41561134017, 41625012, and the China Scholarship Council (CSC) to Yutian Ke (No.201706180008).

Reference

Battin, T. J., Luyssaert, S., Kaplan, L. A., Aufdenkampe, A. K., Richter, A., and Tranvik, L. J. (2009). The boundless carbon cycle. Nature Geoscience, 2(9), 598-600.

Berner, R. A. (1982). Burial of organic carbon and pyrite sulfur in the modern ocean: its geochemical and environmental significance. American Journal of Science, 282.

Berner, R. A. (2004). The Phanerozoic carbon cycle: CO_2 and O_2. Oxford University Press on Demand.

Blair, N. E., and Aller, R. C. (2012). The fate of terrestrial organic carbon in the marine environment. Annual Review of Marine Science, 4, 401-423.

Bouchez, J., Beyssac, O., Galy, V., Gaillardet, J., France-Lanord, C., Maurice, L., and Moreira-Turcq, P. (2010). Oxidation of petrogenic organic carbon in the Amazon floodplain as a source of atmospheric CO_2. Geology, 38(3), 255-258.

Bouchez, J., Gaillardet, J., France-Lanord, C., Maurice, L., and Dutra-Maia, P. (2011a). Grain size control of river suspended sediment geochemistry: Clues from Amazon River depth profiles. Geochemistry, Geophysics, Geosystems, 12(3).

Bouchez, J., Lupker, M., Gaillardet, J., France-Lanord, C., and Maurice, L. (2011b).

How important is it to integrate riverine suspended sediment chemical composition with depth? Clues from Amazon River depth-profiles. Geochimica et Cosmochimica Acta, 75(22), 6955-6970.

Brown, J., Ferrians Jr, O. J., Heginbottom, J. A., and Melnikov, E. S. (1997). Circum-Arctic map of permafrost and ground-ice conditions (p. 45). Reston, VA: US Geological Survey.

Burdige, D. J. (2005). Burial of terrestrial organic matter in marine sediments: A re-assessment. Global Biogeochemical Cycles, 19(4).

Burdige, D. J. (2011). Temperature dependence of organic matter remineralization in deeply-buried marine sediments. Earth and Planetary Science Letters, 311(3-4), 396-410.

Cauwet, G., and Mackenzie, F. T. (1993). Carbon inputs and distribution in estuaries of turbid rivers: the Yang Tze and Yellow rivers (China). Marine Chemistry, 43(1-4), 235-246.

Changjiang Sediment Bulletin (2013), Press of Changjiang Water Conservation, the Ministry of Water Resources of the People's Republic of China, Beijing. [Available at http:// www.cjh.com.cn/.]

Changjiang Sediment Bulletin (2014), Press of Changjiang Water Conservation, the Ministry of Water Resources of the People's Republic of China, Beijing. [Available at http:// www.cjh.com.cn/.]

Changjiang Sediment Bulletin (2015), Press of Changjiang Water Conservation, the Ministry of Water Resources of the People's Republic of China, Beijing. [Available at http:// www.cjh.com.cn/.]

Changjiang Sediment Bulletin (2016), Press of Changjiang Water Conservation, the Ministry of Water Resources of the People's Republic of China, Beijing. [Available at http:// www.cjh.com.cn/.]

Changjiang Sediment Bulletin (2017), Press of Changjiang Water Conservation, the Ministry of Water Resources of the People's Republic of China, Beijing. [Available at http:// www.cjh.com.cn/.]

Dai, S. B., and Lu, X. X. (2014). Sediment load change in the Yangtze River (Changjiang): a review. Geomorphology, 215, 60-73.

Dai, S. B., Yang, S. L., Zhu, J., Gao, A., and Li, P. (2005). The role of Lake Dongting in regulating the sediment budget of the Yangtze River. Hydrology and Earth System Sciences, 9(6), 692-698.

Dai, Z., Mei, X., Darby, S. E., Lou, Y., and Li, W. (2018). Fluvial sediment transfer in the Changjiang (Yangtze) river-estuary depositional system. Journal of Hydrology, 566, 719-734.

Dean, W. E., and Gorham, E. (1998). Magnitude and significance of carbon burial in lakes, reservoirs, and peatlands. Geology, 26(6), 535-538.

Deng, B., Zhang, J., and Wu, Y. (2006). Recent sediment accumulation and carbon burial in the East China Sea. Global Biogeochemical Cycles, 20(3).

Duan, S. W. (2000), The distribution and transportation of nutrients and carbon in the Yangtze River, Ph.D. thesis, Institute of Geography of Academic Science, Beijing, P.R. China.

Duan, S., Liang, T., Zhang, S., Wang, L., Zhang, X., and Chen, X. (2008). Seasonal changes in nitrogen and phosphorus transport in the lower Changjiang River before the construction of the Three Gorges Dam. Estuarine, coastal and shelf science, 79(2), 239-250.

Eglinton, T. I., Galy, V. V., Hemingway, J. D., Feng, X., Bao, H., Blattmann, T. M., ... and Zhao, M. (2021). Climate control on terrestrial biospheric carbon turnover. Proceedings of the National Academy of Sciences, 118(8).

Fick, S. E., and Hijmans, R. J. (2017). WorldClim 2: new 1-km spatial resolution climate surfaces for global land areas. International Journal of Climatology, 37(12), 4302-4315.

France-Lanord, C., and Derry, L. A. (1997). Organic carbon burial forcing of the carbon cycle from Himalayan erosion. Nature, 390(6655), 65-67.

Galy, V., Beyssac, O., France-Lanord, C., and Eglinton, T. (2008a). Recycling of graphite during Himalayan erosion: a geological stabilization of carbon in the crust. Science, 322(5903), 943-945.

Galy, V., France-Lanord, C., and Lartiges, B. (2008b). Loading and fate of particulate organic carbon from the Himalaya to the Ganga–Brahmaputra delta. Geochimica et Cosmochimica Acta, 72(7), 1767-1787.

Galy, V., France-Lanord, C., Beyssac, O., Faure, P., Kudrass, H., and Palhol, F. (2007). Efficient organic carbon burial in the Bengal fan sustained by the Himalayan erosional system. Nature, 450(7168), 407-410.

Galy, V., Peucker-Ehrenbrink, B., and Eglinton, T. (2015). Global carbon export from the terrestrial biosphere controlled by erosion. Nature, 521(7551), 204-207.

Gao, J. H., Jia, J., Kettner, A. J., Xing, F., Wang, Y. P., Li, J., ... and Gao, S. (2018).

Reservoir-induced changes to fluvial fluxes and their downstream impacts on sedimentary processes: The Changjiang (Yangtze) River, China. Quaternary International, 493, 187-197.

Gao, J. H., Jia, J., Kettner, A. J., Xing, F., Wang, Y. P., Xu, X. N., ... and Liao, F. (2014). Changes in water and sediment exchange between the Changjiang River and Poyang Lake under natural and anthropogenic conditions, China. Science of the Total Environment, 481, 542-553.

Gao, T., Zhang, Y., Kang, S., Abbott, B. W., Wang, X., Zhang, T., ... and Gustafsson, O. (2021). Accelerating permafrost collapse on the Eastern Tibetan Plateau. Environmental Research Letters.

Grill, G., Lehner, B., Thieme, M., Geenen, B., Tickner, D., Antonelli, F., ... and Zarfl, C. (2019). Mapping the world's free-flowing rivers. Nature, 569(7755), 215-221.

Guo, C., Jin, Z., Guo, L., Lu, J., Ren, S., and Zhou, Y. (2020). On the cumulative dam impact in the upper Changjiang River: Streamflow and sediment load changes. Catena, 184, 104250.

Guo, L., Ping, C. L., and Macdonald, R. W. (2007). Mobilization pathways of organic carbon from permafrost to arctic rivers in a changing climate. Geophysical Research Letters, 34(13).

Hilton, R. G. (2017). Climate regulates the erosional carbon export from the terrestrial biosphere. Geomorphology, 277, 118-132.

Hilton, R. G., Gaillardet, J., Calmels, D., and Birck, J. L. (2014). Geological respiration of a mountain belt revealed by the trace element rhenium. Earth and Planetary Science Letters, 403, 27-36.

Hilton, R. G., Galy, A., Hovius, N., Chen, M. C., Horng, M. J., and Chen, H. (2008). Tropical-cyclone-driven erosion of the terrestrial biosphere from mountains. Nature Geoscience, 1(11), 759-762.

Hilton, R. G., Galy, A., Hovius, N., Horng, M. J., and Chen, H. (2011). Efficient transport of fossil organic carbon to the ocean by steep mountain rivers: An orogenic carbon sequestration mechanism. Geology, 39(1), 71-74.

Hilton, R. G., Galy, V., Gaillardet, J., Dellinger, M., Bryant, C., O'Regan, M., ... and Calmels, D. (2015). Erosion of organic carbon in the Arctic as a geological carbon dioxide sink. Nature, 524(7563), 84-87.

Jin, Z., West, A. J., Zhang, F., An, Z., Hilton, R. G., Yu, J., ... and Wang, X. (2016). Seismically enhanced solute fluxes in the Yangtze River headwaters following the

AD 2008 Wenchuan earthquake. Geology, 44(1), 47-50.

Keil, R. G., Mayer, L. M., Quay, P. D., Richey, J. E., and Hedges, J. I. (1997). Loss of organic matter from riverine particles in deltas. Geochimica et Cosmochimica acta, 61(7), 1507-1511.

Lai, X., Yin, D., Finlayson, B. L., Wei, T., Li, M., Yuan, W., ... and Chen, Z. (2017). Will river erosion below the Three Gorges Dam stop in the middle Yangtze?. Journal of Hydrology, 554, 24-31.

Larsen, I. J., Montgomery, D. R., and Greenberg, H. M. (2014). The contribution of mountains to global denudation. Geology, 42(6), 527-530.

Lehner, B., Liermann, C. R., Revenga, C., Vörösmarty, C., Fekete, B., Crouzet, P., ... and Wisser, D. (2011). High-resolution mapping of the world's reservoirs and dams for sustainable river-flow management. Frontiers in Ecology and the Environment, 9(9), 494-502.

Li, D., Lu, X. X., Chen, L., and Wasson, R. J. (2019). Downstream geomorphic impact of the Three Gorges Dam: With special reference to the channel bars in the Middle Yangtze River. Earth Surface Processes and Landforms, 44(13), 2660-2670.

Li, D., Lu, X. X., Yang, X., Chen, L., and Lin, L. (2018). Sediment load responses to climate variation and cascade reservoirs in the Yangtze River: A case study of the Jinsha River. Geomorphology, 322, 41-52.

Li, G. K., Fischer, W. W., Lamb, M. P., West, A. J., Zhang, T., Galy, V., ... and Ji, J. (2021). Coal fly ash is a major carbon flux in the Chang Jiang (Yangtze River) basin. Proceedings of the National Academy of Sciences, 118(21).

Li, G., Wang, X. T., Yang, Z., Mao, C., West, A. J., and Ji, J. (2015). Dam-triggered organic carbon sequestration makes the Changjiang (Yangtze) river basin (China) a significant carbon sink. Journal of Geophysical Research: Biogeosciences, 120(1), 39-53.

Li, S., Wang, F., Luo, W., Wang, Y., and Deng, B. (2017). Carbon dioxide emissions from the Three Gorges Reservoir, China. Acta Geochimica, 36(4), 645-657.

Lupker, M., France-Lanord, C., Lavé, J., Bouchez, J., Galy, V., Métivier, F., ... and Mugnier, J. L.(2011). A Rouse-based method to integrate the chemical composition of river sediments: Application to the Ganga basin. Journal of Geophysical Research: Earth Surface, 116(F4).

Maavara, T., Lauerwald, R., Regnier, P., and Van Cappellen, P. (2017). Global perturbation of organic carbon cycling by river damming. Nature communications,

8(1), 1-10.

McLennan, S. M. (1993). Weathering and global denudation. The Journal of Geology, 101(2), 295-303.

Mendonca, R., Kosten, S., Sobek, S., Barros, N., Cole, J. J., Tranvik, L., and Roland, F. (2012). Hydroelectric carbon sequestration. Nature Geoscience, 5(12), 838-840.

Mendonça, R., Kosten, S., Sobek, S., Cardoso, S. J., Figueiredo-Barros, M. P., Estrada, C. H. D., and Roland, F. (2016). Organic carbon burial efficiency in a subtropical hydroelectric reservoir. Biogeosciences, 13(11), 3331-3342.

Mendonça, R., Müller, R. A., Clow, D., Verpoorter, C., Raymond, P., Tranvik, L. J., and Sobek, S. (2017). Organic carbon burial in global lakes and reservoirs. Nature Communications, 8(1), 1-7.

Meybeck, M. (1982). Carbon, nitrogen, and phosphorus transport by world rivers. American Journal of Science, 282(4), 401-450.

Milliman, J. D., & Farnsworth, K. L. (2011). River discharge to the coastal ocean: a global synthesis. Cambridge University Press.

Parnell, A. C., Inger, R., Bearhop, S., and Jackson, A. L. (2010). Source partitioning using stable isotopes: coping with too much variation. PloS One, 5(3), e9672.

Petsch, S. T., Berner, R. A., and Eglinton, T. I. (2000). A field study of the chemical weathering of ancient sedimentary organic matter. Organic Geochemistry, 31(5), 475-487.

Qu, Y., Jin, Z., Wang, J., Wang, Y., Xiao, J., Gou, L. F., ... and Xu, X. (2020). The sources and seasonal fluxes of particulate organic carbon in the Yellow River. Earth Surface Processes and Landforms, 45(9), 2004-2019.

Rao, Z., Guo, W., Cao, J., Shi, F., Jiang, H., and Li, C. (2017). Relationship between the stable carbon isotopic composition of modern plants and surface soils and climate: A global review. Earth-Science Reviews, 165, 110-119.

Schlünz, B., and Schneider, R. R. (2000). Transport of terrestrial organic carbon to the oceans by rivers: re-estimating flux-and burial rates. International Journal of Earth Sciences, 88(4), 599-606.

Shi, Z., Allison, S. D., He, Y., Levine, P. A., Hoyt, A. M., Beem-Miller, J., ... and Randerson, J. T. (2020). The age distribution of global soil carbon inferred from radiocarbon measurements. Nature Geoscience, 13(8), 555-559.

Sobek, S., Durisch-Kaiser, E., Zurbrügg, R., Wongfun, N., Wessels, M., Pasche, N., and Wehrli, B. (2009). Organic carbon burial efficiency in lake sediments controlled

by oxygen exposure time and sediment source. Limnology and Oceanography, 54(6), 2243-2254.

Stock, B. C., Jackson, A. L., Ward, E. J., Parnell, A. C., Phillips, D. L., and Semmens, B. X. (2018). Analyzing mixing systems using a new generation of Bayesian tracer mixing models. PeerJ, 6, e5096.

Suckow, A., Morgenstern, U., and Kudrass, H. R. (2001). Absolute dating of recent sediments in the cyclone-influenced shelf area off Bangladesh: Comparison of gamma spectrometric (137 Cs, 210 Pb, 228 Ra), radiocarbon, and 32 Si ages. Radiocarbon, 43(2B), 917-927.

Syvitski, J. P., Vörösmarty, C. J., Kettner, A. J., and Green, P. (2005). Impact of humans on the flux of terrestrial sediment to the global coastal ocean. Science, 308(5720), 376-380.

Tao, S., Eglinton, T. I., Montluçon, D. B., McIntyre, C., and Zhao, M. (2016). Diverse origins and pre-depositional histories of organic matter in contemporary Chinese marginal sea sediments. Geochimica et Cosmochimica Acta, 191, 70-88.

Teodoru, C. R., Del Giorgio, P. A., Prairie, Y. T., and St-Pierre, A. (2013). Depositional fluxes and sources of particulate carbon and nitrogen in natural lakes and a young boreal reservoir in Northern Québec. Biogeochemistry, 113(1), 323-339.

Tranvik, L. J., Downing, J. A., Cotner, J. B., Loiselle, S. A., Striegl, R. G., Ballatore, T. J., ... and Weyhenmeyer, G. A. (2009). Lakes and reservoirs as regulators of carbon cycling and climate. Limnology and Oceanography, 54(6part2), 2298-2314.

Vonk, J. E., Sánchez-García, L., Van Dongen, B. E., Alling, V., Kosmach, D., Charkin, A., ... and Gustafsson, Ö. (2012). Activation of old carbon by erosion of coastal and subsea permafrost in Arctic Siberia. Nature, 489(7414), 137-140.

Vonk, J. E., Tank, S. E., Bowden, W. B., Laurion, I., Vincent, W. F., Alekseychik, P., ... and Wickland, K. P. (2015). Reviews and syntheses: Effects of permafrost thaw on Arctic aquatic ecosystems. Biogeosciences, 12(23), 7129-7167.

Walling, D. E. (2008). The changing sediment loads of the world's rivers. Annals of Warsaw University of Life Sciences-SGGW. Land Reclamation, 39.

Wang, T., Yang, D., Yang, Y., Piao, S., Li, X., Cheng, G., and Fu, B. (2020). Permafrost thawing puts the frozen carbon at risk over the Tibetan Plateau. Science Advances, 6(19), eaaz3513.

Wang, Z. Y., Li, Y., and He, Y. (2007). Sediment budget of the Yangtze River. Water Resources Research, 43(4).

West, A. J., Lin, C. W., Lin, T. C., Hilton, R. G., Liu, S. H., Chang, C. T., ... and Hovius, N. (2011). Mobilization and transport of coarse woody debris to the oceans triggered by an extreme tropical storm. Limnology and Oceanography, 56(1), 77-85.

Wild, B., Andersson, A., Bröder, L., Vonk, J., Hugelius, G., McClelland, J. W., ... and Gustafsson, Ö. (2019). Rivers across the Siberian Arctic unearth the patterns of carbon release from thawing permafrost. Proceedings of the National Academy of Sciences, 116(21), 10280-10285.

Wu, Y., Eglinton, T. I., Zhang, J., and Montlucon, D. B. (2018). Spatiotemporal variation of the quality, origin, and age of particulate organic matter transported by the Yangtze River (Changjiang). Journal of Geophysical Research: Biogeosciences, 123(9), 2908-2921.

Wu, Y., Eglinton, T., Yang, L., Deng, B., Montluçon, D., and Zhang, J. (2013). Spatial variability in the abundance, composition, and age of organic matter in surficial sediments of the East China Sea. Journal of Geophysical Research: Biogeosciences, 118(4), 1495-1507.

Wu, Y., Fang, H., Huang, L., and Cui, Z. (2020). Particulate organic carbon dynamics with sediment transport in the upper Yangtze River. Water Research, 184, 116193.

Wu, Y., Zhang, J., Liu, S. M., Zhang, Z. F., Yao, Q. Z., Hong, G. H., and Cooper, L. (2007). Sources and distribution of carbon within the Yangtze River system. Estuarine, Coastal and Shelf Science, 71(1-2), 13-25.

Yang, C., Yang, S., Song, J., and Vigier, N. (2019). Progressive evolution of the Changjiang (Yangtze River) sediment weathering intensity since the three gorges dam operation. Journal of Geophysical Research: Earth Surface, 124(10), 2402-2416.

Yang, H. F., Yang, S. L., Xu, K. H., Milliman, J. D., Wang, H., Yang, Z., ... and Zhang, C. Y. (2018). Human impacts on sediment in the Yangtze River: A review and new perspectives. Global and Planetary Change, 162, 8-17.

Yang, L., Lu, F., Wang, X., Duan, X., Song, W., Sun, B., ... and Zhou, Y. (2013). Spatial and seasonal variability of diffusive methane emissions from the Three Gorges Reservoir. Journal of Geophysical Research: Biogeosciences, 118(2), 471-481.

Yang, S. L., Zhang, J., Zhu, J., Smith, J. P., Dai, S. B., Gao, A., and Li, P. (2005). Impact of dams on Yangtze River sediment supply to the sea and delta intertidal wetland response. Journal of Geophysical Research: Earth Surface, 110(F3).

Yu, H., Wu, Y., Zhang, J., Deng, B., and Zhu, Z. (2011). Impact of extreme drought and the Three Gorges Dam on transport of particulate terrestrial organic carbon in

the Changjiang (Yangtze) River. Journal of Geophysical Research: Earth Surface, 116(F4).

Yu, Y., Mei, X., Dai, Z., Gao, J., Li, J., Wang, J., and Lou, Y. (2018). Hydromorphological processes of Dongting Lake in China between 1951 and 2014. Journal of Hydrology, 562, 254-266.

Zhang, L., Xue, M., Wang, M., Cai, W. J., Wang, L., and Yu, Z. (2014). The spatiotemporal distribution of dissolved inorganic and organic carbon in the main stem of the Changjiang (Yangtze) River and the effect of the Three Gorges Reservoir. Journal of Geophysical Research: Biogeosciences, 119(5), 741-757.

Zhang, X. F., Yan, H. C., Yue, Y., and Xu, Q. X. (2019). Quantifying natural and anthropogenic impacts on runoff and sediment load: An investigation on the middle and lower reaches of the Jinsha River Basin. Journal of Hydrology: Regional Studies, 25, 100617.

Zhao, Y., Zou, X., Gao, J., Wang, C., Li, Y., Yao, Y., ... and Xu, M. (2018). Clay mineralogy and source-to-sink transport processes of Changjiang River sediments in the estuarine and inner shelf areas of the East China Sea. Journal of Asian Earth Sciences, 152, 91-102.

Supplementary Materials

The Enhanced Organic Carbon Sequestration induced by Massive Dam-building in the Changjiang River Basin, A Preliminary Investigation on Cascade Mega Reservoirs

Yutian Ke[1], Damien Calmels[1], Julien Bouchez[2], Marc Massault[1], Aurélie Noret[1], Hongming Cai[2], Jiubin Chen[3], Benjamin Chetelat[3], Jérôme Gaillardet[2], Cécile Quantin[1]

[1] GEOPS, Université Paris-Saclay-CNRS, 91405 Orsay, France

[2] Université de Paris, Institut de Physique du Globe de Paris, CNRS, 75005 Paris, France

[3] School of Earth System Science, Institute of Surface-Earth System Science, Tianjin University, 300072 Tianjin, China

Contents of this file

Figure S1-9

Table S1-2

Method for flux calculation

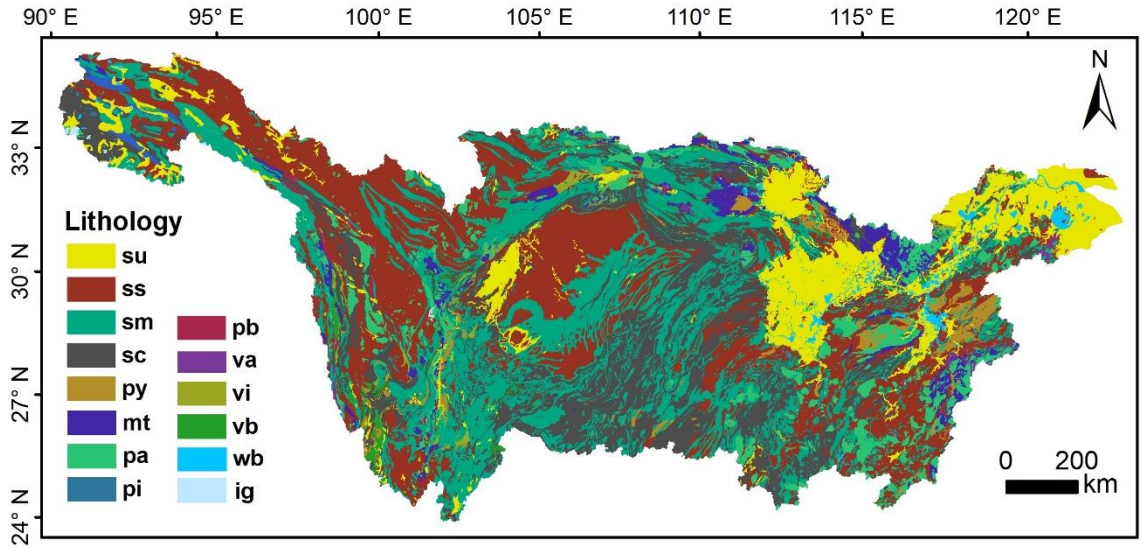

Fig. S1 Lithological map of the Changjiang river basin. (data are from the GLiM v1.1 database by Hartmann and Mossdorf, 2012). Except for no data (ND) and water body (wb), the lithology is as follows. ***su****: Unconsolidated Sediments;* ***ss****: Siliciclastic Sedimentary Rocks;* ***sm****: Mixed Sedimentary Rocks;* ***sc****: Carbonate Sedimentary Rocks;* ***py****: Pyroclastics;* ***mt****: Metamorphic Rocks;* ***pa****: Acid Plutonic Rocks;* ***pi****: Intermediate Plutonic Rocks;* ***pb****: Basic Plutonic Rocks;* ***va****: Acid Volcanic Rocks;* ***vi****: Intermediate Volcanic Rocks;* ***vb****: Basic Volcanic Rocks;* ***ig****: Ice and Glaciers.*

Annual Flux Calculation Method

At NX sampling site, SPM and POC concentration were used to construct a linear correlation between the two parameters (Fig. S2). SPM concentration is obtained by dividing monthly sediment load by monthly water discharge (Changjiang Sediment Bulletin, 2016, 2017). POC concentration is the result of POC content times SPM concentration. Through the linear regression, we could have the simulated POC content of months without POC data in 2016 and 2017 and the corresponding monthly POC flux. Notably, we did not use the adjusted depth-integrating POC to either make the estimation or calculate the annual flux. There is approximately a 10% difference between the POC content of NX 3-3 and the cross-section integration, and the integration value is higher. As we only sampled the depth profiles in flooding season, the pattern for POC transportation in dry seasons due to hydrodynamics is not clear, so we used the POC content of the monthly sampled SPM at 0.5 m water depth to calculate the annual flux, a reasonable uncertainty should be around 10%. Annual sediment load is the sum of monthly sediment load, and annual POC flux was calculated as the sum of monthly POC flux, the equation is shown as below:

$$Flux_{POC} = \sum_{month} (Q_{w_{month}} \times POC_{month})$$

where $Q_{w_{month}}$ is the monthly water discharge, and POC_{month} is the monthly POC concentration.

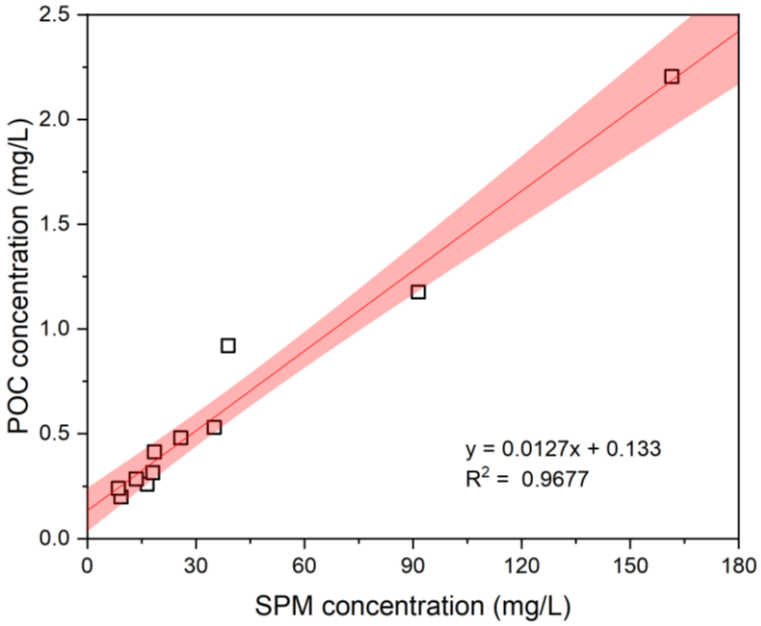

Fig. S2 Relation between SPM concentration and POC concentration of time-series sampling at Nanxi. The red line is the linear regression, the red shadow represents the 95% confidence area of the regression. SPM data was calculated based on hydrological data retrieved from the Annual Hydrological Review of Changjiang 2015, 2016. There is no gauging station at Nanxi after the confluence of Changjiang with Minjiang.

This same method is adopted in the calculation of annual POC flux at DT, we used monthly sampled depth profiles from 2015 to 2016 by Liu et al., (2019) and the cross-section depth profiles in this study (Fig. S3). A depth-integrating average POC concentration was used to predict the POC content for months without POC data.

A simple estimation of annual POC flux for sampling sites (PZH, SDZ, YL, 2009NX) in the Jinshajiang drainage basin was adopted due to the lack of historic POC data. We arbitrarily took the depth-integrating average POC content times the annual sediment load as the annual POC flux. As the depth profiles are collected in the wet seasons, the POC content is commonly lower than in the dry seasons, thus possibly result in a relatively low flux estimation.

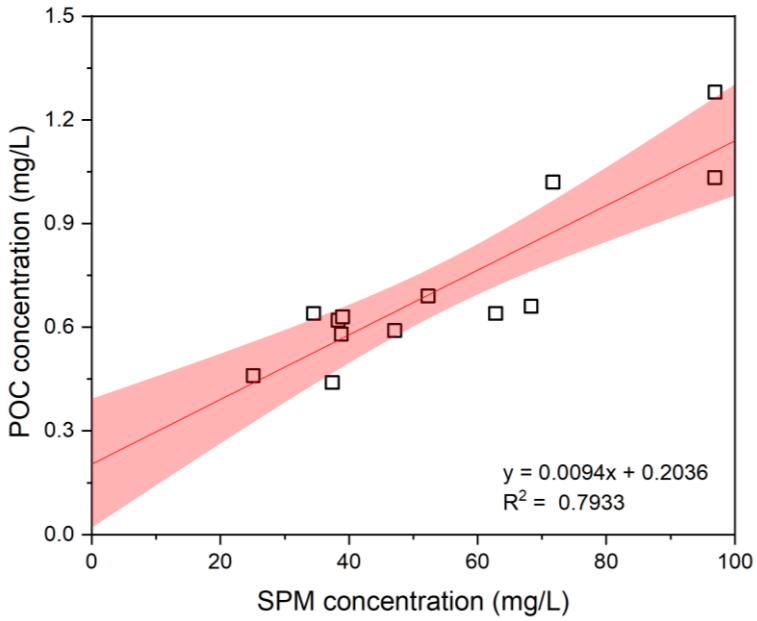

Fig. S3 Relation between SPM concentration and POC concentration of time-series sampling at Datong between May 2015 and April 2016 (Liu et al., 2019), with August 2017 (this study). The red line is the linear regression, the red shadow represents the 95% confidence area of the regression.

Concerning the factional OC flux based on the results of the binary mixing and the MIXSIAR model, the fractional OC flux was calculated using the annual POC flux times the corresponding fraction content of each OC source. At Datong (DT), the average POC_{petro} (0.112±0.027%) is significantly lower compared to the results of Li et al., (2015) of ~0.46%, but comparable to Wu et al., (2018) of ~0.07%-0.13%, we used the estimated POC_{petro} obtained by the binary mixing model. We did not apply the MIXSIAR model for DT because a majority of $\delta^{13}C$ values of SOC, petrogenic OC, and modern plants OC was found in the upper basins, which is not representative to constrain each fractional OC endmember for the entire Changjiang River basin. For other depth profile sampling sites, the MIXSIAR model was adopted to estimate the integrated fractional OC contribution, and the fractional OC flux was calculated accordingly.

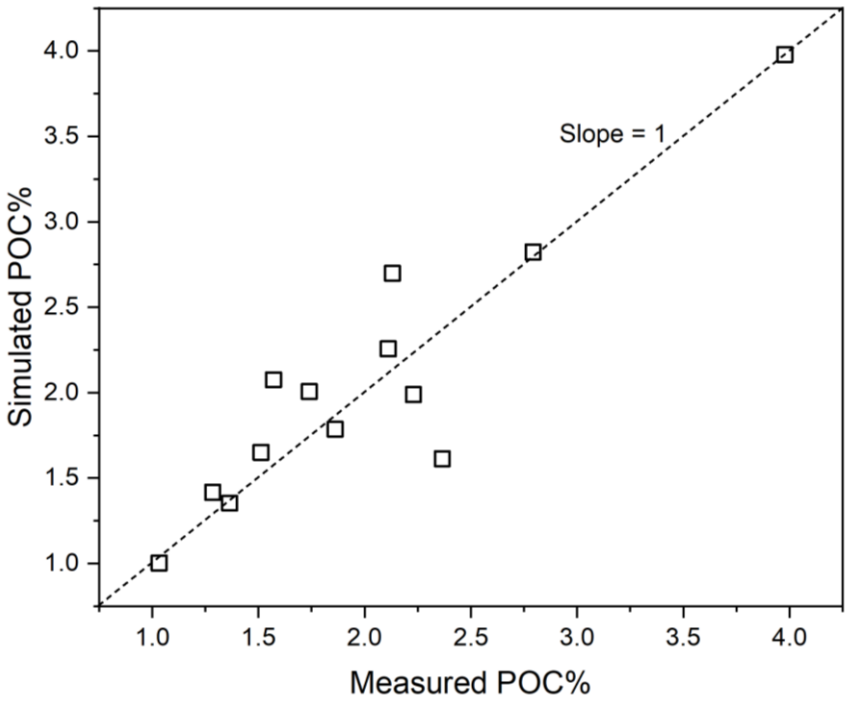

Fig. S4 Plot of measured POC% versus simulated POC% of SPM collected at Nanxi and Datong.

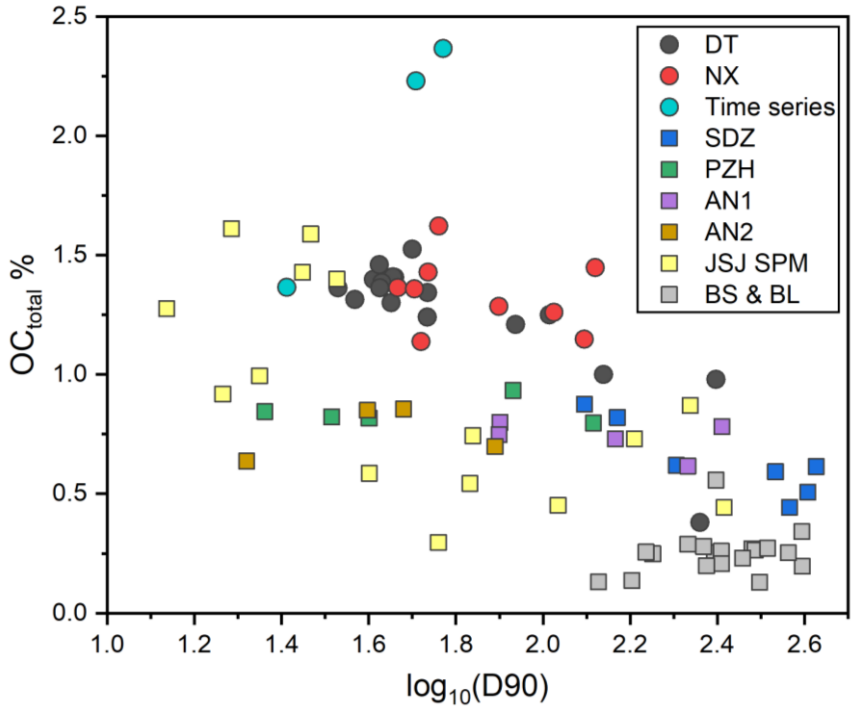

Fig. S5 Plot of SPM particle size versus its POC content

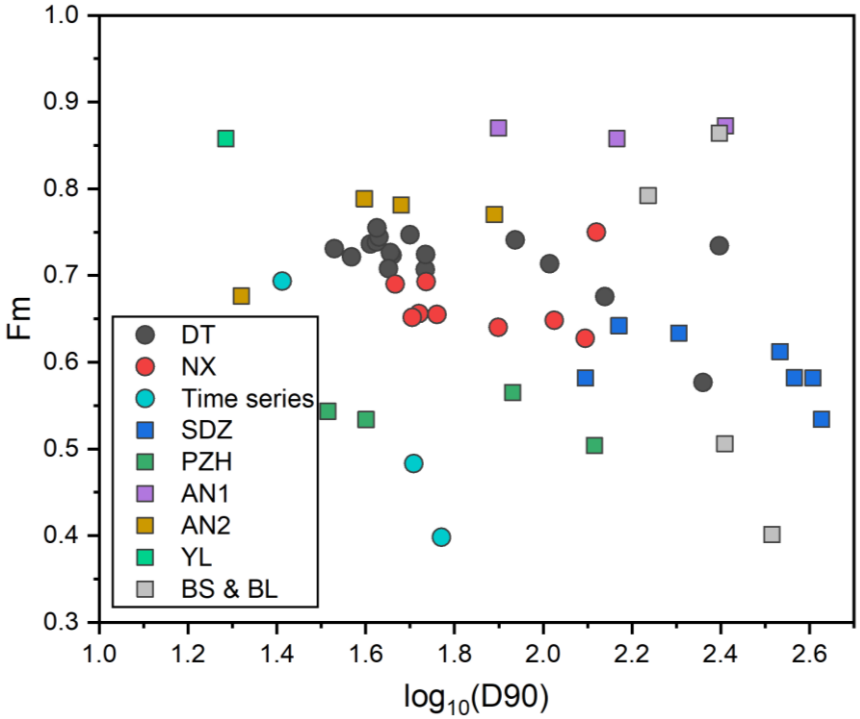

Fig. S6 Plot of SPM particle size versus Fm of POC.

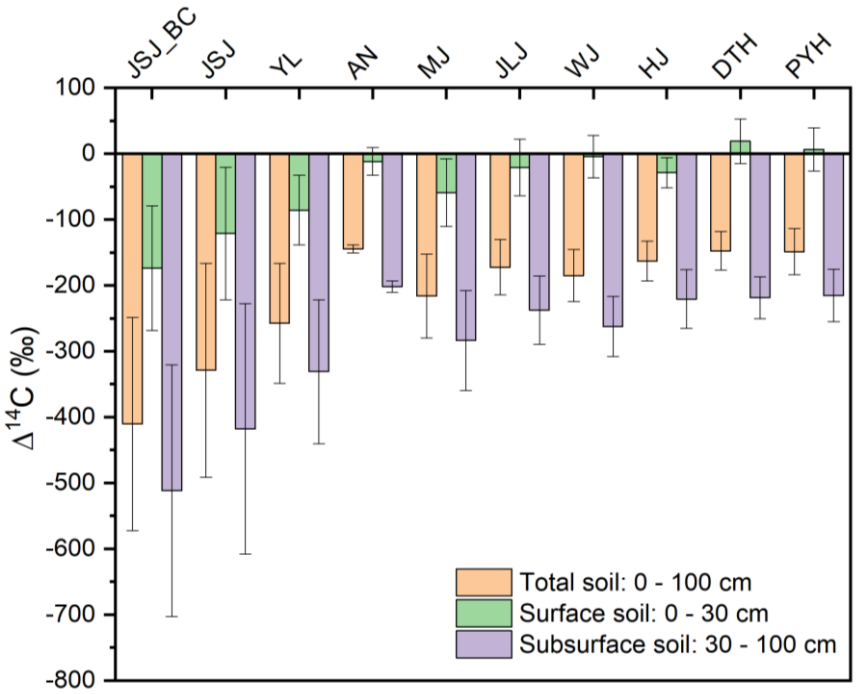

Fig. S7 $\Delta^{14}C$ values of soil organic carbon of different catchment for Changjiang. JSJ_BC, the Jinshajiang River before the confluence with the Yalong; JSJ, Jinshajiang; YL, Yalong; AN, Anning; MJ, Minjiang; JLJ, Jialingjiang; WJ, Wujiang; HJ, Hanjiang; DTH, the Dongtinghu Lake; PYH, the Poyanghu Lake River. Data were extracted from the global soil organic radiocarbon dataset at 0.5° resolution from Shi et al., (2020) in ArcGIS 10.3 (ESRI) environment.

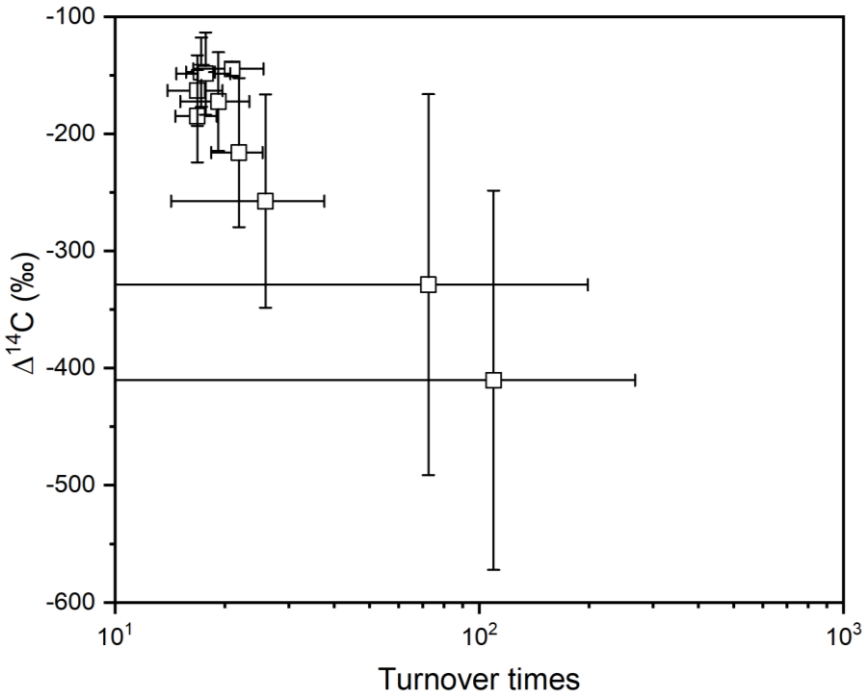

Fig. S8 Cross-plot of average turnover times versus $\Delta^{14}C$ values of soil organic carbon of different catchments for Changjiang. Soil organic carbon turnover times were extracted from the global dataset at 0.5° resolution built by Carvalhais et al. (2014) in ArcGIS 10.3 (ESRI) environment.

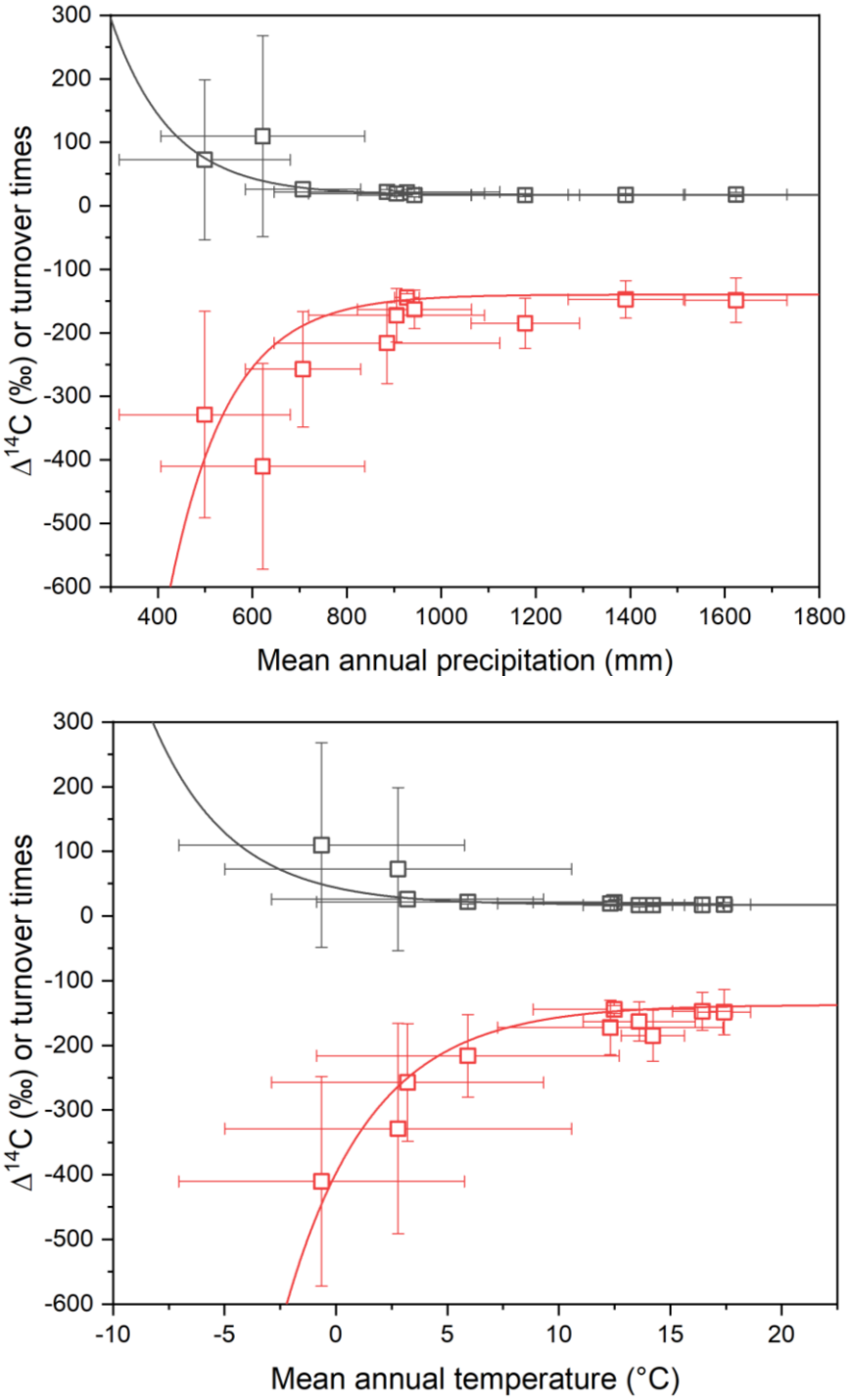

Fig. S9 Correlation between the climate of each subbasin with radiocarbon and turnover times of SOC. Climate parameters are summarized as the mean annual precipitation (mm) and mean annual temperature (°C) of each subbasin. SOC radiocarbon values are marked as red squares, and SOC turnover times are marked as black squares. Climate data is extracted from the WorldClim 2 database by Fick and Hijmans, (2017).

Table. S1 Fractional contribution percentages of different sources to riverine POC

Profile	Sample ID	Petrogenic OC	SD	Modern plant OC	SD	Site-dependant SOC	SD	Minjiang SOC	SD	POC_{petro}	POC_{bio}
Time series	NX 16.08	31.4	3.4	20.4	13.0	13.2	8.8	35	13.1	31.4	68.6
Time series	NX 16.09	41.0	7.2	17.5	13.9	10.4	9.1	31.1	16.1	41.0	59.0
Time series	NX 16.10	42.7	7.7	16.3	13.3	9.3	8.2	31.6	16.0	42.7	57.2
Time series	NX 16.11	36.7	11.1	14.2	12.9	6.0	5.4	43.1	19.3	36.7	63.3
Time series	NX 16.12	29.5	9.0	17.8	16.3	6.5	5.6	46.2	19.8	29.5	70.5
Time series	NX 17.02	29.4	9.5	16.5	15.3	6.2	5.4	47.9	19.5	29.4	70.6
Time series	NX 17.03	34.0	13.4	13.1	12.8	4.7	4.3	48.1	21.8	34.0	65.9
Time series	NX 17.04	32.2	9.5	16	15.1	6.2	5.3	45.6	19.1	32.2	67.8
Time series	NX 17.05	46.3	7.0	15.9	12.3	11.6	10.3	26.2	14.3	46.3	53.7
Time series	NX 17.06	27.1	8.6	21.6	16.9	28.5	17.6	22.8	13.8	27.1	72.9
Time series	NX 17.07	55.2	7.0	12.7	9.8	11.7	10.8	20.4	12	55.2	44.8
NX	NX-1-1	30.5	3.3	20.7	13.3	12.8	8.4	36	13.5	30.5	69.5
NX	NX-1-2	30.1	3.3	20.9	13.4	13.0	8.6	36	13.4	30.1	69.9
NX	NX-1-3	30.7	3.3	20.6	13.2	12.7	8.3	36	13.5	30.7	69.3
NX	NX 2-1	31.4	3.4	20.4	12.9	12.9	8.5	35.2	13.2	31.4	68.5
NX	NX 2-2	30.5	3.3	20.8	13.4	13.4	9.1	35.3	13.2	30.5	69.5
NX	NX 2-3	30.9	3.2	20.6	13.1	13.1	8.8	35.3	13.2	30.9	69.0
NX	NX-3-1	29.1	3.7	21.3	13.9	13.1	8.7	36.5	13.6	29.1	70.9
NX	NX-3-2	30.9	3.2	20.6	13.1	12.9	8.5	35.7	13.3	30.9	69.2
NX	NX-3-3	31.4	3.4	20.4	13	13.2	8.8	35	13.1	31.4	68.6
AN1	AN-A	14.0	3.5	48.0	15.7	38.0	15.7	0.0	0.0	13.1	86.0
AN1	AN-C	13.7	3.4	47.8	15.7	38.6	15.7	0.0	0.0	13.0	86.4
AN1	AN-E	13.5	3.5	50.4	16.2	36.2	16.0	0.0	0.0	12.9	86.6
AN2	AN-A2	28.2	4.5	35.9	13.8	35.9	13.2	0.0	0.0	23.4	71.8
AN2	AN-B2	22.6	3.5	39.7	15.0	37.7	15.2	0.0	0.0	22.8	77.4

AN2	AN-C2	23.1	3.5	39.7	14.9	37.3	15.0	0.0	0.0	22.7	77.0
AN2	AN-D2	23.4	3.4	39.5	14.9	37.0	14.7	0.0	0.0	22.8	76.5
PZH	JSJ-A	43.4	5.1	40.2	10.1	16.4	11.5	0.0	0.0	42.5	56.6
PZH	JSJ-C	42.6	5.2	40.8	10.3	16.6	11.6	0.0	0.0	42.2	57.4
PZH	JSJ-D	43.6	5.1	40.2	9.9	16.2	11.0	0.0	0.0	42.4	56.4
PZH	JSJ-E	45.1	5.0	39.5	9.6	15.4	10.6	0.0	0.0	42.6	54.9
SDZ	PZH-A	38.2	2.8	39.1	8.7	22.7	10.3	0.0	0.0	38.2	61.8
SDZ	PZH-B	35.2	2.7	41.6	9.8	23.2	10.6	0.0	0.0	35.2	64.8
SDZ	PZH-C	40.8	3.4	37.2	8.1	22.0	9.9	0.0	0.0	40.8	59.2
SDZ	PZH-D	35.6	2.6	41.3	9.7	23.1	10.5	0.0	0.0	35.6	64.4
SDZ	PZH-E	36.8	2.5	40.5	9.3	22.7	10.4	0.0	0.0	36.8	63.2
SDZ	PZH-F	38.3	2.8	39.2	8.7	22.5	10.2	0.0	0.0	38.3	61.7
SDZ	PZH-G	38.2	2.8	39.2	8.8	22.6	10.2	0.0	0.0	38.2	61.8
JSJ SPM	YLJ	8.1	4.8	30.4	22.3	61.5	23.8	0.0	0.0	8.1	91.9
2009XJB[a]	2009XJB1	31.5	9.3	21.0	13.9	47.5	16.7	0.0	0.0	36.8	68.5
2009XJB[a]	2009XJB2	29.9	9.2	21.9	14.8	48.2	17.1	0.0	0.0	36.5	70.1
2009XJB[a]	2009XJB3	33.8	9.0	22.8	14.2	43.4	16.0	0.0	0.0	36.8	66.2
2009XJB[a]	2009XJB4	37.5	10.5	19.0	12.1	43.5	15.9	0.0	0.0	38.1	62.5

[a] SPM samples collected at Xiangjiaba (mouth of Jinshajiang) in 2009 by Wu et al., (2018).

Table. S2 Fractional OC content of different sources in SPM

Profile	Sample ID	Petrogenic OC	SD	Modern plant OC	SD	Site-dependant SOC	SD	Minjiang SOC	SD	POC_{petro}	POC_{bio}
Time series	YB 16.08	0.404	0.044	0.262	0.167	0.170	0.113	0.450	0.168	0.404	0.882
Time series	YB 16.09	0.527	0.109	0.265	0.179	0.157	0.117	0.470	0.207	0.527	0.892
Time series	YB 16.10	0.549	0.121	0.256	0.171	0.146	0.105	0.497	0.206	0.549	0.899
Time series	YB 16.11	0.472	0.193	0.247	0.166	0.104	0.069	0.750	0.248	0.472	1.101
Time series	YB 16.12	0.379	0.192	0.379	0.210	0.139	0.072	0.985	0.254	0.379	1.503
Time series	YB 17.02	0.378	0.265	0.461	0.197	0.173	0.069	1.338	0.251	0.378	1.972
Time series	YB 17.03	0.437	0.283	0.277	0.165	0.099	0.055	1.016	0.280	0.437	1.392
Time series	YB 17.04	0.414	0.177	0.298	0.194	0.115	0.068	0.849	0.246	0.414	1.262
Time series	YB 17.05	0.595	0.156	0.355	0.158	0.259	0.132	0.584	0.184	0.595	1.197
Time series	YB 17.06	0.348	0.117	0.295	0.217	0.389	0.226	0.311	0.177	0.348	0.995
Time series	YB 17.07	0.710	0.166	0.300	0.126	0.277	0.139	0.483	0.154	0.710	1.060
NX	NX-1-1	0.392	0.078	0.490	0.171	0.303	0.108	0.852	0.174	0.392	1.644
NX	NX-1-2	0.387	0.078	0.494	0.172	0.308	0.111	0.852	0.172	0.387	1.653
NX	NX-1-3	0.395	0.078	0.487	0.170	0.300	0.107	0.852	0.174	0.395	1.639
NX	NX 2-1	0.404	0.039	0.234	0.166	0.148	0.109	0.404	0.170	0.404	0.786
NX	NX 2-2	0.392	0.047	0.297	0.172	0.191	0.117	0.504	0.170	0.392	0.993
NX	NX 2-3	0.397	0.052	0.334	0.168	0.212	0.113	0.572	0.170	0.397	1.119
NX	NX-3-1	0.374	0.060	0.345	0.179	0.212	0.112	0.592	0.175	0.374	1.150
NX	NX-3-2	0.397	0.052	0.334	0.168	0.209	0.109	0.579	0.171	0.397	1.122
NX	NX-3-3	0.404	0.055	0.331	0.167	0.214	0.113	0.568	0.168	0.404	1.112
AN1	AN-A	0.102	0.026	0.350	0.115	0.277	0.115			0.102	0.627
AN1	AN-C	0.102	0.025	0.357	0.117	0.288	0.117			0.102	0.646
AN1	AN-E	0.105	0.027	0.394	0.127	0.283	0.125			0.105	0.676
AN2	AN-A2	0.180	0.029	0.229	0.088	0.229	0.084			0.180	0.457
AN2	AN-B2	0.192	0.030	0.337	0.127	0.320	0.129			0.192	0.658

AN2	AN-C2	0.198	0.030	0.339	0.127	0.319	0.128	0.198	0.658
AN2	AN-D2	0.163	0.024	0.275	0.104	0.258	0.103	0.163	0.533
PZH	JSJ-A	0.357	0.042	0.331	0.083	0.135	0.095	0.357	0.466
PZH	JSJ-C	0.397	0.048	0.381	0.096	0.155	0.108	0.397	0.535
PZH	JSJ-D	0.356	0.042	0.328	0.081	0.132	0.090	0.356	0.460
PZH	JSJ-E	0.359	0.040	0.314	0.076	0.123	0.084	0.359	0.437
SDZ	PZH-A	0.304	0.022	0.311	0.069	0.181	0.082	0.304	0.492
SDZ	PZH-B	0.280	0.021	0.331	0.078	0.185	0.084	0.280	0.516
SDZ	PZH-C	0.325	0.027	0.296	0.064	0.175	0.079	0.325	0.471
SDZ	PZH-D	0.220	0.016	0.256	0.060	0.143	0.065	0.220	0.399
SDZ	PZH-E	0.218	0.015	0.240	0.055	0.134	0.062	0.218	0.374
SDZ	PZH-F	0.170	0.012	0.174	0.039	0.100	0.045	0.170	0.273
SDZ	PZH-G	0.193	0.014	0.199	0.045	0.114	0.052	0.193	0.313
JSJ SPM	YLJ	0.130	0.077	0.490	0.359	0.990	0.383	0.130	1.480
2009XJB	2009XJB1	0.164	0.048	0.109	0.072	0.247	0.087	0.164	0.356
2009XJB	2009XJB2	0.152	0.047	0.112	0.075	0.246	0.087	0.152	0.358
2009XJB	2009XJB3	0.155	0.041	0.105	0.065	0.200	0.074	0.155	0.305
2009XJB	2009XJB4	0.188	0.053	0.095	0.061	0.218	0.080	0.188	0.313

[a] SPM samples collected at Xiangjiaba (mouth of Jinshajiang) in 2009 by Wu et al., (2018).

Table. S3 Results comparison between the binary mixing model and the MIXSIAR model

Sampling site	POC_{int}[a]	Binary mixing model				MIXSIAR model	
		Fm_{bio}	SD	OC_{petro} %	SD	OC_{petro} %	SD
DT	1.067	0.796	0.018	0.112	0.027		
NX	1.406	0.807	0.117	0.228	0.162	0.433	0.038
SDZ	0.732	0.637	0.069	0.040	0.067	0.286	0.045
PZH	0.962	0.850	0.116	0.309	0.073	0.419	0.062
AN1	0.734	1.062	0.110	0.138	0.064	0.105	0.040
AN2	0.849	1.036	0.120	0.203	0.065	0.205	0.047
YL	1.025	0.882		0.045	0.058	0.089	0.059

[a]POC_{int} is the integrated POC content over the river transect based on the ADCP or velocity profile simulation. SD represents 1 standard deviation.

Table. S4 Flux and yield of SPM and POC in 2016 and 2017

Sampling Site	SPM Load Mt			POC Flux Mt								
	2016	2017	Period[a]	2016			2017			Period[a]		
				Total	OC_{petro}	OC_{bio}	Total	OC_{petro}	OC_{bio}	Total	OC_{petro}	OC_{bio}
DT	152	104	110	1.66	0.21	1.45	1.19	0.15	1.04	1.23	0.15	1.07
NX	27	25	11	0.37	0.08	0.29	0.36	0.08	0.28	0.16	0.06	0.11
SDZ	24	14	13	0.18	0.07	0.11	0.11	0.04	0.07	0.10	0.04	0.06
PZH	8	5	6	0.08	0.03	0.04	0.04	0.02	0.03	0.05	0.02	0.03
YL	15	11	8	0.16	0.03	0.13	0.11	0.02	0.09	0.08	0.01	0.07
	SPM yield t/yr/km^2			POC yield Ct/yr/km^2								
	2016	2017	Period[a]	2016			2017			Period[a]		
				Total	OC_{petro}	OC_{bio}	Total	OC_{petro}	OC_{bio}	Total	OC_{petro}	OC_{bio}
DT	89	61	65	0.98	0.13	0.85	0.70	0.09	0.61	0.72	0.09	0.63
NX	45	41	17	0.60	0.13	0.47	0.58	0.14	0.45	0.27	0.10	0.17
SDZ	62	37	34	0.46	0.17	0.29	0.27	0.10	0.17	0.25	0.09	0.16
PZH	30	18	21	0.29	0.12	0.17	0.17	0.07	0.10	0.21	0.09	0.12
YL	118	84	62	1.21	0.21	1.00	0.87	0.15	0.72	0.64	0.11	0.53

[a] Time series SPM sampling period (August 2016 - July 2017).

Reference

Hartmann, J., and Moosdorf, N. (2012). The new global lithological map database GLiM: A representation of rock properties at the Earth surface. Geochemistry, Geophysics, Geosystems, 13(12).

Annual Hydrological Review of Changjiang (2015), Press of the Ministry of Water Resources of the People's Republic of China, Beijing.

Annual Hydrological Review of Changjiang (2016), Press of the Ministry of Water Resources of the People's Republic of China, Beijing.

Carvalhais, N., Forkel, M., Khomik, M., Bellarby, J., Jung, M., Migliavacca, M., ... and Reichstein, M. (2014). Global covariation of carbon turnover times with climate in terrestrial ecosystems. Nature, 514(7521), 213-217.

Fick, S. E., and Hijmans, R. J. (2017). WorldClim 2: new 1-km spatial resolution climate surfaces for global land areas. International Journal of Climatology, 37(12), 4302-4315.

Liu, D., Bai, Y., He, X., Tao, B., Pan, D., Chen, C. T. A., ... and Gong, C. (2019). Satellite estimation of particulate organic carbon flux from Changjiang River to the estuary. Remote Sensing of Environment, 223, 307-319.

Chapter 5

MOdern River archivEs of Particulate Organic Carbon: MOREPOC

Yutian Ke[1], Damien Calmels[1], Julien Bouchez[2], Cécile Quantin[1]

[1] GEOPS, Université Paris-Saclay-CNRS, 91405 Orsay, France,

[2] Université de Paris, Institut de Physique du Globe de Paris, CNRS, 75005 Paris, France

Abstract

Rivers deliver terrestrial solids associated with particulate organic carbon (POC) into the ocean, playing a significant role in the global carbon cycle. To advance our understanding of the source, transport, and fate of fluvial POC from a regional to a global scale, a systematical database of riverine POC compositions in global contrasted basins in terms of geomorphology, lithology, climate, and anthropogenic pressure is constructed. To this end, building a georeferenced global database archiving the elemental and isotopic POC composition with open access is required. Here, we present a globally representative elemental and isotopic carbon composition set of POC: Modern River Archives of Particulate Organic Carbon (MOREPOC) version 1.0, recording the fluvial memory of suspended particulate matters (SPM) collected at 229 main channels and tributaries in 118 river systems referenced from the sprung up research on POC in the last two decades. This database records 3,298 SPM, including 2,847 with POC content, 3,151 with stable carbon isotope $\delta^{13}C$ values, 1,874 with radiocarbon activity $\Delta^{14}C$ values, and 1,883 with total nitrogen content as well as 487 with aluminum to silicon mass ratios (Al/Si). Together with CASCADE (Circum-Arctic Sediment Carbon DatabasE, Martens et al., 2021) and MOSAIC (Modern Ocean Sediment Archive and Inventory of Carbon, van der Voort et al., 2021), MOREPOC could help to build a powerful framework on mobilization, alteration, and final fate of terrestrial POC from source to sink in contrasting fluvial systems. The database will be available at Zenodo in machine-readable format (.csv, .mat), all map data layers, including attribute tables, are provided in ESRI Shapefile format.

Keywords: SPM, Riverine POC, global compilation, radiocarbon activity, $\delta^{13}C$ values

1. Introduction

In the delivery trajectory of sediments from source to sink in the Earth's sedimentary cycle, rivers are the main conveyor of terrestrial materials in the form of suspended particulate matter (SPM) carrying particulate organic carbon (POC) from mountainous regions to continental margins (Leithold et al., 2016; Blair and Aller, 2012). The focus of the compiled MOREPOC v1.0 dataset is on the POC because of its high involvement in the long-term carbon cycle. The massive input of terrestrial POC in the coastal and ocean environment leads to changes in carbon alteration (loss and gain) and circulation, thus it also helps to understand the rapidly changing ocean under the accelerating and intensified anthropogenic interventions.

The riverine POC is the mixing of organic carbon (OC or C_{org}) from varying sources, representing the superposition of biospheric POC (POC_{bio}) and petrogenic POC (POC_{petro}) (Blair et al., 2003; 2004; Galy et al., 2007; Hilton et al., 2008). The biosphere, consisting of modern plants, soils, and autochthonous organisms, contributes a dominant fraction of POC_{bio} which is radiocarbon-enriched with ages ranging from modern to multi-millennial to riverine POC (Galy et al 2007; Blair et al., 2010; Hilton et al., 2011). Radiocarbon-dead POC_{petro} is from extensively degraded ancient sedimentary rocks with ages of millions of years (Galy et al., 2008a; Hilton et al., 2011). Understanding the role Earth surface processes and the subsequent river-linked source-to-sink system play in the carbon cycle at a regional to global scale is crucial. The release of CO_2 by oxidation of POC_{petro} and the drawdown of CO_2 by burial of POC_{bio} in marine sediments are key mechanisms that control the atmospheric CO_2 level at a geological time scale (> 100,000 years). The induced global carbon fluxes have a similar magnitude to those from silicate weathering and volcanism (Berner, 2003; Hilton et al., 2014; Petsch, 2014; Galy et al., 2007, 2011; Hilton and West, 2020). Thus, it is fundamental to quantitatively understand the alteration extent and bulk fluxes of different POC fractions (sources) to better constrain the net effect induced by the oxidation or burial of riverine POC. Radiocarbon activities give unique information on residence time, ages, and fractional compositions of POC in different reservoirs (atmosphere, lithosphere, and biosphere). Together with $\delta^{13}C$, or POC content or some other organic-inorganic proxies (*e.g.*, C_{org}/N ratio, Al/OC ratio), it helps to better

resolve the signature overlapping from varying sources, providing powerful and sensitive sentinel on unraveling the source, transport, and fate of riverine POC_{bio} and POC_{petro} (Raymond and Bauer, 2001).

Global rivers are contrasted in draining areas subjected to varying environmental drivers including climate, tectonic, geomorphic, and anthropogenic activities. The very complex contributions from different OC sources result in the widely heterogeneous elemental and isotopic signals compositions within the riverine POC. Soil organic carbon (SOC) represents a dominant component of the terrestrial POC exported by many fluvial systems (*e.g.*, Tao et al., 2015; Wu et al., 2018; Wild et al., 2019). Temperature and precipitation exert dominant control over surface SOC radiocarbon activities and turnover times globally (Shi et al., 2020; Carvalhais et al., 2014), the present increasing trend of temperature and precipitation is likely to mobilize more biospheric OC into fluvial systems due to the enhanced perturbation to SOC pools (Eglinton et al., 2021). In cold biomes such as permafrost regions, SOC has the longest turnover times and the most depleted ^{14}C, whereas SOC with the shortest turnover times and the most enriched ^{14}C are found in tropical forests and savannah (Shi et al., 2020; Carvalhais et al., 2014). The exported POC is significantly older in Arctic rivers (*e.g.*, Kolyma, Lena rivers) while considerably younger in tropical rivers such as Congo or Amazon (Holmes et al., 2021; Marwick et al., 2015; Mayorga et al., 2005). Besides, there are seasonal variations in POC composition at a catchment scale (*e.g.*, Wang et al., 2012; Liu et al., 2017). In terms of tectonics, sediment experiences more erosion-deposition cycles on passive margins relative to active margins because of the relatively long path from the upland source to the burial in the ocean (Blair and Aller, 2012). Consequently, original POC source signals are transmitted through the system with greater fidelity on active margins (Blair and Aller, 2012). For example, POC in the Mekong and small rivers in Taiwan can have very contrasted transportation processes and final fates in the ocean (Martin et al., 2013; Hilton et al., 2011). Due to perturbations of anthropogenic activities such as land-use change and dam-building, the delivery of POC in global rivers are modified to varying degrees, mainly by the massive temporal storage of POC before reservoirs and the largely altered POC that is exported to the ocean (Best et al., 2020; Battin et al., 2009). Even though recent research has advanced the understanding of bulk and molecular composition of POC from different sources and the governing environmental controls from a catchment scale to a global scale

(Galy et al., 2015; Hilton 2008; Coppola et al., 2018; Hemingway et al., 2019; Eglinton et al., 2021), there is still a lack of numerical constraints to quantify the effect of environmental drivers on the carbon isotopic composition of riverine POC. Therefore, developing Earth system models is highly needed to push forward the recognition of the riverine POC dynamics and its changing role in the carbon cycle from past to future.

The release of the International Soil Radiocarbon Database (ISRaD) (Lawrence et al., 2020) favors the establishment of state-of-the-art Earth system models on predicting global SOC radiocarbon distribution and turnover times in different depths (Shi et al., 2020; Carvalhais et al., 2014). For global fluvial systems, no such radiocarbon prediction for POC exists, even though there are rising studies on simulation of water discharge, SPM concentration, and POC content based on compiled global water quality datasets (Ittekkot, 1988; Ludwig et al., 1996, Meybeck, 1993), such as the WBMsed global hydrology model (Cohen et al., 2014), Global NEWS2 (Mayorga et al., 2010), etc. Therefore, we built a dataset for riverine POC compiling 1,847 $\Delta^{14}C$ data, which is a great update to the previously reported global dataset by Marwick et al. (2015) with only 531 $\Delta^{14}C$ data. MOREPOC v1.0 incorporates data from international peer-viewed articles and newly analyzed (unpublished) data of four large rivers (Heilongjiang, Zhujiang, Changjiang, and Huanghe) in China from this thesis. This database would provide a basic database to 1) uncover the fundamental mechanisms of preservation and alteration on bulk POC and its fractional compositions (*e.g.*, POC_{bio} and POC_{petro}) in the source-to-sink sedimentary system around the globe; and 2) help with the construction of numerical models to simulate isotopic compositions of POC under the evolving coupled driving of different environmental and anthropogenic variables.

2. Data compilation on global riverine POC

2.1 Collection of data

Taking advantage of the improved carbon-dating technology and the easily accessible accelerator mass spectrometry (AMS), the radiocarbon abundance of riverine POC has been extensively measured during the last two decades. In MOREPOC v1.0, we compiled 3,297 SPM data, including 1,995 with SPM concentration, 2,847 with POC content, 3,151 with stable carbon isotope $\delta^{13}C$ values, 1,874 with radiocarbon activity $\Delta^{14}C$ values, and 1,883 with total nitrogen content as well as 487 with aluminum to

silicon mass ratios (Al/Si) through extensive literature investigation on 118 peer-reviewed articles together with some unpublished data of SPM from the four largest Chinese rivers in this study. We selectively compiled data from studies reporting at least one carbon isotopic data, and those with paired elemental and dual carbon isotopic values are favored. Most data points are from Asian rivers while the least from Oceanic rivers (Figure 1 and Table. 1). Data quality was carefully checked through manual examination, duplicate data was removed, false data was either removed or corrected.

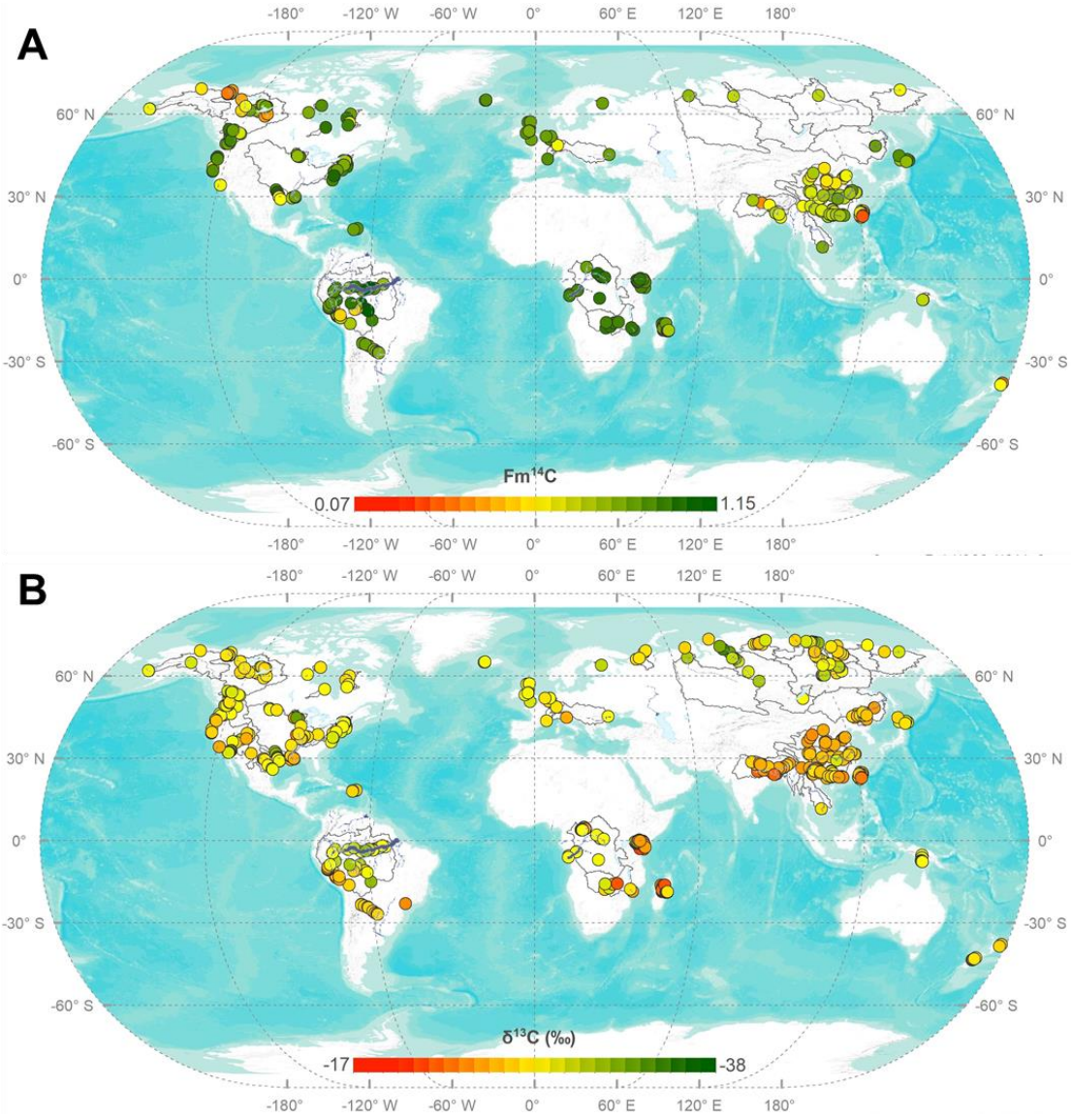

Fig.1 Dual carbon isotopic inventory of riverine POC in global rivers. A, $\delta^{13}C$ values; B, $Fm^{14}C$ values. Samples with the same coordinate location presented in the maps are their averaged values calculated automatically using Matlab 2015, correspondingly. A full reference list for the dual carbon isotopic data is provided in the supplementary materials.

2.2 Georeferenced system

If available, SPM sampling locations are projected in a Geographic Coordinate System using the World Geodetic System 1984 (WGS1984). Because some references only provide a sampling map without giving the numeric coordinate information, we manually extracted the coordinate using ArcGIS 10.3 after georeferenced adjustment. Among the 3,297 compiled SPM samples, 3,072 of them have coordinate information (Figure 1).

Table.1 Data availability for riverine SPM in different continents.

Continent	Samples	SPM	POC	TN	$\delta^{13}C$	$\Delta^{14}C$
	n	n	n	n	n	n
Asia	1,768	1,029	1,697	1,151	1,708	1,050
Africa	277	277	277	103	277	114
Europe	128	81	99	23	123	111
Oceania	94	62	94	92	94	26
North America	755	330	425	379	675	475
South America	275	216	255	135	274	98
Total	3,297	1,995	2,847	1,883	3,151	1,874

2.3 Database structure

To provide a machine-readable database, different parameters are labeled with a name in short in the respective columns in the MOREPOC v1.0 datasheet, which are shown in Table. 2.

Table. 2 Parameter description of the MOREPOC datasheet.

Parameters	Description	Column name
River name	Name of the (major) river	riv_na
Sub river name	Name of the main channel or tributaries	bas_na
Continent	Name of the (resided) continent	cont
Sampling site/code	Expedition sampling ID	code
Sampling date	The time when SPM were collected	time
Latitude	Decimal latitude using WGS 1984	lat
Longitude	Decimal latitude using WGS 1984	lon
Sampling technique	Method of SPM sampling	type_spm
Size fraction of SPM	Reported size fractions analyzed	fra_spm
SPM concentration (mg/L)	The total dry weight of SPM in mg per litter water column	conc_spm
POC concentration (mg/L)	The total dry weight of POC in mg per litter water column	conc_poc
POC content (%)	The total POC content of SPM in wt %	per_poc
$\delta^{13}C$ (‰)	$\delta^{13}C$ values of POC (decarbonated)	d13c_poc
$\Delta^{14}C$ (‰)	$\Delta^{14}C$ values of POC (decarbonated)	D14c_poc

Fraction modern (Fm)	Fraction modern of POC	f14c
Radiocarbon ages (year)	Radiocarbon ages before present (1950)	rca
TN content (%)	The total nitrogen content of SPM in wt %	per_tn
C_{org}/N mass ratio	Mass ratios of POC to TN	cn_mar
Al/Si mass ratio	Mass ratios of Al to Si in SPM	as_mar
Reference	Brief citation of the data source	ref
Notes	Additional information, such as sampling water depth, climate, etc.	note

2.4 Summary of sampling strategy

Different sampling strategies in the river expedition have been reported in the selected articles. In summary, there are five types, which are surface SPM sampling, mid-depth SPM sampling, mixing sampling in depth profiles, depth profile integrated sampling, transect depth profile integrated sampling. An improved and more detailed sampling technique increases the potentials to understand the nature and transport of riverine POC. A brief description of the different sampling techniques is as follows:

Surface SPM sampling collects surface suspended load (SSL), the SPM delivered in the channel surface. This sampling scheme is the most frequently used and widely adopted in riverine POC studies.

Middle-depth SPM sampling collects mid-depth suspended load (MD-SL), the SPM delivered in the water column near the middle between the river surface and bottom. This sampling strategy is relatively rarely adopted and was carried out in the Mekong (Martin et al., 2013) and the Mackenzie (Campeau et al., 2020).

Mixing sampling in depth profiles collects SPM in water columns in different depths below the river surface, then the collected water samples are mixed with a specific ratio to obtain the mixed suspended load (MDL). This sampling strategy is only adopted in the Huanghe and Changjiang (Wang et al., 2012), and in the Zengjiang, a tributary of the Zhujiang (Gao et al., 2007).

Depth profile integrated sampling collects SPM in several water columns at an individual depth profile from different depths. In that case, each SPM at an ideal depth is an individual sample for subsequent pretreatment and laboratory analysis. We classify SPM collected under this sampling scheme as the depth-integrated suspended load (DSL). The advantage of accessing the full range of particle sizes of SPM in the channel makes this sampling scheme become widely accepted (*e.g.*, Ganges-Brahmaputra, Mackenzie, Amazon, etc.).

Transect depth profile integrated sampling collects SPM in several depth profiles across the channel section. Each depth profile sampling follows the strategy adopted in collecting DSL. SPM collected under this sophisticated sampling scheme is the transect depth-integrated suspended load (TSL). This sophisticated sampling scheme further explores the potentials of understanding the SPM transport mode and compositional heterogeneity within a channel transect profile. It has been recently carried out in some large river systems, like the four largest Chinese rivers in this study, the Salween and the Irrawaddy (Baronas et al., 2020), as well as the Danube (Freymond et al., 2018).

2.5 Summary of decarbonization method

Particulate inorganic carbon (PIC) and POC have distinct carbon isotopic signals, and $\delta^{13}C$ and $\Delta^{14}C$ values could be compromised if PIC is not efficiently removed from POC. To accurately determine the elemental and isotopic compositions of POC, it is essential to remove the PIC by acidification (Komada et al., 2008). Three methods are most frequently adopted in references compiled in MOREPOC v1.0, namely, the "rinse method", the "aqueous method", and the "vaporous method". Based on the physical and chemical nature of sediments, there are control variables including acid concentration, reaction time, and reaction temperature. After the acidification process, sediment samples are dried before chemical analysis. For reference, the carbonate removal treatment methods are provided in an independent file with details (acid type and quality, decarbonization method, reaction time, etc.), allowing a manual quality evaluation of the data by the expert user. Meanwhile, a brief description of the three decarbonization methods are provided as follows:

- Rinse method, sediment samples are acidified under an ideal environmental temperature for reaction temperature for a given time, then rinsed with water.
- Aqueous method, pre-weighted sediment samples are acidified in capsules.
- Vaporous method, sediment samples are exposed to vaporous concentrated hydrochloride acid in a closed system under an ideal temperature for a given time.

2.6 Physical and chemical statistics

SPM and POC concentration are reported as dry weight per liter (mg/L), POC content (POC%), and total nitrogen content (TN%) are reported as dry weight percentage (%), thus we also have the POC to TN ratio (C_{org}/N) (Table 2). The fundamental component of MOREPOC v1.0 is the extensively collected stable carbon isotope values ($\delta^{13}C$, ‰ in relative with VPDB) and radiocarbon compositions (both as $\Delta^{14}C$ in ‰ or as $F^{14}C$).

Inorganic chemistry aluminum to silicon ratio (Al/Si) is compiled as well, an efficient proxy for particle size of riverine sediment (Bouchez et al., 2011; Galy et al., 2007; Hilton et al., 2015). All data are either taken directly from references or calculated after the papers' data.

Conventional Radiocarbon Ages (RCA) are quoted for standards as discussed by Stuiver and Polach (1977) using the Libby half-life of 5,567 years with the mean life of 8,033 for ^{14}C. RCA is expressed in units of years before present (BP), with year zero being 1950.

$$\mathrm{RCA} = -8033 \ln (F^{14}\mathrm{C})$$

Δ^{14}C value, the relative difference between the absolute international standard (the base year 1950) and sample activity corrected for age and δ^{13}C (Stuiver and Polach, 1977), was reported as well. A positive Δ^{14}C indicates the presence of bomb carbon, whereas a negative Δ^{14}C indicates that the radioactive decay of C overwhelms any incorporation of bomb carbon into the sample. The Δ^{14}C calculation is defined as below.

$$\Delta^{14}\mathrm{C}\ (\text{in } ‰) = [F^{14}\mathrm{C} * exp\left(\frac{1950 - yr}{8267}\right) - 1] * 1000$$

Where *yr* is the year when the sediment was collected, 8,267 is the true mean life of ^{14}C using the Cambridge half-life of 5,730 years.

To fill blank values of some parameters such as POC content, we also performed the following calculation and conversion.

Calculation of POC concentration $\mathrm{C_{POC}}$,

$$\mathrm{C_{POC}} = \mathrm{C_{SPM}} \times \mathrm{P_{POC}}$$

where $\mathrm{C_{SPM}}$ is the SPM concentration, and $\mathrm{P_{POC}}$ is the percentage content of POC in the corresponding SPM.

C_{org}/N mole and mass ratio conversion:

$$C_{org}/\mathrm{N}\ (\text{mole ratio}) = C_{org}/\mathrm{N}(\text{mass ratio}) \times (\mathrm{Atom_N}/\mathrm{Atom_C})$$

where $\mathrm{Atom_C}$ and $\mathrm{Atom_N}$ are the atomic weight of C (26.982) and N (26.982), respectively.

Al/Si mole and mass ratio conversion:

$$\mathrm{Al/Si}\ (\text{mole ratio}) = \mathrm{Al/Si}\ (\text{mass ratio}) \times (\mathrm{Atom_{Si}}/\mathrm{Atom_{Al}})$$

where $\mathrm{Atom_{Al}}$ is the atomic weight of Al (26.982), and $\mathrm{Atom_{Si}}$ is the atomic weight of

Si (28.085).

2.7 Extent and limitations

Even though this database addresses the globally extensive research on different river systems spanning almost all continents (except the Antarctic), there are certain limitations. For instance, elemental and dual isotopic compositions of molecular compounds (plant-wax fatty-acid and lignin-phenol), thermal labile fractions, and black carbon are not compiled into the MOREPOC v1.0 dataset, which needs to be added in the updated version in the future.

3. Results and discussions

3.1 $\delta^{13}C$ and $\Delta^{14}C$ from the MOREPOC dataset

Global river basins mobilize terrestrial organic matter into the fluvial systems under the complex coupling interplay of tectonics, climate, geomorphology, lithology, and anthropogenic activities, resulting in varying compositions of riverine POC (Blair and Leithold, 2010; Eglinton et al., 2021). In a given river basin, the alteration on POC composition through mineralization, degradation, and gain and loss of C_{org} components is continuous during the transit (Blair and Aller, 2012).

As shown in Figure 2, riverine POC has great heterogeneity in elemental and isotopic carbon compositions around the globe. $\delta^{13}C$ values (n=3,151) ranges from -38‰ to -17‰ with a statistical average of -26.3‰. The majority of data falls between -28‰ to -24‰ (n=1,697), which is consistent with the main isotopic signature of the terrestrial biosphere of -26±7% (Schidlowski et al., 1988). Global riverine POC spans from modern recording bomb carbon to ancient representing fossil petrogenic source, $\Delta^{14}C$ values (n=1,874) ranges from -990‰ to 148‰ with a statistical average of -386.4‰, there is no big difference shows in the distribution for each interval of 100‰ in the range of from -900‰ to 100‰. However, it still exerts a dominant distribution (n=753) in the range from -300‰ to 0‰, a ^{14}C-depleted shifting exists compared to the range of -200‰ – 100‰ (n=323) reported by Marwick et al (2015). It has to be pointed out that the weighted average value of each POC parameter should be more reasonable by considering the corresponding fractional sediment contribution of each basin to the global sediment load, but there are very little water discharge data which makes the calculation hard to fulfill, averaged values presented here could be influenced by data

frequency. Notably, the global dual carbon isotopic data show that POC is more depleted in ^{14}C with the enrichment of ^{13}C, yet there is a slight trend that ^{14}C is getting depleted with the depletion of ^{13}C. This phenomenon matches cases in the Ganges-Brahmaputra River system, ^{13}C is found either more depleted in SPM or bed load but the latter usually has much-depleted ^{14}C (Galy et al., 2008b; Galy and Eglinton, 2011). Meanwhile, in general, $\Delta^{14}C$ increases and $\delta^{13}C$ decreases with the increasing POC content. In the global spatial distribution of POC (Figure 3), $\delta^{13}C$ values tend to be more depleted in high latitude regions; $\Delta^{14}C$ values are enriched in low latitude tropical regions while depleted in high latitude permafrost regions, it spans a large range in the lower latitude regions between 20°N and 30°N. Overall, using POC content and dual carbon isotopic favors the quantification of fraction contribution from either binary sources (biospheric vs petrogenic) or multiple sources (fossil, soil, and plant, etc) (Galy et al., 2007; Tao et al., 2015; Lin et al., 2020).

It is worth finding the extremum of different POC parameters to reveal the contrasting environmental conditions in different river basins. The most ancient POC ($\Delta^{14}C$: -990‰) is detected in small mountainous rivers (Hoping, Hsiukuluan, Peinan, and Yenping, etc) in Taiwan (Hilton et al., 2010), almost representing the fossil OC from sedimentary rocks. In the riverine POC, bomb carbon signals are abundant ($\Delta^{14}C > 0$‰), particularly for African rivers such as Athi-Galana-Sabaki, Tana, Zambezi, and Congo in tropical regions (Marwick et al., 2015; Spencer et al., 2012), rivers in North America including Hudson, Siuslaw, York, and rivers exported to the Hudson Bay (Leithold et al., 2006; Raymond and Bauer, 2001; Godin et al., 2017; Longworth et al., 2007), and source regions of Amazon (Mayorga et al., 2005; Townsend-Small et al., 2007). The most depleted ^{13}C signatures (less than -35‰) are mostly present in POC from the Arctic rivers, such as Ob', Yukon, and Kolyma (Holmes et al., 2021). The most abundant ^{13}C signals (larger than -22‰) are from rivers in Africa (Athi-Galana-Sabaki, Betsiboka, and Tana; Marwick et al., 2015; Tamooh et al., 2012) and mountainous rivers (for example, SMR in Taiwan, Ganges, Minjiang; Hilton et al., 2010; Galy et al., 2007; Galy et al., 2008b; Wang et al., 2019). All the aforementioned data could provide information on the climate, geomorphology, and tectonics, etc. of the given river basin. MOREPOC v1.0 dataset has great potential in exploring the complex environmental drivers over the nature of riverine POC.

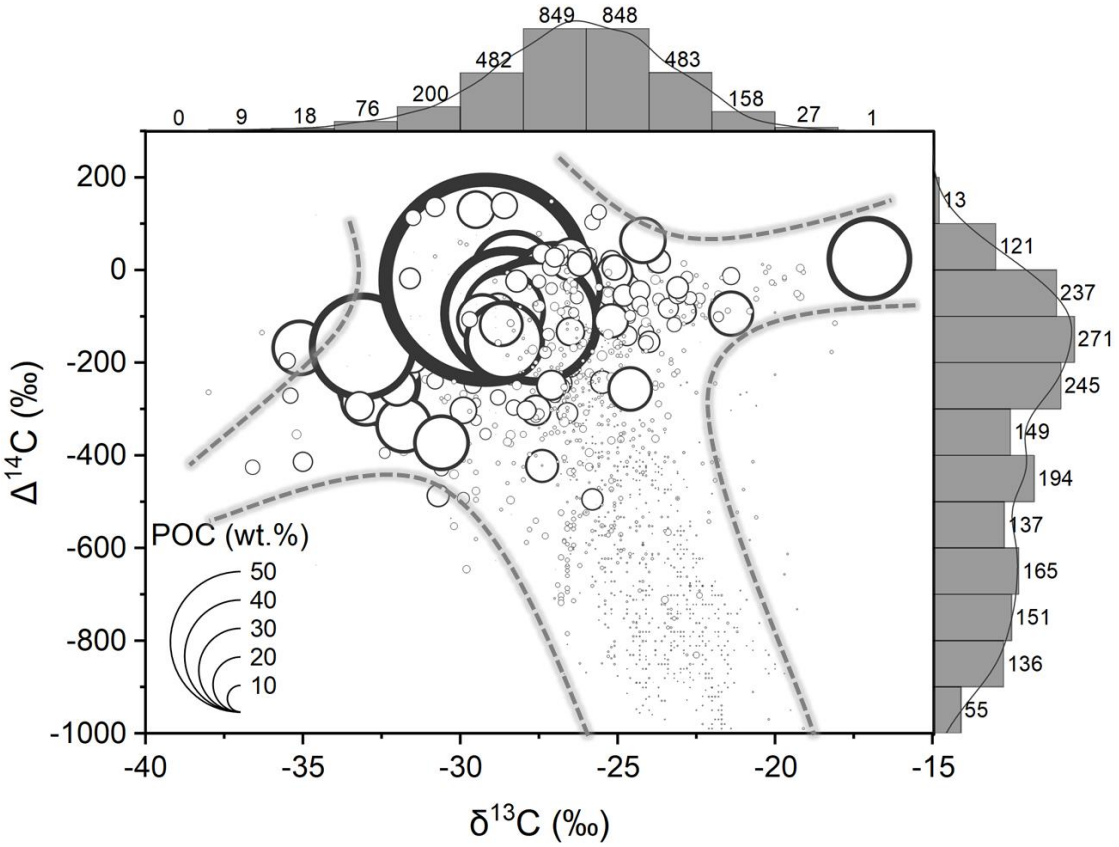

Fig. 2 Plot of $\delta^{13}C$ versus $\Delta^{14}C$, size of open circles indicates POC content (wt. %). Marginal columns are count statistics for $\delta^{13}C$ (x-axial) and $\Delta^{14}C$ (y-axial) of MOREPOC v1.0, including the paired dual carbon isotopic data (n=1,753) in the plot. $\delta^{13}C$ values are classified with a -2.5‰ interval in the range from -40‰ to -15‰, and $\Delta^{14}C$ values are classified with a -50‰ interval in the range from -1000‰ to 200‰. Dot lines represent rough boundaries of data distribution.

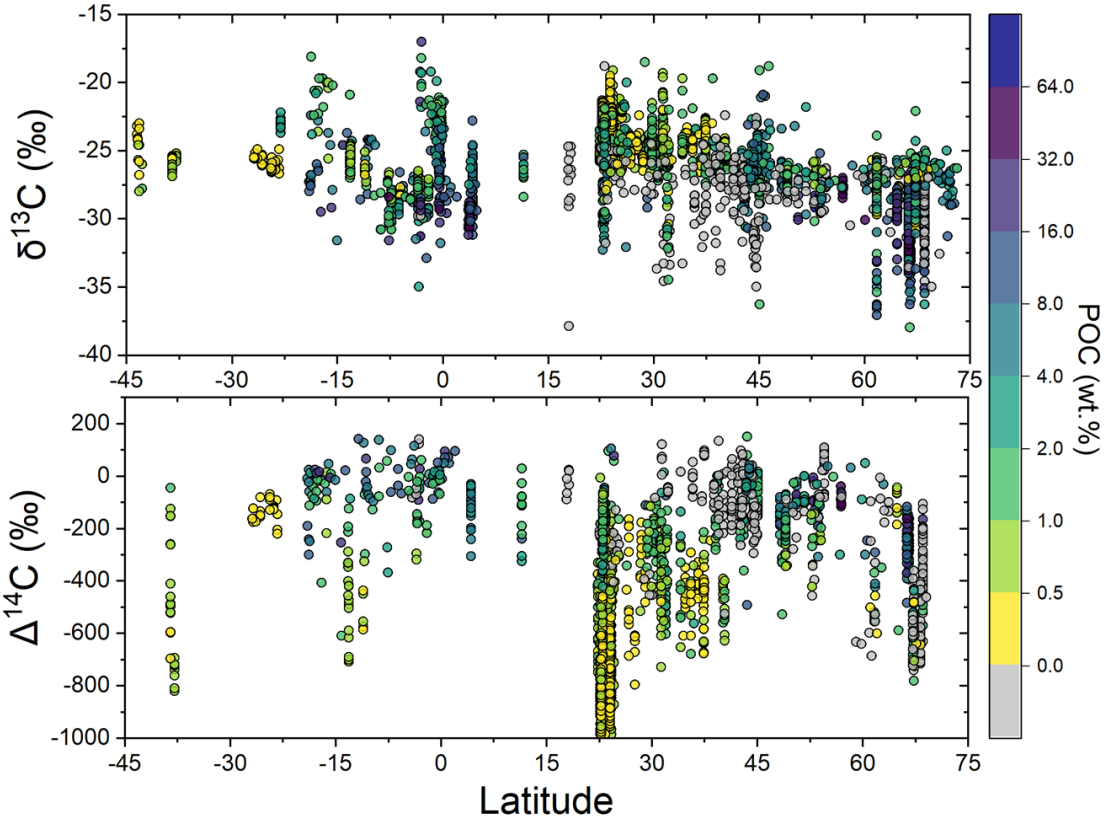

Fig. 3 Latitude versus $\delta^{13}C$ (n=2,940) and $\Delta^{14}C$ (n=1,800), colors indicate POC content (wt. %). $\delta^{13}C$ values tend to be more depleted in high latitude regions; $\Delta^{14}C$ values are enriched in low latitude tropical regions while depleted in high latitude permafrost regions, it spans a large range in the lower latitude regions between 20°N and 30°N.

3.2 Nature of riverine SPM and POC around the globe

Non-turbid and turbid river systems deliver SPM (range: 0.35 – 199,000 mg/L) carrying contrasting POC contents (0.21% – 91.67%). The global pairs of SPM and POC concentration (in mg/L) data (n=1,944) show the positive correlation between the two parameters. However, a larger SPM concentration is usually accompanied by a lower POC content (in %) globally (Ittekkot, 1998; Ludwig et al., 1996; Meybeck, 1993). In MOREPOC, large SPM concentrations (over 10,000 mg/L) are generally spotted in mountainous tectonic-active rivers, such as Choshui and Liwu (Taiwan) (Hilton et al., 2008; Gao et al., 2014), Santa Clara (USA) (Masiello and Druffel, 2001), Minjiang (a major tributary of upper Changjiang, China) (Wang et al., 2019). Huanghe is an exception in that it has very large SPM concentrations in the middle reaches where the section flows through the Chinese Loess Plateau instead of a mountainous area (Qu et al., 2020; Hu et al., 2015). Turbid rivers usually have a large capability of delivering

substantial amounts of POC even though it is relatively OC-poor (Figure 4), underlining the importance of sediment delivery near river bottom due to hydrodynamics, and extreme events such as storms, landslides, and earthquakes, etc (Hilton et al., 2008). Very small SPM concentrations (less than 10 mg/L) are usually characterizing rivers in tropical areas and Circum-Arctic permafrost where the POC content is relatively high (Gao et al., 2007; Holmes et al., 2021). The MOREPOC dataset covers approximately half of the surface area of global river basins, invoked by the extensively collected carbon isotopic data, it enables a better quantification of components of POC from different sources. If with the aid of a water discharge dataset, a more robust flux estimate for bulk POC and its varying fractions can be obtained (*e.g.*, Milliman and Farnsworth, 2011).

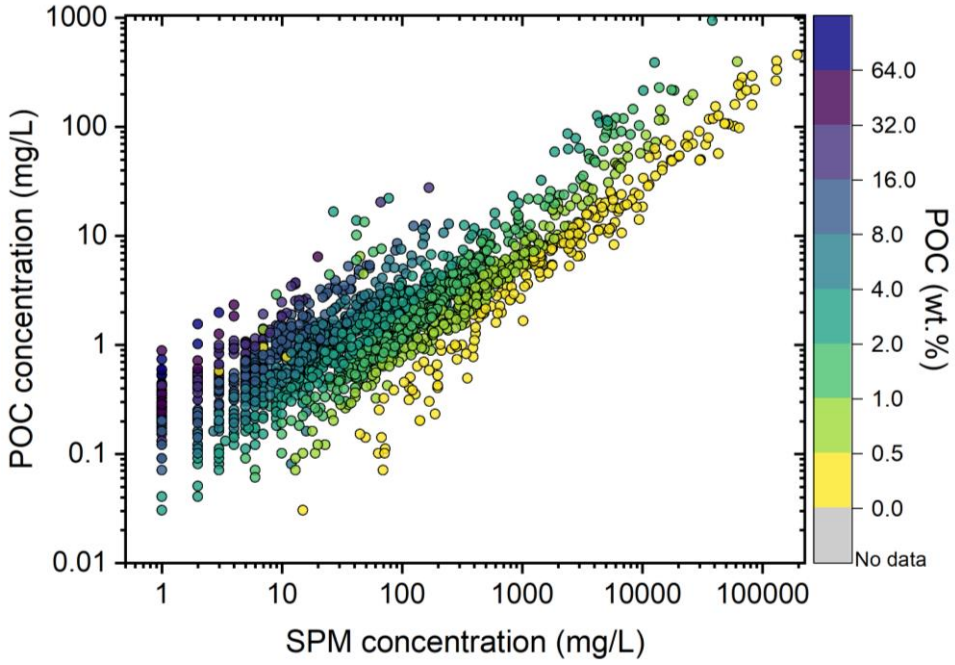

Fig. 4 Pairwise plot of SPM concentration with POC concentration in log metric scale (n=1,947), colors indicate POC content (wt. %). It shows a general trend that POC concentration increases with SPM concentration, accompanied by decreased POC content.

The riverine SPM transport follows a general pattern of depleting POC ^{14}C with increasing suspended sediment load (Figure 5) whereas with decreasing POC content at regional-global scale (Figure 6). The strong inverse relations are generally caused by the dilution of modern OC by the fossil sources associated with lithogenic sediment.

However, SPM with similar concentrations could span a large spatial range with great variations in ^{14}C compositions. For example, SPM with relatively less ^{14}C abundance is usually found in low-latitude tropical regions (30°N - 30°S) and high-latitude permafrost regions (60°N - 75°N), but in general, POC of the former is very young while the latter is significantly older. This phenomenon is largely owing to the contrasting radiocarbon activities of the eroded soil organic carbon (SOC) and turnovers that drove primarily by climate (Eglinton et al., 2021; Marwick et al., 2015; Wild et al., 2019; Vonk et al., 2015). The dataset also reveals that river systems under similar climate conditions could have heterogeneous transport in SPM and associated POC. In Circum Arctic rivers, the Mackenzie River has a relatively large SPM load of 162.3 mg/L on average (n=118) with 2.4% (n=109) POC, and the $\Delta^{14}C$ is comparatively small with an average value of -571‰ (n=130) (Schwab et al., 2020; Holmes et al., 2021; Hilton et al., 2015; Campeau et al., 2020). In contrast, the Yenisei River only has an average sediment load of 5.7 mg/L (n=83) but with a much higher POC content of 17.4% (n=81) and a higher $\Delta^{14}C$ value of -264‰ (n=27) (Holmes et al., 2021). Therefore, lithology plays an important role by providing a substantial fraction of fossil OC (Hilton et al., 2015). Small Mountain Rivers in Taiwan and mountainous regions of Pan-Himalaya rivers show large SPM concentrations, low POC contents with low radiocarbon activities. These regions are with active tectonics, steep terrain, and intense precipitation, acting as sediment hotspots to the global sediment export by rivers (Milliman and Farnsworth, 2011). In the global context, the mechanism behind POC components and mineralization needs further comparative analysis on a given environmental control at inter and intra basin scale. MOREPOC provides a favorable basic data framework for the further comparison and investigation of riverine POC in different conditions from regional to global scale.

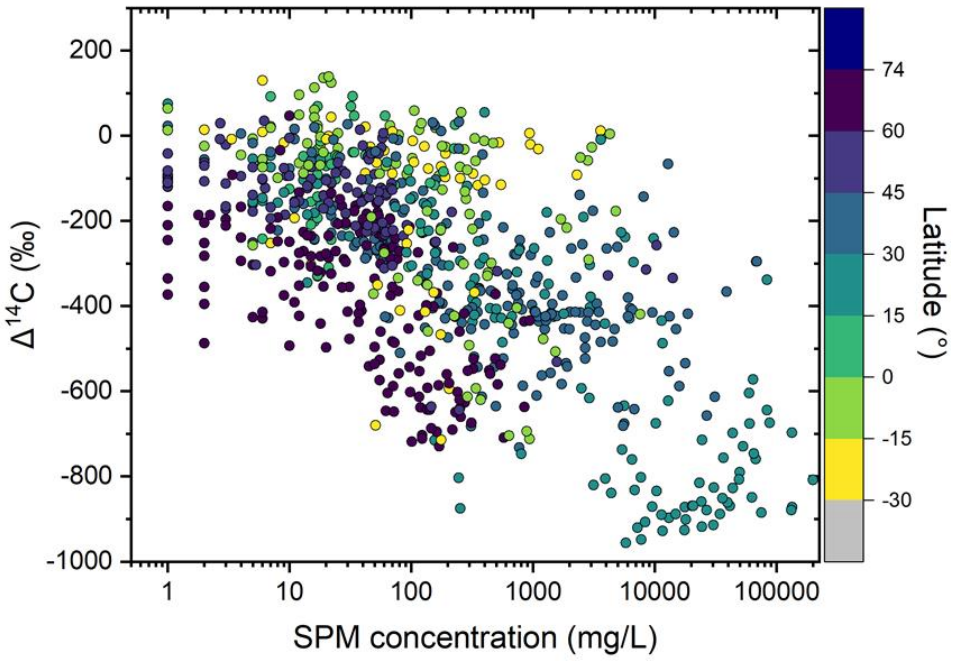

Fig. 5 Variation relation between SPM concentration and POC $\Delta^{14}C$ (n=812). Colors indicate latitudes of SPM samples; the SPM concentration plot uses a log metric scale. A general trend shows the depleting POC ^{14}C with the increasing SPM concentration.

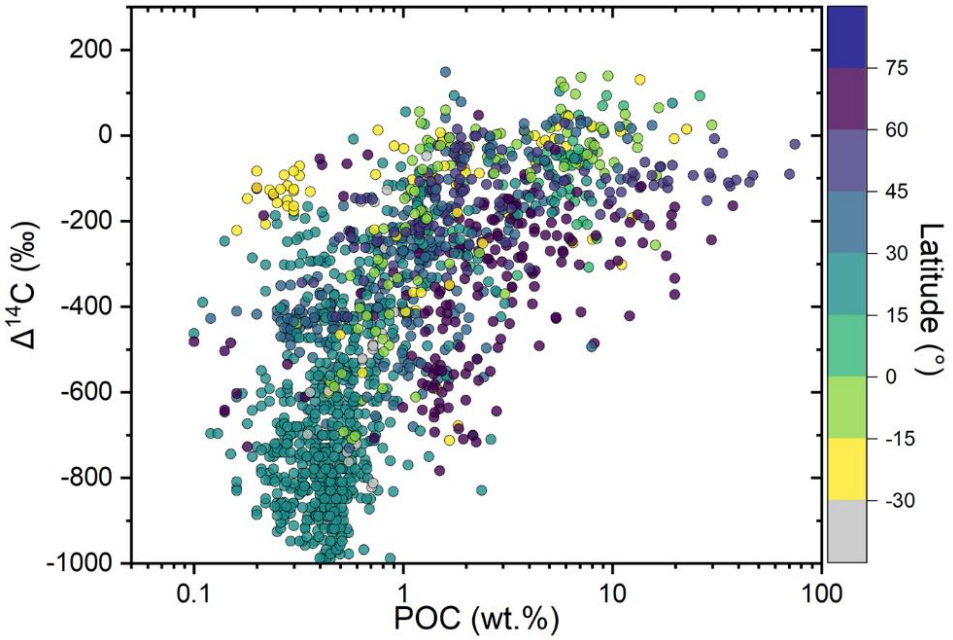

Fig. 6 Variation relation between POC content and $\Delta^{14}C$ (n=1,497). Colors indicate latitudes of SPM samples; the SPM concentration plot uses a log metric scale. A general pattern shows the depleting POC ^{14}C with the decreasing POC content.

4. Database availability

MOREPOC v1.0 database will be available at Zenodo in machine-readable format (.csv, mat), all map data layers, including attribute tables, are provided in ESRI Shapefile format. An ESRI application will be used to make a user-friendly web interface to visually present the data.

5. Conclusions

In this paper, we introduce MOREPOC, the largest and most comprehensive database focusing on riverine SPM and POC composition, including POC and TN content, stable carbon isotope (^{13}C), cosmogenic carbon isotope (^{14}C), as well as Al/Si mass ratios. MOREPOC benefits research on understanding basic characteristics of riverine POC sources, components, and transport processes. With the aid of the ocean sediment database, *i.e.*, CASCADE (Circum-Arctic Sediment Carbon DatabasE, Martens et al., 2021) and MOSAIC (Modern Ocean Sediment Archive and Inventory of Carbon, van der Voort et al., 2021), the fate of POC can be better constrained. Moreover, there are considerable mature environmental raster datasets at global scales concerning climate, geomorphology, lithology, tectonics, hydrology, and anthropology, and so on. Meanwhile, as the advancing of statistical analysis and machine learning models, it enables MOREPOC more potentials to help to quantitatively comprehend the complex coupled environmental driving forces on the nature of POC at large intra- and inter-basin scales. Future updating will incorporate bulk POC parameters from up-to-date literature, meanwhile, synthesize published data on molecular, thermal labile fractions, and specific components (black carbon, fossil carbon, etc) to provide more insight into the research on the alteration of riverine POC from source to sink, thus better constraining the carbon cycle.

6. Revisiting the riverine POC around the globe

This section is a separated section with the above MOREPOC dataset description, function as the extension to investigate the mechanism of possible environmental controls on the radiocarbon signatures of POC in global rivers.

6.1 Geospatial data collection and analysis

In this study, a set of well-established global-scale digital databases involving hydrology, geomorphology, geology and soils, climate, land cover and land use, anthropology was considered. River basin outline and subbasin information was extracted from the global HydroSHEDS database (15 arc-second, 500 m resolution). We take the advantage of HydroATLAS, a high-resolution global database providing a standardized compendium of hydro-environmental attribute information for all watersheds and rivers of the world (Linke et al., 2019). We extracted and compiled a series of environmental parameters of geomorphology, lithology, and soil, climate, and anthropogenic activity for each basin (See supplementary information 1 for the full raster list). Here, we focus on geomorphology (slope and stream gradient) and climate (air temperature and precipitation), the referred global rasters are as follows:

- EarthEnv-DEM90: elevation (meters, m), terrain slope (degrees, °), stream gradient (degrees, ° or decimeter per kilometer, dm/km) (Robinson et al., 2014);
- WorldClim v1.4: mean annual precipitation (MAP, millimeter per year [mm/yr]) and mean annual temperature (MAT, Celsius degrees [°C]) (Hijmans et al., 2005).

All geospatial analyses were performed in ArcGIS version 10.3 (ESRI Corporation) and QGIS version 3.18.

6.2 Classification of river systems

Based on the geometric sizes and geomorphic features of each basin, we classified the global river systems into three types, namely large rivers (LRs), small mountainous rivers (SMRs), and small plain rivers (SPRs). We arbitrarily define rivers with basin sizes less than 50,000 km^2 as small river systems, among which those with a mountain-dominated terrain and an average stream gradient of more than 100 dm/km (or 0.6°) are SMRs, while the remaining are SPRs dominated by plain, and hill geomorphic units. In

general, LRs should possess mountainous geomorphology in the upper reaches and fluvial plains in the lower reaches, besides with a basin area of more than 50,000 km^2. In this circumstance, there are 37 LRs, 39 SMRs, and 25 SPRs among the 101 river systems (the full list of rivers is in Table S1).

To better represent the overall characteristics of riverine POC in a given fluvial system, data points from SPM collected near or at the river mouth (less than 250 km) in LRs are kept for further calculation. While for SMRs and SPRs, all data points are kept, most SPM samples were collected downstream. We consider each sampling at a specific location on a specific date as an individual valid data point by calculating the corresponding average value, subsequently, we calculated the average value of these processed valid data to represent the overall signal of SPM and POC that is exported to the ocean by a given river system (Figure 7).

6.3 General properties of riverine POC around the globe

Fm ranges from 0.23 to1.09 (ca. -771‰ to 84‰, Figure 7A) and $\delta^{13}C$ ranges from -31.2‰ to -18.5‰ (Figure 7B). POC has relatively old radiocarbon ages in northern high-latitude Circum-Arctic rivers (*e.g.*, Mackenzie, Yukon, Kolyma) and low-latitude rivers in tectonically active mountain belts (*e.g.*, Pan-Himalayan rivers: upper reaches of Changjiang, Huanghe, Brahmaputra; SMRs in Taiwan and New Zealand orogens). While relatively young POC is from rivers in tropical savannah areas (*e.g.*, Zambezi, Tana) and in middle-latitude Europe and North America (*e.g.*, Mattaponi, Siuslaw, Meuse). Concerning POC $\delta^{13}C$, it also has very contrasted features between Circum-Arctic tundra and tropical savannah regions, the former is much more depleted in ^{13}C while the latter is significantly ^{13}C enriched. Rivers in orogens with steep terrains deliver relatively ^{13}C enriched POC as well, such as in Ganges-Brahmaputra fluvial system, SMRs in Taiwan and New Zealand, etc.

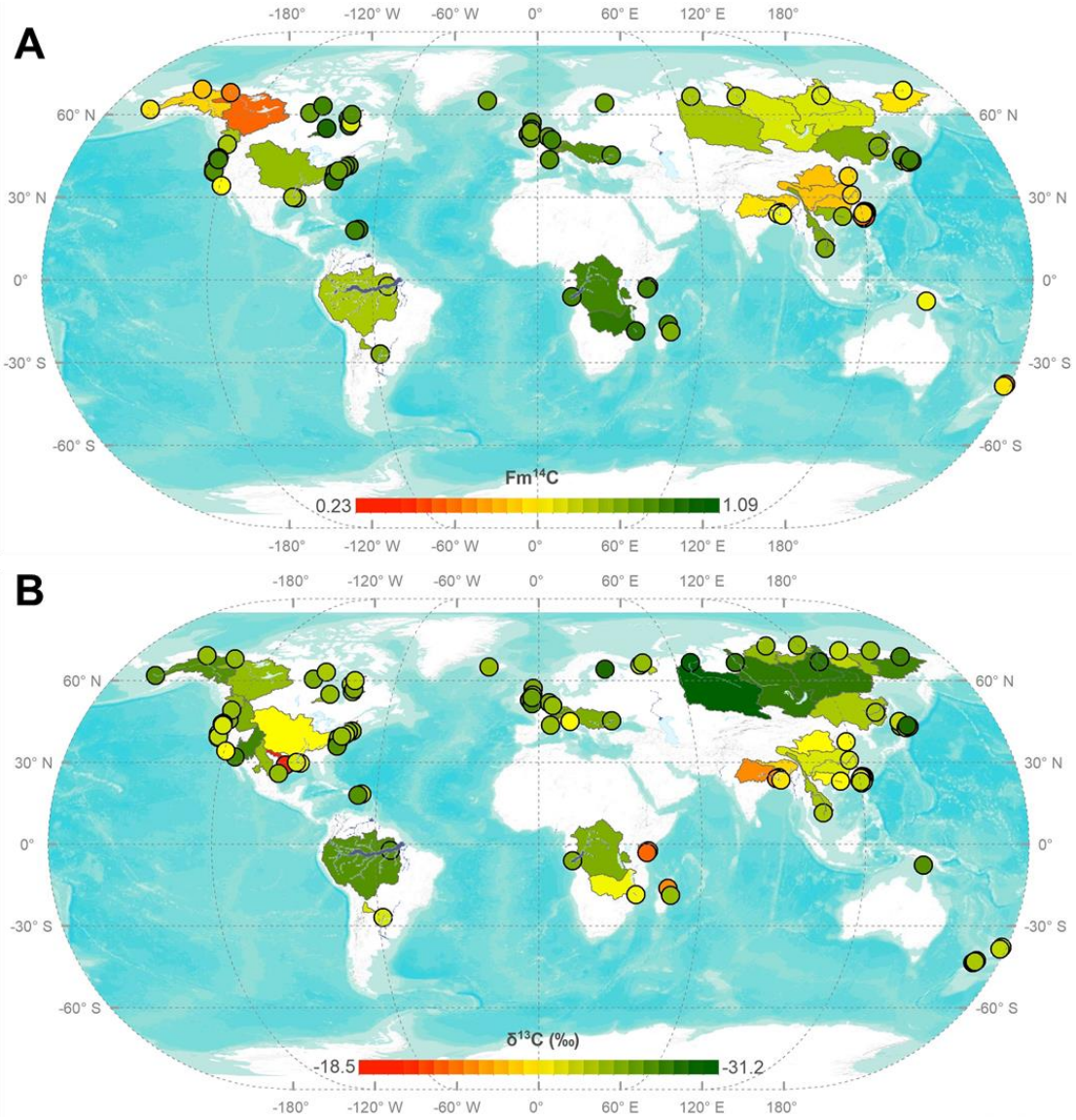

Fig. 7 Fraction modern (Fm) and Stable carbon isotope ($\delta^{13}C$) of riverine POC in global rivers. A) Fm; B) $\delta^{13}C$ values. Solid circles are located within river mouths and 250 km upstream. The colors of river basins and solid circles represent the corresponding average carbon isotopic values.

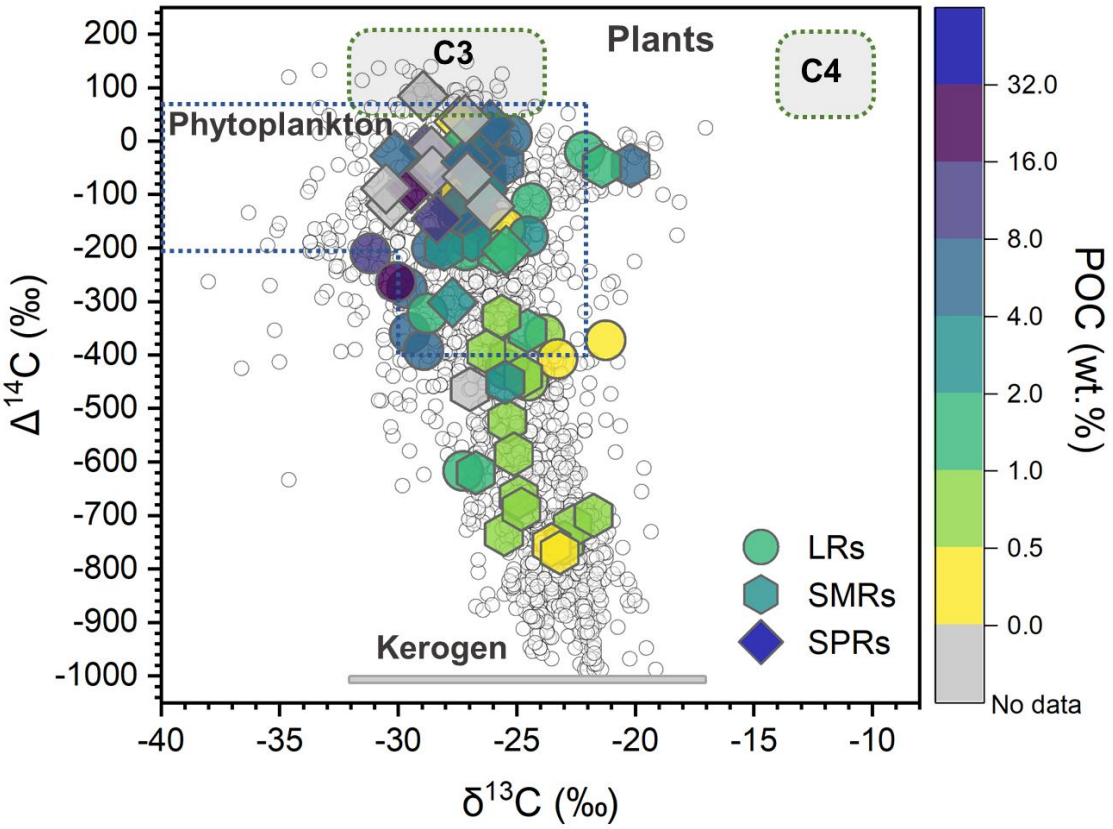

Fig. 8 The plot of $\delta^{13}C$ versus $\Delta^{14}C$ of POC in the global rivers. Colors indicate POC content (wt. %), shapes of points represent different types of river systems, open circles are data from MOREPOC v1.0. The $\Delta^{14}C$ of atmospheric CO_2 (206‰ – 40‰) is the record between 1985 and 2010 (Hua et al., 2013); the globally dominant modern C3- and C4- pathway plants have identical radiocarbon activity as that of atmospheric CO_2, whereas with $\delta^{13}C$ in the range of from -32‰ to -24‰ (Kohn, 2010) and from -14‰ to -10‰, respectively (Cerling et al., 1997). Stable and radiogenic carbon isotopic ranges of phytoplankton are from Marwick et al (2015). ^{14}C-dead (-1000‰) source is kerogen with $\delta^{13}C$ between -32‰ and -17‰ (Whiticar, 1996).

In general, global rivers deliver POC from modern to multi-millennia and to even over ten thousand years (Figure 8). Notably, some rivers (*e.g.*, Zambezi) have an average POC $\Delta^{14}C$ larger than 0, suggesting the incorporation of radiocarbon from atmospheric nuclear weapons testing, which could conceal the aged OC signatures and needs to be paid attention to (Hemingway et al., 2016). In the global context, the composition of riverine POC can be simply explained by a binary mixing of POC_{bio} and POC_{petro} (Blair et al., 2003; 2004; Galy et al., 2007; Hilton et al., 2008). As a fraction of POC_{bio}, the modern plant-derived OC (C3- and C4- pathway plant) set up an upper

limit for POC abundance and radiogenic activities, while POC_{petro} (kerogen or fossil OC) from the lithosphere (sedimentary and metamorphic rocks) acts to the contrary. As the degradation and mineralization as well as formation of organo-mineral aggregates going on, alteration and aging of OC continuously happen during the preservation in soils, where there are minor fractions of radiocarbon-dead POC_{petro} inherited from parent minerals. As a mixture of mainly C3 and C4 sourced OC, soil OC of varying ages is a major component of riverine POC (Tao et al., 2015; Blair and Aller, 2012; Leithold et al., 2006). Besides, the contemporary in-channel autochthonous production could contribute to riverine POC to a minor extent (Cole et al., 2007; Marwick et al., 2015; Wu et al., 2018). Under tectonic and climatic forcings, physical erosion rates vary among global river basins, controlling yields of POC_{bio} and POC_{petro} (Galy et al., 2015; Hilton, 2017), and influencing their relative proportions in the riverine transport, thus the elemental and isotopic signatures of POC. Generally, the intense physical erosion will result in high yields of POC, eventually favoring the sequestration of both POC_{bio} and POC_{petro} (Hilton and West, 2020).

There are systematic variations in elemental and dual carbon isotopic behaviors (represented by the average value) of POC among SMRs, LRs, and SPRs (Figure 9). Overall, compared to LRs, SMRs generally deliver more depleted and ancient POC with relatively more enriched ^{13}C. The average values for POC content, $\delta^{13}C$, and $\Delta^{14}C$ are 1.92 ± 2.13%, -25.3 ± 1.8‰, and -351 ± 280‰, respectively. On the contrary, SPM in SPRs are relatively enriched in POC of comparatively abundant ^{14}C and depleted ^{13}C. The average values for POC content, $\delta^{13}C$, and $\Delta^{14}C$ are 9.33 ± 11.71%, -27.8 ± 1.4‰, and -66 ± 85‰, respectively. Average values of the three POC parameters of LRs are in the middle of that between SMRs and SPRs, which are 3.74 ± 3.49% for POC content, -26.4 ± 2.6‰ for $\delta^{13}C$ and -233 ± 157‰ for $\Delta^{14}C$. In some SMRs, the very low $\Delta^{14}C$ values suggest the preferential mechanical erosion (*e.g.* landslide, gully erosion, glacier cutting) to unweathered rocks, bringing substantial petrogenic OC into the riverine transport, while the delivery of very young POC indicates the primary fraction from the biospheric sources including the recent degraded OC and modern discrete OC debris from a shallow erosion to soil (Leithold et al., 2006; Alin et al., 2008; Godin et al., 2017; Hilton, 2017; Blair and Aller, 2012; Hilton and West, 2020). In general, SPRs transport very young POC ($\Delta^{14}C$ > -200‰, ca. 1,800 yrs before present), showing a dominant young POC_{bio} fraction that is eroded from the surface

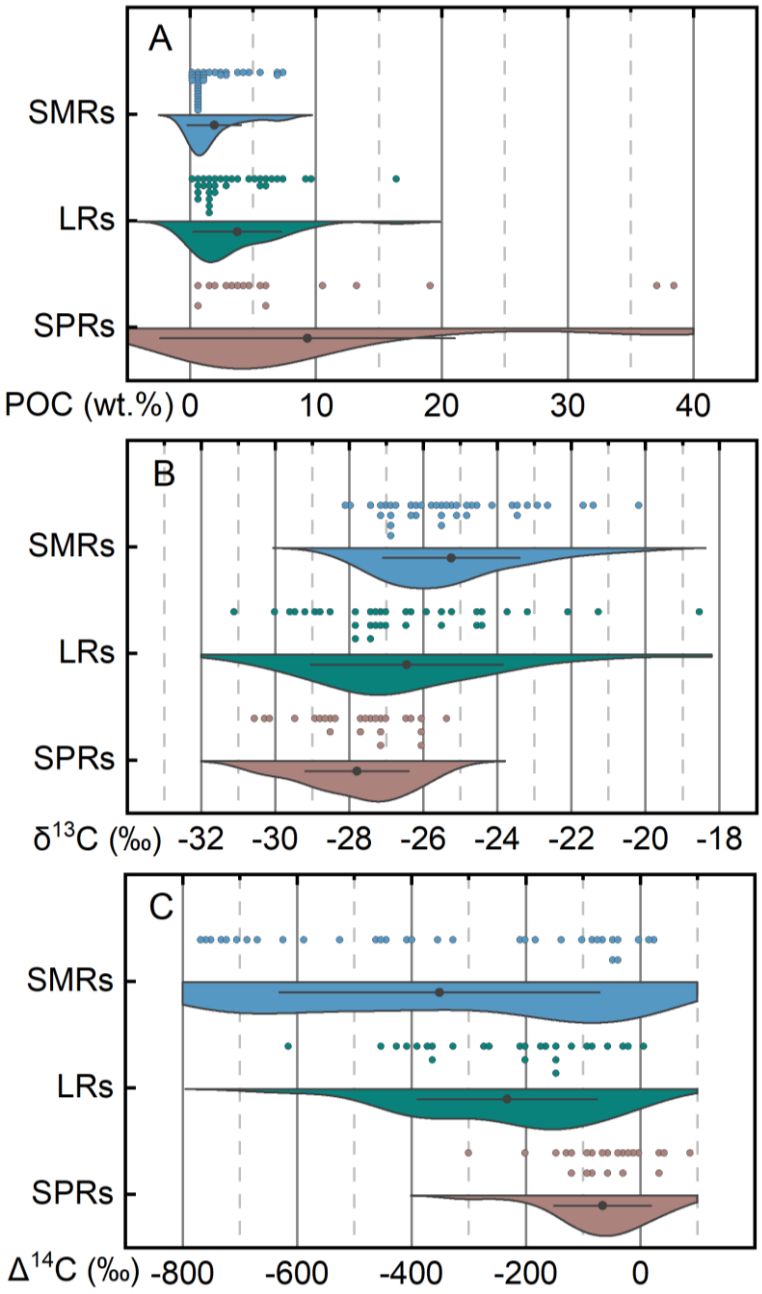

Fig. 9 Summarization and statistic distribution of elemental composition and dual carbon isotopes of POC in SMRs, LRs, and SPRs. A) POC content (wt.%); B) $\delta^{13}C$; C) $\Delta^{14}C$. Circles represent the corresponding values of each POC parameter of global rivers systems; blue, green, and brown represents SMRs, LRs, and SPRs, respectively. Black dots with error bars are the averaged statistics with one uncertainty of the three types of river systems.

and shallow horizons of soils, such as POC from rivers around the Hudson Bay in Canada and small rivers in Britain such as Dee and Conwy (Godin et al., 2017; Adam

et al., 2015). The climate and geomorphology in SMRs and SPRs should be less complicated compared to that of LRs, each factor could have a dramatic impact on the POC yields and components due to the small basin size. LRs usually have more intense physical erosion in the upper mountainous regions of the main channel and major tributaries, and with external supplies of OC from a weaker erosion to the lower plain regions (*e.g.*, Amazon, Mayorga et al., 2005). The POC in the river mouth is a very complex integration of OC from different sources that go through varying extents of chemical and physical alterations during the fluvial transit. As the classification of different river systems is based on geomorphic features, which could be partially responsible for the systematic differences in POC characteristics.

6.4 Geomorphology, climate, and tectonics

In this section, the relationships between geomorphic features (terrain slope and stream gradient) and climatic parameters (MAT and MAP) with the radiocarbon of exported POC by global rivers are investigated. Overall, both terrain slope and stream gradients present a clear inverse relationship with $\Delta^{14}C$ values (Figure 10). However, this pattern seems to be mainly regulated by SMRs and is not obvious in SPRs (Figure 11). Meanwhile, it can be observed that POC is generally depleted in rivers characterized by high gradients. SMRs in Taiwan (Liwu, Chenyoulan, Hualian rivers) and New Zealand (Waiho, Fox rivers) orogens have the highest gradients and POC of the most depleted ^{14}C, while SPRs around the Hudson Bay (Winisk, Nastapoka rivers) and in Britain (Dee, Conwy rivers) have the lowest gradients and the most abundant POC ^{14}C. Radiocarbon of POC in rivers of very low relief (*e.g.*, less than 0.5° for stream gradient and less than 5.0° for terrain slope) is not sensitive to the weak variation of gradients, other factors should play a more important role in POC regulation.

Eglinton et al (2020) reported that temperature and precipitation exert primary controls on biospheric-carbon turnover within river basins by identifying their inverse relationships with both the catchment biospheric SOC turnover and biomarker ^{14}C ages of different types of fluvial sediments. In Figure 12, we hypothesize POC $\Delta^{14}C$ values are in a multi-linear function with both the MAT and the MAP, which has distinct discrepancies with the linear correlation presented in Eglinton et al (2020). We suppose this discrepancy is mainly owing to the incorporation of petrogenic organic matter to varying degrees. Looking into the SPRs of similar topographic features around the

Hudson Bay, these continental passive margin exported rivers are observed a sensitive response of the POC $\Delta^{14}C$ to the climate change especially the temperature, a higher MAP and MAT both result in a younger POC delivery. Comparatively, SMRs in Taiwan orogens have contrasted draining environment in terms of geomorphology (steep slopes) and tectonics (active tectonics), POC $\Delta^{14}C$ still sensitively responds to climate change with a similar pattern, and this correlation pattern also occurs among LRs systems at passive continental margins, for example, the Circum-Arctic riverine POC is getting younger with a higher MAP and MAP. We assume river basins with similar geomorphic and tectonic features, the POC radiocarbon signatures are mainly drove by the climate. A steeper terrain and more active tectonic activities enhanced the potential of mechanical erosion to bedrock when coupled with intensive precipitation and higher temperature (Figure 12). In pan-Himalayas LRs systems, Changjiang and Ganges-Brahmaputra have higher MAP and MAT compared to permafrost LRs, but the delivered POC is comparatively old due to a significant fraction contributed by the intensive erosion to upper steep and active mountain belts. However, other factors are exerting a significant impact on the POC composition revealed by the radiocarbon activity, such as lithology and anthropogenic activities, etc. Mackenzie transports the most ancient POC among LRs, which is mainly attributed to the dominant contribution of petrogenic OC from vastly distributed organic-rich shales (Hilton et al., 2015; Horan et al., 2019) coupled with aged-OC from erosion to the thawing permafrost and riverbank (Feng et al., 2013; Vonk et al., 2015). Huanghe is also a special case (see Chapter 3), over 90% of the POC load originates from the massive loess regions due to the gigantic contribution of unconsolidated materials in the Chinese Loess Plateau. Even though it is estimated to have a relatively fast SOC turnover (ca. 34 years, see Table S1), the riverine POC is significantly old. Meanwhile, it is worth pointing out that the release of deeper permafrost and peat OC and mobilization of deeper loess-paleosol sequence OC, might both respond positively to a global warming climate, increased temperature and precipitation will together enhance the relatively aged OC transfer into fluvial systems, and the final burial in ocean sediments. Anthropogenic perturbation impacts the natural source-to-sink delivery of POC to a large extent (Maavara et al., 2017; Best, 2019). Changjiang (see Chapter 4) is largely regulated by the massive building of dams, extensive mining and constructions, deforestation, etc. during the last several decades. Dominated by the drastic-channel blocking and temporal-sediment trapping by densely distributed dams in the upper reaches,

Changjiang has experienced dramatically sediment load reduction in the after-dam transport and the final exported load to oceans, thus impacting the POC greatly as well. POC that can be delivered to oceans is becoming younger due to the dam-building. Under the current human-driven global warming, we estimate a universal shortening of SOC turnover time and intensified physical erosion, finally resulting in the accelerated transfer of atmospheric CO_2 to the terrestrial biosphere and the final sequestration in ocean sediment, which should be an Earth's self-regulation of climate.

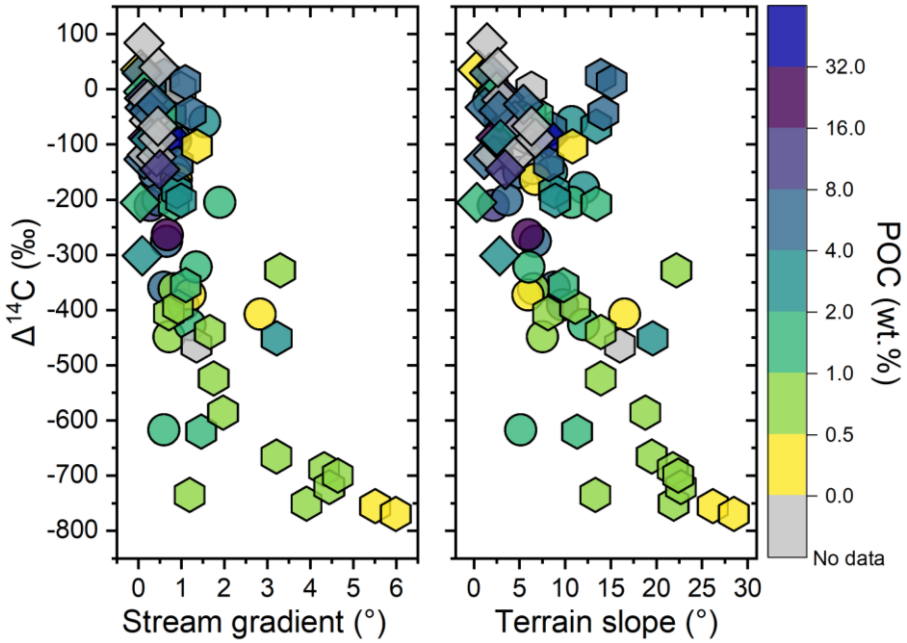

Fig. 10 Relationships between stream gradient, terrain slope with the average POC $\Delta^{14}C$ around the globe. Colors indicate POC content (wt. %), shapes of points represent different types of river systems.

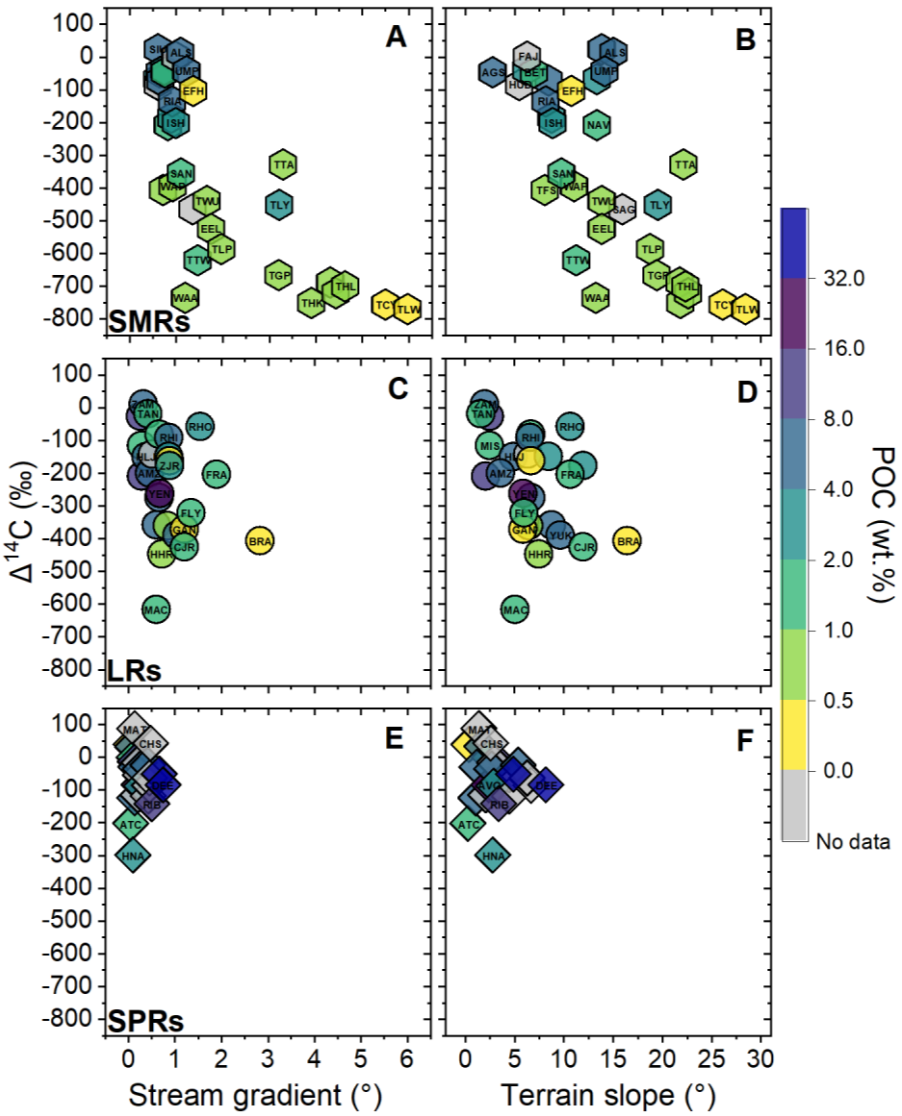

Fig. 11 Relationships between stream gradient, terrain slope with the average POC $\Delta^{14}C$ in global large rivers. Colors indicate POC content (wt. %), shapes of points represent different types of river systems: SMRs (A, B), LRs (C, D), SPRs (E, F).

Rivers export POC containing information of OC over the watershed, together with the developed environmental data rasters on broad spatial scales, enabling great potentials to assess possible controls on riverine POC delivery. Temperature and precipitation exert strong control on the ages and compositions of POC, both high temperature and precipitation favor the transport of young POC due to enhanced erosion to the SOC of short turnovers over their watersheds. A steep topography within the watershed provides an advantageous environment for erosion and mobilization to petrogenic OC from weathered and unweathered bedrocks. Besides, active tectonics, for example, mountain building generally results in steep terrain associated active

seismic activities, landslides, resulting in an increased transfer of terrestrial OC into fluvial systems. Lithology and anthropogenic activities are important, it is necessary to build quantitative correlations to examine how each factor interplays in regulating the terrestrial transport of organic matter by rivers to better constrain the organic carbon cycle from past to future.

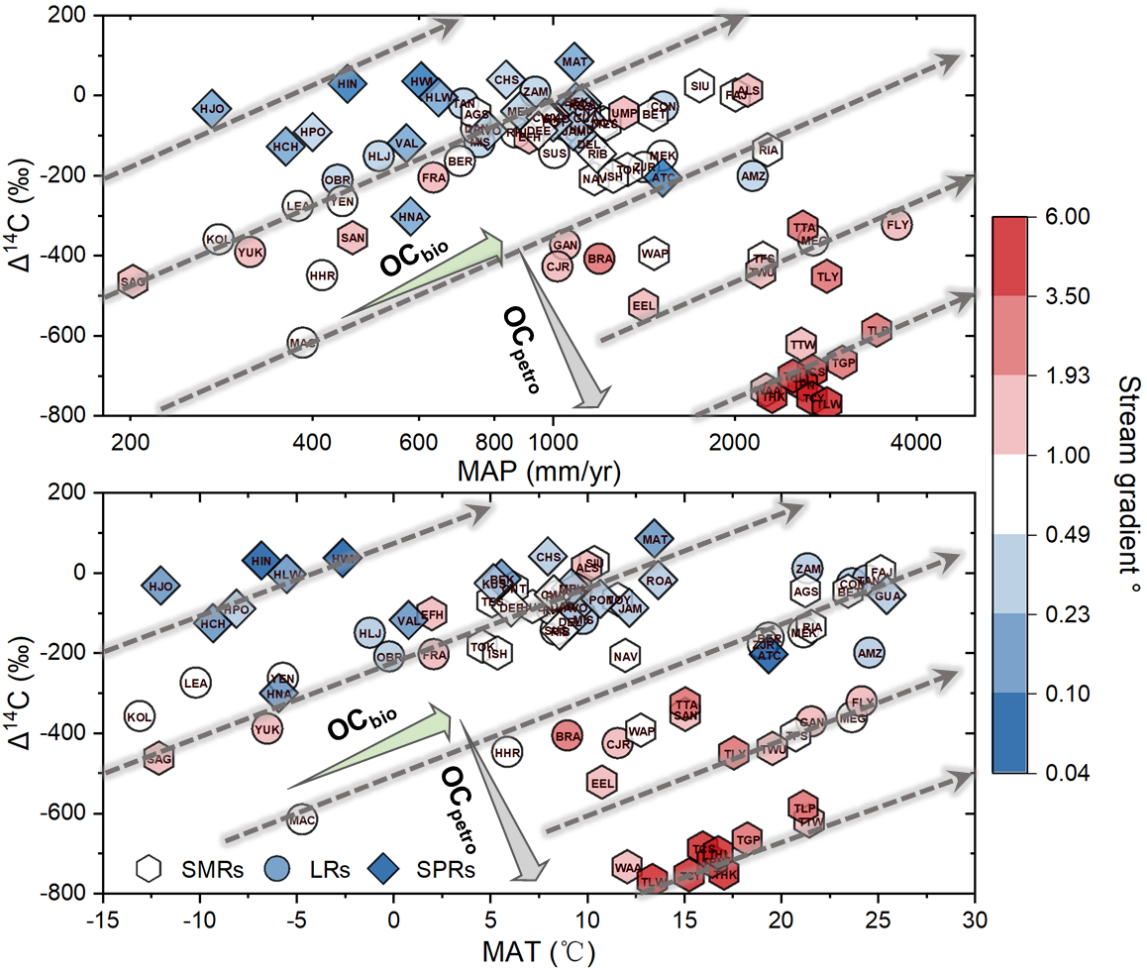

Fig. 12 Relationships between MAP, MAT with the POC $\Delta^{14}C$ in global rivers. In MAP-$\Delta^{14}C$ and MAT-$\Delta^{14}C$ plots, colors indicate stream gradients, intervals are determined using a probability distribution. Shapes of points represent different types of river systems. Grey dot lines with arrows stand for the hypothesized multi-linear variation trend, the green arrows indicate the enhanced erosion to biospheric OC (OC_{bio}), and the grey arrows indicate the enhanced erosion to petrogenic OC (OC_{petro}).

6.5 Fluvial POC loading

Riverine POC is a complex mixture of produced and decomposed organic carbon from discrete organic particles and rock-eroded minerals, chemical and physical properties of SPM together exert a control on the relative abundance of POC (Galy et al., 2008b; Blair and Aller, 2012; Bouchez et al., 2014). It is widely recognized that POC can be interspersed across all particle sizes of the riverine load, with a general pattern showing OC enrichment in fine fractions and OC depletion in coarse factions because a finer particle can offer a larger mineral surface area which can usually load more POC (*e.g.*, Bouchez et al, 2014; Keil et al., 1997; Galy et al., 2008b). Aside from the specific area of mineral particles and particle sizes, the mineralogy of SPM is a key factor that determines POC loading. There are very strong relationships between very fine-grained minerals and organic matter in sediments, Al-Fe oxyhydroxides and phyllosilicates (micrometer-sized aluminosilicate minerals/clay minerals) are particularly important in the stabilization of organic matter (Keil, 2014). Al/Si ratio is a proxy for particle size and mineralogy of SPM, a higher Al/Si generally indicates a more clay-rich nature and finer particles while a lower Al/Si commonly has a more quartz-rich nature and coarser particles. Inferred from the vertical depth profile sampling of SPM from the channel surface to bottom, finer particles are usually delivered in the surface with a younger POC indicating a biospheric OC assemblage, while coarser particles prone to the river bottom with a petrogenic radiocarbon-dead endmember (Bouchez et al., 2014; Galy et al., 2007). In SPM of large rivers around the globe, it shows an obvious broad positive relationship between Al/Si and POC content at either a catchment scale or a global scale (Figure 13). However, the Al/Si-POC correlation intensity (slope) among different basins varies to a great extent, indicating the varying POC loading (Galy et al., 2008b). For example, POC contents increase sharply in the Heilongjiang while gently in the Huanghe with the increase of Al/Si ratios. The slope defined by the correlation between Al/Si and POC in sediments of Ganges is likely to set a lower limit for the global compilation. In addition, this variation also exists among different tributaries and channel sections within an independent fluvial system, such as in Ganges-Brahmaputra, Amazon, and Changjiang, etc. (Galy et al., 2008b, Bouchez et al., 2014; Ke et al., unpublished data). Each river system is characterized by different POC loading mechanisms.

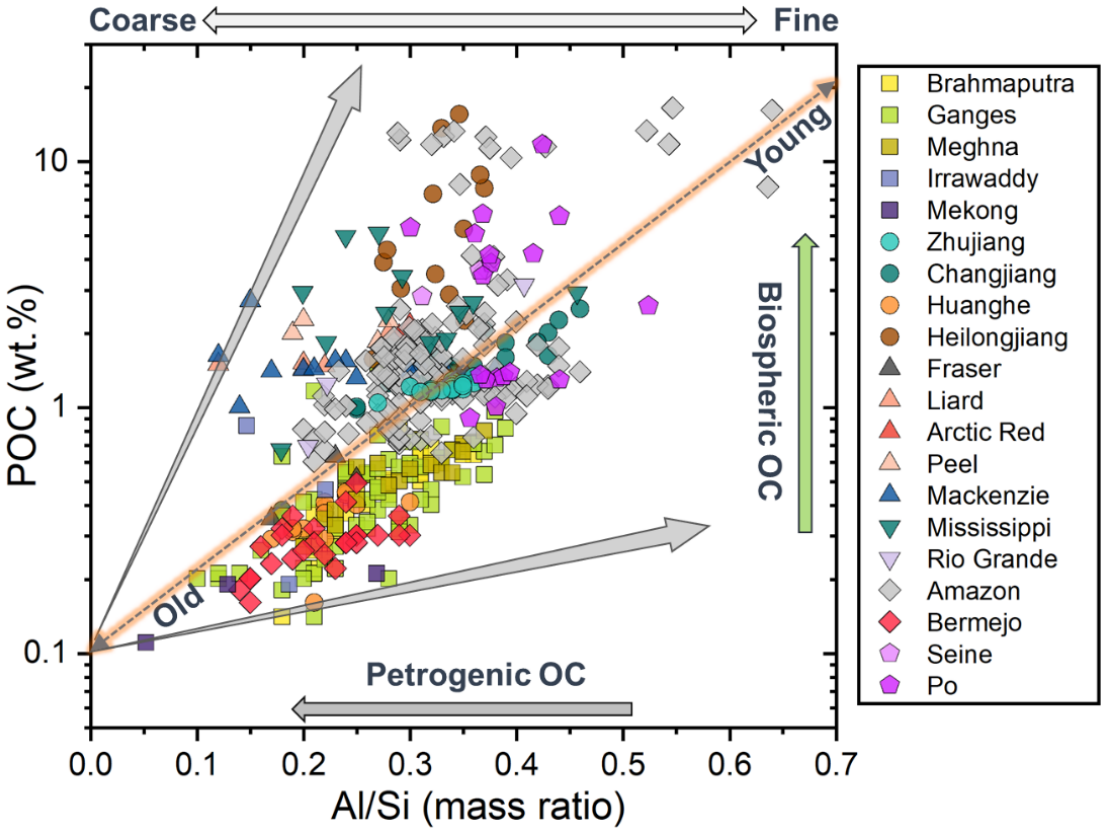

Fig. 13 Relationships between Al/Si mass ratios and POC content of suspended load in global large rivers. POC content is plotted using the log metric scale. Each river is marked with an independent color, squares represent major pan-Himalaya rivers, circles are the four largest Chinese rivers, upward triangles are rivers in northern North America, inverted triangles are rivers in southern North America, parallelograms are rivers in South America, and pentagons are rivers in Europe. The slope of POC-Al/Si in each large river represents the corresponding POC loading (Galy et al., 2008b), the orange shaded line represents the best fit for the entire dataset using linear regression, representing the global averaged POC loading. Two grey arrows are estimated boundaries for the data distribution and POC loading using the upper and lower exterior data points. The high Al/Si and POC content are prone to young biospheric OC, while the low Al/Si and POC content are prone to ancient petrogenic OC. Rivers in high-latitude permafrost regions deliver SPM with low Al/Si but high POC, representing the aged biospheric endmember from the thawing permafrost. Data from Aucour et al. (2006), Galy et al. (2007; 2008b), Galy and Eglinton. 2011; Li et al., (2015); Qu et al. (2020); Voss (2014); Hilton et al. (2015); Bouchez et al. (2014); Scheingross et al. (2021); Hossain et al. (2017); Guinoiseau et al. (2016); Davide et al. 2003; Canfield. (1997).

To the first order, the contrasting environmental condition in each river system could result in a complex coupled effect on POC loading by altering components of terrestrial materials, especially discrete organic matter and minerals within the basin and the fraction that will be transferred into the river delivery. Secondly, the temporal hydrodynamic within river channels could yield a contrasted segregation effect on particles, which leads to mineral and organic carbon sorting. To be more specific, mineral phases within the basin reflects weathering and thus climate, geomorphological and sediment recycling factors (Gaillardet et al., 1999), climate is a major factor that controls the turnover of soil OC, a longer turnover time favors some OC fraction becoming strongly bound to pedogenic minerals (Eglinton et al., 2021; Kögel-Knabner et al., 2008; Hemingway et al., 2019). Soil OC as a primary fraction of riverine POC is observed from high-latitude permafrost rivers to low-latitude tropical rivers (Guo et al., 2007; Tao et al., 2015; Marwick et al., 2015). However, the major clay-sized minerals vary among different basins, Fe-oxyhydroxides are the dominant clay-sized minerals in Siberian permafrost soil, Al-oxyhydroxides and clay mineral are relatively depleted (Kawahigashi et al., 2006), highly possible to result in relatively low Al/Si ratios, which is confirmed by the report of Tipper et al (2021) that SPM Al/Si is ca. 0.20 for the Yenisei and ca. 0.24 for Ob'. We infer POC loading should be high in SPM of Circum-Arctic rivers even though Al/Si ratios are low due to the input of discrete biospheric OC and mineral-bound organic aggregates. However, POC content may be inversely correlated with Al/Si ratio in these large Circum-Arctic rivers, the reason is that the rapid oxidation of the abundant discrete biospheric OC in the low-concentrated SPM (Wild et al., 2019). In addition, we propose to look into Fe-related proxies (*e.g.*, Fe/Si) to infer the mineral protection to POC and the corresponding maximum efficiency in these permafrost rivers in future research. While in tropical rivers in Amazon, OC preservation is likely protected by Al-oxyhydroxides and phyllosilicates (*e.g.*, smectite), resulting in high POC loading with high Al/Si (Aucour et al., 2006; Bouchez et al., 2014). Meanwhile, clay-sized SPM in the Congo River was observed to contain POC derived from much older carbon pools (Spencer et al., 2012). It is commonly assumed that mainly young organic material is discharged from flat tropical watersheds due to their extensive plant cover and rapid carbon turnover. Aside from the anoxic environment in wetlands, effective mineral protection can provide a reasonable explanation due to high Al/Si (mass ratio: 0.46; Tipper et al., 2021). In the tectonic active mountainous belts, the POC content is low because the preferable erosion to bed

rocks create substantial quartz-rich clastic, resulting in the low fraction of clay size minerals in the SPM. Even though discrete organic particles such as plant debris could carry substantial OC contributing to riverine POC (Galy et al., 2008b; Alin et al. 2008), it could be diluted by the fossil OC from denudated materials by mechanical weathering (Blair and Aller, 2012). The dilution effect could be elevated by a largely enhanced physical erosion rate, which will directly contribute a progressively larger fraction of POC from bedrock erosion via deep gully incision (Leithold et al., 2016; Galy et al., 2015; Hilton, 2017). For small mountainous rivers in Taiwan and New Zealand orogens, we estimate an equal or lower POC loading compared to that of the Ganges due to the extremely high sediment yield. Even though terrestrial erosion determines inorganic minerals and organic carbon delivered in the fluvial system, POC will go through physical loss and chemical oxidation along the source-to-sink delivery pathway. It is crucial to explore the information revealed by the correlation between the organic carbon aboundance and the inorganic mineral proxy Al/Si ratio, *i.e.*, the occurrence (mineral protection, mineral surface attachement, mineral aggregation or discreted form, etc) of POC speciations (*e.g.*, OC_{bio} and OC_{petro}) in sediments, the oxidation rate of POC during transportation, the possible burial efficiency of POC in the ocean environment.

Acknowledgment

This projected was study was financially supported by the Agence Nationale de la Recherche (ANR) SEDIMAN (Grant ANR-15-CE01-0012), the authors acknowledge the Ph.D. scholarship awarded to Yutian Ke (No. 201706180008) by the China Scholarship Council.

Reference

Aucour, A. M., France-Lanord, C., Pedoja, K., Pierson-Wickmann, A. C., and Sheppard, S. M. (2006). Fluxes and sources of particulate organic carbon in the Ganga-Brahmaputra River system. Global Biogeochemical Cycles, 20(2).

Best, J. (2019). Anthropogenic stresses on the world's big rivers. Nature Geoscience, 12(1), 7-21.

Berner, R. A. (2003). The long-term carbon cycle, fossil fuels and atmospheric composition. Nature, 426(6964), 323-326.

Blair, N. E., and Aller, R. C. (2012). The fate of terrestrial organic carbon in the marine

environment. Annual Review of Marine Science, 4, 401-423.

Blair, N. E., Leithold, E. L., and Aller, R. C. (2004). From bedrock to burial: the evolution of particulate organic carbon across coupled watershed-continental margin systems. Marine Chemistry, 92(1-4), 141-156.

Blair, N. E., Leithold, E. L., Brackley, H., Trustrum, N., Page, M., and Childress, L. (2010). Terrestrial sources and export of particulate organic carbon in the Waipaoa sedimentary system: Problems, progress and processes. Marine Geology, 270(1-4), 108-118.

Blair, N. E., Leithold, E. L., Ford, S. T., Peeler, K. A., Holmes, J. C., and Perkey, D. W. (2003). The persistence of memory: The fate of ancient sedimentary organic carbon in a modern sedimentary system. Geochimica et Cosmochimica Acta, 67(1), 63-73.

Canfield, D. E. (1997). The geochemistry of river particulates from the continental USA: Major elements. Geochimica et Cosmochimica Acta, 61(16), 3349-3365.

Carvalhais, N., Forkel, M., Khomik, M., Bellarby, J., Jung, M., Migliavacca, M., ... and Reichstein, M. (2014). Global covariation of carbon turnover times with climate in terrestrial ecosystems. Nature, 514(7521), 213-217.

Cerling, T. E., Harris, J. M., MacFadden, B. J., Leakey, M. G., Quade, J., Eisenmann, V., and Ehleringer, J. R. (1997). Global vegetation change through the Miocene/Pliocene boundary. Nature, 389(6647), 153-158.

Cohen, S., Kettner, A. J., and Syvitski, J. P. (2014). Global suspended sediment and water discharge dynamics between 1960 and 2010: Continental trends and intra-basin sensitivity. Global and Planetary Change, 115, 44-58.

Cole, J. J., Prairie, Y. T., Caraco, N. F., McDowell, W. H., Tranvik, L. J., Striegl, R. G., ... and Melack, J. (2007). Plumbing the global carbon cycle: integrating inland waters into the terrestrial carbon budget. Ecosystems, 10(1), 172-185.

Davide, V., Pardos, M., Diserens, J., Ugazio, G., Thomas, R., and Dominik, J. (2003). Characterisation of bed sediments and suspension of the river Po (Italy) during normal and high flow conditions. Water Research, 37(12), 2847-2864.

Eglinton, T. I., Galy, V. V., Hemingway, J. D., Feng, X., Bao, H., Blattmann, T. M., ... and Zhao, M. (2021). Climate control on terrestrial biospheric carbon turnover. Proceedings of the National Academy of Sciences, 118(8).

Feng, X., Vonk, J. E., Van Dongen, B. E., Gustafsson, Ö., Semiletov, I. P., Dudarev, O. V., ... and Eglinton, T. I. (2013). Differential mobilization of terrestrial carbon pools

in Eurasian Arctic river basins. Proceedings of the National Academy of Sciences, 110(35), 14168-14173.

Galy, V., and Eglinton, T. (2011). Protracted storage of biospheric carbon in the Ganges–Brahmaputra basin. Nature Geoscience, 4(12), 843-847.

Galy, V., Beyssac, O., France-Lanord, C., and Eglinton, T. (2008a). Recycling of graphite during Himalayan erosion: A geological stabilization of carbon in the crust. Science, 322(5903), 943-945.

Galy, V., France-Lanord, C., and Lartiges, B. (2008b). Loading and fate of particulate organic carbon from the Himalaya to the Ganga–Brahmaputra delta. Geochimica et Cosmochimica Acta, 72(7), 1767-1787.

Galy, V., France-Lanord, C., Beyssac, O., Faure, P., Kudrass, H., and Palhol, F. (2007). Efficient organic carbon burial in the Bengal fan sustained by the Himalayan erosional system. Nature, 450(7168), 407-410.

Galy, V., Peucker-Ehrenbrink, B., & Eglinton, T. (2015). Global carbon export from the terrestrial biosphere controlled by erosion. Nature, 521(7551), 204-207.

Gaillardet, J., Dupré, B., Louvat, P., and Allegre, C. J. (1999). Global silicate weathering and CO_2 consumption rates deduced from the chemistry of large rivers. Chemical geology, 159(1-4), 3-30.

Guinoiseau, D., Bouchez, J., Gélabert, A., Louvat, P., Filizola, N., and Benedetti, M. F. (2016). The geochemical filter of large river confluences. Chemical Geology, 441, 191-203.

Guo, L., Ping, C. L., and Macdonald, R. W. (2007). Mobilization pathways of organic carbon from permafrost to arctic rivers in a changing climate. Geophysical Research Letters, 34(13).

Hilton, R. G., and West, A. J. (2020). Mountains, erosion and the carbon cycle. Nature Reviews Earth and Environment, 1(6), 284-299.

Hilton, R. G., Galy, A., Hovius, N., Chen, M. C., Horng, M. J., and Chen, H. (2008). Tropical-cyclone-driven erosion of the terrestrial biosphere from mountains. Nature Geoscience, 1(11), 759-762.

Hilton, R. G., Galy, A., Hovius, N., Horng, M. J., and Chen, H. (2011). Efficient transport of fossil organic carbon to the ocean by steep mountain rivers: An orogenic carbon sequestration mechanism. Geology, 39(1), 71-74.

Hilton, R. G., Galy, V., Gaillardet, J., Dellinger, M., Bryant, C., O'Regan, M., ... & Calmels, D. (2015). Erosion of organic carbon in the Arctic as a geological carbon

dioxide sink. Nature, 524(7563), 84-87.

Hilton, R. G., Gaillardet, J., Calmels, D., & Birck, J. L. (2014). Geological respiration of a mountain belt revealed by the trace element rhenium. Earth and Planetary Science Letters, 403, 27-36.

Holmes, R.M., J.W. McClelland, S.E. Tank, R.G.M. Spencer, and A.I. Shiklomanov. 2021. Arctic Great Rivers Observatory. Water Quality Dataset, Version 20210608. https://www.arcticgreatrivers.org/data

Horan, K., Hilton, R. G., Dellinger, M., Tipper, E., Galy, V., Calmels, D., ... and Burton, K. W. (2019). Carbon dioxide emissions by rock organic carbon oxidation and the net geochemical carbon budget of the Mackenzie River Basin. American Journal of Science, 319(6), 473-499.

Hossain, H. Z., Kawahata, H., Roser, B. P., Sampei, Y., Manaka, T., and Otani, S. (2017). Geochemical characteristics of modern river sediments in Myanmar and Thailand: implications for provenance and weathering. Geochemistry, 77(3), 443-458.

Hua, Q., Barbetti, M., and Rakowski, A. Z. (2013). Atmospheric radiocarbon for the period 1950–2010. Radiocarbon, 55(4), 2059-2072.

Ittekkot, V. (1988). Global trends in the nature of organic matter in river suspensions. Nature, 332(6163), 436-438.

Kawahigashi, M., Kaiser, K., Rodionov, A., and Guggenberger, G. (2006). Sorption of dissolved organic matter by mineral soils of the Siberian forest tundra. Global Change Biology, 12(10), 1868-1877.

Kögel-Knabner, I., Guggenberger, G., Kleber, M., Kandeler, E., Kalbitz, K., Scheu, S., ... and Leinweber, P. (2008). Organo-mineral associations in temperate soils: Integrating biology, mineralogy, and organic matter chemistry. Journal of Plant Nutrition and Soil Science, 171(1), 61-82.

Kohn, M. J. (2010). Carbon isotope compositions of terrestrial C3 plants as indicators of (paleo) ecology and (paleo) climate. Proceedings of the National Academy of Sciences, 107(46), 19691-19695.

Komada, T., Anderson, M. R., and Dorfmeier, C. L. (2008). Carbonate removal from coastal sediments for the determination of organic carbon and its isotopic signatures, $\delta^{13}C$ and $\Delta^{14}C$: comparison of fumigation and direct acidification by hydrochloric acid. Limnology and Oceanography: Methods, 6(6), 254-262.

Lawrence, C. R., Beem-Miller, J., Hoyt, A. M., Monroe, G., Sierra, C. A., Stoner, S., ...

and Wagai, R. (2020). An open-source database for the synthesis of soil radiocarbon data: International Soil Radiocarbon Database (ISRaD) version 1.0. Earth System Science Data, 12(1), 61-76.

Leithold, E. L., Blair, N. E., and Perkey, D. W. (2006). Geomorphologic controls on the age of particulate organic carbon from small mountainous and upland rivers. Global Biogeochemical Cycles, 20(3).

Leithold, E. L., Blair, N. E., and Wegmann, K. W. (2016). Source-to-sink sedimentary systems and global carbon burial: A river runs through it. Earth-Science Reviews, 153, 30-42.

Li, G., Wang, X. T., Yang, Z., Mao, C., West, A. J., and Ji, J. (2015). Dam-triggered organic carbon sequestration makes the Changjiang (Yangtze) river basin (China) a significant carbon sink. Journal of Geophysical Research: Biogeosciences, 120(1), 39-53.

Ludwig, W., Probst, J. L., and Kempe, S. (1996). Predicting the oceanic input of organic carbon by continental erosion. Global Biogeochemical Cycles, 10(1), 23-41.

Maavara, T., Lauerwald, R., Regnier, P., and Van Cappellen, P. (2017). Global perturbation of organic carbon cycling by river damming. Nature communications, 8(1), 1-10.

Martens, J., Romankevich, E., Semiletov, I., Wild, B., van Dongen, B., Vonk, J., ... and Gustafsson, Ö. (2021). CASCADE–The Circum-Arctic Sediment CArbon DatabasE. Earth System Science Data, 13(6), 2561-2572.

Mayorga, E., Seitzinger, S. P., Harrison, J. A., Dumont, E., Beusen, A. H., Bouwman, A. F., ... and Van Drecht, G. (2010). Global nutrient export from WaterSheds 2 (NEWS 2): model development and implementation. Environmental Modelling and Software, 25(7), 837-853.

Meybeck, M. (1993). Riverine transport of atmospheric carbon: sources, global typology and budget. Water, Air, and Soil Pollution, 70(1), 443-463.

Petsch S. T. (2014). Weathering of organic carbon: Treatise on Geochemistry, Second Edition, 12, 217-238.

Qu, Y., Jin, Z., Wang, J., Wang, Y., Xiao, J., Gou, L. F., ... and Xu, X. (2020). The sources and seasonal fluxes of particulate organic carbon in the Yellow River. Earth Surface Processes and Landforms, 45(9), 2004-2019.

Scheingross, J. S., Repasch, M. N., Hovius, N., Sachse, D., Lupker, M., Fuchs, M., ... and Schleicher, A. M. (2021). The fate of fluvially-deposited organic carbon during

transient floodplain storage. Earth and Planetary Science Letters, 561, 116822.

Schidlowski, M. (1988). A 3,800-million-year isotopic record of life from carbon in sedimentary rocks. Nature, 333(6171), 313-318.

Schefuß, E., Eglinton, T. I., Spencer-Jones, C. L., Rullkötter, J., De Pol-Holz, R., Talbot, H. M., ... and Schneider, R. R. (2016). Hydrologic control of carbon cycling and aged carbon discharge in the Congo River basin. Nature Geoscience, 9(9), 687-690.

Shi, Z., Allison, S. D., He, Y., Levine, P. A., Hoyt, A. M., Beem-Miller, J., ... and Randerson, J. T. (2020). The age distribution of global soil carbon inferred from radiocarbon measurements. Nature Geoscience, 13(8), 555-559.

Stuiver, M., and Polach, H. A. (1977). Discussion reporting of ^{14}C data. Radiocarbon, 19(3), 355-363.

Van der Voort, T. S., Blattmann, T. M., Usman, M., Montluçon, D., Loeffler, T., Tavagna, M. L., ... and Eglinton, T. I. (2020). MOSAIC (Modern Ocean Sediment Archive and Inventory of Carbon). Earth System Science Data Discussions.

Vonk, J. E., Tank, S. E., Bowden, W. B., Laurion, I., Vincent, W. F., Alekseychik, P., ... and Wickland, K. P. (2015). Reviews and syntheses: Effects of permafrost thaw on Arctic aquatic ecosystems. Biogeosciences, 12(23), 7129-7167.

Voss, B. M. (2014). Spatial and temporal dynamics of biogeochemical processes in the Fraser River, Canada: A coupled organic-inorganic perspective (Doctoral dissertation, Massachusetts Institute of Technology).

Wild, B., Andersson, A., Bröder, L., Vonk, J., Hugelius, G., McClelland, J. W., ... and Gustafsson, Ö. (2019). Rivers across the Siberian Arctic unearth the patterns of carbon release from thawing permafrost. Proceedings of the National Academy of Sciences, 116(21), 10280-10285.

Supplementary information S1

The extracted environmental rasters for each river basin are as follows:

- WaterGAP v2.2: water discharge (cubic meters per second, m^3/s), land surface runoff (millimeters, mm) (Döll et al., 2003);
- EarthEnv-DEM90: elevation (meters, m), terrain slope (degrees, °), stream gradient (degrees, ° or decimeter per kilometer, dm/km) (Robinson et al., 2014);
- WorldClim v1.4: mean annual precipitation (MAP, millimeter per year [mm/yr]) and mean annual temperature (MAT, Celsius degrees [°C]) (Hijmans et al., 2005);
- SoilGrids1km: fractions (%) of clay, silt, and sand in soils (Hengl et al., 2014);
- GloSEM v1.2: soil erosion rate (kilogram per square kilometer per year: $kg/km^2/yr$) (Borrelli et al. 2017).
- Soil organic carbon within one-meter depth: soil organic carbon storage (kilograms carbon per square kilometer, kg C/km^2), radiocarbon activity of soil organic carbon ($\Delta^{14}C$, per mil ‰), and turnover times (years, yrs), gross primary production (GPP, ton carbon per square kilometer per year, $tC/km^2/yr$), net primary production (NPP, $tC/km^2/yr$) (Shi et al., 2020; Carvalhais et al., 2014);
- GLiM (covering percent of sedimentary lithology units, including siliciclastics, carbonate, and unconsolidated materials, %, (Hartmann and Moosdorf 2012);
- GLC2000: anthropogenic fraction (covering percent of cropland and urban area of the terrain, %) (Bartholomé and Belward, 2005);
- GRanD v1.4: degree of regulation (Lehner et al. 2011).

Table. S1 Summary of average basic parameters of POC and SPM exported to the estuary by global rivers.

River system	River	ID	River type	Continent	SPM mg/L	POC mg/L	POC %	$\delta^{13}C_{POC}$ ‰	$\Delta^{14}C_{POC}$ ‰	Age yr BP	Fm	N %	C/N mass ratio
Athi-Galana-Sabaki	Athi-Galana-Sabaki	AGS	SMRs	Africa	2137.1	50.0	7.58	-20.2	-46.5	533	0.96		
Betsiboka	Betsiboka	BET	SMRs	Africa	1978.8	15.5	1.95	-21.4	-47.8	591	0.96		
Congo	Congo	CON	LRs	Africa	16.4	1.1	9.72	-27.5	-28.0	448	0.98	0.80	12.4
Rianila	Rianila	RIA	SMRs	Africa	38.2	2.2	7.01	-27.2	-136.1	1866	0.87		
Tana	Tana	TAN	LRs	Africa	2961.0	51.8	1.92	-22.1	-20.4	143	0.99		
Zambezi	Zambezi	ZAM	LRs	Africa	37.9	1.7	7.41	-25.2	9.4		1.02		
Brahmaputra	Brahmaputra	BRA	LRs	Asia	2346.6	7.7	0.48	-23.2	-408.5	4247	0.59		
Changjiang	Changjiang	CJR	LRs	Asia	81.3	1.0	1.37	-25.5	-427.4	4781	0.57	0.19	7.7
Ganges	Ganges	GAN	LRs	Asia	1250.7	6.0	0.49	-21.2	-373.6	5324	0.63		
Heilongjiang	Heilongjiang	HLJ	LRs	Asia	60.8	2.1	6.15	-26.5	-151.5	1263	0.86	1.34	5.8
Huanghe	Huanghe	HHR	LRs	Asia	2995.5	16.9	0.56	-24.5	-449.5	4882	0.55	0.09	5.7
Indigirka	Indigirka	IND	LRs	Asia	170.0	3.5	2.06	-27.4				0.24	8.5
Irrawaddy	Irrawaddy	IRR	LRs	Asia									
Japan rivers	Teshio	TES	SMRs	Asia	35.2	1.5	4.76	-26.2	-71.9	703	0.93	0.62	8.4
Japan rivers	Tokachi	TOK	SMRs	Asia	34.3	0.7	2.98	-26.9	-185.7	1614	0.82	0.33	8.2
Japan rivers	Ishikari	ISH	SMRs	Asia	101.9	1.9	2.87	-28.0	-202.4	1803	0.80		
Japan rivers	Bekanbeushi	BEK	SPRs	Asia	20.9	2.1	10.36	-28.8	-16.8	820	0.99	0.66	15.6
Japan rivers	Kushiro	KUS	SPRs	Asia	10.9	0.5	6.03	-30.1	-28.0	176	0.98		
Khatanga	Khatanga	KHA	LRs	Asia	42.4	1.2	3.23	-27.3				0.36	9.2
Kolyma	Kolyma	KOL	LRs	Asia	47.6	0.8	6.65	-29.5	-359.8	3704	0.64	1.29	7.1
Lena	Lena	LEA	LRs	Asia	30.3	0.9	5.73	-29.6	-276.3	2573	0.73	0.75	8.4
Meghna	Meghna	MEG	LRs	Asia	1063.1	5.1	0.56	-23.8	-362.5	3265	0.67		19.7
Mekong	Mekong	MEK	LRs	Asia	113.3	1.8	2.42	-26.4	-150.5	1460	0.86	0.25	9.5
Ob'	Ob'	OBR	LRs	Asia	34.7	1.4	9.06	-31.2	-211.1	1863	0.79	1.12	8.1
Olenyok	Olenyok	OLE	LRs	Asia	25.7	1.0	5.48	-27.2				0.74	8.6
Taiwan rivers	Fonshan	TFS	SMRs	Asia	500.0	3.4	0.67	-25.3	-407.0	4155	0.60		
Taiwan rivers	Tsengwen	TTW	SMRs	Asia	12900.0	63.2	1.15	-26.7	-622.0	7772	0.38	0.21	4.9
Taiwan rivers	Wu	TWU	SMRs	Asia	3900.0	26.5	0.68	-24.7	-441.0	4629	0.56		
Taiwan rivers	Linpien	TLP	SMRs	Asia			0.83	-25.1	-587.2	7354	0.42	0.14	5.6
Taiwan rivers	Gaoping	TGP	SMRs	Asia	3600.0	20.9	0.56	-24.9	-667.2	10017	0.34	0.10	5.1
Taiwan rivers	Lanyang	TLY	SMRs	Asia	6041.4	39.1	2.39	-25.5	-452.5	8227	0.55		
Taiwan rivers	Taan	TTA	SMRs	Asia			0.92	-25.6	-329.2	3382	0.68	0.09	8.0

Taiwan rivers	Hsiukuluan	THK	SMRs	Asia			0.69	-23.0	-752.5	14077	0.25	0.10	6.2
Taiwan rivers	Choshui	TCS	SMRs	Asia	76776.9	225.5	0.56	-24.8	-690.1	10861	0.31	0.11	5.5
Taiwan rivers	Peinan	TPN	SMRs	Asia			0.53	-22.6	-722.6	12782	0.28	0.09	5.6
Taiwan rivers	Hualien	THL	SMRs	Asia			0.54	-21.7	-701.7	11236	0.30	0.06	8.6
Taiwan rivers	Chenyoulan	TCY	SMRs	Asia			0.47	-23.5	-757.3	12210	0.24	0.08	5.6
Taiwan rivers	Liwu	TLW	SMRs	Asia	27241.3	66.9	0.29	-23.1	-771.4	13040	0.23	0.05	6.2
Taiwan rivers	Erhjen	TEJ	SPRs	Asia			2.77	-26.1				0.49	4.9
Yana	Yana	YAN	LRs	Asia	48.9	1.2	3.62	-26.3				0.33	10.7
Yenisei	Yenisei	YEN	LRs	Asia	5.9	0.4	16.43	-30.1	-264.3	2471	0.74	2.18	7.4
Zhujiang	Zhujiang	ZJR	LRs	Asia	31.9	1.2	2.95	-24.5	-179.0	1632	0.83	0.61	8.1
British rivers	Conwy	CWY	SPRs	Europe	2.7	1.0	37.27	-28.7	-55.6	540	0.95		
British rivers	Dee	DEE	SPRs	Europe	0.9	0.3	38.25	-27.7	-88.6	686	0.92		
British rivers	Avon	AVO	SPRs	Europe	8.1	1.6	19.06	-29.4	-88.5	683	0.92		
British rivers	Cottage	CHS	SPRs	Europe				-27.1	39.0	484	1.05		
British rivers	Ribble	RIB	SPRs	Europe	29.4	2.5	13.01	-28.4	-146.4	1231	0.86		
Danube	Danube	DAN	LRs	Europe	48.6	0.8	1.73	-27.9	-83.0	704	0.92		
Efri Haukadals	Efri Haukadals	EFH	SMRs	Europe			0.40	-27.4	-104.2	833	0.90		
Meuse	Meuse	MEU	SPRs	Europe			4.40	-27.1	-40.0	286	0.97		
Mezen	Mezen	MEZ	LRs	Europe	209.3	1.8	0.85	-25.9				0.06	13.2
Po	Po	POR	LRs	Europe	4.9	0.2	5.06	-24.4				0.93	5.6
Rhine	Rhine	RHI	LRs	Europe			4.67	-27.8	-93.0	742	0.91		
Rhone	Rhone	RHO	LRs	Europe			2.90	-27.0	-59.3	2165	0.95		
Valipuro	Valipuro	VAL	SPRs	Europe		1.5		-30.3	-119.7	969	0.89		
Vizhas	Vizhas	VIZ	SPRs	Europe	214.3	0.9	0.41	-27.1				0.03	12.4
Alsea	Alsea	ALS	SMRs	N. America	61.1	3.3	7.14	-26.1	12.4	245	1.02	0.54	15.1
Atchafalaya	Atchafalaya	ATC	SPRs	N. America	184.0		1.50	-25.4	-206.0	1841	0.80	0.19	10.2
Brazos	Brazos	BRZ	LRs	N. America			1.21	-18.5				0.12	11.8
Colorado	Colorado	COL	LRs	N. America	36.6	7.8	1.44	-29.2				0.04	61.3
Columbia	Columbia	CLB	LRs	N. America	39.3			-27.8					10.6
Connecticut	Connecticut	CNT	SMRs	N. America			3.84	-27.1	-39.8	814	0.97	0.37	12.1
Delaware	Delaware	DEL	SPRs	N. America		0.5		-26.1	-122.8	1193	0.88		
Eel	Eel	EEL	SMRs	N. America	1578.8	15.1	0.93	-25.4	-525.4	6023	0.48	0.07	13.1
Fraser	Fraser	FRA	LRs	N. America	40.6	0.5	1.80	-27.1	-205.5	1885	0.80	0.20	9.6
Hudson	Hudson	HUD	SMRs	N. America		0.5		-28.0	-86.2	1142	0.93		5.9
Hudson	Winisk	HWI	SPRs	N. America	1409.1	6.2	0.44	-27.4	35.0	0	1.04		
Hudson	Innuksuac	HIN	SPRs	N. America	2.7	0.2	5.93	-26.1	29.2	0	1.04		

Hudson	Nastapoka	HNA	SPRs	N. America	5.3	0.2	3.21	-27.7	-303.0	2839	0.70		
Hudson	Little Whale	HLW	SPRs	N. America	10.0	0.2	1.90	-27.2	-4.9	0	1.00		
Hudson	Churchill	HCH	SPRs	N. America	11.0	0.5	4.86	-27.5	-128.1	2839	0.88		
Hudson	Josephine	HJO	SPRs	N. America	8.4	0.5	5.36	-26.5	-33.5	215	0.97		
Hudson	Povungnituk	HPO	SPRs	N. America	3.4	0.1	3.82	-26.4	-91.8	715	0.91		
James	James	JAM	SPRs	N. America		0.2		-30.5	-89.5	753	0.92		
Mackenzie	Mackenzie	MAC	LRs	N. America	187.6	4.3	1.60	-27.2	-618.4	7878	0.38	0.19	9.7
Mississippi	Mississippi	MIS	LRs	N. America	118.9	1.6	1.41	-24.4	-117.0	1400	0.84	0.20	9.3
Navarro	Navarro	NAV	SMRs	N. America			1.29	-25.8	-208.6	1840	0.80	0.09	14.4
Noyo	Noyo	NOY	SMRs	N. America			2.39	-26.3	-67.9	683	0.94	0.13	18.6
Potmac	Potomac	POT	SPRs	N. America				-27.1	-67.4	522	0.94		
Rio Grande	Rio	RIO	LRs	N. America	251.0			-27.0					10.4
Roanoke	Roanoke	ROA	SPRs	N. America				-28.6	-19.9	471	0.99		
Sag	Sag	SAG	SMRs	N. America				-26.9	-465.5	4975	0.54		
Santa Clara	Santa	SAN	SMRs	N. America	14126.6	133.6	1.50	-24.5	-356.0	4052	0.65	0.17	9.1
Siuslaw	Siuslaw	SIU	SMRs	N. America			5.76	-27.0	23.8	0	1.03	0.29	20.0
Susquehanna	Susquehanna	SUS	LRs	N. America				-27.4	-144.1	1218	0.88		
Umpqua	Umpqua	UMP	SMRs	N. America	145.2	4.1	4.29	-25.5	-44.0	305	0.96	0.41	12.2
York	Mattaponi	MAT	SPRs	N. America		1.4		-28.9	83.7	0	1.09		16.3
Yukon	Yukon	YUK	LRs	N. America	222.5	2.3	6.99	-28.9	-391.7	4067	0.61	0.48	17.5
Fly	Fly	FLY	LRs	Oceania	323.7	3.5	1.36	-28.7	-323.1	3099	0.68	0.14	8.7
NZE rivers	Whataroa	WHA	SMRs	Oceania	93.3	0.5	0.59	-26.9				0.03	17.7
NZE rivers	Waipaoa	WAP	SMRs	Oceania			0.72	-26.3	-395.4	4405	0.61	0.06	12.7
NZE rivers	Waiapu	WAA	SMRs	Oceania			0.58	-25.5	-736.8	10861	0.27	0.05	12.2
NZE rivers	Poerua	POE	SMRs	Oceania	390.0	1.3	0.35	-23.7				0.02	16.7
NZE rivers	Waitangitanoa	WAT	SMRs	Oceania	57.0	0.4	0.66	-25.2				0.03	19.0
NZE rivers	Hokitika	HOK	SMRs	Oceania	14.5	0.1	0.78	-26.9				0.05	15.5
NZE rivers	Fox	FOX	SMRs	Oceania	119.0	0.3	0.29	-23.5				0.03	10.5
NZE rivers	Waiho	WAH	SMRs	Oceania	56.5	0.1	0.27	-24.2				0.03	9.8
Amazon	Amazon	AMZ	LRs	S. America	87.9	1.6	5.92	-28.6	-201.4	2887	0.80	1.32	7.5
Fajardo	Fajardo	FAJ	SMRs	S. America		2.1		-26.4	0.5	240	1.01		
Guanica	Guanica	GUA	SPRs	S. America		14.2		-28.5	-57.5	427	0.95		
Parana	Bermejo	BER	LRs	S. America			0.28	-25.5	-163.9	1374	0.84	0.04	7.5

Notice: NZE, New Zealand; N. America, North Americ; S. America, South America

To be continued.

ID	Slope	Stream gradient	MAT	MAP	Erosion rate	SC	SS	τ	SD	SOCS	SD	SRCA	SD	NPP	SD	GPP	SD
	°	dm/km	℃	mm/yr	kg/km^2	%	%			kgC/m^2		RCA		kgC/m^2		kgC/m^2	
AGS	2.9	113	21.3	748	61.9	1.21	9.97	19	9.7	21	9	2356	374	0.75	0.45	1.51	0.93
BET	7.1	132	23.5	1471	0.2			132	16.9	93	12	4644	475	1.22	0.50	2.58	1.11
CON	2.6	46	23.7	1527	18.4	0.01	15.90	10	2.7	9	2	1874	458	1.07	0.64	2.21	1.38
RIA	8.3	160	21.6	2275	17.0		3.48	15	2.5	15	3	2413	533	2.32	0.19	4.77	0.32
TAN	1.7	73	24.5	713	42.3		2.93	16	5.7	19	8	2886	1689	0.70	0.19	1.40	0.38
ZAM	2.1	55	21.4	938	38.0	0.23	9.63	10	2.7	10	3	2039	646	2.84	0.62	6.27	1.63
BRA	16.6	496	9.0	1198	91.5	2.10	12.48	48	42.9	50	42	3325	1816	1.34	1.06	2.76	2.18
CJR	12.1	211	11.6	1020	89.8	17.17	28.58	23	20.9	25	24	3822	5072	1.11	0.14	2.24	0.27
GAN	6	212	21.6	1051	115.2	1.61	11.84	19	36.2	19	37	2762	1426	1.76	0.10	3.69	0.25
HLJ	5	66	-1.2	516	8.6	0.44	16.63	48	14.6	45	15	5419	2560	1.20	0.08	2.47	0.14
HHR	7.6	125	5.9	416	36.4	3.93	21.44	34	20.1	37	22	4918	3782	1.71	0.38	3.64	0.81
IND	9.7	127	-16.2	266	54.8	4.15	24.04	205	41.4	172	44	16107	1959	1.17	0.60	2.43	1.24
IRR	10.1	305	21.8	1700	44.4	8.01	25.31	13	3.6	14	4	2132	504	1.37	0.86	2.79	1.76
TES	8.6	117	5.1	1230	10.7	4.48	0.29	29	6.2	27	7	2995	423	0.53	0.10	1.07	0.20
TOK	8.9	157	4.6	1334	45.3		72.96	16	0.7	16	1	2069	525	1.26	1.29	2.99	3.03
ISH	9	174	5.4	1263	7.6		92.71	17	1.4					1.52	0.56	3.42	1.31
BEK	3.4	26	5.6	1095	15.6		48.89	16	2.7					0.16	0.03	0.33	0.04
KUS	5.5	74	5.2	1113	36.8		0.15	11	0.8	11	1	2428	313	2.06	1.53	4.91	3.66
KHA	4.9	115	-13.6	328	8.1	21.47	25.39	227	44.7	192	53	12861	2543	1.61	0.23	3.37	0.54
KOL	8.9	105	-13.1	280	18.9	5.43	20.48	183	42.8	134	42	15574	3325	1.29	0.01	2.70	0.02
LEA	6.8	116	-10.2	379	10.7	21.24	27.79	111	52.8	86	45	12704	3217	1.64	0.21	3.43	0.42
MEG	6.6	147	23.7	2711	75.8		40.22	11	2.7	11	3	2645	685	1.82	1.29	3.62	2.56
MEK	8.6	151	21.2	1522	64.9	5.78	14.00	17	14.6	17	16	2685	2226	0.79	0.17	1.60	0.35
OBR	2.2	49	-0.2	441	2.3	5.27	15.96	71	39.7	63	43	4843	1986	0.47	0.12	0.93	0.25
OLE	4.6	90	-13.2	272	2.0	55.93	13.97	185	34.1	162	33	14489	2491	1.43	0.30	2.98	0.67
TFS	8.2	126	20.8	2236	40.9		48.31	39	3.9	42	5	2584	244	1.46	1.36	3.39	3.16
TTW	11.4	257	21.5	2589	55.0		13.74	10	3.6	8	6	3249	554	0.00	1.71	0.01	4.11
TWU	14	291	19.6	2220	74.7	0.20	2.99	49	15.2	49	15	6766	1979	1.61	0.93	3.55	2.06
TLP	18.9	345	21.2	3451	35.8							2240	565	2.42		5.82	
TGP	19.6	562	18.3	3029	28.2		64.71	18	3.8					1.13		2.47	
TLY	19.7	565	17.6	2855	59.4			128	1.5	99	5	3549	187	0.89	0.31	1.81	0.65
TTA	22.3	579	15.1	2605	37.8			62	17.1	64	18	7367	2005	2.02	0.26	4.26	0.57
THK	22	686	17.1	2317	73.5		0.68	119	27.9	128	32	5719	2710	1.90	0.28	4.01	0.48
TCS	21.9	757	16.0	2700	3.6		94.28	13	0.0					2.33		5.17	

TPN	22.8	779	16.5	2603	35.1		5.39	117	26.7	126	31	5543		1.91	0.14	4.04	0.32
THL	22.5	814	16.8	2507	62.0		80.49	18	1.4	17	1	1703		2.56	1.81	5.94	4.20
TCY	26.3	966	15.3	2698	57.9	1.02	0.03					1432		2.35	0.71	5.38	1.73
TLW	28.6	1051	13.4	2857	67.0		3.91					2650		1.82	1.23	4.01	2.78
TEJ	2.8	31	23.7	2153	11.4	8.15	39.20	13	1.4	13	2	1720	364	2.56	0.17	5.48	0.40
YAN	9	134	-16.8	272	41.7	1.08	18.19	180	48.2	165	45	16062	2104	0.53	0.00	1.05	0.01
YEN	6	119	-5.7	449	5.2	14.22	16.68	87	50.9	69	38	8704	2892	1.49	0.17	3.12	0.35
ZJR	12.1	155	19.1	1419	72.5	40.04	19.54	13	3.6	14	4	2267	535	1.13	0.11	2.29	0.22
CWY	5	117	8.3	975	34.4		8.56	36	4.8	40	5	2743	274				
DEE	8.3	131	6.1	949	3.0	51.42	12.48	17	1.8	17	2	3303	520	0.95	0.42	1.94	0.89
AVO	2.5	40	9.4	783	0.1		0.42	79	13.0	74	9	3509	230	1.68	0.38	3.68	0.89
CHS	2.7	84	8.0	839	1.2			289	76.3	154	95	11756	876	1.02	0.81	2.29	1.90
RIB	3.5	89	8.6	1187	36.8		0.02	30	10.4	17	7	2041	529	1.13		2.47	
DAN	6.8	115	8.7	748	13.9	18.07	35.65	22	7.0	23	7	2970	808	1.54	0.44	3.19	0.88
EFH	10.9	240	2.0	916	7.9	28.52	40.78	29	5.4	24	3	2626	1628	0.41	0.06	0.83	0.11
MEU	2.8	46	9.2	885	1.9		0.43	139	22.1	54	16	9680	906	0.29	0.03	0.58	0.05
MEZ	2.5	51	-0.8	575	0.1		3.12	73	22.8	53	14	4009	400	1.08	0.44	2.21	0.94
POR	12.4	362	9.3	1012	43.1	24.24	2.68	20	7.8	23	9	3014	1282	0.74	0.08	1.62	0.16
RHI	6.7	151	8.2	871	10.2	24.43	14.19	24	11.8	25	14	2649	1149	0.79	0.34	1.76	0.83
RHO	10.8	270	8.5	1018	29.7	35.99	8.48	25	11.2	27	16	3080	1420	3.14	0.71	7.36	1.68
VAL	2.2	37	0.8	574	3.4			258	48.7	184	27	11081	1291	0.28	0.02	0.58	0.01
VIZ	1.1	21	-0.9	504	2.8	33.01	23.79	17	3.7	17	4	2391	427	0.49	0.31	0.98	0.66
ALS	15.2	192	10.0	2109	56.8		93.97	17	1.6	16	2	2373	473	1.46	1.36	3.39	3.16
ATC	0.4	8	19.4	1526	7.9	9.09	51.10	27	21.0	26	21	1850	603	1.98	0.98	4.27	2.11
BRZ	1	29	17.4	708	20.7	6.40	24.93	25	7.6	28	9	3036	715	2.20	1.09	4.71	2.32
COL	6.4	171	11.2	325	19.6	5.44	44.99	27	13.1			3192	1057	0.38	0.21	0.78	0.43
CLB	11.4	283	5.2	616	17.3	5.13	19.08	31	12.5			1275	1751	0.85	0.12	1.87	0.27
CNT	6.3	131	6.2	1137	8.5	0.10	12.36	13	1.1	12	1	2138	57	2.14	0.11	4.49	0.21
DEL	4.6	75	9.1	1148	21.0		79.63	15	2.0			0	0	0.36	0.03	0.73	0.06
EEL	14	308	10.8	1418	42.0		80.83	17		16		2023	435	2.72		6.29	
FRA	10.8	331	2.1	636	12.1	3.39	17.39	46	28.0					2.21		4.79	
HUD	5.6	108	7.2	1118	6.7		7.60	37	4.0	37	4	2578	230	2.56	1.81	5.94	4.20
HWI	0.5	11	-2.6	607	0.2		0.27	114	38.2	45	21	4544	1157	1.11	0.38	2.25	0.78
HIN	1.8	16	-6.8	458	119.7		8.13	19	8.4	25	10	2300	416	1.32	0.07	2.90	0.10
HNA	2.9	18	-5.9	583	12.6		4.28	36	2.5	38	3	2598	794	1.82	1.28	3.61	2.55
HLW	2.6	22	-5.5	648	10.8	1.47	14.80	12	1.8	12	2	2238	502	1.13		2.47	
HCH	1.2	24	-9.3	362	25.6	23.48	50.73	15	2.4	15	2	2350	515	1.18	0.26	2.43	0.54

HJO	1.3	28	-12.0	273	3.2	8.63	14.16	24	6.3	22	6	1889	612	0.27	0.01	0.57	0.01
HPO	3	48	-8.1	401	2.6			149	20.0	59	7	9718	1224	0.80	0.27	1.62	0.55
JAM	6.8	80	12.2	1084	0.6			328	18.6	270	40	12405	511	2.11	0.85	4.86	2.04
MAC	5.2	104	-4.7	386	7.6	4.87	28.57	133	84.7					1.29	0.16	2.80	0.24
MIS	2.6	49	9.8	758	30.4	16.55	43.48	25	12.3	26	13	3253	1161	1.61	1.22	3.49	2.63
NAV	13.5	145	12.0	1175	35.4		68.79	15	2.2	15	3	1968	689	2.42	0.23	5.83	0.52
NOY	13.5	105	11.6	1214	60.8		6.19	14	1.0	14	1	2766	54	0.41	1.66	0.95	3.84
POT	6.4	81	10.7	1004	52.3		69.57	14	3.6	14	4	2123	694	1.55	1.23	3.71	2.88
RIO	4.2	100	16.0	382	19.0	21.39	20.79	30	10.9	39	16	3342	883	2.02	1.43	4.31	3.06
ROA	3.1	41	13.7	1122	96.8	37.47	23.06	269	84.0					0.87	0.40	1.86	0.90
SAG	16.1	238	-12.1	202	48.2		2.84					2581	501	2.72		6.29	
SAN	9.9	193	15.1	467	6.2	20.09	35.29	21	11.4	18	12	3658	1950	0.96	0.37	1.97	0.78
SIU	14	106	10.4	1755	8.1		83.21	18	3.4					0.33	0.09	0.66	0.18
SUS	6.5	90	8.4	1008	19.7	7.33	79.93	19	4.1	19	4	2334	368	0.99	0.53	2.02	1.11
UMP	14.3	215	9.5	1315	12.8		97.09	15	3.5					1.13		2.47	
MAT	1.5	24	13.5	1088	15.8	7.58	65.35	21	4.6	20	4	1997	426	0.14	0.03	0.30	0.07
YUK	9.8	184	-6.5	316	10.5	3.06	27.01	127	48.8					1.04	0.62	2.17	1.29
FLY	6.1	235	24.2	3727	4.0	18.10	0.73	18	3.8	15	4	2867	588				
WAP	11.2	163	12.8	1476	3.8	38.27	47.36	21	0.7	20	0	2966	839	0.42	0.08	0.84	0.16
WAA	13.4	209	12.1	2264	53.5		18.76	6	5.2	1	9	3224	557	1.08	1.31	2.59	3.15
POE	12.8	398	10.3	3675	28.0		42.36	12	1.7	12	3	2547	550	1.71	0.80	3.73	1.77
WAT	15.5	489	10.1	4046	58.6		3.89	15		15		2690		2.72		6.29	
HOK	19.2	502	8.9	3401	97.7		0.09	64	25.7	66	27	9419	2742	2.65	0.05	5.71	0.07
WHA	20.8	698	8.1	3322	40.1		66.33	10		11		2618	944	2.75		6.57	
FOX	20.4	714	7.6	4170	80.7			115	48.4	124	54	9730	3263				
WAH	21.4	735	7.2	3967	42.6		53.51	15	3.7	17	4	815	492	2.74	0.23	6.56	0.52
AMZ	3.7	81	24.6	2149	19.2	1.60	23.90	13	8.3	13	10	2259	547	0.78	0.22	1.65	0.48
FAJ	6.4	172	25.2	2014	45.4		58.40	12	3.0	12	5	3078	656	2.55	1.48	6.12	3.54
GUA	4.6	45	25.5	1133	2.2			200	14.7	159	16	9425	1018	0.38	0.00	0.78	0.02
BER	6.8	156	19.4	703	43.4		6.91	13	14.1	13	14	2516	657	0.44	0.20	0.93	0.46

Supplementary information 2

The full reference list for the MOREPOC v1.0 dataset

Reference

Adams, J. L., Tipping, E., Bryant, C. L., Helliwell, R. C., Toberman, H., and Quinton, J. (2015). Aged riverine particulate organic carbon in four UK catchments. Science of the Total Environment, 536, 648-654.

Alam, M. J., Nagao, S., and Quayum, M. E. (2012). Transport behavior of particulate organic matter in river water during snow melting in the Ishikari, Tokachi, Teshio and Kushiro Rivers, Japan. Journal of the Asiatic Society of Bangladesh, Science, 38(2), 163-173.

Alam, M. J., Nagao, S., Aramaki, T., Shibata, Y., and Yoneda, M. (2007). Transport of particulate organic matter in the Ishikari River, Japan during spring and summer. Nuclear Instruments and Methods in Physics Research Section B: Beam Interactions with Materials and Atoms, 259(1), 513-517.

Alin, S. R., Aalto, R., Goni, M. A., Richey, J. E., and Dietrich, W. E. (2008). Biogeochemical characterization of carbon sources in the Strickland and Fly rivers, Papua New Guinea. Journal of Geophysical Research: Earth Surface, 113(F1).

Aramaki, T., Nagao, S., Nakamura, Y. H., Uchida, M., and Shibata, Y. (2010). The effects of rainfall on carbon isotopes of POC in the Teshio River, Northern Japan. Radiocarbon, 52(2), 808-814.

Aucour, A. M., France-Lanord, C., Pedoja, K., Pierson-Wickmann, A. C., and Sheppard, S. M. (2006). Fluxes and sources of particulate organic carbon in the Ganga-Brahmaputra River system. Global Biogeochemical Cycles, 20(2).

Barros, G. V., Martinelli, L. A., Novais, T. M. O., Ometto, J. P. H., and Zuppi, G. M. (2010). Stable isotopes of bulk organic matter to trace carbon and nitrogen dynamics in an estuarine ecosystem in Babitonga Bay (Santa Catarina, Brazil). Science of the Total Environment, 408(10), 2226-2232.

Bianchi, T. S., Mitra, S., and McKee, B. A. (2002). Sources of terrestrially derived organic carbon in lower Mississippi River and Louisiana shelf sediments: implications for differential sedimentation and transport at the coastal margin. Marine Chemistry, 77(2-3), 211-223.

Bianchi, T. S., Wysocki, L. A., Stewart, M., Filley, T. R., and McKee, B. A. (2007). Temporal variability in terrestrially derived sources of particulate organic carbon in

the lower Mississippi River and its upper tributaries. Geochimica et Cosmochimica Acta, 71(18), 4425-4437.

Billett, M. F., Dinsmore, K. J., Smart, R. P., Garnett, M. H., Holden, J., Chapman, P., ... and Stott, A. W. (2012). Variable source and age of different forms of carbon released from natural peatland pipes. Journal of Geophysical Research: Biogeosciences, 117(G2).

Billett, M. F., Garnett, M. H., Dinsmore, K. J., Dyson, K. E., Harvey, F., Thomson, A. M., ... and Kortelainen, P. (2012). Age and source of different forms of carbon released from boreal peatland streams during spring snowmelt in E. Finland. Biogeochemistry, 111(1), 273-286.

Bird, M. I., Giresse, P., and Ngos, S. (1998). A seasonal cycle in the carbon-isotope composition of organic carbon in the Sanaga River, Cameroon. Limnology and Oceanography, 43(1), 143-146.

Blair, N. E., Leithold, E. L., Brackley, H., Trustrum, N., Page, M., and Childress, L. (2010). Terrestrial sources and export of particulate organic carbon in the Waipaoa sedimentary system: Problems, progress and processes. Marine Geology, 270(1-4), 108-118.

Bouchez, J., Galy, V., Hilton, R. G., Gaillardet, J., Moreira-Turcq, P., Pérez, M. A., ... and Maurice, L. (2014). Source, transport and fluxes of Amazon River particulate organic carbon: insights from river sediment depth-profiles. Geochimica et Cosmochimica Acta, 133, 280-298.

Bouchez, J., Beyssac, O., Galy, V., Gaillardet, J., France-Lanord, C., Maurice, L., and Moreira-Turcq, P. (2010). Oxidation of petrogenic organic carbon in the Amazon floodplain as a source of atmospheric CO_2. Geology, 38(3), 255-258.

Bouillon, S., Abril, G., Borges, A. V., Dehairs, F., Govers, G., Hughes, H. J., ... and Middelburg, J. J. (2009). Distribution, origin and cycling of carbon in the Tana River (Kenya): a dry season basin-scale survey from headwaters to the delta. Biogeosciences, 6(11), 2475-2493.

Bouillon, S., Yambélé, A., Gillikin, D. P., Teodoru, C., Darchambeau, F., Lambert, T., and Borges, A. V. (2014). Contrasting biogeochemical characteristics of the Oubangui River and tributaries (Congo River basin). Scientific Reports, 4, 5402.

Bröder, L., Davydova, A., Davydov, S., Zimov, N., Haghipour, N., Eglinton, T. I., and Vonk, J. E. (2020). Particulate organic matter dynamics in a permafrost headwater stream and the Kolyma River mainstem. Journal of Geophysical Research:

Biogeosciences, 125(2).

Cai, Y., Guo, L., and Douglas, T. A. (2008). Temporal variations in organic carbon species and fluxes from the Chena River, Alaska. Limnology and Oceanography, 53(4), 1408-1419.

Cai, Y., Guo, L., Wang, X., and Aiken, G. (2015). Abundance, stable isotopic composition, and export fluxes of DOC, POC, and DIC from the Lower Mississippi River during 2006–2008. Journal of Geophysical Research: Biogeosciences, 120(11), 2273-2288.

Campeau, A., Soerensen, A. L., Martma, T., Åkerblom, S., and Zdanowicz, C. (2020). Controls on the ^{14}C Content of Dissolved and Particulate Organic Carbon Mobilized Across the Mackenzie River Basin, Canada. Global Biogeochemical Cycles, 34(12).

Caraco, N., Bauer, J. E., Cole, J. J., Petsch, S., and Raymond, P. (2010). Millennial-aged organic carbon subsidies to a modern river food web. Ecology, 91(8), 2385-2393.

Cathalot, C., Rabouille, C., Tisnérat-Laborde, N., Toussaint, F., Kerhervé, P., Buscail, R., ... and Lansard, B. (2013). The fate of river organic carbon in coastal areas: a study in the Rhône River delta using multiple isotopic ($\delta^{13}C$, $\Delta^{14}C$) and organic tracers. Geochimica et Cosmochimica Acta, 118, 33-55.

Clark, K. E., Hilton, R. G., West, A. J., Malhi, Y., Gröcke, D. R., Bryant, C. L., ... and New, M. (2013). New views on "old" carbon in the Amazon River: Insight from the source of organic carbon eroded from the Peruvian Andes. Geochemistry, Geophysics, Geosystems, 14(5), 1644-1659.

Daessle, L. W., Orozco, A., Struck, U., Camacho-Ibar, V. F., van Geldern, R., Santamaría-del-Ángel, E., and Barth, J. A. C. (2017). Sources and sinks of nutrients and organic carbon during the 2014 pulse flow of the Colorado River into Mexico. Ecological Engineering, 106, 799-808.

De Jonge, C., Stadnitskaia, A., Hopmans, E. C., Cherkashov, G., Fedotov, A., Streletskaya, I. D., ... and Damsté, J. S. S. (2015). Drastic changes in the distribution of branched tetraether lipids in suspended matter and sediments from the Yenisei River and Kara Sea (Siberia): Implications for the use of brGDGT-based proxies in coastal marine sediments. Geochimica et Cosmochimica Acta, 165, 200-225.

Dudarev, O. V., Charkin, A. N., Semiletov, I. P., and Krukhmalev, A. V. (2010, August). Spatiotemporal variability of the organic carbon isotopic composition of suspended matter at the lower stream and estuary of the Amur River. Doklady Earth Sciences,

433(2), 1132-1140.

Fernandes, A. M., Hissler, C., da Conceição, F. T., Junior, E. P. S., and Mortatti, J. (2016). Combined analysis of trace elements and isotopic composition of particulate organic matter in suspended sediment to assess their origin and flux in a tropical disturbed watershed. Environmental Pollution, 218, 844-854.

Freymond, C. V., Lupker, M., Peterse, F., Haghipour, N., Wacker, L., Filip, F., ... and Eglinton, T. I. (2018). Constraining instantaneous fluxes and integrated compositions of fluvially discharged organic matter. Geochemistry, Geophysics, Geosystems, 19(8), 2453-2462.

Galy, V., and Eglinton, T. (2011). Protracted storage of biospheric carbon in the Ganges-Brahmaputra basin. Nature Geoscience, 4(12), 843.

Galy, V., France-Lanord, C., Beyssac, O., Faure, P., Kudrass, H., and Palhol, F. (2007). Efficient organic carbon burial in the Bengal fan sustained by the Himalayan erosional system. Nature, 450(7168), 407.

Galy, V., Beyssac, O., France-Lanord, C., and Eglinton, T. (2008). Recycling of graphite during Himalayan erosion: a geological stabilization of carbon in the crust. Science, 322(5903), 943-945.

Galy, V., Peucker-Ehrenbrink, B., and Eglinton, T. (2015). Global carbon export from the terrestrial biosphere controlled by erosion. Nature, 521(7551), 204.

Gao, Q., Tao, Z., Yao, G., Ding, J., Liu, Z., and Liu, K. (2007). Elemental and isotopic signatures of particulate organic carbon in the Zengjiang River, southern China. Hydrological Processes: An International Journal, 21(10), 1318-1327.

Ge, T., Xue, Y., Jiang, X., Zou, L., and Wang, X. (2020). Sources and radiocarbon ages of organic carbon in different grain size fractions of Yellow River-transported particles and coastal sediments. Chemical Geology, 534, 119452.

Godin, P., Macdonald, R. W., Kuzyk, Z. Z. A., Goñi, M. A., and Stern, G. A. (2017). Organic matter compositions of rivers draining into Hudson Bay: Present-day trends and potential as recorders of future climate change. Journal of Geophysical Research: Biogeosciences, 122(7), 1848-1869.

Gomez, B., Baisden, W. T., and Rogers, K. M. (2010). Variable composition of particle-bound organic carbon in steepland river systems. Journal of Geophysical Research: Earth Surface, 115(F4).

Goñi, M. A., Hatten, J. A., Wheatcroft, R. A., and Borgeld, J. C. (2013). Particulate organic matter export by two contrasting small mountainous rivers from the Pacific

Northwest, USA. Journal of Geophysical Research: Biogeosciences, 118(1), 112-134.

Goni, M. A., Yunker, M. B., Macdonald, R. W., and Eglinton, T. I. (2005). The supply and preservation of ancient and modern components of organic carbon in the Canadian Beaufort Shelf of the Arctic Ocean. Marine Chemistry, 93(1), 53-73.

Goñi, M. A., Moore, E., Kurtz, A., Portier, E., Alleau, Y., and Merrell, D. (2014). Organic matter compositions and loadings in soils and sediments along the Fly River, Papua New Guinea. Geochimica et Cosmochimica Acta, 140, 275-296.

Gordon, E. S., and Goñi, M. A. (2003). Sources and distribution of terrigenous organic matter delivered by the Atchafalaya River to sediments in the northern Gulf of Mexico. Geochimica et Cosmochimica Acta, 67(13), 2359-2375.

Guo, L., and Macdonald, R. W. (2006). Source and transport of terrigenous organic matter in the upper Yukon River: Evidence from isotope ($\delta^{13}C$, $\Delta^{14}C$, and $\delta^{15}N$) composition of dissolved, colloidal, and particulate phases. Global Biogeochemical Cycles, 20(2).

Guo, L., Ping, C. L., and Macdonald, R. W. (2007). Mobilization pathways of organic carbon from permafrost to arctic rivers in a changing climate. Geophysical Research Letters, 34(13).

Hatten, J. A., Goñi, M. A., and Wheatcroft, R. A. (2012). Chemical characteristics of particulate organic matter from a small, mountainous river system in the Oregon Coast Range, USA. Biogeochemistry, 107(1), 43-66.

Hélie, J. F., and Hillaire-Marcel, C. (2006). Sources of particulate and dissolved organic carbon in the St Lawrence River: isotopic approach. Hydrological Processes: An International Journal, 20(9), 1945-1959.

Hemingway, J. D. (2017). Understanding terrestrial organic carbon export: a time-series approach (Doctoral dissertation, Massachusetts Institute of Technology).

Hemingway, J. D., Schefuß, E., Spencer, R. G., Dinga, B. J., Eglinton, T. I., McIntyre, C., and Galy, V. V. (2017). Hydrologic controls on seasonal and inter-annual variability of Congo River particulate organic matter source and reservoir age. Chemical Geology, 466, 454-465.

Hilton, R. G. (2017). Climate regulates the erosional carbon export from the terrestrial biosphere. Geomorphology, 277, 118-132.

Hilton, R. G., Galy, A., Hovius, N., Chen, M. C., Horng, M. J., and Chen, H. (2008). Tropical-cyclone-driven erosion of the terrestrial biosphere from mountains. Nature

Geoscience, 1(11), 759-762.

Hilton, R. G., Galy, A., Hovius, N., Horng, M. J., and Chen, H. (2010). The isotopic composition of particulate organic carbon in mountain rivers of Taiwan. Geochimica et Cosmochimica Acta, 74(11), 3164-3181.

Hilton, R. G., Galy, V., Gaillardet, J., Dellinger, M., Bryant, C., O'regan, M., ... and Calmels, D. (2015). Erosion of organic carbon in the Arctic as a geological carbon dioxide sink. Nature, 524(7563), 84.

Hossain, H. Z., Kawahata, H., Roser, B. P., Sampei, Y., Manaka, T., and Otani, S. (2017). Geochemical characteristics of modern river sediments in Myanmar and Thailand: implications for provenance and weathering. Geochemistry, 77(3), 443-458.

Hossler, K., and Bauer, J. E. (2012). Estimation of riverine carbon and organic matter source contributions using time-based isotope mixing models. Journal of Geophysical Research: Biogeosciences, 117(G3).

Hu, B., Li, J., Bi, N., Wang, H., Wei, H., Zhao, J., ... and Liu, M. (2015). Effect of human-controlled hydrological regime on the source, transport, and flux of particulate organic carbon from the lower Huanghe (Yellow River). Earth Surface Processes and Landforms, 40(8), 1029-1042.

Kao, S. J., and Liu, K. K. (1996). Particulate organic carbon export from a subtropical mountainous river (Lanyang Hsi) in Taiwan. Limnology and Oceanography, 41(8), 1749-1757.

Kao, S. J., and Liu, K. K. (1997). Fluxes of dissolved and nonfossil particulate organic carbon from an Oceania small river (Lanyang Hsi) in Taiwan. Biogeochemistry, 39(3), 255-269.

Kao, S. J., Hilton, R. G., Selvaraj, K., Dai, M., Zehetner, F., Huang, J. C., ... and Hovius, N. (2014). Preservation of terrestrial organic carbon in marine sediments offshore Taiwan: mountain building and atmospheric carbon dioxide sequestration. Earth Surface Dynamics, 2(1), 127-139.

Kendall, C., Silva, S. R., and Kelly, V. J. (2001). Carbon and nitrogen isotopic compositions of particulate organic matter in four large river systems across the United States. Hydrological Processes, 15(7), 1301-1346.

Kim, J. H., Zell, C., Moreira-Turcq, P., Pérez, M. A., Abril, G., Mortillaro, J. M., ... and Damsté, J. S. S. (2012). Tracing soil organic carbon in the lower Amazon River and its tributaries using GDGT distributions and bulk organic matter properties.

Geochimica et Cosmochimica Acta, 90, 163-180.

Komada, T., Druffel, E. R., and Hwang, J. (2005). Sedimentary rocks as sources of ancient organic carbon to the ocean: An investigation through $\Delta^{14}C$ and $\delta^{13}C$ signatures of organic compound classes. Global Biogeochemical Cycles, 19(2).

Komada, T., Druffel, E. R., and Trumbore, S. E. (2004). Oceanic export of relict carbon by small mountainous rivers. Geophysical Research Letters, 31(7).

Leithold, E. L., Blair, N. E., and Perkey, D. W. (2006). Geomorphologic controls on the age of particulate organic carbon from small mountainous and upland rivers. Global Biogeochemical Cycles, 20(3).

Li, G., Wang, X. T., Yang, Z., Mao, C., West, A. J., and Ji, J. (2015a). Dam-triggered organic carbon sequestration makes the Changjiang (Yangtze) river basin (China) a significant carbon sink. Journal of Geophysical Research: Biogeosciences, 120(1), 39-53.

Li, Z., Peterse, F., Wu, Y., Bao, H., Eglinton, T. I., and Zhang, J. (2015b). Sources of organic matter in Changjiang (Yangtze River) bed sediments: preliminary insights from organic geochemical proxies. Organic Geochemistry, 85, 11-21.

Liu, Z., Zhao, M., Sun, H., Yang, R., Chen, B., Yang, M., ... and Zeng, H. (2017). "Old" carbon entering the South China Sea from the carbonate-rich Pearl River Basin: Coupled action of carbonate weathering and aquatic photosynthesis. Applied geochemistry, 78, 96-104.

Lobbes, J. M., Fitznar, H. P., and Kattner, G. (2000). Biogeochemical characteristics of dissolved and particulate organic matter in Russian rivers entering the Arctic Ocean. Geochimica et Cosmochimica Acta, 64(17), 2973-2983.

Longworth, B. E., Petsch, S. T., Raymond, P. A., and Bauer, J. E. (2007). Linking lithology and land use to sources of dissolved and particulate organic matter in headwaters of a temperate, passive-margin river system. Geochimica et Cosmochimica Acta, 71(17), 4233-4250.

Lu, F., Liu, Z., and Ji, H. (2013). Carbon and nitrogen isotopes analysis and sources of organic matter in the upper reaches of the Chaobai River near Beijing, China. Science China Earth Sciences, 56(2), 217-227.

Lu, Y. H., Bauer, J. E., Canuel, E. A., Chambers, R. M., Yamashita, Y., Jaffé, R., and Barrett, A. (2014). Effects of land use on sources and ages of inorganic and organic carbon in temperate headwater streams. Biogeochemistry, 119(1), 275-292.

Martin, E. E., Ingalls, A. E., Richey, J. E., Keil, R. G., Santos, G. M., Truxal, L. T., ...

and Druffel, E. R. (2013). Age of riverine carbon suggests rapid export of terrestrial primary production in tropics. Geophysical Research Letters, 40(21), 5687-5691.

Marwick, T. R., Tamooh, F., Teodoru, C. R., Borges, A. V., Darchambeau, F., and Bouillon, S. (2015). The age of river-transported carbon: A global perspective. Global Biogeochemical Cycles, 29(2), 122-137.

Masiello, C. A., and Druffel, E. R. (2001). Carbon isotope geochemistry of the Santa Clara River. Global Biogeochemical Cycles, 15(2), 407-416.

Mayorga, E., Aufdenkampe, A. K., Masiello, C. A., Krusche, A. V., Hedges, J. I., Quay, P. D., ... and Brown, T. A. (2005). Young organic matter as a source of carbon dioxide outgassing from Amazonian rivers. Nature, 436(7050), 538-541.

McClelland, J. W., Holmes, R. M., Peterson, B. J., Raymond, P. A., Striegl, R. G., Zhulidov, A. V., ... and Staples, R. (2016). Particulate organic carbon and nitrogen export from major Arctic rivers. Global Biogeochemical Cycles, 30(5), 629-643.

McIntosh, H. A. (2013). Composition, sources, and age of dissolved and particulate organic matter in the Delaware River and estuary. (Mater dissertation)

Megens, L., Van der Plicht, J., and De Leeuw, J. W. (2001). Temporal variations in ^{13}C and ^{14}C concentrations in particulate organic matter from the southern North Sea. Geochimica et Cosmochimica Acta, 65(17), 2899-2911.

Moyer, R. P., Bauer, J. E., and Grottoli, A. G. (2013). Carbon isotope biogeochemistry of tropical small mountainous river, estuarine, and coastal systems of Puerto Rico. Biogeochemistry, 112(1), 589-612.

Nagao, S., Aramaki, T., Seki, O., Uchida, M., and Shibata, Y. (2010). Carbon isotopes and lignin composition of POC in a small river in Bekanbeushi Moor, northern Japan. Nuclear Instruments and Methods in Physics Research Section B: Beam Interactions with Materials and Atoms, 268(7-8), 1098-1101.

Nagao, S., Usui, T., Yamamoto, M., Minagawa, M., Iwatsuki, T., and Noda, A. (2005). Combined use of $\Delta^{14}C$ and $\delta^{13}C$ values to trace transportation and deposition processes of terrestrial particulate organic matter in coastal marine environments. Chemical Geology, 218(1-2), 63-72.

Onstad, G. D., Canfield, D. E., Quay, P. D., and Hedges, J. I. (2000). Sources of particulate organic matter in rivers from the continental USA: lignin phenol and stable carbon isotope compositions. Geochimica et Cosmochimica Acta, 64(20), 3539-3546.

Qu, Y., Jin, Z., Wang, J., Wang, Y., Xiao, J., Gou, L. F., ... and Xu, X. (2020). The

sources and seasonal fluxes of particulate organic carbon in the Yellow River. Earth Surface Processes and Landforms, 45(9), 2004-2019.

Rachold, V., and Hubberten, H. W. (1999). Carbon isotope composition of particulate organic material in East Siberian rivers. In Land-Ocean Systems in the Siberian Arctic (pp. 223-238). Springer, Berlin, Heidelberg.

Raymond, P. A., and Bauer, J. E. (2001). Riverine export of aged terrestrial organic matter to the North Atlantic Ocean. Nature, 409(6819), 497.

Raymond, P. A., Bauer, J. E., Caraco, N. F., Cole, J. J., Longworth, B., and Petsch, S. T. (2004). Controls on the variability of organic matter and dissolved inorganic carbon ages in northeast US rivers. Marine Chemistry, 92(1-4), 353-366.

Rosenheim, B. E., Roe, K. M., Roberts, B. J., Kolker, A. S., Allison, M. A., and Johannesson, K. H. (2013). River discharge influences on particulate organic carbon age structure in the Mississippi/Atchafalaya River System. Global Biogeochemical Cycles, 27(1), 154-166.

Scheingross, J. S., Repasch, M. N., Hovius, N., Sachse, D., Lupker, M., Fuchs, M., ... and Schleicher, A. M. (2021). The fate of fluvially-deposited organic carbon during transient floodplain storage. Earth and Planetary Science Letters, 561, 116822.

Schwab, M. S., Hilton, R. G., Raymond, P. A., Haghipour, N., Amos, E., Tank, S. E., ... and Eglinton, T. I. (2020). An abrupt aging of dissolved organic carbon in large Arctic rivers. Geophysical Research Letters, 47(23).

Smith, J. C., Galy, A., Hovius, N., Tye, A. M., Turowski, J. M., and Schleppi, P. (2013). Runoff-driven export of particulate organic carbon from soil in temperate forested uplands. Earth and Planetary Science Letters, 365, 198-208.

Spencer, R. G., Hernes, P. J., Aufdenkampe, A. K., Baker, A., Gulliver, P., Stubbins, A., ... and Six, J. (2012). An initial investigation into the organic matter biogeochemistry of the Congo River. Geochimica et Cosmochimica Acta, 84, 614-627.

Striegl, R. G., Dornblaser, M. M., Aiken, G. R., Wickland, K. P., and Raymond, P. A. (2007). Carbon export and cycling by the Yukon, Tanana, and Porcupine rivers, Alaska, 2001–2005. Water Resources Research, 43(2).

Sun, H. G., Han, J. T., Zhang, S. R., and Lu, X. X. (2011). Transformation of dissolved inorganic carbon (DIC) into particulate organic carbon (POC) in the lower Xijiang River, SE China: an isotopic approach. Biogeosciences Discussions, 8(5), 9471-9501.

Sun, H., Han, J., Li, D., Lu, X., Zhang, H., and Zhao, W. (2017). Organic carbon transport in the Songhua River, NE China: influence of land use. Hydrological Processes, 31(11), 2062-2075.

Sun, S., Schefuß, E., Mulitza, S., Chiessi, C. M., Sawakuchi, A. O., Zabel, M., ... and Mollenhauer, G. (2017). Origin and processing of terrestrial organic carbon in the Amazon system: lignin phenols in river, shelf, and fan sediments. Biogeosciences, 14(9).

Tamooh, F., Van den Meersche, K., Meysman, F., Marwick, T. R., Borges, A. V., Merckx, R., ... and Bouillon, S. (2012). Distribution and origin of suspended sediments and organic carbon pools in the Tana River Basin, Kenya. Biogeosciences Discussions, 9(3), 2523-2566.

Tao, S., Eglinton, T. I., Montluçon, D. B., McIntyre, C., and Zhao, M. (2015). Pre-aged soil organic carbon as a major component of the Yellow River suspended load: Regional significance and global relevance. Earth and Planetary Science Letters, 414, 77-86.

Tao, Z. Q., Gao, Z., Huang, X. K. , Liu, K. X. , and Fu, D. P. (2012). Biogeochemical cycle of riverine carbon in the Guijiang River: tracing with ^{14}C and ^{13}C. Quaternary Research, 03, 95-102. (In Chinese with English abstract).

Teodoru, C., unpublished data (2011) from Marwick et al., 2015.

Tesi, T., Miserocchi, S., Goñi, M. A., Turchetto, M., Langone, L., De Lazzari, A., ... and Correggiari, A. (2011). Influence of distributary channels on sediment and organic matter supply in event-dominated coastal margins: the Po prodelta as a study case. Biogeosciences, 8(2), 365.

Torres, M. A., Kemeny, P. C., Lamb, M. P., Cole, T. L., and Fischer, W. W. (2020). Long-Term Storage and Age-Biased Export of Fluvial Organic Carbon: Field Evidence From West Iceland. Geochemistry, Geophysics, Geosystems, 21(4), e2019GC008632.

Townsend-Small, A., Noguera, J. L., McClain, M. E., and Brandes, J. A. (2007). Radiocarbon and stable isotope geochemistry of organic matter in the Amazon headwaters, Peruvian Andes. Global Biogeochemical Cycles, 21(2).

Tripti, M., Gurumurthy, G. P., Lambs, L., Riotte, J., and Balakrishna, K. (2018). Water and Organic Carbon Cycles in Monsoon-driven Humid Tropics of the Western Ghats Mountain Belt, India: Insights from Stable Isotope Approach. Journal of the Geological Society of India, 92(5), 579-587.

Voss, B. M. (2014). Spatial and temporal dynamics of biogeochemical processes in the Fraser River, Canada: A coupled organic-inorganic perspective (Doctoral dissertation, Massachusetts Institute of Technology).

Voss, B. M., Peucker-Ehrenbrink, B., Eglinton, T. I., Spencer, R. G., Bulygina, E., Galy, V., ... and Gillies, S. L. (2015). Seasonal hydrology drives rapid shifts in the flux and composition of dissolved and particulate organic carbon and major and trace ions in the Fraser River, Canada.

Voss, B. M., Wickland, K. P., Aiken, G. R., and Striegl, R. G. (2017). Biological and land use controls on the isotopic composition of aquatic carbon in the Upper Mississippi River Basin. Global Biogeochemical Cycles, 31(8), 1271-1288.

Wakeham, S. G., Canuel, E. A., Lerberg, E. J., Mason, P., Sampere, T. P., and Bianchi, T. S. (2009). Partitioning of organic matter in continental margin sediments among density fractions. Marine Chemistry, 115(3-4), 211-225.

Wang, J., Hilton, R. G., Jin, Z., Zhang, F., Densmore, A. L., Gröcke, D. R., ... and West, A. J. (2019). The isotopic composition and fluxes of particulate organic carbon exported from the eastern margin of the Tibetan Plateau. Geochimica et Cosmochimica Acta.

Wang, J., Jin, Z., Hilton, R. G., Zhang, F., Li, G., Densmore, A. L., ... and West, A. J. (2016). Earthquake-triggered increase in biospheric carbon export from a mountain belt. Geology, 44(6), 471-474.

Wang, X., Ma, H., Li, R., Song, Z., and Wu, J. (2012). Seasonal fluxes and source variation of organic carbon transported by two major Chinese Rivers: The Yellow River and Changjiang (Yangtze) River. Global Biogeochemical Cycles, 26(2).

Wang, X., Xu, C., Druffel, E. M., Xue, Y., and Qi, Y. (2016). Two black carbon pools transported by the Changjiang and Huanghe Rivers in China. Global Biogeochemical Cycles, 30(12), 1778-1790.

Wei, X., Yi, W., Shen, C., Yechieli, Y., Li, N., Ding, P., ... and Liu, K. (2010). ^{14}C as a tool for evaluating riverine POC sources and erosion of the Zhujiang (Pearl River) drainage basin, South China. Nuclear Instruments and Methods in Physics Research Section B: Beam Interactions with Materials and Atoms, 268(7-8), 1094-1097.

Wu, Y., Bao, H. Y., Unger, D., Herbeck, L. S., Zhu, Z. Y., Zhang, J., and Jennerjahn, T. C. (2013). Biogeochemical behavior of organic carbon in a small tropical river and estuary, Hainan, China. Continental Shelf Research, 57, 32-43.

Wu, Y., Bao, H., Yu, H., Zhang, J., and Kattner, G. (2015). Temporal variability of

particulate organic carbon in the lower Changjiang (Yangtze River) in the post-Three Gorges Dam period: Links to anthropogenic and climate impacts. Journal of Geophysical Research: Biogeosciences, 120(11), 2194-2211.

Wu, Y., Eglinton, T. I., Zhang, J., & Montlucon, D. B. (2018). Spatiotemporal variation of the quality, origin, and age of particulate organic matter transported by the Yangtze River (Changjiang). Journal of Geophysical Research: Biogeosciences, 123(9), 2908-2921.

Wu, Y., Zhang, J., Liu, S. M., Zhang, Z. F., Yao, Q. Z., Hong, G. H., and Cooper, L. (2007). Sources and distribution of carbon within the Yangtze River system. Estuarine, Coastal and Shelf Science, 71(1-2), 13-25.

Xue, Y., Zou, L., Ge, T., and Wang, X. (2017). Mobilization and export of millennial-aged organic carbon by the Yellow River. Limnology and Oceanography, 62(S1), S95-S111.

Yu, M., Eglinton, T. I., Haghipour, N., Montluçon, D. B., Wacker, L., Hou, P., ... and Zhao, M. (2019). Impacts of natural and human-induced hydrological variability on particulate organic carbon dynamics in the Yellow River. Environmental science and technology.

Zeng, F. W. (2011). The Effects of Land Use and Human Activities on Carbon Cycling in Texas Rivers. (Doctoral dissertation, Rice University).

Zheng, L. W., Ding, X., Liu, J. T., Li, D., Lee, T. Y., Zheng, X., ... and Kao, S. J. (2017). Isotopic evidence for the influence of typhoons and submarine canyons on the sourcing and transport behavior of biospheric organic carbon to the deep sea. Earth and Planetary Science Letters, 465, 103-111.

Chapter 6

Conclusions and Perspectives

It is a fundamental issue to understand the Earth's carbon cycle, in which rivers play a significant role by transferring inorganic and organic material from continents to the ocean. As a constituent of eroded material transiting through river systems, riverine particulate organic carbon (POC) represent a main component of the global carbon cycle. The global carbon cycle is continuously and sensitively adapting to external environmental perturbations, yet the feedback mechanism needs to be further constrained. In response to current anthropogenic interventions, the natural transport of riverine POC has been greatly modified, influencing long-term carbon exchange fluxes between Earth's reservoirs as well as other biogeochemical cycles. In this section, I summarize the major conclusions of this thesis and put up some new thoughts for future research.

1. General conclusions

1.1 Major sources of fluvial POC

In large river systems, active carbon cycling between the terrestrial and aquatic environment happens throughout the entire river source-to-sink routing. Each river section contributes sediments and associated POC to fluvial transport in its own way. Among the POC that is eventually exported to the ocean from the Huanghe, over 90% is supplied by erosion of the Chinese Loess Plateau (CLP) located in the middle reaches while bank erosion in the flat region of the lower reaches could be an important POC supplying mechanism. In this regard, the physical erosion rate of the CLP controls POC yields of the entire river basin. The biospheric organic carbon fraction derived from the topsoil and deeper loess-paleosol sequences constitutes 60% and 20% of the riverine POC, respectively. This deep contribution explains the significantly ^{14}C-depleted nature of bulk POC ($\Delta^{14}C$: −398 ± 38‰). The situation is quite different for the Changjiang river where fluvial POC under natural flow conditions (non-perturbated by human activities) would be mainly derived from mountainous regions in the upper reaches. In the Jinshajiang (upper Changjiang reaches), POC is radiocarbon depleted

($\Delta^{14}C$ values: −431 ± 40‰) consistent with mobilization of petrogenic carbon (about 40% of POC) in high physical erosion rates mountainous region and the possible contribution of aged organic carbon from permafrost thawing in the Qinghai-Tibet Plateau. However, since massive dam-building in the last few decades, especially after the Three Gorges Dam operation, POC from the upper reaches have been temporally stored in artificial reservoirs and not delivered anymore at the mouth. In addition, the mid reaches have shifted from a net sediment sink to a net sediment source to the river system. Recycling of pre-deposited materials from the upper Changjiang, instantaneous bank erosion, and sediments supply of mid tributaries reshape the POC components, resulting in elevated biospheric organic fraction (~90%). Therefore, region-specific controls on physical erosion rate should be emphasized to address POC composition and yield of an entire fluvial system. Furthermore, it has been shown that small catchments like the Anning river basin, which only accounts for only 1/150 of the total Changjiang basin, can yield comparable POC flux under storm events than the whole Changjiang. Intensive storm events in small catchments should be highlighted, especially in monsoon-impacted river systems, due to their capability to quickly mobilize a large amount of POC into fluvial systems. Finally, anthropogenic activities, such as dam-building, perturbs the natural transport of sediments and POC from source to sink. Humans profoundly modify the long-term contributions of the different continental POC pools exported to the ocean and potentially modify the feedback between organic carbon cycling and climate. Source-to-sink alteration of POC in large rivers over the Anthropocene should be systematically investigated.

1.2 Transport behavior

In global river systems, POC shows a general depleting trend of elemental and radiocarbon compositions with increasing turbidity (suspended sediment load), suggesting dilution by old-aged POC-poor materials from deep soil horizons and/or source rocks. This variation is observed at depth profile scale but also laterally along channel transects. Hydrological segregation is at play and generates elemental and isotopic heterogeneities of POC. For the first time, the transect sampling scheme has been adopted in the four largest Chinese rivers, granting access to the full range of sediment particle sizes. In general, SPM shows an increasing concentration and particle size with depth, and a depleting trend of POC content and radiocarbon activity (^{14}C). This sorting effect is pronounced in the Huanghe, resulting in the conspicuously higher

POC load near the river bottom compared to that transiting at the surface. Lateral heterogeneities are also observed at other sampling sites (*e.g.*, Jibei in the Huanghe, Nanxi in the Changjiang, Shapu in the Zhujiang, Fuyuan in the Heilongjiang), as a result of the coupled effect of hydrodynamics, river turbidity, channel geometry, and bank erosion, etc. Anthropogenic regulation is a strong force on the POC heterogeneity and loading by exerting primary control reducing the turbidity of post-dam sediment transport. Preferential deposition of coarse sediments accompanied by post-dam transport of fine sediments, the intrinsic physical and chemical heterogeneities are reduced to varying extents. In this manner, the POC loading (constrained by the slope between POC content and Al/Si ratios in this thesis) is increasing due to the changing mineralogy, loss of coarse particles and rock-derived organic carbon. A quantitative assessment framework of the effect of different environmental variables (lithology, geomorphology, climate, anthropogenic activities, etc) on POC loading should be built.

1.3 Shifting POC burial from ocean to continent

The sediment load of large Chinese rivers has considerabely decreased over the last 70 years in response to anthropogenic activities, especially dam building. For instance, the Huanghe and Changjiang rivers experience a decrease in the sediment load of about 99% and 70%, respectively. As a consequence, large amounts of POC have been buried in pre-dam reservoirs with a high preservation efficiency instead of entering the ocean. It is estimated that artificial reservoirs in the Changjiang collect a POC flux of approximately 6.6 MtC/yr, consisting of 0.8 - 3.1 MtC/yr for POC_{petro} and 3.5 - 5.8 MtC/yr for POC_{bio}. These fluxes are equivalent to 5 times the amount of POC arriving at the mouth. The shifting and massive burial of riverine POC at reservoirs will last for, at least, the lifespan of the dams (decades to millennials). From a global carbon cycle perspective, it is crucial to quantify the accumulation and preservation fluxes of POC in reservoirs. A highlight is raised to the dam-building in the upper mountainous regions of large rivers, because it is expected to represent a rapid and efficient burial environment for POC. For example, it is shown that cascade reservoirs in the lower Jinshajiang prevent almost all headwater sediments from entering the Changjiang mainstream. Steep terrains favor high erosion rates and rapid transfer leading to efficient burial due to high accumulation rate and low oxygen exposure. In addition, it is anticipated that the in-river mineralization rate of POC is lower for material traveling a short distance before being buried in dam reservoirs compared to material transported

over a long pathway down to the accumulation site in the estuary. Substantial POC_{bio} and POC_{petro} survive from oxidation during transport and deposition processes in the passive margins. Concerning large rivers in the pan-QTP regions, dam-building is expected to efficiently counteract the delivery of massive terrestrial eroded organic matter into the Ocean, which would represent negative feedback on global warming due to temporary negation of CO_2 release.

1.4 MOREPOC database: environmental driving forces

This thesis presents a globally representative elemental and isotopic carbon composition dataset of fluvial POC: Modern River Archives of Particulate Organic Carbon (MOREPOC) version 1.0, recording the fluvial memory of suspended particulate matters (SPM) collected at 229 main channels and tributaries in 118 river systems referenced from the sprung up researches on POC in the last two decades. This database records 3,298 SPM, including 2,847 with POC content, 3,151 with stable carbon isotope $\delta^{13}C$ values, and 1,874 with radiocarbon activity $\Delta^{14}C$ values. MOREPOC dataset is aimed to help to explore potentials to quantitatively comprehend the complex coupled environmental drivers on the nature of POC at large intra- and inter-basin scales. Geomorphic features (slope and stream gradient), climatic (mean annual precipitation and mean annual temperature), tectonic (passive and active continental margins), and lithologic control on radiocarbon signatures of riverine POC are analyzed. A steep terrain favors the erosion to OC_{petro} resulting in depleted ^{14}C compositions. Temperature and precipitation together control the ^{14}C and turnover of soil organic carbon within the catchment, thus affecting POC characteristics in the fluvial system, low temperature and precipitation result in the delivery of ^{14}C-depleted POC. This response is sensitive in river basins with similar geomorphic and tectonic features, such as in Circum-Arctic rivers. The lithogenic features should be an important factor, the erosion to the vast organic-rich shales makes Mackenzie deliver the most ^{14}C-depleted POC in large river systems. To better constrain the organic carbon cycle from past to future, it is necessary to build quantitative correlations and numerical models to examine and to predict how each factor interplays in regulating the terrestrial mobilization of organic matter into fluvial transport.

2. Perspectives

2.1 Rock landslides: fast CO_2 release at high temperature

Landslide-induced thermal decomposition of carbonate and organic carbon enters the long-term carbon cycle as a net source. Landslides, especially rock avalanches, are of substantial large volumes, long runouts, high velocities (Heim, 1932; Keefer and Larsen, 2007; Pudasaini and Miller, 2013). This type of landslides is widely and frequently happened in tectonically-active mountainous regions around the globe (Fan et al., 2019). It is evidenced that there are substantial thermal reactions during the sliding process due to the intensive friction (Aharonov and Anders, 2006, Goren et al., 2010), accompanying by the thermal decomposition of basal carbonates (Anders et al., 2000, Mitchell et al., 2015; Hu et al., 2018; 2019). In two large landslides located at the upper reaches of Changjiang, it is observed that the temperature of the sliding surface can reach over 850 ℃ due to the dramatic frictional heating (Figure 1 shows Daguangbao landslide) (Hu et al., 2018; 2019). The temperature is much higher than the reaction temperature for amphibolite-grade metamorphism (300 ℃: initiation of reactions, over 650 ℃: reaching the equilibrium) (Schidlowski, 1998). Other studies report the bulk decarbonization temperature for dolomite is ca. 600 ℃ and is ca. 750 ℃ for decarbonating calcite (De Paola et al., 2011; Karunadasa et al., 2019). The pyrolysis formulas of dolomite and calcite could be as follows:

$$2CaMg(CO_3)_2 + SiO_2 \rightarrow Mg_2SiO_4 + 2CaCO_3 + 2CO_2 \quad (1)$$

$$CaCO_3 \rightarrow CaO + CO_2 \quad (2)$$

Petrogenic OC in ancient sedimentary rocks can be oxidized at a temperature of over 650 ℃ (Rosenheim and Galy, 2012), the formula is as follows:

$$CH_2O + O_2 \rightarrow H_2O + CO_2 \quad (3)$$

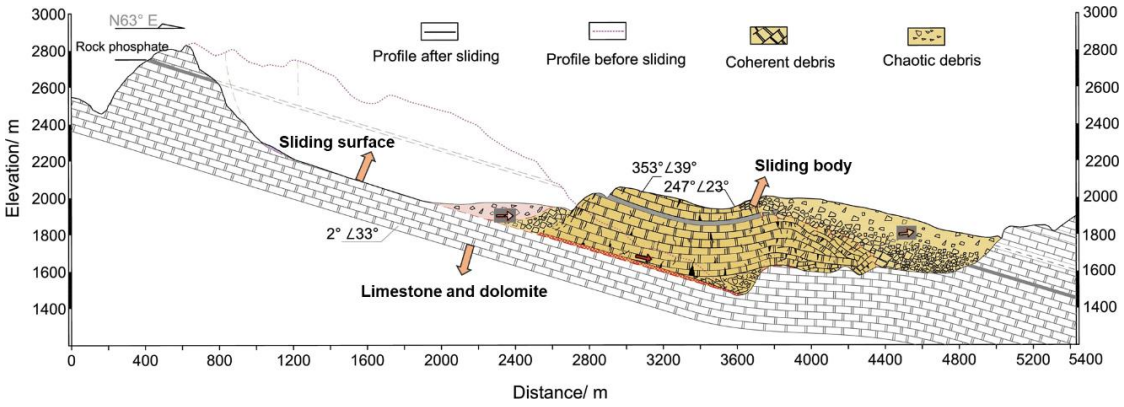

Fig. 1 Geological longitudinal section of Daguangbao landslide drawn through the sampling site. The sliding surface can reach over 850 °C during the long-runout movement of the sliding body, the high frictional heating enables the thermal decomposition of calcite and dolomite. Figure modified from Hu et al. (2019).

These pyrolysis processes to carbonate and organic carbon indicate the release of CO_2 that will impact the Earth's geological carbon cycle. Recent studies already show that the occurrence of landslides could facilitate organic carbon degradation (Emberson et al., 2018; Hemingway et al., 2019) and sulfide oxidation (Emberson et al., 2016; Bufe et al., 2021; Nevers et al., 2021) due to the increased exposure of rock surface, both processes represent a net source of CO_2 to the atmosphere (Hilton et al., 2014; Horan et al., 2019; Calmels et al., 2007). Sedimentary OC is oxidized under low temperatures at a measurable rate (Soulet et al., 2018, 2021). The quantity of CO_2 released from rock organic carbon oxidation is demonstrated to be seasonally variable, showing an increasing CO_2 release by a factor of 2.2 when temperature increased by 10 °C. CO_2 release in summer is 5 times higher than that in winter (Soulet et al., 2021). Therefore, it can be reasonably hypothesized that rapid rock sliding would be capable of producing substantial CO_2 to the atmosphere in a very short time promoted by instantaneous high temperature. These fluxes need to be quantitatively constrained. On the contrary, landslides can also facilitate the mobilization of biospheric OC into rivers by stripping vegetation and soils and favor silicate weathering through exposing fresh silicate minerals, which plays as the long-term CO_2 sink (Hilton et al 2008; Emberson et al., 2018; Bufe et al., 2021). However, due to the counteracting effect of CO_2 drawdown or release of these processes, it is unknown whether landslides play as a net source or net sink of atmospheric CO_2 in the long-term carbon cycle. The thermal release of geological CO_2 might be fast and large in the upper reaches of the Changjiang,

where there are intensive and active seismic activities (*e.g.*, Wenchuan earthquake), inducing massive destruction of relief and causing intensive and widely extended mass wasting, especially in the form of landslides (Fan et al., 2019). The dynamic geomorphic process gives rise to the kinetics limitation of rock weathering reactions. The thermal release of CO_2 might counteract the CO_2 sink associated with silicate weathering and POC_{bio} burial favored by increasing sediment supply. This process should be explored to evaluate the overall rock-atmosphere CO_2 exchange of landslides.

2.2 Unconstrained organic carbon cycles in the largest Chinese rivers

To adequately understand to what extent the large fluvial system affects the geologic carbon cycle, it is important to determine the possible processes in the catchment that will lead to net atmospheric CO_2 change. On the one hand, some natural processes involved in the carbon cycle need to be explored; on the other hand, the rate and the scale of anthropogenic alterations to the carbon cycle need to be further discussed.

[1] Oxidation of petrogenic OC at low temperature

Even though provenances of POC have been extensively studied in large rivers, many important carbon cycling processes are yet poorly constrained. The Mackenzie is the only large fluvial system for which net CO_2 exchange between the lithosphere and the atmosphere has been quantified (*i.e.*, sink: silicate weathering and biospheric OC burial; source: oxidation of sulfides and petrogenic OC) (Horan et al., 2019; Märki et al., 2021). Regarding the organic carbon cycle, oxidative weathering of petrogenic OC in sedimentary rocks is a major source of atmospheric CO_2 (Chang and Berner, 1999; Derry, 2014; Petsch, 2014; Hilton et al., 2014; Soulet et al., 2021), which remains unknown in the four largest river systems mentioned in this thesis, further exploration is highly needed. With a special concern to the upper mountainous regions, especially of the Changjiang and the Huanghe, where the continental surface is characterized by high proportions of sedimentary rocks, and is constantly experiencing uplifting and mountain building in active tectonic belts, the high physical erosion rate favors both the oxidation of petrogenic OC and fluvial transfer of biospheric OC, the imbalance between two processes should be more precisely quantified. In addition, it is demonstrated that the oxidation of petrogenic OC meditated by microbial activities during exhumation and subsequent erosion of mountain ranges is a considerable source of CO_2 to the atmosphere. From 56% to 78% of the petrogenic OC initially resent in bedrock exhumed from the tropical, rapidly eroding Central Range of Taiwan is

oxidized (Hemingway et al., 2018). This mechanism needs to be examined in the mountainous ranges of similar active tectonic activities and climate (high temperature and precipitation) in the largest Chinese rivers. Meanwhile, it is worth noting that glaciers are an important element of the environment in the source regions of the Changjiang and the Huanghe on the Qinghai-Tibet Plateau. Glaciation is reported to favor oxidation of petrogenic OC (Horan et al., 2017), but the mode, the quantity, and the rate at which glacier evolution affects this CO_2 release process needs to be further constrained by looking into the fluvial memory of sensitive solids and solutes.

At present, some methods have been applied to determine the petrogenic OC loss, *e.g.*, using the ^{14}C content of riverine POC (Bouchez et al., 2010), using the trace element rhenium (Re) of soluble phases due to the close association between OC and redox-sensitive metals (Petsch, 2014; Horan et al., 2019; Hilton et al., 2014); a chamber-based method allows direct measurements of CO_2 emissions (Soulet et al., 2018); ramped pyrolysis radiocarbon analysis to OC from different sources (Hemingway et al., 2018). Appropriate analysis schemes should be carried out to better constrain the varying processes of petrogenic OC oxidation in large rivers.

[2] POC burial efficiency in the artificial reservoirs

As discussed in Chapter 4, the Changjiang case study, it is of crucial importance to know the interference by dam-building to the carbon cycle over different timescales. Dam-building creates reservoirs upstream that store a massive amount of terrestrial OC (24-100 MtC/yr) and potentially emit significant amounts of greenhouse gases (51 MtC/yr) (Mendonça et al., 2017; Barros et al., 2011). However, reservoirs will lead to the exposure of drawdown areas, therefore increasing the mineralization to OC enhancing the carbon source effect to the atmosphere by ~53%, an updated estimate is 43-80 MtC/yr (Keller et al., 2021). Thus, the counterbalance between emissions and burial in global reservoirs needs to be quantified at high resolution to define the role that reservoirs can play in the carbon cycle. Inland waters are more efficiently burying C than oceans, since a higher fraction of settling OC escapes mineralization and stays in the sediments, the burial efficiency of OC in reservoirs is even higher than in lakes (Burdige, 2007; Blair and Aller, 2012; Mendonça et al., 2017). The present global estimates of OC burial in reservoirs are relying on few systematic measurements, limited geographical distribution, and many assumptions, resulting in relatively large uncertainty and discrepancy of and among different estimates (*e.g.*, Mendonça et al.,

2017; Keller et al., 2021). The burial efficiency of OC in artificial reservoirs is determined by the sediment accumulation rate and oxygen exposure time (Sobek et al., 2009; Burdige, 2007). On this basis, the elemental and isotopic composition of organic carbon entering and being buried in reservoirs is needed to infer their metabolism state during the transport and the sedimentation processes. Compound-specific carbon analysis and ramped pyrolysis are recommended (Galy and Eglinton, 2011; Hemingway et al., 2018). The Changjiang alone has over 50,000 dams in operation or under construction. The enhanced terrestrial erosion rate brought increased inputs of terrestrial OC, and the increased reservoir area favors the aquatic primary production, two processes coupled to enhance riverine OC (allochthonous and autochthonous) into the burial in the reservoirs. In Chapter 4, we estimate that reservoirs in Changjiang receive a total POC flux of 6.6 MtC/yr and assume that the emission of greenhouse gases is significantly low based on the case study in the Three Gorges Dam, thus leading to the conclusion that reservoirs enhance the role that the Changjiang River Basin plays as a carbon sink at least over decadal to centennial timescales. There are two implications behind this conclusion, the first is that reservoirs in Changjiang as a whole are carbon sink; the second is that the Changjiang since dam-building regulation has enhanced its carbon sink effect since the operation of dams in its catchment. This should be clarified in a global estimate to better illustrate how artificial reservoirs affect the carbon cycle. In the Changjiang basin, the remineralization rate of fluvial POC in reservoirs is still poorly constrained, accurate quantifications are recommended. Nevertheless, understanding the redox status of buried OC can also help to advance the prediction of the fate of the accumulated OC after the operating life of reservoirs. Massive reservoir buried sediments will be eventually delivered into the ocean or redistributed in the after-dam channels. The Three Gorges Dam alone has been accumulating ca. 20 MtC (2003-2021, a maximum estimate considering complete POC preservation), representing 10% of the estimated global POC flux (200 MtC/yr). This massive release will surely cause a high-turbidity transport of sediments accompanied by many processes involving reburial and oxidation of biospheric and petrogenic OC, the role in the carbon cycle needs further understanding.

Reference

Aharonov, E., and Anders, M. H. (2006). Hot water: A solution to the Heart Mountain detachment problem?. Geology, 34(3), 165-168.

Anders, M. H., Aharonov, E., and Walsh, J. J. (2000). Stratified granular media beneath large slide blocks: Implications for mode of emplacement. Geology, 28(11), 971-974.

Barros, N., Cole, J. J., Tranvik, L. J., Prairie, Y. T., Bastviken, D., Huszar, V. L., ... and Roland, F. (2011). Carbon emission from hydroelectric reservoirs linked to reservoir age and latitude. Nature Geoscience, 4(9), 593-596.

Bouchez, J., Beyssac, O., Galy, V., Gaillardet, J., France-Lanord, C., Maurice, L., and Moreira-Turcq, P. (2010). Oxidation of petrogenic organic carbon in the Amazon floodplain as a source of atmospheric CO_2. Geology, 38(3), 255-258.

Bufe, A., Hovius, N., Emberson, R., Rugenstein, J. K., Galy, A., Hassenruck-Gudipati, H. J., and Chang, J. M. (2021). Co-variation of silicate, carbonate and sulfide weathering drives CO_2 release with erosion. Nature Geoscience, 14(4), 211-216.

Calmels, D., Gaillardet, J., Brenot, A., & France-Lanord, C. (2007). Sustained sulfide oxidation by physical erosion processes in the Mackenzie River basin: Climatic perspectives. Geology, 35(11), 1003-1006.

De Paola, N., Hirose, T., Mitchell, T., Di Toro, G., Viti, C., and Shimamoto, T. (2011). Fault lubrication and earthquake propagation in thermally unstable rocks. Geology, 39(1), 35-38.

Emberson, R., Galy, A., and Hovius, N. (2018). Weathering of reactive mineral phases in landslides acts as a source of carbon dioxide in mountain belts. Journal of Geophysical Research: Earth Surface, 123(10), 2695-2713.

Emberson, R., Hovius, N., Galy, A., and Marc, O. (2016). Oxidation of sulfides and rapid weathering in recent landslides. Earth Surface Dynamics, 4(3), 727-742.

Galy, V., and Eglinton, T. (2011). Protracted storage of biospheric carbon in the Ganges–Brahmaputra basin. Nature Geoscience, 4(12), 843-847.

Goren, L., Aharonov, E., and Anders, M. H. (2010). The long runout of the Heart Mountain landslide: Heating, pressurization, and carbonate decomposition. Journal of Geophysical Research: Solid Earth, 115(B10).

Heim, A. (1932). Bergsturz und menschenleben (No. 20). Fretz and Wasmuth.

Hemingway, J. D., Hilton, R. G., Hovius, N., Eglinton, T. I., Haghipour, N., Wacker, L., ... and Galy, V. V. (2018). Microbial oxidation of lithospheric organic carbon in rapidly eroding tropical mountain soils. Science, 360(6385), 209-212.

Hilton, R. G., Gaillardet, J., Calmels, D., and Birck, J. L. (2014). Geological respiration of a mountain belt revealed by the trace element rhenium. Earth and Planetary Science Letters, 403, 27-36.

Hilton, R. G., Galy, A., and Hovius, N. (2008). Riverine particulate organic carbon from an active mountain belt: Importance of landslides. Global Biogeochemical Cycles, 22(1).

Horan, K., Hilton, R. G., Dellinger, M., Tipper, E., Galy, V., Calmels, D., ... and Burton, K. W. (2019). Carbon dioxide emissions by rock organic carbon oxidation and the net geochemical carbon budget of the Mackenzie River Basin. American Journal of Science, 319(6), 473-499.

Horan, K., Hilton, R. G., Selby, D., Ottley, C. J., Gröcke, D. R., Hicks, M., and Burton, K. W. (2017). Mountain glaciation drives rapid oxidation of rock-bound organic carbon. Science Advances, 3(10), e1701107.

Hu, W., Huang, R., McSaveney, M., Yao, L., Xu, Q., Feng, M., and Zhang, X. (2019). Superheated steam, hot CO_2 and dynamic recrystallization from frictional heat jointly lubricated a giant landslide: field and experimental evidence. Earth and Planetary Science Letters, 510, 85-93.

Hu, W., Huang, R., McSaveney, M., Zhang, X. H., Yao, L., and Shimamoto, T. (2018). Mineral changes quantify frictional heating during a large low-friction landslide. Geology, 46(3), 223-226.

Karunadasa, K. S., Manoratne, C. H., Pitawala, H. M. T. G. A., and Rajapakse, R. M. G. (2019). Thermal decomposition of calcium carbonate (calcite polymorph) as examined by in-situ high-temperature X-ray powder diffraction. Journal of Physics and Chemistry of Solids, 134, 21-28.

Keller, P. S., Marcé, R., Obrador, B., and Koschorreck, M. (2021). Global carbon budget of reservoirs is overturned by the quantification of drawdown areas. Nature Geoscience, 1-7.

Märki, L., Lupker, M., France-Lanord, C., Lavé, J., Gallen, S., Gajurel, A. P., ... & Eglinton, T. (2021). An unshakable carbon budget for the Himalaya. Nature Geoscience, 14(10), 745-750.

Mendonça, R., Müller, R. A., Clow, D., Verpoorter, C., Raymond, P., Tranvik, L. J., and Sobek, S. (2017). Organic carbon burial in global lakes and reservoirs. Nature Communications, 8(1), 1-7.

Mitchell, T. M., Smith, S. A., Anders, M. H., Di Toro, G., Nielsen, S., Cavallo, A., and Beard, A. D. (2015). Catastrophic emplacement of giant landslides aided by thermal decomposition: Heart Mountain, Wyoming. Earth and Planetary Science Letters, 411, 199-207.

Pudasaini, S. P., and Miller, S. A. (2013). The hypermobility of huge landslides and avalanches. Engineering Geology, 157, 124-132.

Rosenheim, B. E., and Galy, V. (2012). Direct measurement of riverine particulate organic carbon age structure. Geophysical Research Letters, 39(19).

Sobek, S., Durisch-Kaiser, E., Zurbrügg, R., Wongfun, N., Wessels, M., Pasche, N., and Wehrli, B. (2009). Organic carbon burial efficiency in lake sediments controlled by oxygen exposure time and sediment source. Limnology and Oceanography, 54(6), 2243-2254.

Soulet, G., Hilton, R. G., Garnett, M. H., Dellinger, M., Croissant, T., Ogrič, M., and Klotz, S. (2018). In situ measurement of flux and isotopic composition of CO 2 released during oxidative weathering of sedimentary rocks. Biogeosciences, 15(13), 4087-4102.

Soulet, G., Hilton, R.G., Garnett, M.H., Roylands, T., Klotz, S., Croissant, T., Dellinger, M., Bouteiller, C. (2021). Temperature control on CO_2 emissions from the weathering of sedimentary rocks. Nature Geoscience. https://doi.org/10.1038/s41561-021-00805-1

Tranvik, L. J., Downing, J. A., Cotner, J. B., Loiselle, S. A., Striegl, R. G., Ballatore, T. J., ... and Weyhenmeyer, G. A. (2009). Lakes and reservoirs as regulators of carbon cycling and climate. Limnology and Oceanography, 54(6part2), 2298-2314.

ÉCOLE DOCTORALE
Sciences mécaniques et énergétiques, matériaux et géosciences (SMEMAG)

Titre : Origine et devenir du carbone organique particulaire transporté par les plus grands fleuves de Chine

Mots clés : grands fleuves de Chine, carbone organique particulaire, géochimie isotopique, radiocarbone

Résumé : Les processus d'érosion et de transport de carbone organique particulaire (POC) des continents vers l'océan jouent un rôle central dans le cycle du carbone. Les rivières fournissent des informations clés et intégrées sur l'origine, les processus de mobilisation et le métabolisme du carbone organique transitant des réservoirs terrestres aux réservoirs marins. Cet apport de POC à l'océan peut avoir des impacts variés sur la teneur en CO_2 de l'atmosphère à long terme, suivant son origine (biosphérique vs pétrogénique) et son devenir (enfouissement vs minéralisation). Il est donc crucial d'améliorer notre compréhension des processus de mobilisation et de transport de POC dans les fleuves et d'en identifier les sources, notamment face aux perturbations anthropiques actuelles. En ce sens, les grands fleuves chinois sont des terrains d'études privilégiés car ils sont caractérisés par une diversité de conditions climatiques et géomorphologiques, drainent des lithologies variées et sont soumis à une pression anthropique variable mais croissante.

Cette thèse se décompose en trois parties : 1) quantifier les sources et mécanismes de transport du POC dans un grand fleuve ayant l'une des charges sédimentaires les plus importantes au monde, le Huanghe ; 2) quantifier l'impact des barrages sur l'export de POC dans le Changjiang, un fleuve soumis à une pression anthropique massive (> 50000 barrages) ; 3) développer une base de données mondiale qui rassemble 3300 données de POC ainsi que des données de ses éventuels contrôles géo-environnementaux. Pour atteindre ces objectifs, des campagnes de prélèvements ont été menées sur les plus grands fleuves de Chine. Il a ainsi été possible d'exploiter des séries temporelles mensuelles de matière en suspension (SPM) prélevée en surface ainsi que de multiples échantillons de SPM prélevés suivant des profils verticaux distribués le long de transects de rivière.

La distribution en taille des grains et la composition chimique de ces SPM ont été analysés au même titre que la teneur en carbone organique et ses compositions isotopiques en $d^{13}C$ et C^{14}.

Le fleuve Huanghe, qui a connu une diminution d'environ 90 % de sa charge sédimentaire depuis 1950, transporte du POC relativement appauvri en C^{14} ($\Delta^{14}C$: -453‰ à -331‰) et cela, bien que la majorité de ce POC provienne de sources biosphériques (67 %-79 %). L'érosion physique intense des séquences de loess-paléosols dans le bassin expliquerait cette mobilisation de carbone relativement ancien (et même "mort" pour partie) provenant d'horizons profonds. De plus, l'hétérogénéité verticale et latérale de la composition élémentaire et isotopique du POC à l'échelle d'un transect de rivière montrent que l'érosion des berges et la remise en suspension du sable de fond sont des processus actifs.

Dans le bassin du fleuve Changjiang, les flux d'érosion à long terme et l'exportation de POC ont été fortement impactés par les activités humaines, notamment par la mise en place de barrages. A l'heure actuelle, il y aurait 4 fois plus de POC retenus à l'arrière des barrages du Changjiang que la quantité de POC exportée à l'embouchure. Le développement des méga-réservoirs en cascade (CMR) dans le Jinshajiang (cours supérieur du Changjiang) a bloqué le transfert jusqu'à l'océan du POC provenant du plateau du Qinghai-Tibet et a favorisé un enfouissement rapide et efficace de ce carbone organique sur le continent plutôt que dans l'océan.

Enfin, une base de données mondiale archivant 3 300 données élémentaires et isotopiques de POC dans le monde : Modern River Archives of Particulate Organic Carbon (MOREPOC), a été construite. Elle enregistre la mémoire fluviale des SPM collectés dans 229 rivières de 118 systèmes fluviaux. MOREPOC est construite pour étudier de manière globale les facteurs environnementaux majeurs pouvant contrôler l'export de POC et sa signature isotopique.

université PARIS-SACLAY

ÉCOLE DOCTORALE
Sciences mécaniques et énergétiques, matériaux et géosciences (SMEMAG)

Title : Source, transport, and fate of particulate organic carbon in the largest Chinese rivers

Keywords : large Chinese rivers, particulate organic carbon, stable isotope geochemistry, radiocarbon

Abstract : Continental erosion and riverine transport of particulate organic carbon (POC) to the Ocean play a central role in the global carbon cycle. Rivers provide key and integrated information on the origin, mobilization processes and metabolism of POC transiting from terrestrial to marine reservoirs. Once in the marine environment, POC may eventually have antagonist feedbacks on the long-term CO_2 content of the atmosphere, depending on its origin (biospheric vs petrogenic) and its fate (burial vs mineralization). Large rivers in China are of crucial importance in our understanding of POC delivery at both regional and global scales, as they encompass a large spectrum of climatic and geomorphic conditions, drain various lithologies, and are subject to varied but increasing anthropogenic pressure.

This thesis focuses on three parts: 1) the sources and transport mechanisms of POC in one of the most turbid large rivers, the Huanghe; 2) the impact of dam-building on POC export in the Changjiang, a large catchment that experiences massive anthropogenic perturbation with > 50,000 dams; 3) the development of a global database that gathers 3,300 data on riverine POC along with co-localized data of its possible geoenvironmental controls. To fulfill the goals of this thesis, multiple sampling expeditions were carried out on the largest rivers in China to collect monthly time series of suspended particulate matter (SPM) at the channel surface and multiple vertical depth profiles of SPM along channel transects. Fluvial sediment was analyzed for particle size and major elements as well as for POC content and dual carbon isotopes (^{13}C and ^{14}C). Coupling POC content with particle size (or aluminum to silicon ratios) and ADCP acquisitions allows accessing the loading and transport mode of POC as well as an accurate estimate of instantaneous POC fluxes.

The Huanghe, which has experienced a 90% decrease in sediment load since the 1950s, carries relatively ^{14}C-depleted POC ($\Delta^{14}C$: −453‰ to −331‰) although POC mainly originates from the biospheric pool (67%-79%). This is explained by enhanced physical erosion of unconsolidated loess-paleosol sequences in the Chinese Loess Plateau region. Gully erosion would mobilize aged (and even dead) carbon from deep horizons that can still be considered as biospheric carbon in the long-term carbon cycle. In addition, POC heterogeneities at the scale of a river cross-section suggest that bank erosion and bedload resuspension are operational processes.

In the Changjiang River system, long-term fluxes of erosion and POC export have been greatly impacted by human activities, especially since the operation of dams. A substantial amount of POC is not anymore transferred to the ocean but end-up buried in reservoirs upstream of dams. Nowadays, there would be 4 times more POC retained in reservoirs along the Changjiang than the amount of POC exported to the ocean at the mouth. For the first time, the impact of cascade mega reservoirs (CMRs) in the lower Jinshajiang (upper reaches of the Changjiang) on fluvial POC transfer is quantitatively evaluated. Distinct POC signature and loading are observed before and after CMRs operation, which prevented POC coming from the Qinghai-Tibet Plateau from traveling downstream and favored rapid and efficient burial of this OC on the continent rather than in the ocean.

Finally, a global database archiving 3,300 published and unpublished elemental and isotopic data on worldwide riverine POC: MOdern River archivEs of Particulate Organic Carbon (MOREPOC) has been built. It records the fluvial memory of SPM collected at 229 main channels and tributaries in 118 river systems. MOREPOC is then used to investigate the global pattern of POC loading and the possible environmental factors (*i.e.*, geomorphology, climate, and tectonics) that can control the radiocarbon signatures of POC in global rivers.